BOUNDARIES OF THE CRYSTAL MEMORY EFFECT IN SATURATED TRIACYLGLYCEROLS

by

Yujing Wang

Submitted in partial fulfillment of the requirements for the degree of Master of Science

at

Dalhousie University
Halifax, Nova Scotia
August 2016

TABLE OF CONTENTS

LIST OF TABLES

LIST OF FIGURES

ABSTRACT

One important factor that determines the crystalline phases formed from liquid triacylglycerols is the "crystal memory": fats that re-crystallize from a liquid obtained by melting a crystal may form the same crystal structure that they had as a solid before melting. The mechanism of this phenomenon is almost unknown, and no systematic research on pure triacylglycerols has been done. To advance the understanding of this effect, pure triacylglycerols and triacylglycerol mixtures were crystallized, tempered and subsequently melted. The liquid was then held at a combination of time and temperature before recrystallizing it. After testing many combinations, the [time + temperature] pairs that produced a recrystallization equal to a crystallization from a random liquid were found. These combinations define a time temperature boundary. Above the boundary, the memory is erased, since the liquid recrystallizes in a different form from the parent crystal present before re-crystallization. These experiments were done in a differential scanning calorimeter, given its precise temperature control.

Two kinds of memory were identified: early formation of the α polymorph, as observed by Arnaud; and the formation of a stable form, β or β', directly from the melt. The time-temperature combinations needed to erase each one of these memories were determined. For pure triacylglycerols, the times and temperatures required were shorter and lower than for their mixtures.

This supports the hypothesis that the liquid structure of pure triacylglycerols is disrupted by thermal fluctuations. In blends, it is additionally necessary to homogenize the concentration of the mixture. The size of the domains of different concentration in the freshly molten liquid, which depends on the history of the crystallization, also influences the memory. The effect on the onset temperature is more difficult to predict.

LIST OF ABBREVIATONS AND SYMBOLS USED

5M5P	50% trimyristin: 50% tripalmitin triacylglycerol mixture by weight
5P5S	50% tripalmitin: 50% tristearin triacylglycerol mixture by weight
C_p	Specific heat capacity at a constant pressure (J/g C°)
DCL	Double Chain Length Structure
DSC	Differential Scanning Calorimetry
FA	Fatty acid
FWHM	Full Width at Half Maximum
g_s	Geometrical factors for surface area A
g_v	Geometrical factors for volume V
G	Gibbs energy (J or J/mol)
LD	Lamellar Distance
LLL	Trilaurin
MMM	Trimyristin
NMR	Nuclear Magnetic Resonance
PLM	Polarized Light Microscopy
PPP	Tripalmitin
Rhdh	Rhombic dodecahedra
S	Entropy (J/K or J/Kmol)
SAXS	Small Angle X-ray Scattering
SF	Solid Fraction
SSS	Tristearin

T	Temperature (°C)
TAGs	Triacylglycerols
TCL	Triple Chain Length Structure
t_H	Holding time (min)
T_M	Melting temperature of trimyristin
T_m	Melting Temperature (°C)
$T_{m,\alpha}$	Melting temperature of $\boldsymbol{\alpha}$ polymorph
T_{max}	The maximum temperature that crystal memory phenomenon occurs
T_{min}	The minimum temperature that crystal memory phenomenon occurs
T_{onset_α}	The onset temperature of "early $\boldsymbol{\alpha}$ memory" during step e
$T_{onset\_\boldsymbol{\alpha}0}$	The onset temperature during step a
T_{onset_β}	The onset temperature of "$\boldsymbol{\beta}$ memory" during step e
T_P	Melting temperature of tripalmitin (°C)
T_{sl}	The highest temperature that exhibited the memory effect (°C)
XRD	X-ray Diffraction
x_M	Mole fraction of solid phase of trimyristin
y_M	Mole fraction of liquid phase of trimyristin
ΔG	Change in Gibbs energy (J)
$\Delta G*(\boldsymbol{\alpha})$	Energy barrier of the formation of polymorphic form $\boldsymbol{\alpha}$ (J)
$\Delta G*(\boldsymbol{\beta})$	Energy barrier of the formation of polymorphic form $\boldsymbol{\beta}$ (J)
$\Delta G*(\boldsymbol{\beta}')$	Energy barrier of the formation of polymorphic form $\boldsymbol{\beta}'$ (J)
ΔG_c	Activation Gibbs energy (J)

ΔG_D	Activation Gibbs energy for molecular diffusion (J)
$\Delta G_f(\boldsymbol{\alpha})$	Gibbs energy of the formation of polymorphic form $\boldsymbol{\alpha}$ (J)
$\Delta G_f(\boldsymbol{\beta})$	Gibbs energy of the formation of polymorphic form $\boldsymbol{\beta}$ (J)
$\Delta G_f(\boldsymbol{\beta}')$	Gibbs energy of the formation of polymorphic form $\boldsymbol{\beta}'$ (J)
ΔH	Enthalpy change at constant temperature and pressure (J)
ΔH_{crys}	Enthalpy of crystallization
ΔS	Entropy change at constant temperature and pressure (J/K)
ΔT_{α}	The difference between $T_{onset\_\alpha 0}$ and T_{onset_α}
$\Delta T_{\alpha\beta}$	The differences between $T_{onset\_\alpha 0}$ and T_{onset_β}
γ_T	Surface tension
γ_P or γ_M	Activity coefficient
ξc	Thickness of nanoplatelet
$a \cdot \xi c$	Width of nanoplatelet
$b \cdot \xi c$	Length of nanoplatelet
N	The number of molecules per mole
k_B	The Boltzmann constant (1.38065×10^{-23} J/K)
h	Plank's constant (6.6261×10^{-34} J·s)
V_{sm}	Molar volume
v_{obs}	Observation volume
τ	Induction time (min)

ACKNOWLEDGEMENTS

Firstly, I would like to gratefully acknowledge my supervisor Dr. Gianfranco Mazzanti, for his encouragement, guidance, inspiration, and patience for not only my project, but also my life. I also want to thank my advisory team Dr. Gill and Dr. Martini for their guidance and assistance for my thesis. To my research colleagues, Omar Qatami, Amro Alkhudair, Pavan Batchu, Pranav Arora, Mohit Kalaria, Liangle Lin, Rong Liu, Xiyan Deng, Tianguang Jia and Yijin Su, your very insightful discussions made this work possible and enjoyable.

Deepest thanks are expressed to my parents, who gave birth to me, raised me, taught me and supported me, and for their endless love for me. It is my parents that have made all the wonderful things happen in my life. Words cannot express how much I love you both.

My appreciation goes to my friends and other family members for their kindness and generous support. One page is not enough to name you all.

CHAPTER 1. INTRODUCTION

Because eating is such a central part of daily life, people are constantly looking for novel methods of food preparation. Indeed, eating can be a mundane activity, and encountering new forms of familiar food can make it more exciting and interesting. With billions of dollars at stake, the food industry makes every effort to improve food and ensure a safe and abundant food supply, striving not just to provide food but also to perfect characteristics like texture and taste. It is therefore very important to understand particular food ingredients and the ways in which they might be modified and manipulated. Food science provides us with a large platform for better understanding food, its ingredients, and how to produce better tasting food.

Dietary fat is one of the main nutrients that humans need; it provides people with an energy storage resource, as well as essential fatty acids that help to regulate body functions and carry fat-soluble vitamins. Dietary fats are key ingredients in many popular foods, such as chocolate, margarine, butter, spreads and baked products. Because the structure and distribution of dietary fats plays a critical role in food structure, they strongly influence the properties of the final products in terms of texture, appearance and mouth feel (Himawan, Starov & Stapley, 2006; Metin & Hartel, 2005). The formation of solid fat, known as fat crystallization, occurs mostly during the industrial manufacture and has a powerful influence on the texture, shelf life and quality of fat-based foods (Metin & Hartel, 2005). In order to get better quality and to meet the current market demands of fat-based foods, a more accurate understanding of the fat crystallization process of dietary fat from physics, chemistry and biochemistry is needed (Kiyotaka Sato, Ueno, & Yano, 1999).

Many sensorial attributes such as texture, stability and mouth feel of common fat-based foods

are derived from the network structure of the crystalline fat (Mazzanti, Guthrie, Sirota, Marangoni, & Idziak, 2003; Narine & Marangoni, 1999) and, depend on the mechanical strength of the fat crystal network (Narine & Marangoni, 1999). Several factors play an important role in determining the characteristics of the crystallized fat, such as composition, solid fraction, the microstructure of the crystals and polymorphic types. The processing conditions, such as crystallization temperatures, process time and cooling rates, determine these characteristics.

During processing and storage, it is common to crystallize the fat from a hot melt, then melt it at moderate temperature and recrystallize it again. If this melting occurs at temperatures close to the melting temperature of the fat, and the fat stays in the liquid state for a short time, there is long standing empirical evidence, backed up by a few documented scientific studies, that the crystals formed are influenced by the type of crystals present before the melting. On the other hand, if the same fat is melted to a temperature that is much higher than the melting temperature, and kept there for a long time, the fat will crystallize to a type of crystal structure that is independent of the type of crystals that existed before the melting. This effect was originally defined as the influence of the thermal history of cocoa butter on its phase behavior (Malssen, Peschar, & Schenk, 1996). The concept has since then, been extended to all fats. However, the precise combinations of time and temperature that return the liquid to the state where it will recrystallize into a crystal unaffected by the crystals from where it came from have not been investigated systematically. These time-temperature combinations constitute a boundary between the liquid that retains a "memory" of its source crystals, and a liquid that "forgot" that memory, i.e. an "amnesiac" liquid. In less anthropomorphic terms, it is the boundary between the region where the molecules of the liquid retain some structure remaining from its source

crystals, and the liquid where this structure has been destroyed by a thermal and diffusional randomization process. For simplicity, we will mostly use memory-type terms during the thesis, with the understanding that they represent molecular structures.

Despite its apparent importance in processing as well as in fundamental physical chemistry, to our knowledge there are no systematic data or methodologies to study the memory effect in pure liquid triacylglycerols (TAGs). This research, then, aims to observe the behavior of selected pure liquid TAGs during a defined melting and recrystallization process, in order to find the temperature-time boundaries needed to erase the crystal memory effect in the liquid.

Our working hypotheses were:

1. That there would be a time-temperature boundary for each pure material, with shorter times corresponding to higher temperatures. At time-temperature combinations above that boundary, the liquid will crystallize in the same polymorph and onset temperature, regardless of the crystal from which it came. At time temperature combinations below that boundary, the liquid will crystallize showing an effect of the crystal from which it came. This effect will produce a different polymorph, onset temperature or both.
2. That there would be a time-temperature boundary for each mixture, shorter times in combination with higher temperatures. The times, however, are expected to be longer than the times of pure materials. The effect of the source crystal structure on the liquid below the boundary will also affect the composition, the polymorphism and onset temperatures upon cooling.

We chose to use differential scanning calorimetry (DSC) to detect the crystallization and melting behavior. DSC estimates the heat flow rate to the sample by measuring the small difference in temperature between a sample pan and a reference pan, while samples are

subjected to a very precisely controlled temperature program. No instrument in our lab can provide better precision in the control of temperature and temperature ramps than the TA-Q100 DSC.

The memory effect was studied in five model molecular materials: three pure mono-saturated triacylglycerols: trimyristin, tripalmitin and tristearin (MMM, PPP and SSS) and two of their binary contiguous mixtures, 50% MMM + 50% PPP (5M5P) and 50% PPP + 50% SSS (5P5S). To determine the temperature-time boundaries the crystalline material was melted just above its melting temperature. Subsequently, the liquid was held at a chosen combination of temperature and time, and then recrystallized by cooling. Depending on the crystallization behavior, it was possible to observe if the liquid had retained or lost memory of its source crystal. By testing many combinations of holding times and temperatures it was possible to determine the boundaries for the memory of these materials.

During the research process, many other useful and interesting aspects of this phenomenon were observed. As a result of the study and these observations, a hypothesis for the molecular mechanism underlying the memory phenomenon is proposed

1.1 Objectives

The general research aim of our lab is to gain a better and wider understanding of the characteristics of the triacylglycerols crystallizing under different conditions, such as temperatures and time.

The specific objectives of this thesis are:

- To find the time-temperature boundaries of the crystal memory effect in three pure saturated triacylglycerols: trimyristin, tripalmitin and tristearin.
- To find the onset temperature of recrystallization from the crystal memory effect of those three pure saturated triacylglycerols.
- To find the time-temperature boundaries of the crystal memory effect in two binary mixtures: 5M5P and 5P5S.
- To find the onset temperature of recrystallization from the crystal memory effect of those two binary mixtures.
- To relate the boundaries to current theory on solid-liquid phase transitions in triacylglycerols.

CHAPTER 2. LITERATURE REVIEW

2.1 Lipids and Crystallization

Lipids are a group of molecules containing fatty acids and their derivatives, or substances that are functionally and biosynthetically related to these compounds. Chemically, oils and fats are multi-component mixtures composed predominantly of triacylglycerols (TAGs), which are composed of esters from glycerol and fatty acids. Specifically, TAGs consist of a glycerol moiety with each hydroxyl group esterified to a fatty acid (Ribeiro *et al.*, 2015).

Lipids are widely used in food industries, cosmetics and pharmaceuticals (Gunstone & B.Padley, 1997). They play a particularly critical role in fat commercial products, such as chocolate, butter, margarine, and baked foods: TAGs are the main component of edible fats, constituting 95% - 98% of their composition (Metin & Hartel, 2005). Not only processing but also storage conditions have determinant effects on food quality and texture, as well as shelf-life (Himawan *et al.*, 2006; Metin & Hartel, 2005).

The general structure of TAG molecules is shown in Figure 2-1 (a) (Sato, 2001): Each glycerol unit is esterified with three fatty acid units (R_1, R_2, R_3). A special sub-cell structure is defined as a lateral cross-sectional packing mode of the hydrocarbon chains of TAGs (Hagemann & Rothfus, 1993; van Langevelde *et al.*, 1999; Vand & Bell, 1951). A capital letter and a symbol are used to describe the sub-cells, with the letter implying the symmetry (e.g., O for orthorhombic, T for triclinic, M for monoclinic, H for hexagonal) and the symbol indicating either a parallel (//) or perpendicular ($\perp$) position between the zigzag planes of the different chains. There are about 10 types of sub-cell structures in crystalline fats, five of which are predominant: H, $O_\perp$, $O'_{//}$, $T_{//}$, and $M_{//}$ (the most frequent ones are H, $O_\perp$, and $T_{//}$).

In the hexagonal (H) sub-cell structure, the two-dimensional lattice is hexagonal. The carbon atoms can rotate and form disordered conformations of hydrocarbon chains. This is why the chain packing of the hexagonal (H) sub-cell structure is loose and the specific chain-chain interactions are lost. In the orthorhombic perpendicular ($O_{\perp}$) sub-cell structure, the two-dimensional lattice is rectangular, leading to a tightly packed lattice with specific chain-chain interactions. The triclinic parallel sub-cell structure (T//) has an oblique two-dimensional lattice, with the tightly packed chains causing strong specific chain-chain interaction (Kiyotaka Sato & Ueno, 2011).

In this research, three simple mono-saturated TAGs were studied, as shown in Table 2-1.

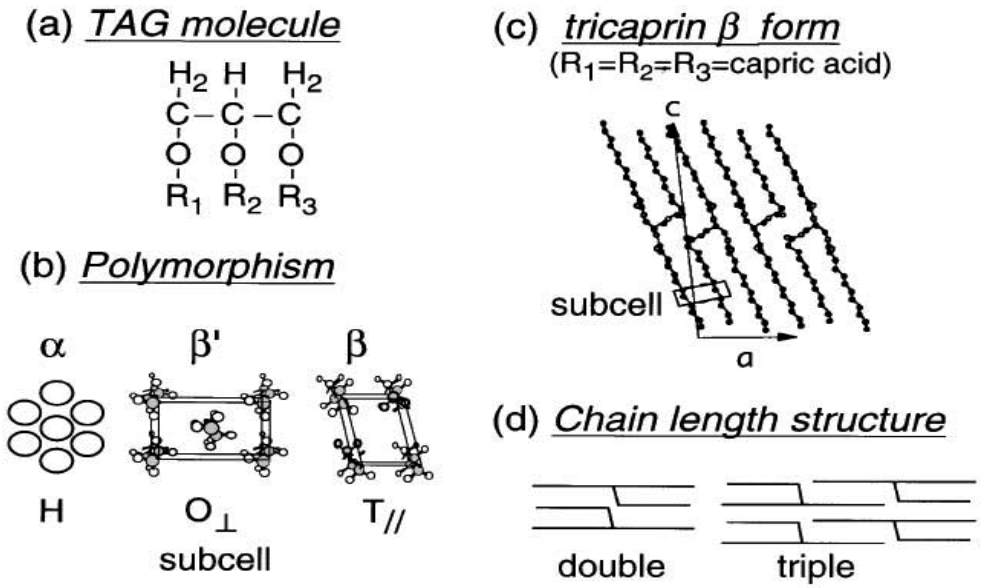

Figure 2-1 (a) a general TAG molecule structure, (b) the sub-cell structure of three most common polymorphisms in TAGs, "α", "β'" and "β", (c) unit cell structure of Tricaprin β form and (d) chain length structure in TAGs (Sato, 2001).

Table 2-1. Fatty acids in TAG samples used in our research.

Code	Fatty Acid	Chain Length
M	Myristic acid (tetradecanoic acid)	14
P	Palmitic acid (hexadecanoic acid)	16
S	Stearic acid (octadecanoic acid)	18

As shown in Figure 2-2, TAG molecules crystallize from the melt, via mass and heat transfer, to form nanocrystals, which then aggregates into particles and larger clusters until a three-dimensional space-filling network forms (Acevedo & Marangoni, 2010).

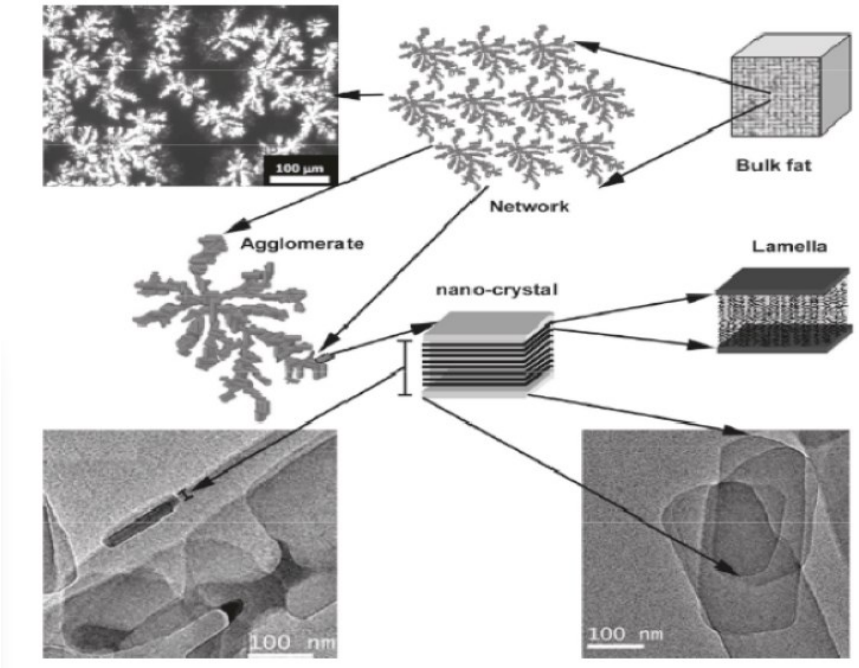

Figure 2-2. Schematic representation of different levels of structure in a bulk fat (Acevedo & Marangoni, 2010).

2.1.1 Polymorphism

Polymorphism is the ability of a TAG molecule to crystallize in more than one crystalline form (polymorph) depending on its arrangement within the crystal lattice (Metin & Hartel, 2005). The crystallization behavior of TAGs is mainly influenced by their molecular structures combined with external factors that include cooling rate, temperature, shear flow, pressure, impurities, and contact surfaces (Sato, 2001). Different crystalline arrangements of TAG molecules show obvious different melting temperatures, as shown in Table 2-2 (Takeuchi *et al.*, 2002).

Table 2-2. Melting points (°C) of three polymorphic forms for MMM, PPP, and SSS (Takeuchi *et al.*, 2002).

	α	***β'***	***B***
MMM	32.6	45.9	57.1
PPP	44.7	55.7	65.9
SSS	54.7	64.3	72.5

There are three main types of polymorphs in fats, ***α***, ***β***, and ***β'*** (Larsson, 1966), which are distinguished by their sub-cell structures, which are apparent from a top view of these planes (Figure 2-1 (b)). ***α*** (hexagonal shape sub-cell) is an unstable form, while ***β'*** (orthorhombic perpendicular shape sub-cell) is a metastable form of hydrocarbon chains inclined with respect to the basal plane by about 108 degrees and ***β*** (triclinic sub-cell) is the most stable form, with a triclinic parallel shape sub-cell with the hydrocarbon chains inclined at about 128 degrees (Takeuchi *et al.*, 2002).

2.1.2 Polymorphic Types and Sub-Cell Structures

Chain length structure plays an important role in the phase behavior of different types of TAGs in solid phase, as it produces a repeating sequence of the acyl chains involved in a unit cell lamella along the long-chain axis. The double chain length structure usually occurs when the chemical properties of the three fatty acid moieties of the TAG are the same or very similar; a triple chain length structure is formed when the chemical properties of one or two of the three fatty acids are greatly different from others (Sato, 2001).

The Gibbs energy (*G*) determines the thermodynamic stability of the polymorphic forms of TAGs, with the most stable polymorph having the lowest *G* value. A *G*-*T* (Temperature) diagram is shown in Figure 2-3 for three basic polymorphs. The plot follows the equation for *G* as a function of enthalpy (*H*), entropy (*S*), and *T*, which are computed as a difference ΔG with respect to a reference state, usually the liquid at zero degrees Celsius:

$$G = H - TS \quad (1)$$

Due to its monotropic nature, the Gibbs energy values are largest for $\boldsymbol{\alpha}$ form (least dense crystal packing), intermediate for $\boldsymbol{\beta}$' form and smallest for $\boldsymbol{\beta}$ form (densest crystal packing). Each polymorphic form has its own melting temperature, T_m, as well as its own melting enthalpy and entropy. The slope of the liquid line is steeper for the liquid and becomes shallower as the polymorphic form is more stable, i.e. going from $\boldsymbol{\alpha}$ to $\boldsymbol{\beta}$. At the melting temperature, the equilibrium condition between liquid and solid requires $\Delta G_{liquid\text{-}solid}$ to be zero, i.e. $\Delta G_{liquid} = \Delta G_{solid}$.

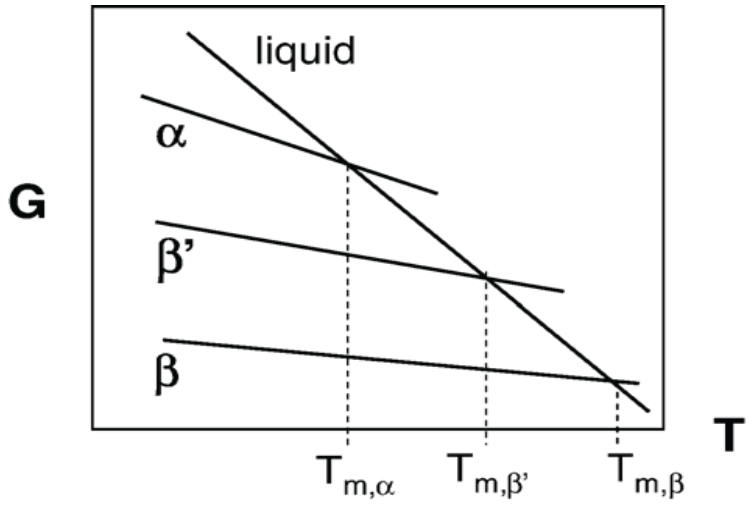

Figure 2-3. The relation between Gibbs energy and temperature for the three main polymorphic forms of TAGs (Himawan *et al.*, 2006).

For crystallization to occur at practical rates, the liquid has to be cooled below the melting temperature of the desired polymorphic form. In this state, the liquid is known by several different names, all having the same meaning: supercooled, subcooled, undercooled. In that situation, the Gibbs energy of the crystalline form is lower than that of the liquid, and therefore $\Delta G_{solid\text{ - }liquid}$ is negative. Thus, the process of crystallization is thermodynamically possible. For low temperatures, for instance, below $T_{m,\alpha}$, a question arises about the fact that there are three different $\Delta G_{solid\text{ - }liquid}$: Which polymorph(s) will then form? This is discussed in the next section.

2.1.3 Polymorphic Transitions

Due to the different stabilities of the polymorphs, all forms of crystals tend to transform to ***β***, the most stable form. Figure 2-3 shows the difference in the Gibbs energy for formation of the three major polymorphic forms (***α***, ***β***', and ***β***). A transition may happen from liquid to any polymorph, or between polymorphs. However, the transition rate depends both on its driving force (the Gibbs energy of formation ΔG_f(***α***), ΔG_f(***β***'), and ΔG_f(***β***)) and on its energy barrier (ΔG^*(***α***), ΔG^*(***β***') and ΔG^*(***β***)). The 'interaction' between these two Gibbs energies (driving

force vs. energy barrier) determines the actual polymorph that is formed when cooling at a given rate to a specific final temperature. In order to form a more stable polymorphic form like ***β***, a higher degree of undercooling below the ***β*** melting point is required; likewise, a lower degree of undercooling below the ***α*** melting point is enough to form the metastable form ***α*** (P. Rousset, 2002). Thus, the polymorphic forms obtained at the onset of a crystallization process are often not stable, eventually transforming into a more stable form.

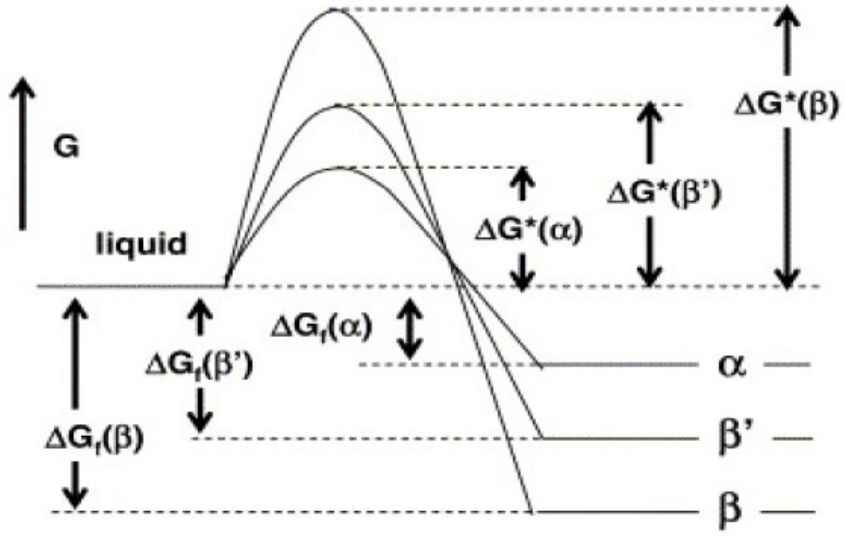

Figure 2-4. Gibbs energy diagram for the 3 main polymorphic forms of a TAG, at a specific temperature below their melting temperatures (P. Rousset, 2002).

The polymorphic transitions are monotropic, meaning that they always progress from a less stable to a more stable polymorphic form, in accordance with Ostwald's step rule (Wesdorp *et al.*, 2013). Figure 2-4 shows that a polymorphic transition within the solid phase may occur from ***α*** to ***β***' or from ***α*** to ***β*** directly. The increase in stability from ***β***' to ***β*** is a consequence of improvement in overall packing (Larsson, 1972). Some (e.g., Sato, 1993) have suggested that all polymorphic forms can perhaps be crystallized directly from a hypothetical liquid crystal structure, although this is still a matter of debate. Nonetheless, it seems clear that recrystallization of a more stable phase from the melting of a less stable phase can reduce the

total activation energy of polymorphic transition if the liquid retains some kind of organization (Sato, 1993).

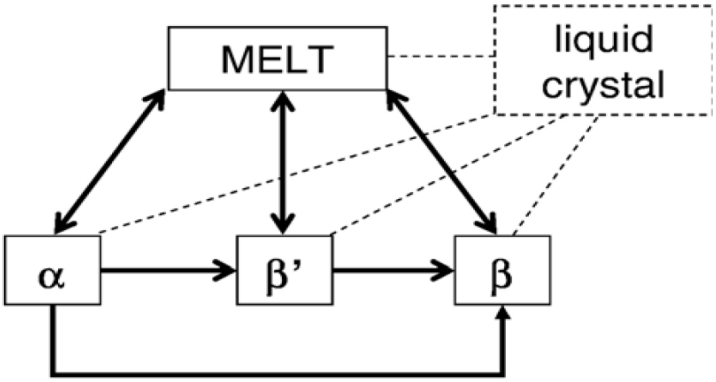

Figure 2-5. The monotropic transformation dynamics from the least to the most stable form in TAGs (Himawan *et al.*, 2006).

The $\beta' \rightarrow \beta$ transition is perhaps the most important one from an economic standpoint because it is associated with the swelling or bloom of saturated triacylglycerols in many food products such as chocolate, shortenings, spreads, and margarine. This phenomenon, often observed in foods that contain hydrogenated fats, is believed to occur due to rapid formation of the β form (K. Sato & Garti, 2001). Swelling can change appearance and texture, in turn causing substantial deterioration of market quality in products.

2.1.4 Liquid phase behavior

Study of the polymorphic crystalline structure of fats long predates any interest in their liquid state, and greatly informed initial ideas regarding the possible structure within the liquid phase (Larsson, 1972).

Several studies have demonstrated that lipids retain some degree of ordering in the liquid phase. To break the ordering, the temperature needs to be far enough above the melting point (Larsson, 1972; Kiyotaka Sato *et al.*, 1999). Below the melting point, the molecules in the liquid phase

are in a metastable state, and will spontaneously organize themselves into certain structures (liquid crystals) prior to the formation of actual crystals. This hypothetical liquid crystal structure may also explain "crystal memory", a phenomenon where fat tends to form the same crystal structure that it had as a solid before melting. It would also describe the ordering of the liquid phase at the beginning of crystallization (Hernqvist, 1984).

Despite theoretical constructs that attempt to describe their order, the actual structure of liquid TAGs remained unclear. Several hypotheses were proposed over the years. Larsson (1972) suggested the first model, which featured a smectic liquid crystal structure for liquid TAGs (Figure 2-6) and was formulated on the basis of X-ray diffraction (XRD) measurements.

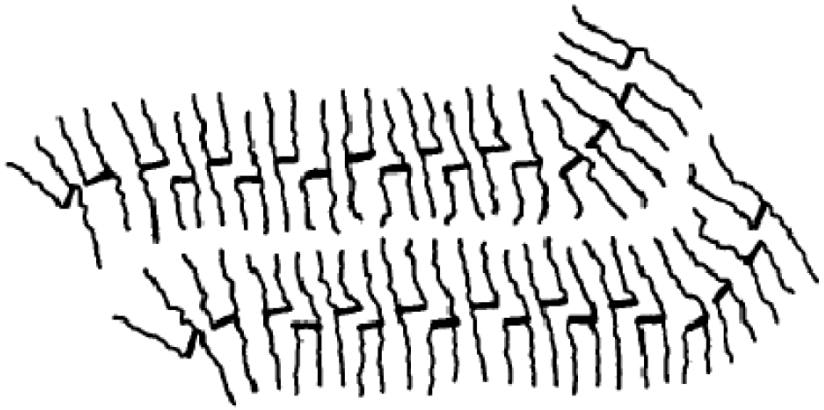

Figure 2-6. The smectic model proposed by Larsson for the structure of TAGs in the liquid state (Larsson, 1972).

Hernqvist (1984) supported Larsson's model and indicated that the order of different segments in the hydrocarbon chains varied with different chain length. The smectic model was also supported by Callaghan & Jolley (1977) through ^{13}C Nuclear Magnetic Resonance (NMR) measurements. However, Cebula, *et al*. (1992), performing SAXS (Small Angle X-ray

Scattering) experiments with desaturated trilaurin, questioned Larsson's model and claimed that a nematic phase of liquid crystals (Figure 2-7) was more consistent with their observations.

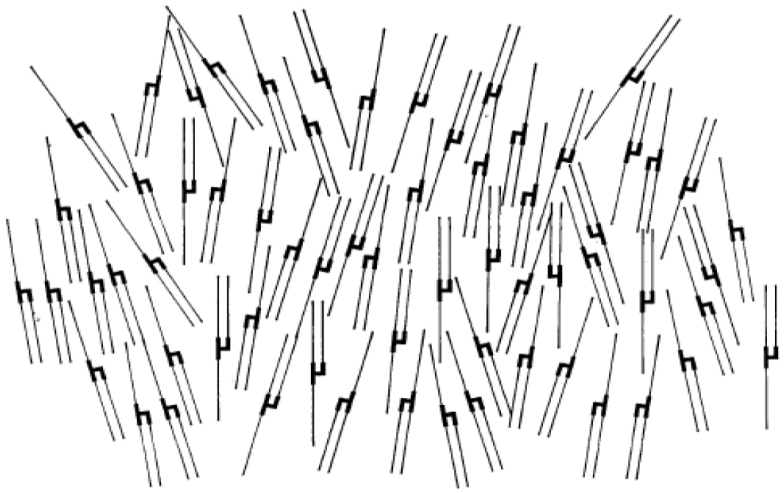

Figure 2-7.Proposed structure of TAGs in the liquid state, the nematic model proposed by Cebula *et al* (Cebula *et al*., 1992).

More recently, molecular modeling by Sum *et al.* (2003) supported the lamellar hypothesis. Later, an alternative discotic model was proposed by Corkery, *et al.* (2007), who suggested that triglyceride molecules exist in the liquid state with fully splayed chains ("Y" shape), forming disc structures (Figure 2-8). However, in a subsequent paper by one of the authors (Pink, 1873), it was shown that these discotic structures were very unlikely to exist.

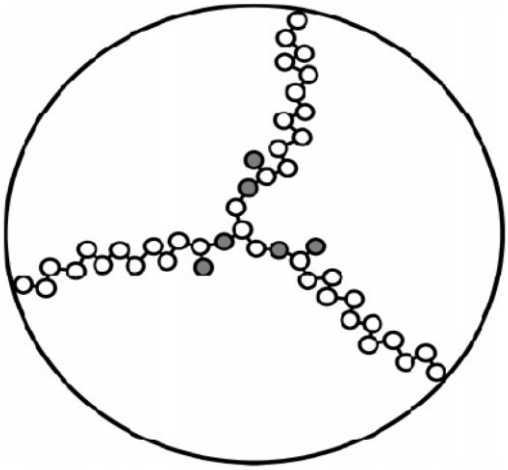

Figure 2-8. Proposed "Y" shaped structure of TAGs within each "disc" in the liquid state, the discotic model proposed by Cokery *et al.* (2007).

In the recent work of Lin (2014), it was noted that the TAG molecules should fill the space of the liquid in such way that the average density of the smaller entities is equal to the density of the bulk fluid, be these entities molecules or groups of attached molecules. The simplest space filling packing of monodisperse (single sized) solid spheres are the hexagonal close packing arrangement and the cubic close packing, but the actual space filling solids is the rhombic dodecahedra that circumscribe the spheres. If it is assumed that the TAG molecules are distributed individually in the liquid, the characteristic average distance between centers of each pair of molecules would be 1.285 nm, which much smaller than the distance measured between scattering centers in small angle x-ray scattering experiments, 2.448 nm.

Therefore, Lin (2014) developed a new conceptual model to describe the clustering of liquid TAGs as “Loose Multimers” based on the clustering suggested by Pink (2010).

It was assumed that the liquid TAGs are clustered together and arranged in such way that the cores are very close together, wrapped in the folded aliphatic chains. These entities were called “Loose Multimers”. The average volume occupied by a cluster corresponds then to that of a rhombic dodecahedron. They are loose because there is no strong chemical bonding between the

molecules in the unit, and molecules can be exchanged between units. Spatially speaking, it is also a flexible unit. It might not be as strict as the rhombic dodecahedron. In extreme cases, the TAG molecules might lie as cylinders and cluster in layers forming cross-like shapes. However, the forces between molecules and the exact shape still need further discussion and advanced simulations.

From the new conceptual model, Lin (2014) estimated that the clusters consist approximately of 5 to 9 molecules. The average number of molecules decreases with temperature and increases with molecular weight.

2.1.5 Liquid-Solid multicomponent equilibrium

The general concepts of thermodynamic equilibrium that are used for any multicomponent system can be, in principle, applied to solid-liquid equilibria as well.

As happens with any other multicomponent states, when the solid crystallizes, its composition is rarely the same as that of the liquid where it came from. Very often, the TAG with highest melting point will crystallize in a ratio that is larger than that it had in the liquid phase. This tends to produce a localized increase in the concentration of the TAG with lowest melting point. The balance of these two opposing trends is controlled by the rate at which the TAGs can move to the interface from the bulk of the liquid, compared to the rate at which the crystals are growing. It also depends on the distribution and rate of nucleation, that will be discussed in the next section.

The system of equations that would govern the equilibrium at the interface of a mixture can be written by considering that the chemical potential of each component in the liquid has to be equal to the chemical potential of that component in the solid phase. If there is more than one

solid phase, then the chemical potential for that component in all the phases has to be the same. Two different components will usually have different chemical potentials, though. For instance, in the hypothetical case of a slow enough equilibrium condition for a binary MMM-PPP blend, with T_m as the equilibrium temperature, the two equations are (Batchu, 2014; Marangoni & Wesdorp, 2012):

$$y_M = x_M \cdot \gamma_M \cdot \exp\left[\frac{\Delta H_M}{R}\left(\frac{1}{T_m} - \frac{1}{T_M}\right)\right]$$

$$1 - y_M = (1 - x_M) \cdot \gamma_P \cdot \exp\left[\frac{\Delta H_P}{R}\left(\frac{1}{T_m} - \frac{1}{T_P}\right)\right]$$

The mole fraction, y_M, of MMM in the liquid must be equal to the product of the mole fraction of MMM in the solid state, x_M, by an activity coefficient γ_M and an exponential temperature factor. This factor appears from the Gibbs energies of the solid and liquid states, once its derivatives (the chemical potential) are equated. Similarly, the mole fractions of PPP in the liquid and solid states, presented as (1- y_M) and (1- x_M), are related to its activity coefficient γ_P and its exponential temperature factor. The enthalpies ΔH_M and ΔH_P, and the melting temperatures T_M and T_P, correspond to the polymorphic form of the pure components that is the same as that of the solid solution crystal. The activity coefficients are often expressed as a function of the composition of the solid phase and a set of interaction parameters, that also correspond to the type of polymorph and the TAGs involved. There is very little experimental or theoretical information available on these parameters, or the activity coefficients of TAG mixtures.

Although the thermodynamics of liquid-solid multicomponent equilibrium are not different from, for instance, vapor-liquid, the immobilization of the molecules in the solid can introduce significant distortions of the concentrations that are present at the interface, with respect to the

bulk concentration of the solid.

On the other hand, the presence of discrete particles or large clusters of particles can introduce dramatic limitations in the mobility of the liquid as well. This is due to the formation of tortuous or closed channels.

These differences in mobility affect also the time that it takes for a mixture of diverse molecules to reach a uniform distribution by diffusion, once the concentration has been affected by crystallization.

2.1.6 Nucleation

Nuclei are the smallest stable crystals that form when a liquid is supersaturated. Supersaturation is the driving force for all solution crystallization processes. For a pure substance it is better expressed as undercooling, i.e. the difference in temperature between the melting point and the crystallization temperature. Often, the undercooling is also used to describe the crystallization of TAGs from a liquid mixture, or melt. Crystallization scientists gain control over crystallization processes and product quality by carefully controlling the prevailing level of supersaturation during these processes. In the case of TAGs, the nucleus formation requires the molecules from the liquid state to organize into crystalline lamellae. The arrangement of molecules depends on several factors like the cooling rate, the crystallization temperature, and the composition of the lipids (Metin & Hartel, 2005). For TAGs, a nucleus starts to form at measurable rates when the temperature of the melt is 5 to 10 C° below the melting point (Marangoni & Wesdorp, 2012). The higher the degree of undercooling, the higher the tendency to form a nucleus. At lower degrees of undercooling, the pre-nuclei called embryos are continuously formed and then broken due to the bombardment by liquid molecules of higher energy. Before nucleation, nonetheless, the average number and size of embryos increases with time, providing a growing

organization of the liquid molecules, until eventually the fat forms coherent, three-dimensional nuclei (Larsson, 1972). The size and number of crystals, and the polymorphic phases formed depend on the nucleation rate. Nucleation is, thus, the formation of a crystalline phase directly from the liquid state, and is the most important process in controlling crystallization.

The memory effect being studied in this Thesis is a return from the recently formed liquid to the solid state. It is clearly a process that is intimately related to the nucleation mechanisms.

Nucleation includes primary and secondary nucleation. Primary nucleation can be homogeneous or heterogeneous, whereas secondary nucleation occurs when crystals spawn new nuclei due to contacts between two crystals, or between a crystal and a surface such as a solid wall, or the stirrer (Herrera & Hartel, 2000).

Primary Nucleation

According to classic nucleation theory, a Gibbs energy barrier must be overcome to form a stable nucleus. This Gibbs energy change is positive for the formation of a nucleus. Once a nucleus has formed, there is an associated release of energy, from the latent heat proportional to its volume. This sum of energy change reaches a maximum value at a critical nucleus size. A stable nucleus can continue to grow beyond the critical size, whereas the smaller one dissolve into the liquid phase. In other words, the critical nucleus size is the minimum size for a stable nucleus (Timms, 1984; Walton, 1969).

Homogeneous nucleation normally happens in a system of a single type of molecule, where molecules come together and form dimers, and subsequently trimers by gathering additional molecules. This accumulation process continues until a stable nucleus forms. However, homogeneous nucleation rarely occurs, especially under commercial conditions due to the presence of foreign nucleation sites such as dirt, dust particles or rough surfaces.

The creation of a solid-liquid interface requires energy, leading to an increase in the Gibbs energy of the system; however, the creation of a nucleus also causes a decrease in the Gibbs energy of the system (Marangoni and Wesdorp, 2013). The balance of these two energies determines the critical size of a nucleus, and its mathematical expression is known as the Gibbs-Thomson equation (Turnbull & Fisher, 1949).

The equation is adapted here for a nanoplatelet of critical thickness ξ_c, width $a \cdot \xi_c$, and length $b \cdot \xi_c$:

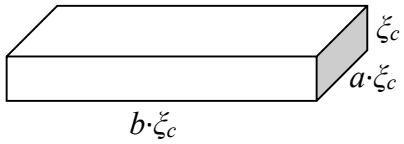

In this case, the geometrical factors for surface area A and volume V, called here g_s and g_v, are expressed as a function of the aspect ratio for width, a, and for length, b.

$$A = g_s \cdot \xi_c^2 \quad g_s = 2(a + b + b \cdot a)$$
$$V = g_v \cdot \xi_c^3 \quad g_v = b \cdot a$$

At a given temperature below the melting point, the size of a nucleus is determined by the balance between two Gibbs energies: the surface energy consumed (also known as surface tension) γ, in J/m^2, multiplied by the surface area created; and the energy of crystallization liberated, ΔG_m, in J/mol, multiplied by the moles of material crystallized.

$$\Delta G_c = \frac{V}{V_m^s}\Delta G_m - A\cdot\gamma_T \quad \Rightarrow \quad \Delta G_c = \frac{g_V\cdot\xi^3}{V_m^s}\Delta G_m - g_S\cdot\xi^2\cdot\gamma_T$$

$$\Delta G_m = \Delta H_m - T\cdot\Delta S_m = \Delta H_m - T\cdot\frac{\Delta H_m{}'}{T_m} = \Delta H_m\cdot\left(\frac{T_m - T}{T_m}\right)$$

$$\Delta G_c = \frac{g_V\cdot\xi^3}{V_m^s}\Delta H_m\cdot\left(\frac{T_m - T}{T_m}\right) - g_S\cdot\xi^2\cdot\gamma_T$$

$$\frac{\partial(\Delta G_c)}{\partial\xi} = \frac{3g_V}{V_m^s}\Delta H_m\cdot\left(\frac{T_m - T}{T_m}\right)\cdot\xi_c^2 - 2g_S\cdot\gamma_T\cdot\xi_c = 0 \quad \Rightarrow \quad \xi_c = \frac{2g_S\cdot V_m^s\cdot\gamma_T}{3g_V\cdot\Delta H_m}\left(\frac{T_m}{T_m - T}\right)$$

$$\xi_c = s_f\cdot\gamma_T\frac{V_m^s}{\Delta H_m}\left(\frac{T_m}{T_m - T}\right) \quad \therefore \quad s_f = \frac{2g_S}{3g_V}$$

$$\Delta G_c = s_g\cdot\gamma_T^3\left[\frac{V_m^s}{\Delta H_m}\left(\frac{T_m}{T_m - T}\right)\right]^2 \quad \therefore \quad s_g = s_f^2\left(g_S - g_V\cdot s_f\right)$$

When nucleation occurs from the melt in the absence of foreign particles, the rate of the nucleation (J), in nuclei per mol per second, depends on the activation Gibbs energy needed to develop a stable nucleus, ΔG_c, and the activation Gibbs energy for molecular diffusion, ΔG_D. The latter is associated with the work involved in the diffusion of molecules from the bulk toward the crystal interface. Since viscosity is a physical parameter inversely proportional to molecular diffusion, as supercooling increases, the viscosity of the liquid phase might become a limiting factor for nucleation or crystal growth. The Fisher-Turnbull equation (Turnbull & Fisher, 1949) describes the relationship of ΔG_c and ΔG_D with J through the following expression:

$$\boldsymbol{J = \left(\frac{N k_B T}{h}\right)\exp\left(\frac{-\Delta G_c}{k_B T}\right)\exp\left(\frac{-\Delta G_D}{k_B T}\right)}$$

N is the number of molecules per mole (Avogadro's number 6.022×10^{23}), k_B is the Boltzmann constant (1.38065×10^{-23} J/K), T is the crystallization temperature, in K, and h is Planck's constant (6.6261×10^{-34} J·s) (Widlak, Hartel, & Narine, 2001).

The Fisher-Turnbull expression for a situation where the diffusion does not play an important role ($\Delta G_D = 0$), as is the case with pure materials, can then be expressed as:

$$J_v = \left(\frac{N k_B T}{h V_m^s}\right) \exp\left(\frac{-s_g \cdot \gamma_T^3}{k_B T}\left[\frac{V_m^s}{\Delta H_m}\left(\frac{T_m}{T_m - T}\right)\right]^2\right)$$

Here the molar volume V^s_m is given in m^3/mol. The rate of nucleation, J_v, in nuclei per unit volume (m^3) per second, is inversely proportional to the induction time of crystallization (τ) in a given observation volume v_{obs}. This induction time should be the time it takes for the first nucleus to reach a critical size. It should be also the moment when the nucleus becomes detectable. However, the experimental limitations usually require some form of backwards extrapolation to estimate τ, because the early changes in the liquid material become detectable only after certain amount of nucleation and growth events have taken place.

$$J_v = \frac{\#_{obs}}{\tau \cdot v_{obs}}$$

Although the counting of $\#_{obs}$, the number of the first nuclei to appear simultaneously, can be difficult at low temperatures, this does not completely preclude the use of the estimates of the onset times. There is a transformation of the Fisher-Turnbull equation that can be used to linearize data of onset times. Since the observation volume is usually constant, it is assumed that the number of nuclei is also constant. The equation then can be treated as follows:

$$\ln(\tau \cdot T) \propto -\ln\left(\frac{N k_B}{h V_m^s}\right) + m_g \frac{1}{T(T_m - T)^2} \quad \therefore \quad m_g = \frac{s_g}{k_B}\left(\frac{V_m^s T_m}{\Delta H_m}\right)^2 \cdot \gamma_T^3$$

A plot with X = 1/ (T (T_m - T)) vs. Y = ln($\tau \cdot T$) will have a slope m_g, from which an approximate value of the interfacial tension γ_T can be estimated. This method has been used by several researchers, using a spherical nucleus model, to report values of γ_T for a variety of fats. The values of γ_T for TAGs depend on the polymorphism of the crystal that they refer to. For pure tripalmitin (Chumpitaz, Coutinho, & Meirelles, 1999) reported values between 2.8 and 2.9 mJ/m^2. Several natural fats and systems blended from modified natural fats have been studied. Examples report values of 3.7 mJ/m^2 for β' from hydrogenated palm oil in sunflower oil ((Kloek, Walstra, & van Vliet, 2000). For alkanes with C_n ~ 21-28 the values of γ_T are around 6.0 mJ/m^2 (Kraack, Deutsch, & Sirota, 2000).

It is clear that, to the extent that the Fisher-Turnbull expression applies to TAGs, temperature has a strong impact on the rate of nucleation, which happens in the liquid as soon as the temperature falls below the melting point of a given polymorphic form. This is a very important concept for this research.

As the temperature decreases, the nucleation frequency increases. The larger the frequency, the smaller the volume of liquid that each nucleus has the chance to seed. This happens because the rate of nucleation increases much faster than the growth rate with the decrease in temperature. As a consequence, increasing the cooling rate produces more nuclei, and therefore more crystals or crystal clusters. On the other hand, the crystals are smaller, because each nucleation center has less liquid available around it.

Secondary Nucleation

Secondary Nucleation is the process where new crystal nuclei form contacts with existing crystals or crystal fragments (Metin & Hartel, 2005). It normally proceeds once some primary homogeneous or heterogeneous nucleation has happened.

Secondary nucleation is affected by many parameters. They include the driving force of crystallization, temperature, foreign matter, agitation, the size and number of existing crystals, and the roughness of crystal surface. When the crystal slurry is agitated in a vessel, the crystals impinge on the vessel walls, other crystals and the stirrer. This may lead to fractures of the existing crystal structure and finally the formation of secondary nuclei (Metin & Hartel, 2005). Secondary nucleation may also occur when microscopic crystalline elements are separated from an existing crystal surface.

Like primary homogeneous and heterogeneous nucleation, secondary nucleation also depends on the crystallization driving force (supersaturation or subcooling). At higher supersaturation there are more stable nuclei being formed (Marangoni and Wesdorp, 2013).

2.1.7 Crystal Growth

Once nuclei have formed and reached the critical size, they grow by incorporating other TAG molecules from the liquid phase. The correct configuration and the correct location on the crystal surface are determinants of the binding into a lattice when a new TAG molecule migrates from the liquid phase to the existing nuclei (Marangoni & Wesdorp, 2013).

For crystal growth to take place, the TAG molecules must migrate from the liquid phase to the crystal surface. A growth unit, which is either an individual molecule or a cluster of molecules, migrates to the surface of the crystal until there is an appropriate site for incorporation into the

lattice. Crystal growth keeps going as long as the driving force for crystallization exists. There is a release of latent heat when the growth unit has been incorporated. This energy diffuses away from the growing surface and makes the temperature of the whole system increase if the system is isolated. When the whole system is either fully crystallized or has reached phase equilibrium, no further overall crystal growth can occur (Metin & Hartel, 2005). If the system is kept isothermal, the heat will be removed until the system reaches phase equilibrium.

The rate of crystal growth depends on several factors. They include the degree of undercooling, the structure of the crystal surface, the rate of the molecular diffusion to the crystal surface, the nature of the surface of crystal-melt and the difference between the rate of the attachment and the detachment of the molecules on the interface (Fisher & Kurz, 1992). The crystal growth is also affected by lipid composition, temperatures, and shear rates (Mazzanti *et al*., 2005).

Many successful theoretical models like the JMAEK (Avrami model) (Avrami, 1939, 1940, 1941; Erofe'ev, 1946; Johnson & Mehl, 1939; Kolmogorov, 1937), the Foubert model (Foubert *et al*., 2002) and the diffusion model (Mazzanti *et al*.,2009) have been developed to predict the growth rate of solid material from a multi-component TAG system, within the boundaries of a limited set of conditions. Solid content curves have been developed through experimentation for many natural fats like cocoa butter (Foubert *et al*., 2002), milk fat (Foubert *et al*., 2002; Mazzanti *et al.*, 2009) etc. Growth parameters were obtained by fitting these theoretical models into experimental data. For a particular set of processing conditions (cooling rate, shear rate, etc.,) the solid content at any point during crystallization bears a direct impact on the bulk physical properties like texture, spreadability, melting point, etc.

Nucleation is the birth of new crystal nuclei - either spontaneously from solution (primary nucleation) or in the presence of existing crystals (secondary nucleation). Crystal growth is the

increase in the size of crystals as solute is deposited from the solution or melt. These often competing mechanisms ultimately determine the final crystal size distribution - an important product attribute. The crystal size also affects several other characteristics, such as melting point, phase behavior and even the crystal memory effect.

The so-called “crystal-memory”, the very intriguing behavior of fats and other materials that is the subject of this thesis, is discussed after the following DSC introduction.

2.2 DSC Technique as Used in Fat Crystallization Studies

Methods for studying the polymorphism of fats include DSC, XRD, NMR, neutron diffraction, infrared absorption spectroscopy and PLM. All of them have been used extensively to study the crystallization and polymorphism of triacylglycerols and their mixtures in the past several decades (Sato, 2001). In this research, DSC is used as a tool to better understand the crystallization of pure triacylglycerols, given its ability to provide very precise temperature control to the sample.

Calorimetry is the primary technique to measure the thermal properties of materials and thereby establish a connection between temperature and specific physical properties of substances. It is the only method for direct determination of the enthalpy associated with the process of interest. Calorimeters are frequently used in chemistry, biochemistry, cell biology, biotechnology, pharmacology and recently, in nanoscience to measure thermodynamic properties of the biomolecules and nano materials.

DSCs allow precise and quick measurement of reaction heats, heats of transition, or heat flow rates and their changes at characteristic temperatures, even on small sample masses (milligram range; in the case of classic calorimeters: gram range). They also allow measurement in very

wide temperature ranges with high accuracy. During a change in temperature, a heat-flux DSC estimates the heat lost or gained by the sample, per unit time. The heat flow is computed from the temperature difference measured between the sample and a reference material.

2.2.1 Definition and basic principles of heat flux Differential Scanning Calorimetry

Based on the mechanism of operation, DSCs can be classified into two types: heat-flux DSCs and power-compensation DSCs. They differ in their design and measuring principle. The instrument used in this research is a heat-flux DSC. In a heat-flux DSC, the sample material is enclosed in a pan and is placed on a thermoelectric disk that is surrounded by a furnace. An empty pan is placed on an adjacent symmetric thermoelectric disk in the same furnace.

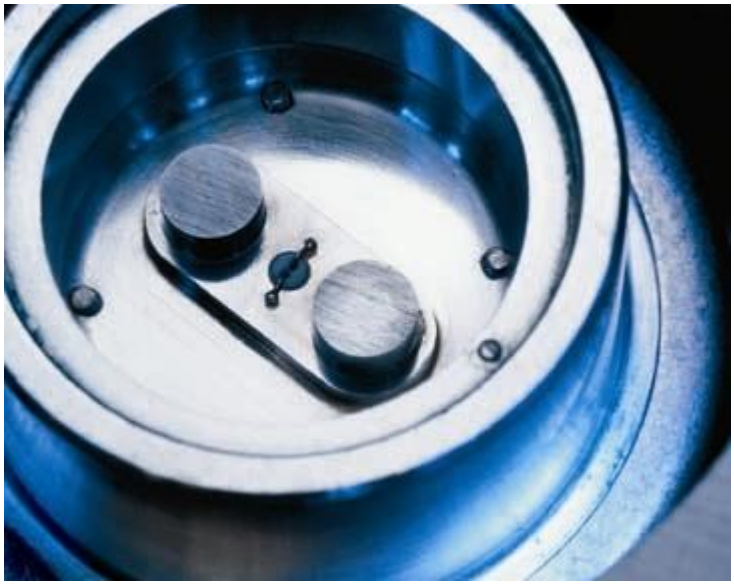

Figure 2-9.The measuring cell for DSC Q100.

As the furnace is heated at a constant rate, heat is transferred to the sample and reference pan through the thermoelectric disk. However, depending on the heat capacity (c_p), thermal conductivity (k) and mass of the sample pan, there will be a temperature difference between the sample and reference pans. This temperature difference is measured by the area thermocouples.

The heat flow is the estimated by the thermal equivalent of Ohm's laws applied to an electrical network:

$$q = \Delta T / R \quad (2)$$

Where q is "sample heat flow", ΔT is "temperature difference between sample and reference", and R is "resistance of the thermoelectric disk".

DSC has been the most commonly used method in oil and fat characterization to determine melting and crystallization profiles, heat capacity, phase diagrams and even solid fat content. DSC is known for its sensitivity, and rapid and reproducible measurements are usually obtained. However, careful interpretation is paramount. Several peaks, which reflect the presence of different thermal transitions, are observed upon heating or cooling of samples, when calorimetry is used in the thermal investigation of fats (Loisel *et al*., 1998). When different cooling and heating rates are employed, different phase transition behaviors will readily be observed on DSC traces (Hagemann & Rothfus, 1993).

The two common approaches to determine transformation kinetics are isothermal and non-isothermal methods. In isothermal experiments, the sample is quickly brought to a predetermined temperature where thermal analysis instrument monitors the heat flow of the system at the constant temperature as the function of time. The other approach uses a temperature ramp (Foubert *et al*., 2003).

The time-temperature program used in most investigations includes four stages: In the first stage, the sample is heated to a higher temperature and is kept at that temperature for enough time to destroy all crystal nuclei. During the second stage, the sample is cooled at a specified cooling rate to a target crystallization temperature. In the third stage the sample is kept isothermal until

crystallization is complete. The final stage is often a destructive test, consisting of heating the sample at a relatively high rate, to observe the trace produced by the material that crystallized during the isothermal stage.

2.2.2 Heat Capacity and Enthalpy Measured by DSC

Integration of DSC curves

In cases where the enthalpy of crystallization is well known, the relative amount of material crystallized as a function of time is calculated by integration of the isothermal DSC curves. The area enclosed between a baseline and the exothermal peak corresponds to the heat of crystallization, ΔH_m. The fraction of crystallized material F at a given time t is approximated by the ratio of the integration of the exothermal rate to the total area in accordance with the following equation (Kawamura, 1979):

$$F = \frac{\int_{t=0}^{t} \frac{d\Delta H(t)}{dt} dt}{\Delta H} \tag{3}$$

It was shown by Foubert, Vanrolleghem, and Dewettinck, that when the start and end point of the integration are determined visually, the resulting area and thus the model parameters vary when different persons perform the integration but also when the same person perform the integration several times.

Figure 2-10 shows a typical DSC thermogram. The heat capacity of the sample is calculated from the shift in the baseline at the starting transient. Glass transitions cause a baseline shift. DSC allows to precisely control the temperature during the heating or cooling of the samples and measure small changes of energy. From the point of view of the calorimeter, these changes

of energy can be visualized as exothermic peaks for fusion, and endothermic peaks for crystallization events.

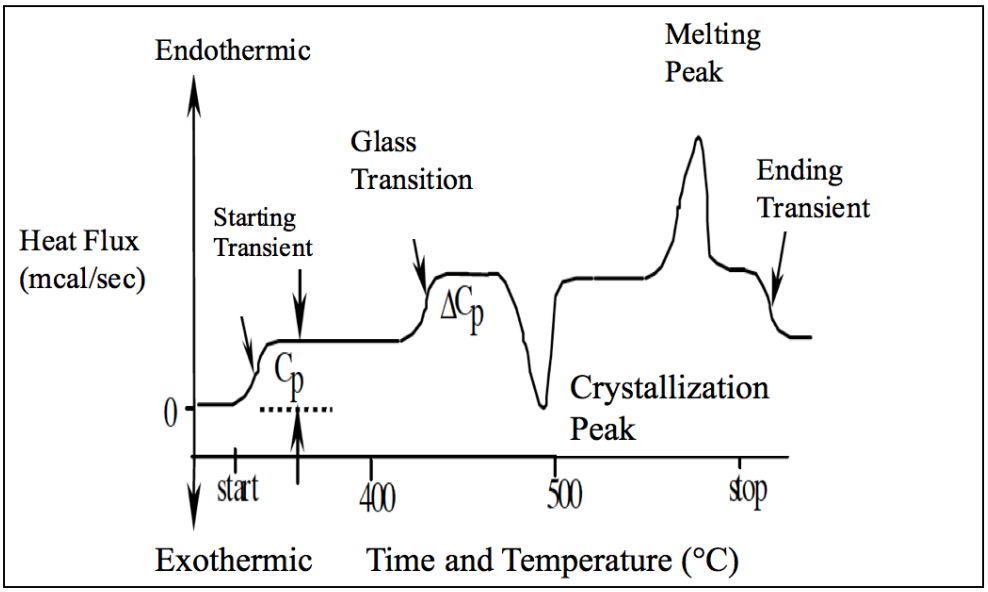

Figure 2-10. Typical DSC scanning process (Thomas, 2005).

DSC provides a convenient and moderately accurate method of measuring heat capacities and enthalpy changes. Commercial instruments provide a recorded output of the constant-pressure heat capacity,

$$c_p = \left(\frac{dq}{dT}\right)_p = \left(\frac{\partial H}{\partial T}\right)_P \tag{4}$$

where $\partial H/\partial T$ is the shift in the baseline of the thermogram, shown in Figure 2-10.

The integral under the DSC peak, above the baseline, gives the total enthalpy change for the process:

$$\Delta H = \int_{T_1}^{T_2} \left(\frac{\partial H}{\partial T}\right)_P dT = \int_{T_1}^{T_2} c_P \, dT \tag{5}$$

Table 2-3 Enthalpy of fusion (kJ/mol; J/g) of the pure triacylglycerols MMM, PPP, SSS at their melting temperatures (Timms, 1978).

	α		*β'*		*β*	
	kJ/mol	*J/g*	*kJ/mol*	*J/g*	*kJ/mol*	*J/g*
MMM	81.9	113.25	106.0	146.58	146.8	203.0
PPP	95.8	118.65	126.5	156.67	171.3	212.15
SSS	108.5	121.71	156.5	175.55	194.2	217.84

2.3 Crystal Memory

It is widely recognized that lipids retain some degree of ordering in the liquid phase, with temperatures well above the melting point needed to fully disrupt this ordering. When melting fats, this liquid ordering is termed the "crystalline memory" effect, where subsequent re-cooling leads to formation of a different (usually more stable) phase than would occur if the fat was heated to higher temperatures to destroy the liquid memory (Metin & Hartel, 2005).

"Crystal memory", also called "memory effect" is a very interesting phenomenon in lipid crystallization. Since most of the research about "crystal memory" was initially done on cocoa butter, it was defined as the influence of the thermal history of cocoa butter on its phase behavior. A more detailed explanation for this effect is that when fats are melted, they tend to retain, or "remember", the compositional and nano-structural organization they had when they were crystalline. Upon re-crystallization, this often produces crystalline structures with undesirable end qualities. This phenomenon is known as crystal memory.

2.3.1 Published research

So far, consistent physical rules describing crystal memory have not been established: for a given fat, it is still hard to tell under which conditions of time and temperature it will persist or be erased. Hernqvist and Larsson (1984) suggested that fat should be heated at least 30 °C above its melting point to avoid any influence of structural "memories" on crystallization. They attribute these memories to partly ordered laminar structures in the liquid that originate from the solid that existed before melting. In accordance with this opinion, it has been a common practice to heat cocoa butter to rather higher temperatures to melt all crystalline remnants. However, seeding experiments of Hachiya *et al* (1989) showed that the seeding effect of nuclei on dynamic crystallization depends strongly on the similarity in polymorphic behavior between seeding crystallites and liquid mass (cocoa butter). The seeding effectiveness of high-melting nuclei of tri-saturated TAG turned out to be much less than that of SOS (1,3-distearoyl, 2-oleoyl-sn - glycerol), BOB (1,3-behenoyl-2-snoleoyl-glycerol), or ***β***-cocoa butter. Therefore, it can be expected that to eliminate memory effects, the temperature needs to be raised only slightly above the melting point. This however, has not become common practice.

The most common way to erase crystal memory is to heat a sample to a high enough temperature and for a long enough time. Several researchers report protocols to erase any memory effect at the beginning of their experiments, such as heating chocolate to 50 °C for 2 h (Svanberg *et al.,* 2013); melting anhydrous milk fat to 80 °C for 30 min (Campos & Marangoni, 2002); or heating refined, bleached & deodorized coconut oil to 80 °C for 10 min to erase crystal memory (Chaleepa *et al.,*2010). The list is far too long to include it here. Frequently the determination of the specific time and temperature is done by trial and error, but in most cases no reason is given for the choice of temperature-time combination selected.

Only a few researchers have tried to define the boundaries of this effect, mostly for the processing of cocoa butter or chocolate, where the memory tends to have a critical impact on the final product quality. A presentation from van Malssen (van Malssen & Smith, 2001) showed that if cocoa butter in the β phase is melted (no visible solid), but remains below 40 °C, it maintains a "memory" of the crystal structure. On subsequent cooling, the crystallization speed of the β phase is increased, apparently re-forming from the melt. This temperature of 40 °C applies irrespective of the origin and composition of the natural cocoa butter. That is, whether the cocoa butter has a melting point of 32 °C or 36 °C, the memory effect for both is lost at 40 °C but not below. From these results, van Malssen gave a short definition for "memory effect": a special type of seeding, or rather of having the right nuclei for fast crystallization, is the memory effect.

Another study by van Malssen (van Malssen *et al.,* 1996) used cocoa butter with fast and slow recrystallization experiments using X-ray powder diffraction, aiming to find the relationship between β memory effect and composition. He subdivided the memory effect into short-term memory effect (memory effect from the fast recrystallization process) and long-term memory effect (memory effect from the slow recrystallization process). The results of this experiment indicated that at least for cocoa butter, even a very small percentage of "β components" in cocoa butter is sufficient to result in a complete β-solidification of the cocoa butter sample.

Foubert (Foubert *et al.,* 2003) also performed three different crystallization experiments with cocoa butter at different time-temperature combinations (65 °C for 15 min, 65 °C for 30 min and 80 °C for 15 min). They found out that holding cocoa butter at 65 °C for 15 min is sufficient to eliminate any evidence of sample history. However, the three protocols that were suggested still can't give a sense of the boundaries in eliminating memory effect.

Rousset (Rousset & Rappaz, 1997) studied the memory effect with two different crystallization processes: "direct crystallization" and the "***α*** melt-mediated crystallization" (Figure 2-11). The liquid -solid transformation was much faster in the "***α*** melt-mediated crystallization" process than under the "direct crystallization" procedure. In direct crystallization, quite large spherulites (average size about 50 μm) were observed, whereas the microstructure obtained during the ***α*** melt-mediated crystallization was fine and the grain size could hardly be estimated (lower than 5-10 μm). In conclusion, if the first plateau is sufficiently long for ***α*** to form, it seems that some structure of ***α*** remains in the melt at the beginning of the second plateau ("memory effect") and that some ***α*** embryos retransform into ***δ*** (the structure formed in previous crystallization), which will dramatically accelerate the formation of ***δ*** nuclei.

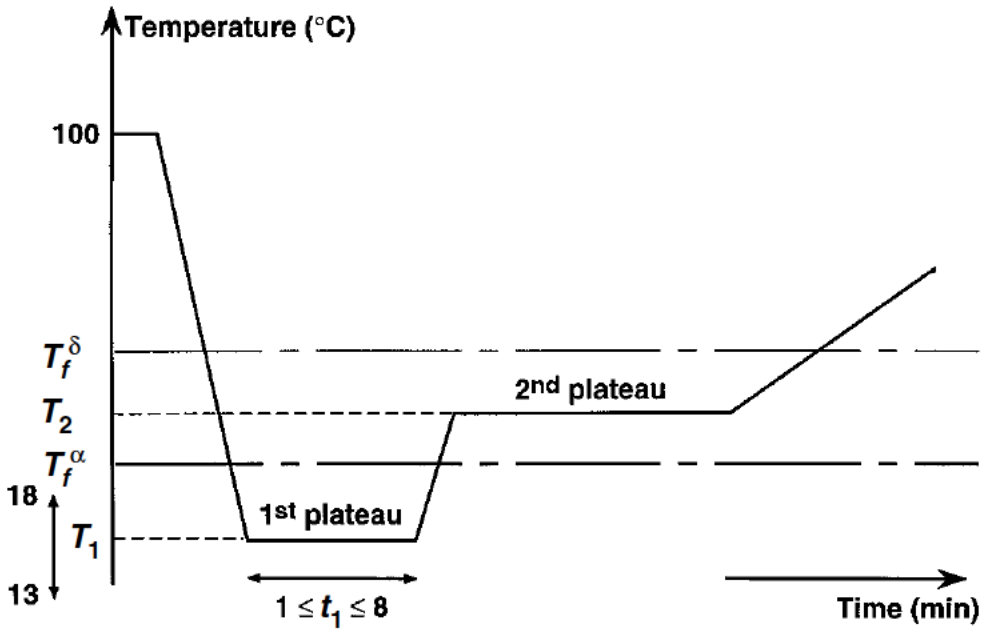

Figure 2-11. Temperature path used for the ***α*** melt-mediated crystallization of POS (P. Rousset, 2002).

However, there has been practically no research on the memory effect of simple pure triacylglycerols or binary mixtures, to define better the underlying mechanisms. That is why in

this research we are trying to find the temperature-time boundaries for the three different pure triacylglycerols MMM, PPP, SSS and two of their binary mixtures 5M5P and 5P5S by using DSC Q100.

2.3.2 Unpublished research of Léa Arnaud

Near the completion of the experimental phase of this thesis, we were made aware of an unpublished work that had been conducted in this area. This was the internship report "Demonstration of a memory effect during the crystallization of tricaprylin, tristearin and trilaurin by DSC", produced by Mlle. Léa Arnaud, supervised by Dr. Derick Rousseau and Dr. Supratim Gosh, at Ryerson University in 2009. The original report, kindly provided by Dr. Rousseau, was written in French, and was freely translated and edited by Dr. Mazzanti. This section presents some aspects of that report, though a more detailed discussion is deferred to Chapter 4.

Crystallization of triacylglycerols was studied as a function of temperature at which they have previously melted. If all the factors that influence crystallization are constant, the crystallization curve should be similar, and it would not matter if the triglyceride was heated slightly or strongly above its melting point. This report attempts to show that triacylglycerols can keep a conformation in the liquid beyond their melting point, which would favor their future recrystallization. This study was done by using the DSC on three pure triacylglycerols: tristearin (C18), trilaurin (C12), and tricaprylin (C8).

Table 2-4. Main data concerning triacylglycerols used, melting points are given for a rate of heating and melting of 1 C˚/min.

	Tristearin	Trilaurin	Tricaprylin
Number of carbon by fatty acid	18	12	8
Polymorph β	72.4˚C	46.5˚C	11˚C
Polymorph β'	65.3˚C	40˚C	β'_2= -12 et β'_1= -19 (*)
Polymorph α	54.9˚C	14˚C	-54 (*)

This study was focused on the effect of temperature and time.

For the first experiment, temperature was changed by heating by an extra 1 C° above its melting point each cycle, with heating rate as 1 C°/min, then cooled down to 10 °C at 1 C° /min as well. The time was constant during this method, as heating was also done with a 10 C° /min rate.

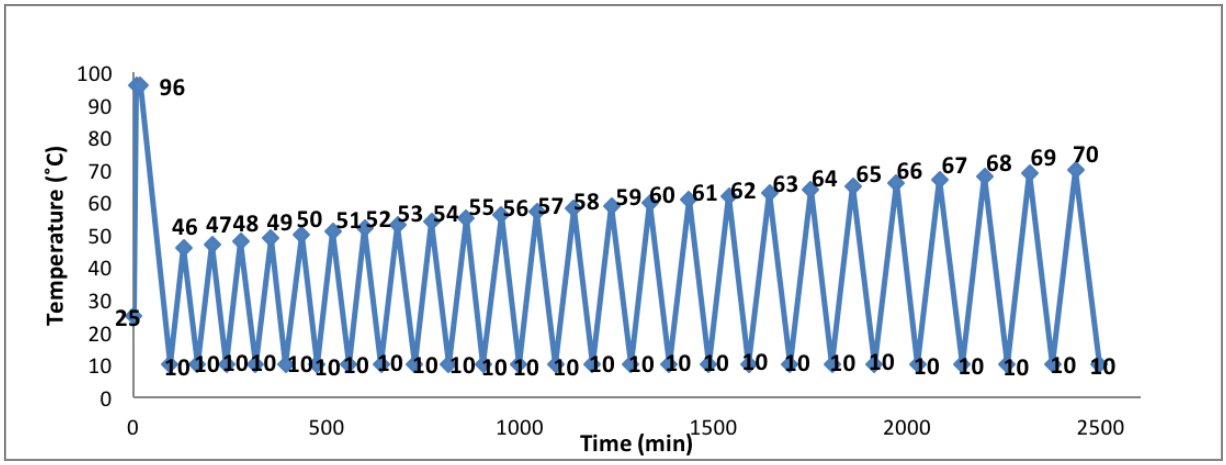

Figure 2-12. Program used to characterize the memory effect of trilaurin (LLL).

The second experiment, conducted on LLL, was used to study the effect that the time spent beyond its melting point has on the recrystallization temperature. The temperature of the liquid was kept constant beyond the melting point (i.e. 50 °C for the LLL when the rate of heating is 10 C°/min) whereas the time at 50 °C varied. The crystallization curves were then compared to see if the time at 50 °C influenced the recrystallization temperature.

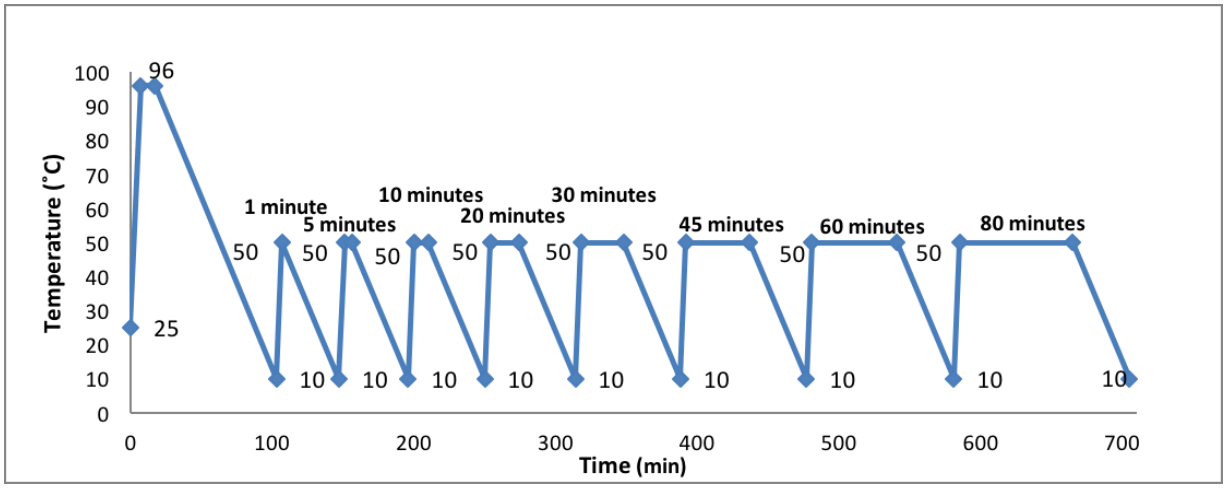

Figure 2-13. Program used to study the effect of the kinetics on the memory effect.

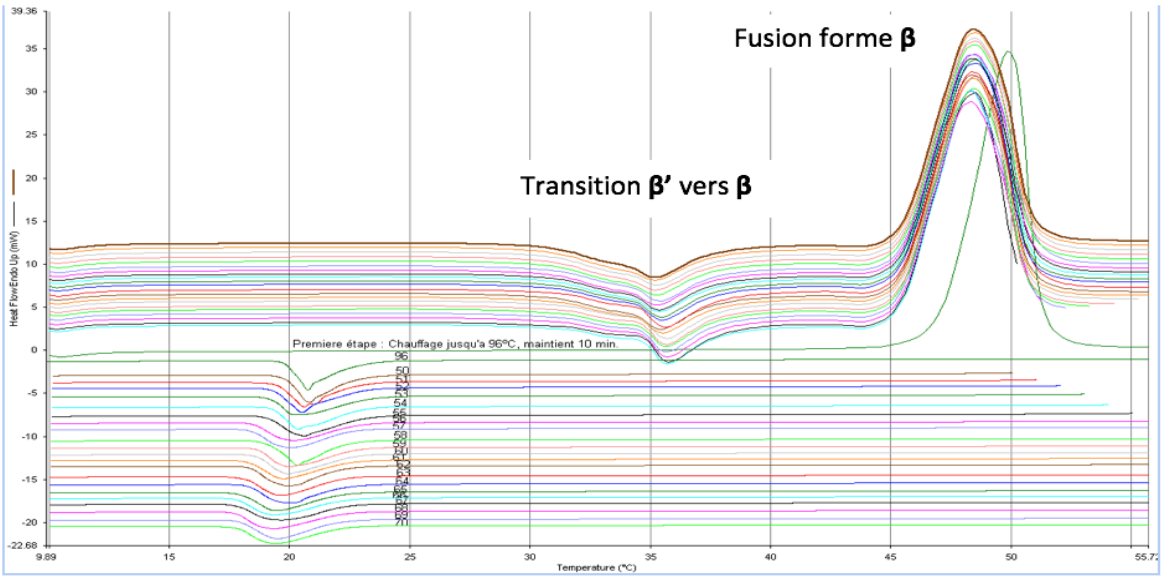

Figure 2-14. Thermograms of crystallization and melting curves obtained for LLL, method 2.

The same methods were used with SSS and CCC. There was one more method applied to CCC to find the effect of sample weight. As shown from the results, for LLL and SSS, a crystal memory effect may persist beyond the melting point. This effect is manifested only in a very small onset change, a few tenths of a degree. The case of CCC requires further study.

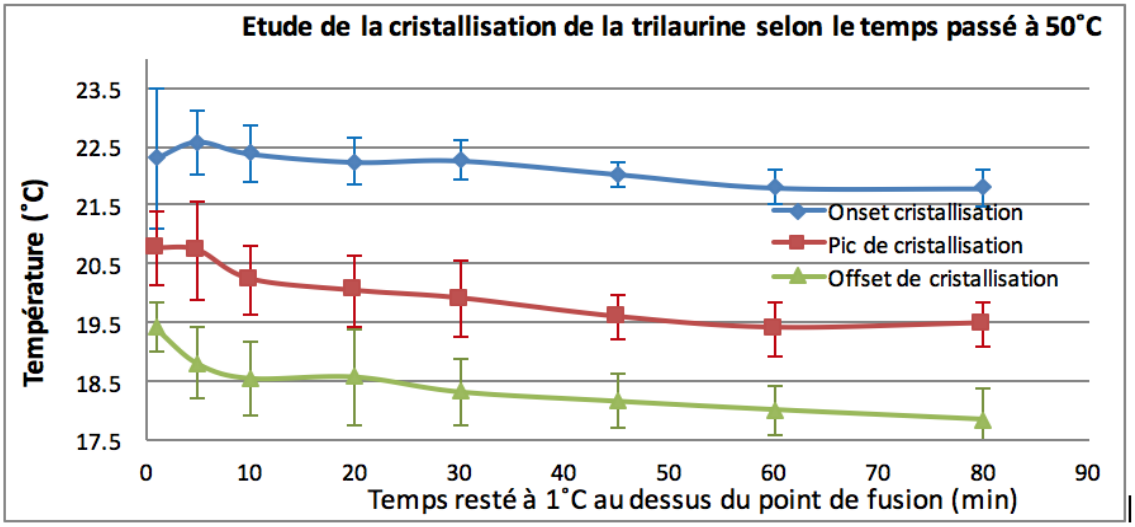

Figure 2-15. Onset, peak, and offset of crystallization of the LLL according to the time spent to 50 °C.

As a conclusion, for LLL they observed a kinetic effect: the time spent beyond the melting point decreases the crystallization temperature. This kinetic effect was also weakly present in SSS. The major difference between these two triacylglycerols is that LLL crystallized initially in the β form, whereas SSS crystallized in the ***α*** form. The ***β***-form may be more sensitive to the kinetic effect than the ***α***-form. This is certainly due to the energy of activation needed for crystallization. In fact, the most stable form, ***β***, requires high activation energy. The ***α*** form, which is the least stable, requires only very little activation energy. The ***β***-form would be more sensitive than the ***α*** form to the persistence of "crystals in solution" favoring its crystallization. Actually the crystallization of α is easy and would be less favored by a persistence of organization in the liquid state in the ***β*** form. Lowering the large energy of activation needed for the crystallization in the ***β***-form would be a most visible memory effect.

CHAPTER 3. EXPERIMENTAL METHODS AND MATERIALS

3.1 Materials

3.1.1 Pure triacylglycerols:

The following triacylglycerols were purchased from Sigma-Aldrich: MMM, (CAS # 555-45-3), PPP, (CAS # 555-44-2) and SSS (CAS # 555-43-1). Each had a purity of at least 99%, as determined by gas chromatography (GC); no further purification was performed.

3.1.2 Mixtures of pure triacylglycerols:

Two binary mixtures (dry blends) were prepared by combining the weighted materials in powder form and subsequently mixing them via melting. The ratios on a weight per weight basis were 50:50%. The blend MMM: PPP was abbreviated as 5M5P, and the blend PPP: SSS was abbreviated as 5P5S, following the naming convention used for many other blends in our lab. Two pans, each with 4 to 7 mg of material, were prepared for each sample for study and three repeating tests were done for each pan in the onset experiments. The weight of material in each pan is reported in Table 3-1.

Table 3-1. Weight of material in each pan, in mg. Two pans were prepared for each material.

Sample	MMM	PPP	SSS	5M5P	5P5S
Sample pan_1 weight (mg)	5.270	5.264	4.603	6.567	4.054
Sample pan_2 weight (mg)	5.132	6.131	4.819	5.355	4.463

3.2 Instruments and Methods

3.2.1 Differential Scanning Calorimetry (DSC)

Differential scanning calorimetry (DSC) determines the heat flow associated with thermal events in a material as a function of temperature and/or time. These events are seen as either exothermic peaks (e.g., heat evolution during crystallization), endothermic peaks (e.g., heat absorption during melting), or as shifts in the baseline (change in the heat capacity). The versatility of DSC makes it useful in investigations that involve melting and boiling points, crystallization time and temperature, heats of fusion and reactions, specific heat capacity, glass transitions, and purity.

All experiments were performed with a DSC Q100 V9.4 Build 287, Standard Cell FC (TA Instruments Q100, New Castle, DE, US) connected to a Microsoft Windows-based computer system. The machine is equipped with a two-stage refrigerated cooling system (RCS) and can perform modulated DSC (MDSC®) (Figure 3-1). The furnace is gray in color and has an auto-lid. The instrument is connected to two gas cylinders, one for nitrogen and the other for clean compressed air. The software Q Series™ Explorer Windows, provided by TA Instruments, was used for setting up the instrument, and for viewing and controlling the experiments. For record keeping and mass-normalized computations, information about the sample is entered into the software that controls the DSC, including sample name, sample weight, operator's notes, and other miscellaneous details.

Figure 3-1. TA Instruments heat flux DSC Q100 equipped with modulated DSC connected to a refrigerated cooling system, RCS (Al-Qatami, 2011).

When the temperature of the furnace in Figure 3-2 is raised or lowered in a linear fashion, the resulting differential heat flow between the sample and the reference is monitored indirectly by chromel-constantan Type-E area thermocouples fixed to the underside of the disk platforms. These thermocouples are connected in series and measure the temperature difference ΔT. From this temperature difference, heat flow is estimated using the thermal equivalent of Ohm's Law, summarized as:

$$\frac{dq}{dt} = \frac{\Delta T}{R_D} \tag{6}$$

where dq/dt is heat flow, ΔT is the temperature difference between the reference and the sample thermocouples, and R_D is the overall thermal resistance between these thermocouple disks. This

simple relationship, however, does not take into account extraneous heat flow within the sensor or between the sensor and the sample pan. The TA Instruments Q Series DSCs is specifically designed to account for those latter heat flows, as explained below.

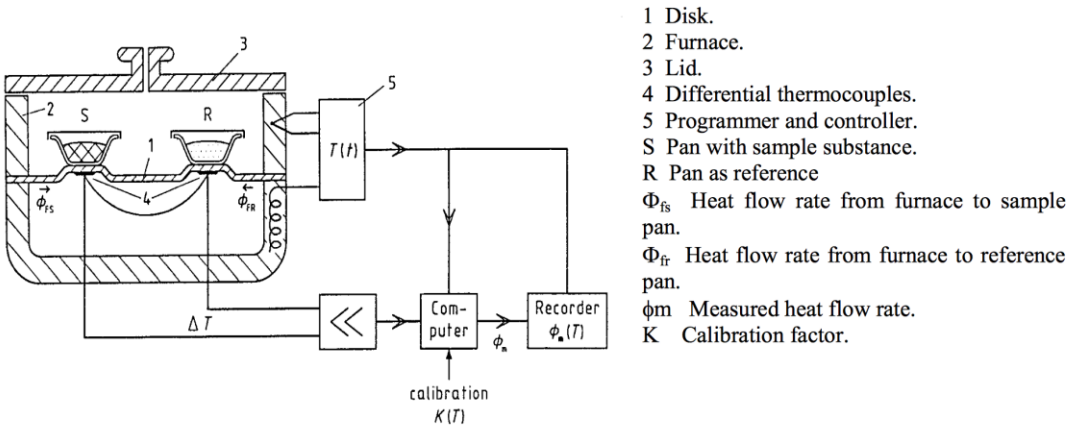

1 Disk.
2 Furnace.
3 Lid.
4 Differential thermocouples.
5 Programmer and controller.
S Pan with sample substance.
R Pan as reference
Φ_{fs} Heat flow rate from furnace to sample pan.
Φ_{fr} Heat flow rate from furnace to reference pan.
ϕm Measured heat flow rate.
K Calibration factor.

Figure 3-2. Scheme of a heat flux DSC system (Danley, 2003).

The cell sensor consists of a constantan body with separate raised platforms to hold the sample and reference. The platforms are connected to the heating block (base) by thin-walled tubes that create thermal resistances between the platforms and the base. Chromel area detectors (thermocouples) on the underside of each platform measure the temperature difference between the sample and reference, as shown in Figure 3-3. A third thermocouple measures the temperature at the base. The equation below shows the expanded thermal network model that represents this cell arrangement, and the resultant heat flow expression that describes it (designated the T_o [Tzero™ cell] method):

$$\frac{dq}{dt} = -\frac{\Delta T}{R_r} + \Delta T_0 \left(\frac{1}{R_S} - \frac{1}{R_r}\right) + (C_r - C_s)\frac{dT_s}{dt} - C_r\frac{d\Delta T}{dt} \qquad (7)$$

where:

dq/dt = differential heat flow rate (mW)

ΔT = temperature difference between the sample and reference sensors (C°)

ΔT_0 = temperature difference between sample sensor and Tzero™ thermocouple (C°)

R_r = thermal resistance (C°/mW) of the reference sensor

R_s = thermal resistance (C°/mW) of the sample sensor

C_r = heat capacitance (mJ/C°) of the reference sensor

C_s = heat capacitance (mJ/C°) of the sample sensor

dT/dt = heating rate of sample sensor (C°/s)

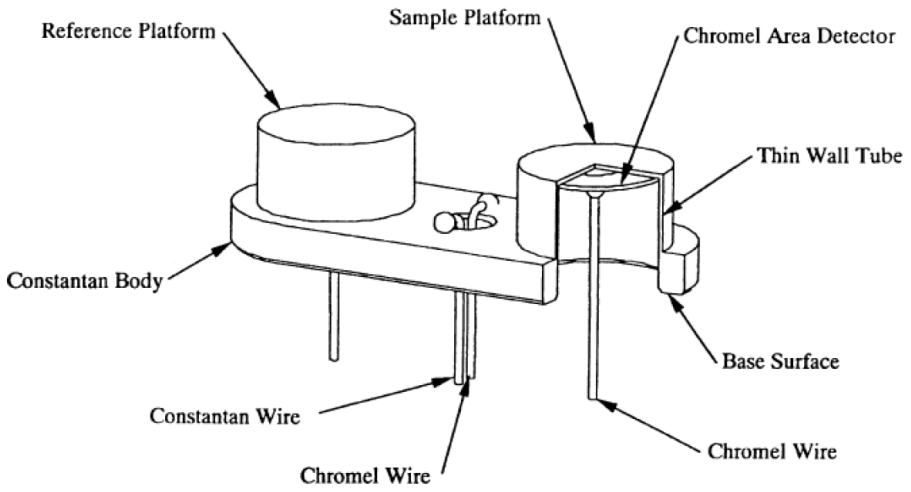

Figure 3-3. DSC Q100 sensor assembled with Tzero™ technology (Danley, 2007). The chromel-constantan pair forms a Type-E thermocouple.

Calibration

Any contaminants left in the cell from previous experiments would distort the DSC traces. Therefore, before calibrating the DSC, the cleanness of the DSC cell, including its two sensors, needed to be confirmed. In order to do so, a cyclic empty cell run was performed (no sample or

reference containers) from -60 to 200 °C at 20 C°/min, with any deviations from the normal trace indicating contamination. A fiberglass brush included in the accessory kit was used to wipe and clean the instrument. The test cycle was then repeated and, if further cleaning is necessary, a burn-up step was done using dry air and high temperature (usually 550 °C for 5 min).

Calorimetric measurements usually drift further from zero-baseline during the first run than they do for subsequent runs under the same conditions. This effect is called the "first run effect". To nullify this effect, a pre-test cycle was done, as recommended by the TA instruments support team. This pre-test cycle is considered a critical step in terms of obtaining a smooth baseline before the calibration process (Al-Qatami, 2011).

After finishing the pre-test cycle, the instrument was calibrated in three steps:

1. Using the "calibration wizard" with the T4 heat flow option with empty cell: cell resistance and capacitance, cell constant and temperature calibration were selected. The T4 heat flow compensates for subtle differences in thermal resistance and capacitance between the reference and sample sensors in the DSC cell. That is, it corrects for the slight asymmetry between the reference and sample sensors.

2. Two sapphire discs with similar masses (provided by the instrument manufacturer) were used to determine R and C values as a function of temperature, for the reference and sample sensors in equation (6). The first two runs were done through the same temperature range using a heating rate of 20 C°/min.

3. Indium was run as a standard with known enthalpy and melting temperature in order to determine the cell constant and the temperature calibration. Indium or other metals are used because they provide a sharp, well-defined melting peak. The cell constant is a correction factor for the heat flow, calculated by dividing the theoretical enthalpy value

of indium by the one measured during the calibration process. The temperature calibration can be done with more than one point, but in this case it was done only with indium. Thus, only a constant term (offset) is used in the temperature calibration (Al-Qatami, 2011).

3.2.2 Sample preparation

The sample mixtures were melted in a 20 mL glass vial at 100 °C using a hot water bath (Cole-Parmer, USA) for ten minutes to ensure that the samples were totally melted and mixed. This step is not necessary for pure samples, since they do not have compositional gradients.

An empty hermetic aluminum pan and lid (TA Instruments, Newcastle, DE, US) were selected and weighed as a reference pan, and other pan-plus-lid sets were selected to fall within the range of the reference pan weight ± 0.05 mg. Clean tweezers were used for all operations in order to avoid any contamination. Weights were measured using a microbalance (Cahn Instruments, C-33 Microbalance Model Number 13633-013, US) with a precision of ≤ 0.001 mg. All the pans and lids were then immersed in acetone for cleaning and left to air dry. Each clean and dry pan-plus-lid set was weighed. Approximately 5 to 10 mg of melted sample was then transferred to the pan using disposable capillary tubes with a wire plunger (Drummond Scientific Company, Wiretrol® II, US, 5 μL and l0 μL). Then the pan and its lid were hermetically crimped using a TA Instruments blue crimping press. The crimped pan was weighed again. The weight of the sample was calculated as the difference between the pan with and without the sample. Each crimped pan was stored in an Eppendorf 1 mL plastic vial that was labeled to indicate the type of sample and its net weight. The empty reference pan was also kept in a labeled Eppendorf vial. The vials were kept in a plastic organizing block.

3.2.3 Experimental Procedures

Prior to each experimental batch, a conditioning cycle was performed with an empty cell by heating and cooling the system between the highest and the lowest temperature settings (- 60 °C to 250 °C) three times at 20 C°/min. The sample and reference pans were then loaded into the cell, and the sample information (sample name, sample weight, saved file name, etc.) was entered into the program. The procedure to be executed by the DSC was then programmed into the software according to the temperatures and times required for each type of sample.

To facilitate understanding and discussion of the procedures and experiments, the constant temperature plateaus have been designated with letters, whereas the cooling or heating ramps have been designated with numbers. As an example, the following list shows the designations for complete experiment with MMM samples; this experiment is illustrated in Figure 3-4.

ⓐ First isothermal step, keeping the sample at a high temperature for 10 min.

① First cooling ramp to 5 °C at 20 C°/min.

ⓑ Second isothermal step, 5 min isothermal plateau at 5 °C.

② Heating ramp at 15 C°/min to a temperature above the melting temperature of $\boldsymbol{\alpha}$.

ⓒ Third isothermal period for 10 min at that temperature.

③ Cooling ramp from the previous temperature to 5 °C at 15 C°/min.

ⓓ Fourth isothermal plateau at 5 °C for 5 min.

④ Heating ramp at 15 C°/min to the holding temperature, in search for the memory effect.

ⓔ Isothermal plateau at the **holding temperature** for the duration of the **holding time**.

⑤ Recrystallization ramp of the sample by cooling it back to 5 °C at 20 C°/min.

ⓕ Isothermal plateau for 5 min at 5 °C, analogous to ⓑ.

⑥ Heating ramp of the sample back to its initial high temperature at 15 C°/min, to observe its melting profile.

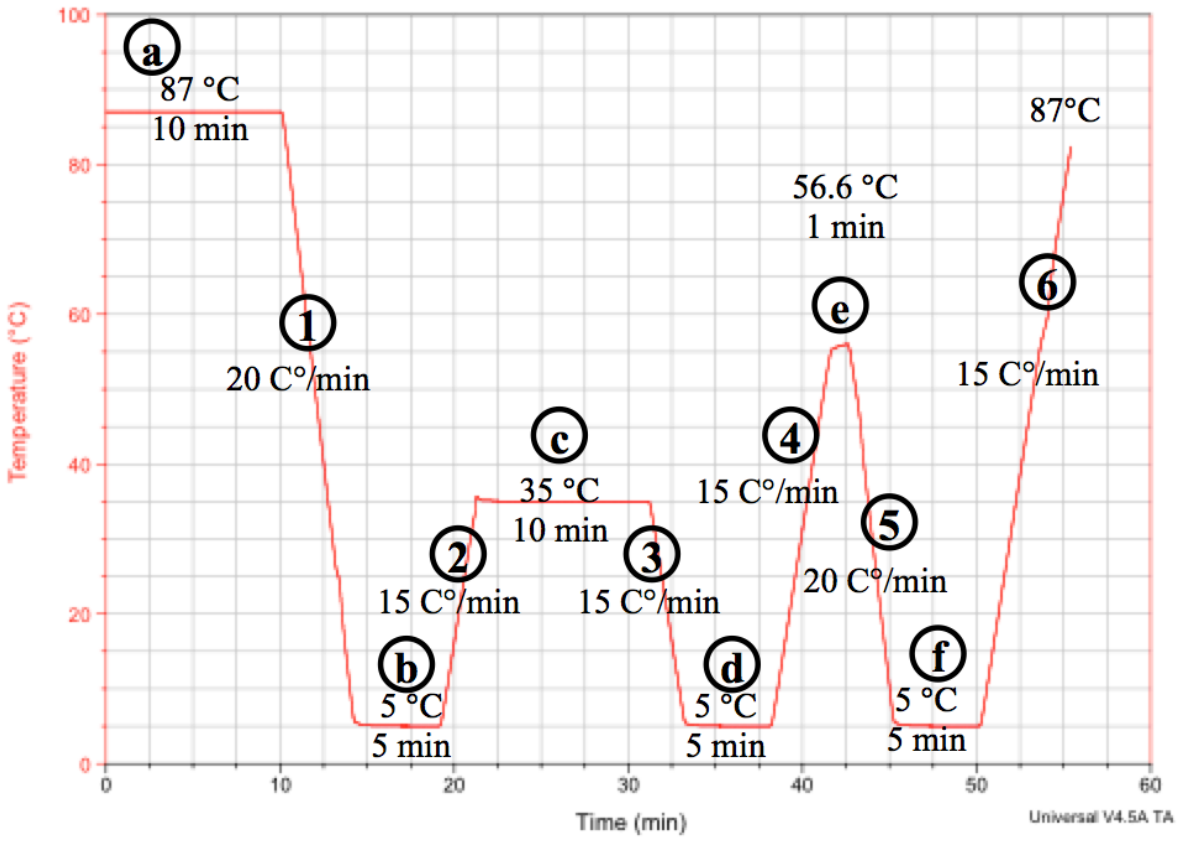

Figure 3-4. Example of temperature-time profile for MMM, labeled with numbers and letters for each step, to illustrate the experimental process.

The first stage (step "a" in Figure 3-4) of the procedure was to melt the material at ~30 °C above the melting temperature of its most stable polymorph, ***β***, regardless of its initial temperature.

The material was then held at this temperature for 10 min in order to ensure a homogeneous temperature and an even molecular distribution within the liquid. The initial temperature in each case (87 °C for MMM, 96 °C for PPP and 103 °C for SSS) was reached by heating at a rate of 15 C°/min.

The next stage (step "1" in Figure 3-4) was to cool the sample at 20 C°/min to 5 °C, and hold it there for 5 min (step "b" in Figure 3-4) in order to initiate the fat crystallization. The fast cooling rate promotes the formation of the α polymorph, since there is not enough time for β' or β to form. This allows the crystallization to proceed quickly, and prepares the material for further tempering. This process also serves for the preparation of a reference thermogram of formation of the α polymorph.

To obtain the reference thermogram, the sample was once again brought back to its initial temperature by heating it at 15 C°/min (dashed line "α standard" in Figure 3-5). This is equivalent to extending step "2" in Figure 3-4 all the way to the initial molten temperature in step "a" in the same figure. This generates a typical melting trace of the α polymorph, which is later used to check whether the α polymorph is formed alone or not. This "α standard melting profile" procedure was done for each pan of each material.

The tempering stage was performed next in order to recrystallize the sample material in the β form. After the step at 5 °C for 5 min (step "b" in Figure 3-4), the sample was subsequently heated to a temperature above the melting point of α (35 °C for MMM, 48 °C for PPP and 56 °C for SSS) and kept at that temperature for 10 min (step "c" in Figure 3-4). This ensures the melting of α and the recrystallization of the material into the β form. The sample was then cooled to 5 °C again at 15 C°/min and kept for 5 min (steps "3" and "d" in Figure 3-4). These steps were used to prepare a fully crystalline sample in the β form as a starting point for the memory experiments.

A reference sample melting thermogram for the $\boldsymbol{\beta}$ polymorph was obtained by heating up the sample at 15 C°/min to its initial molten temperature (dashed line "β standard" in Figure 3-5). This is equivalent to extending step "4" in Figure 3-4 all the way to the initial molten temperature in step "a" in the same figure. This "$\boldsymbol{\beta}$ standard melting profile" procedure was obtained for each pan.

Once the standard traces for $\boldsymbol{\alpha}$ and $\boldsymbol{\beta}$ were obtained, the procedure from step "a" to "d" in Figure 3-4 was performed for each experiment to produce a fully crystalline sample in the $\boldsymbol{\beta}$ form as a starting point for each memory test.

Therefore, for regular experimental runs (not for standard traces), a tempering procedure tailored to each specific sample was performed after step "b" (Figure 3-4). To melt the $\boldsymbol{\alpha}$ polymorph crystals, the sample was heated at 15 C°/min, to 35 °C for MMM, to 48 °C for PPP, and to 56 °C for SSS (step "2" in Figure 3-4). The material was kept at this temperature for 10 min (step "c" in Figure 3-4). The sample was then recrystallized by cooling it at 15 C°/min to 5 °C (step "3" in Figure 3-4), and left there for 5 min (step "d" in Figure 3-4). At this point all the $\boldsymbol{\alpha}$ -crystals had been melted or transformed. Thus, the material was fully crystalline and only in the $\boldsymbol{\beta}$ polymorph phase.

The memory experiments involve three steps: 1) melting the $\boldsymbol{\beta}$ polymorph, 2) keeping the resulting liquid at a particular holding temperature for a given holding time, and 3) recrystallizing the liquid material by cooling it to its original temperature. If, upon fast cooling of this liquid, the $\boldsymbol{\beta}$ polymorph is formed, it is deemed that some kind of structure has persisted in the liquid. This structure must have served as a precursor for the formation of the $\boldsymbol{\beta}$ polymorph. In contrast, formation of the $\boldsymbol{\alpha}$ polymorph suggests that the liquid went back to the same state that it had when it had been heated at high temperature for a long time (step "**a**" of the general

procedure). The capacity to go back directly to the β polymorph without the need for tempering is known as the "memory effect"; that is, it is assumed that some kind of structure remains in the liquid. Otherwise, if that liquid structure has been destroyed, that "memory" is said to be erased.

A vast number of holding temperature-time combinations had to be tested (steps "4", "e" and "5") in order to determine the combinations (Figure 3-5) beyond which the memory was lost. Those time-temperature combinations would be considered the boundary of the memory effect. As the holding temperature above the melting point is increased, the time needed to erase the memory is reduced, such that higher temperatures required shorter times. Each material had its own boundaries, that had to be painstakingly found. They constitute the core new knowledge that this thesis contributes to the understanding of triglyceride crystallization, along with additional information related to their recrystallization temperatures.

The final step (step "6" in Figure 3-4) is to melt the sample to its initial temperature at 15 C°/min.

All the thermograms obtained from the DSC experiments were initially analyzed using the TA Instruments Analysis program to obtain the signals of temperature, time and heat flow. Selected data were exported to MS Excel for inclusion in this thesis.

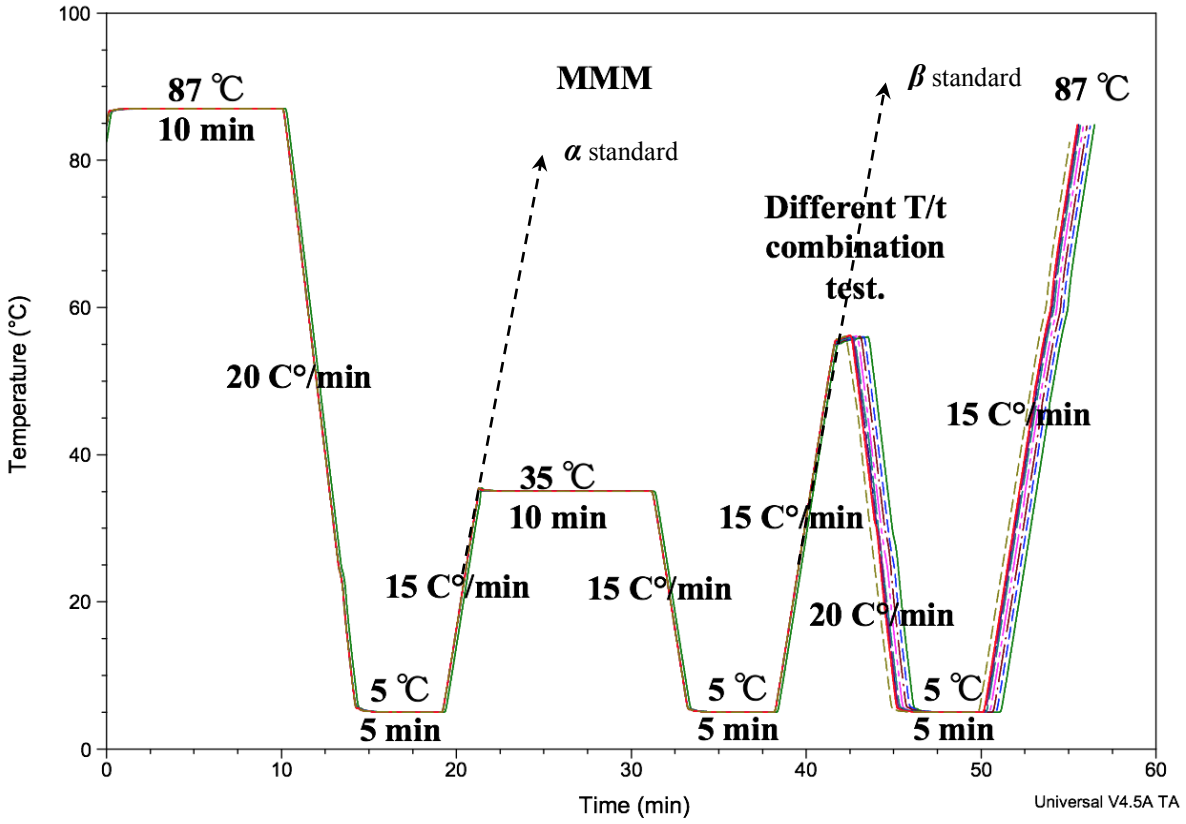

Figure 3-5. Experimental procedure of MMM in this research, extracted from the data recorded by the DSC. The dashed blue and red traces represent the various time-temperature combinations tested for each of the samples.

The DSC experiments produced three synchronized "signals": heat flow (the energy flow difference between reference pan and sample pan), temperature and time. Thermograms can be plotted with two or even three of the signals. Figure 3-6 shows a thermogram with heat flow as the Y-axis and time as the X-axis. This plot provides information sequentially, and is therefore useful for following the events in the order in which they were programmed.

Plots with temperature on the X-axis requires more training to interpret, but are essential for relating events to the temperatures at which they occur. An example is shown in Figure 3-7 with heat flow on the Y-axis, as in the Figure 3-6, and temperature on the X-axis. From this plot, we

can get information about the onset temperature of crystallization and melting, as well as the temperature at the end of crystallization and melting (offset), and the enthalpy of the peak.

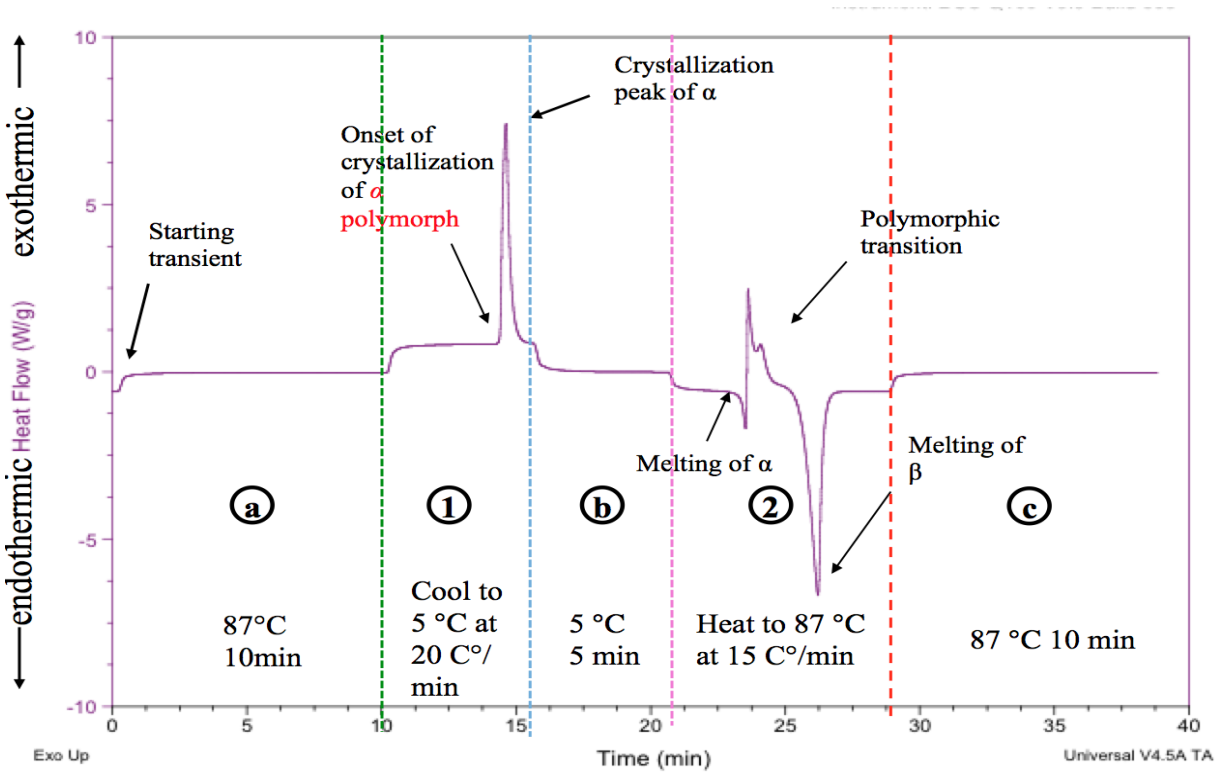

Figure 3-6. Example of a heat-flow versus time thermogram of MMM. The letters designate the temporal relationship among "plateau" regions where temperature has been held constant; numbers represent the temporal sequence of heating and cooling at constant rates of temperature change.

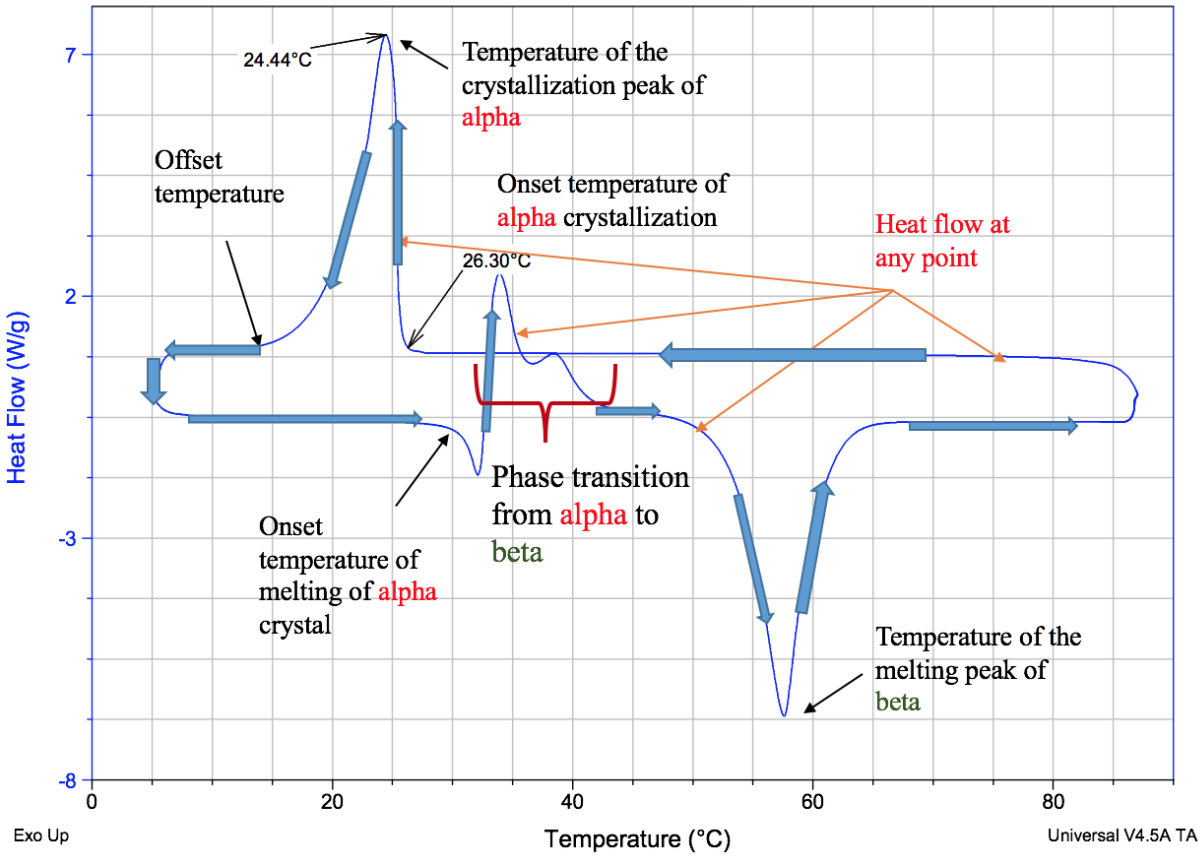

Figure 3-7. Example of a heat-flow versus temperature thermogram of MMM. The data are the same as in Figure 3-6, but they have been plotted as a function of temperature. Blue arrows on the thermogram traces show the temporal sequence of events. The onset of crystallization is around 26.3 °C.

In order to get more information from the experiment, one can plot the three signals together, as shown in Figure 3-8. It is easier to compare time and temperature, as well as time with energy. This arrangement often aids in interpretation of thermal events observed as a function of temperature. However, sometimes it is ideal to use only two signals in order to make the thermogram simple and clear.

The integral under the phase-change peaks provides an estimate of the enthalpy change involved, as seen in Figure 3-9. The TA software estimates a sigmoidal baseline, though it is limited to horizontal take-off and landing, so it does not successfully account for the change in specific heat (i.e., the slope of the signal before and after the transition).

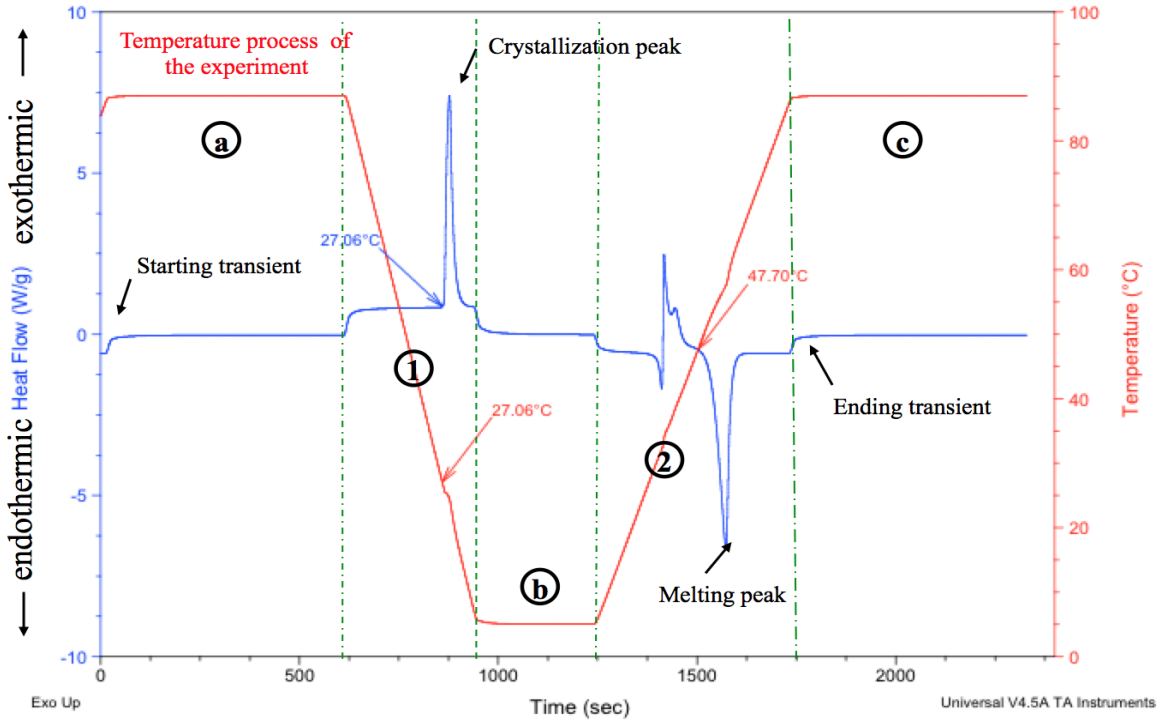

Figure 3-8. Thermogram of MMM showing temperature (red) and heat flow (blue) as a function of time.

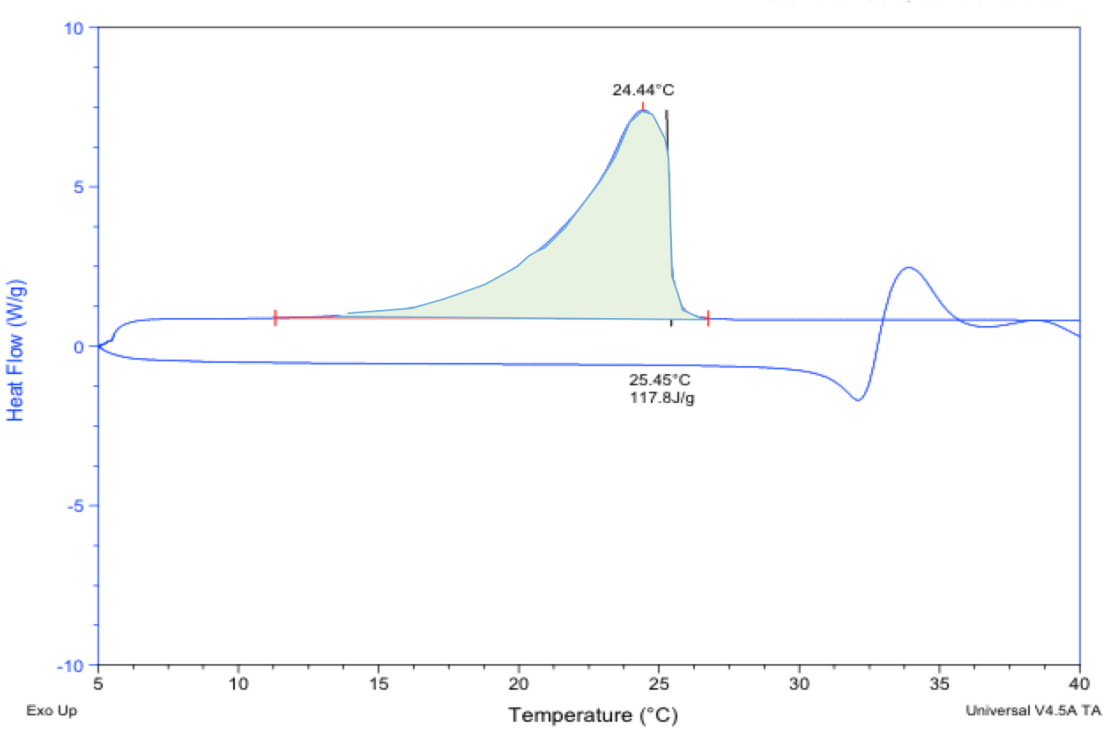

Figure 3-9. Thermogram of MMM showing the estimate of enthalpy as the area under a crystallization peak (the shaded green area). The heat flow maximum is at 24.44ºC.

CHAPTER 4. RESULTS AND DISCUSSION – I TIME-TEMPERATURE BOUNDARIES OF CRYSTAL MEMORY IN PURE TRIACYLGLYCEROLS

4.1 Formation and characterization of the *α* and *β* polymorphs

As described in Chapter 3, the first step in this research was the formation of the ***α*** polymorph for the three materials. This served as a reference via comparison of its thermogram with that of the materials formed upon re-cooling the liquid. A sample temperature profile for forming and analyzing the ***α*** polymorph for MMM is shown in Figure 4-1. Its corresponding thermogram is shown in Figure 4-2. Three replicates were done for each sample.

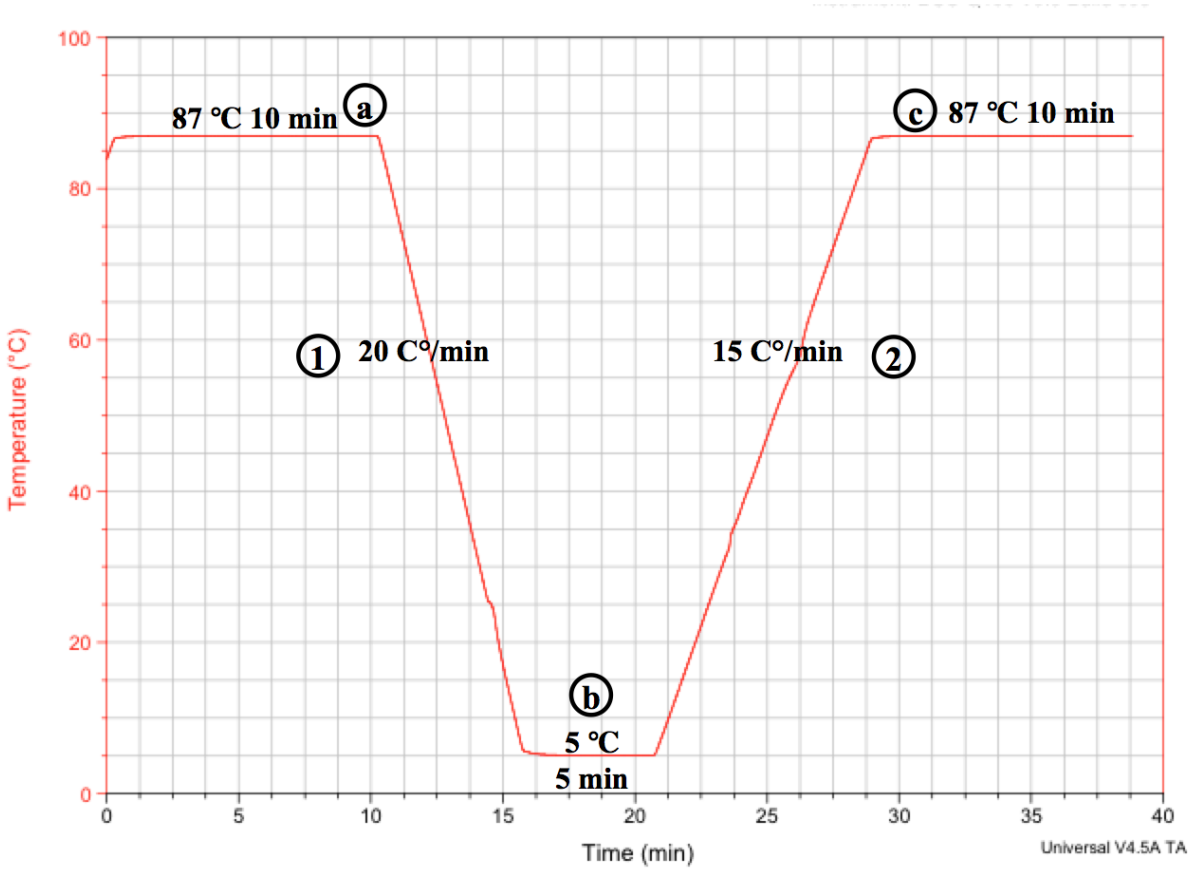

Figure 4-1. Temperature-time plot of MMM ***α*** polymorph formation and analysis.

4.1.1 Formation and characterization of the α polymorph

Trimyristin

The crystallization peak of MMM during cooling at 20 C°/min (step "1" in Figure 4-1) started at 26.3 ± 0.1 °C (Figure 4-2). The enthalpy under the crystallization peak was estimated as 114.8 ± 0.2 J/g. The literature values for melting point and enthalpy of the ***α*** polymorph for MMM are 32.6 °C and 113.25 J/g (Hui.Y.H & Sherkat, 2013) (see Chapter 2).

According to Table 2-2 and Table 2-3, the undercooling onset was 6.3 ± 0.1 C°. The enthalpy measured here was relatively close to the reference value; however, since we did not observe exactly the same melting temperature, the enthalpy cannot be exactly the same. As the crystallization temperature is lowered, the enthalpy becomes larger because the c_p of the liquid is larger than that of the crystal (Hampson & Rothbart, 1983; Morad, Idrees, & Hasan, 1995).

A melting temperature profile with a heating rate of 15 C°/min (step "2" in Figure 4-1) was applied after a holding time of 5 min at 5 °C (step "b" in Figure 4-2) in order to make sure that the polymorph formed during cooling from 87 °C to 5 °C (step "1" in Figure 4-2) was ***α***. A melt-mediated polymorphic transition from ***α*** to ***β*** occurred during step "2" in Figure 4-2. This increase in temperature caused the melting first of the unstable forms and then of the more stable forms. The first peak observed was exothermic (step "1" in Figure 4-2) and corresponds to the onset of melting of ***α*** as the temperature reaches ~ 32 °C, followed by crystallization to ***β'*** and transformation to ***β***. As the temperature rose above 55.9 °C, the melting of ***β*** started, continuing until the whole mass has become liquid again.

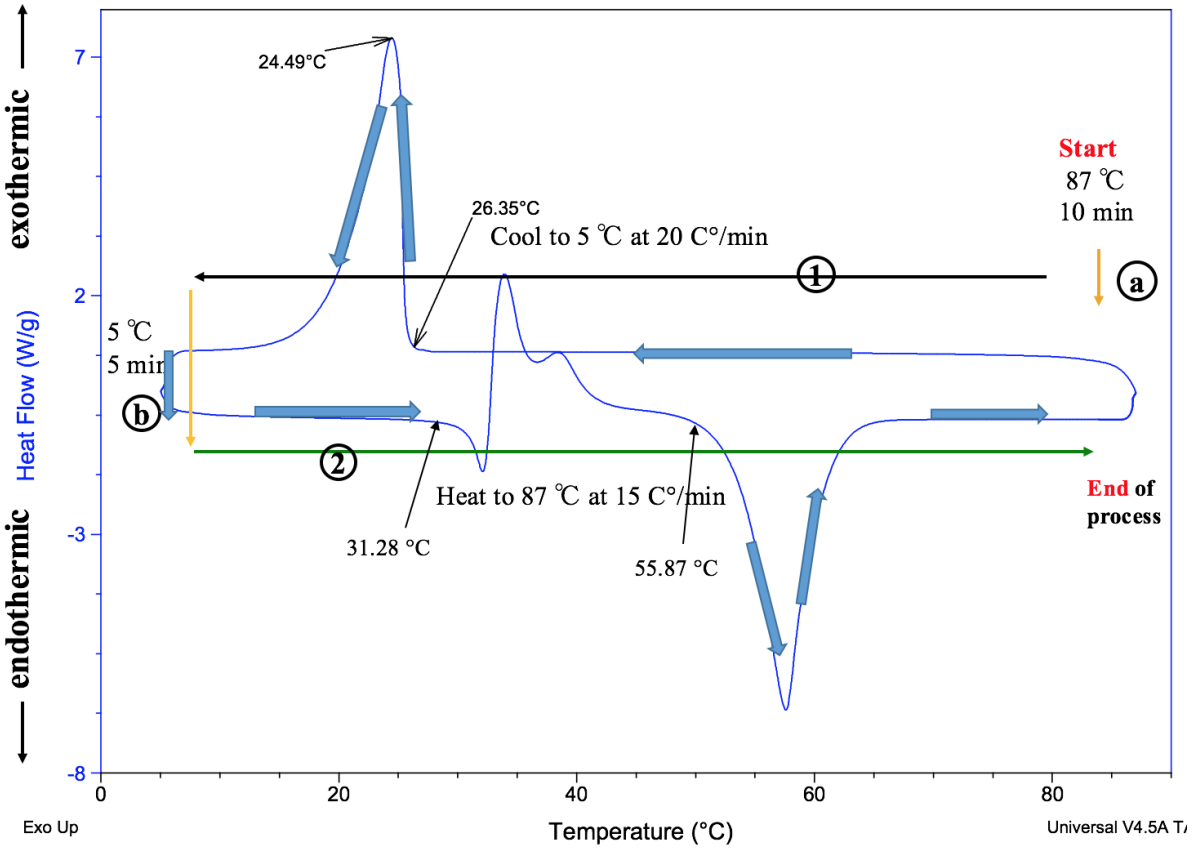

Figure 4-2. Thermogram of the process to form and analyze the ***α*** polymorph in MMM, indicating the cooling and heating directions and conditions. (For step numbers and letters see Figure 4-1).

Figure 4-3 illustrates literature data of how the cooling rate affected the onset temperature for the crystallization of the ***α*** form in MMM. Similar behavior was observed with the other TAGs. The onset temperature reported in the literature was recorded for cooling rates of 7.5 C°/min, 10 C°/min, 15 C°/min and 20 C°/min (Data from Anom, E. 2009). The literature reported onset temperature of ***α*** crystallization in MMM at the hypothetical zero cooling rate was the melting temperature, 32.6 °C. The reported crystallization onset temperature at 20 C°/min was seen at around 27.0 °C, which is similar to the onset temperature of 26.3 °C observed in our experiments.

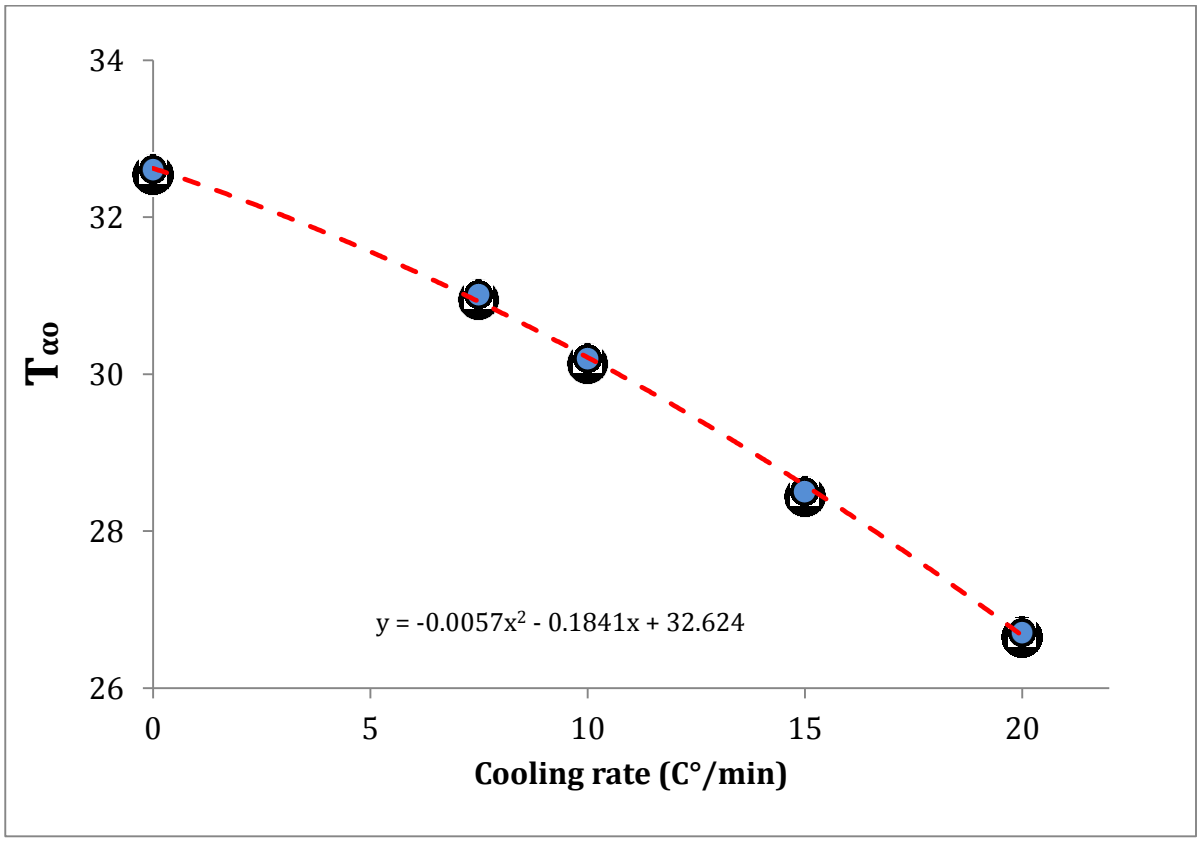

Figure 4-3. Onset temperature for ***α*** form in MMM at different cooling rates (Data from Anom, E. 2009).

Tripalmitin

Figure 4-4 shows the reference ***α*** trace of PPP. Crystallization (step "1" in Figure 4-4) started at 37.4 ± 0.1 °C the enthalpy under the crystallization peak was estimated as 119.7 ± 0.1 J/g.

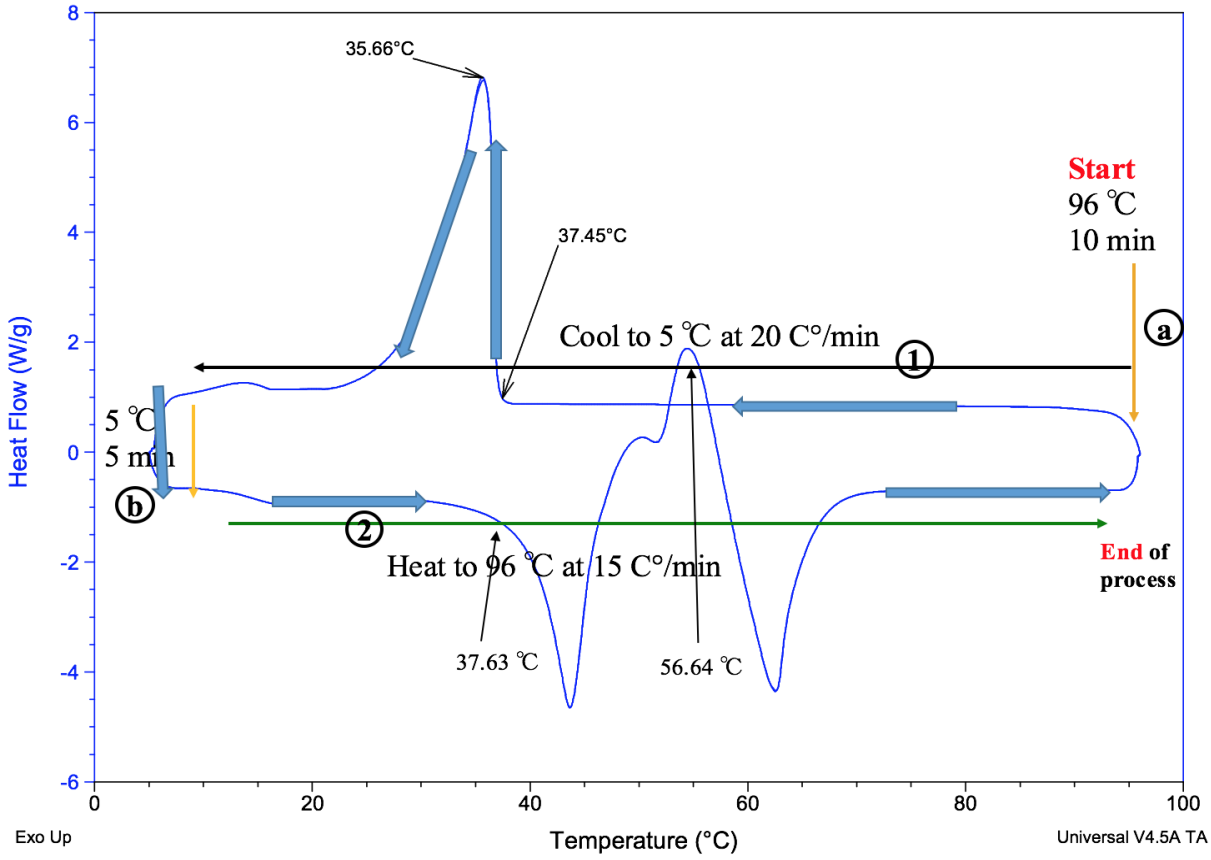

Figure 4-4. Thermogram of the process to form and analyze the ***α*** polymorph in PPP, indicating the cooling and heating directions and conditions. (For step numbers and letters see Figure 4-1).

The literature values for the melting point and the enthalpy of the ***α*** polymorph for PPP are 44.7 °C and 118.65 J/g (Hui.Y.H & Sherkat, 2013). The undercooling onset would thus be 7.3 ± 0.1 C°. The enthalpy of crystallization peak is reasonably close to the expected value for ***α*** PPP. While melting at 15 C°/min (step "2" in Figure 4-4), the ***α*** form (unstable form) starts to melt at 37.6 °C. The melting temperature of ***α*** in PPP was considerably lower than the theoretical value, perhaps due to the very small nanoplatelet size formed by PPP. After melting, the liquid re-solidified in a more stable form, the ***β'*** polymorph. As the temperature rose above 56.6 °C, the melting of ***β'*** started. There was no appreciable transformation to ***β***, given that the melting peak of early ***α*** and ***β*** would be almost over at 65.9 °C.

Tristearin

Figure 4-5 displays the reference ***α*** trace of a SSS sample. The onset of crystallization (step "1" in Figure 4-5) started at 49.6 ± 0.04 °C, and the enthalpy under the crystallization peak was estimated as 125.1 ± 0.1 J/g. The melting point and the enthalpy of the ***α*** polymorph reported in the literature for SSS are 54.7 °C and 121.71 J/g (Hui.Y.H. & Sherkat, 2013). The undercooling onset would thus be 5.1 ± 0.04 C°.

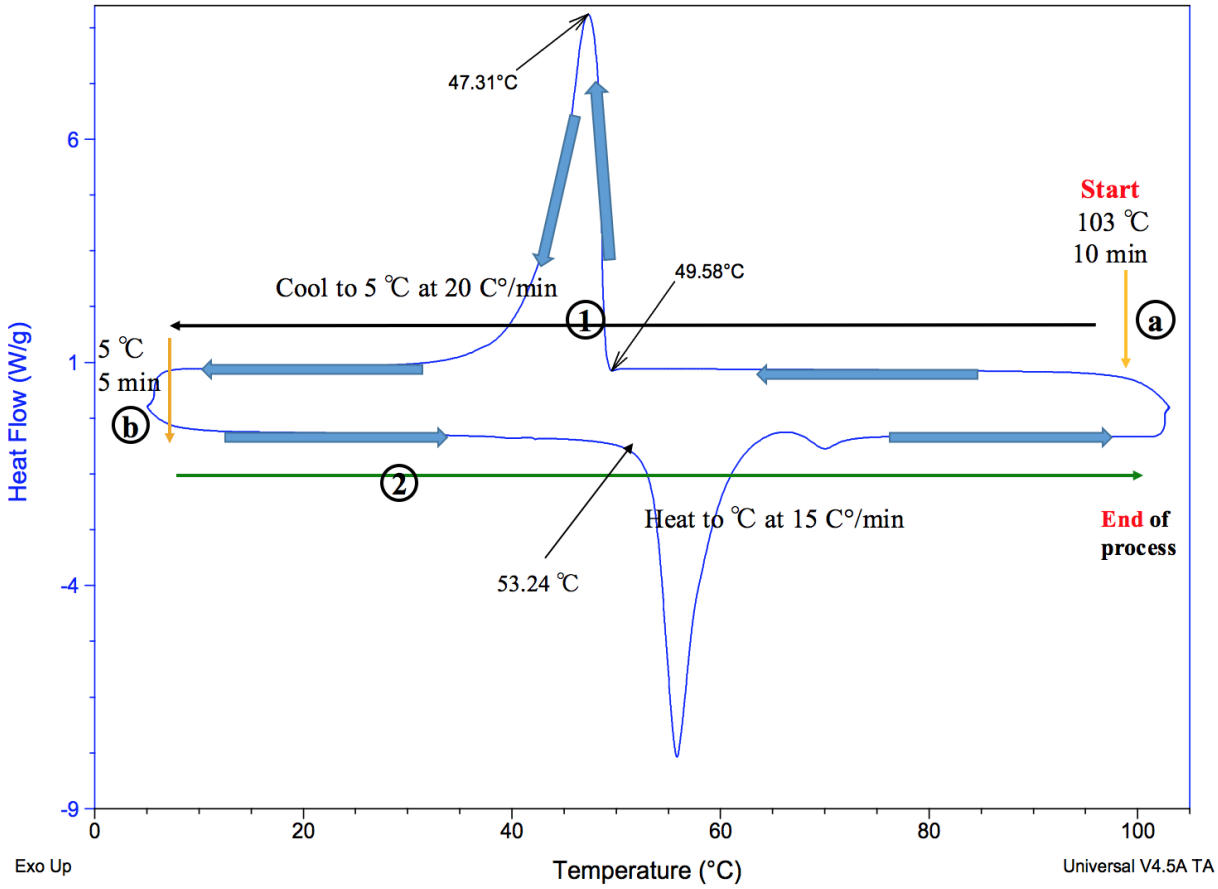

Figure 4-5. Thermogram of the process to form and analyze the ***α*** polymorph in SSS, indicating the cooling and heating directions and conditions. (For step numbers and letters see Figure 4-1).

The difference in the enthalpy is small, but larger than for the other two materials. The reason for this somewhat larger difference is not clear. During melting (step "2" in Figure 4-5), ***α*** started

to melt after heating to 53.24 °C, and a small peak of melting can be noticed after the melting peak (during step "2" in Figure 4-5) of ***α***, indicating that there might have been a transformation to ***β'*** that was not able to finish.

The three thermograms of pure triacylglycerols suggest that the melting temperature becomes higher for materials with higher carbon numbers, and thus higher molecular weights. This can be perhaps attributed to the increase in the strength of the van der Waals interactions between molecules, thereby requiring more energy to break the larger molecules apart from the crystal structure. The differences are noticeable not just at equilibrium but also during the melting process. The ***α*** structure of MMM could easily be broken; as a result, complicated polymorphic transitions happen and molecules re-organize into different polymorphs. For PPP, it's harder to break the ***β'*** organization; for SSS, it is just enough to break the network of ***α***. This is because both the energy barrier and the driving force increase with carbon number.

4.1.2 Tempering: Formation and characterization of the β polymorph

Figure 4-6 is the temperature-time diagram that includes the tempering process of MMM, and defines the names of the steps of this process as letters and numbers. A temperature of 35 °C and a time of 10 min were chosen for the tempering process (step "c" in Figure 4-6) after trying many different combinations. The tempering conditions for PPP and SSS were 48 °C, 10 min and 56 °C, 10 min, respectively. Temperatures slightly above the melting point of ***α*** are enough to melt the ***α*** polymorph in a relatively short time.

The heat flow from the thermogram in Figure 4-7 revealed a small melting peak from the ***α*** polymorph after heating the MMM sample at 35 °C for 10 min (step "c" in Figure 4-7). When we recrystallized the sample, no peak was formed during the cooling period (step "3" in Figure 4-7). While reheating (step "4" in Figure 4-7), only one peak appeared at 58.52 °C. This melting

event started at 50.8 °C. Since the melting point of ***β'*** MMM is 45.9 °C, the endothermic peak should be the melting peak of ***β***. Although the melting point of large ***β*** MMM crystals is 57.1 °C (Hui.Y.H. & Sherkat, 2013), it is common to observe melting onsets at lower temperatures due to the formation of nanoplatelets. Thus, the tempering program totally melted the ***α*** polymorph and forms the desired ***β*** polymorph.

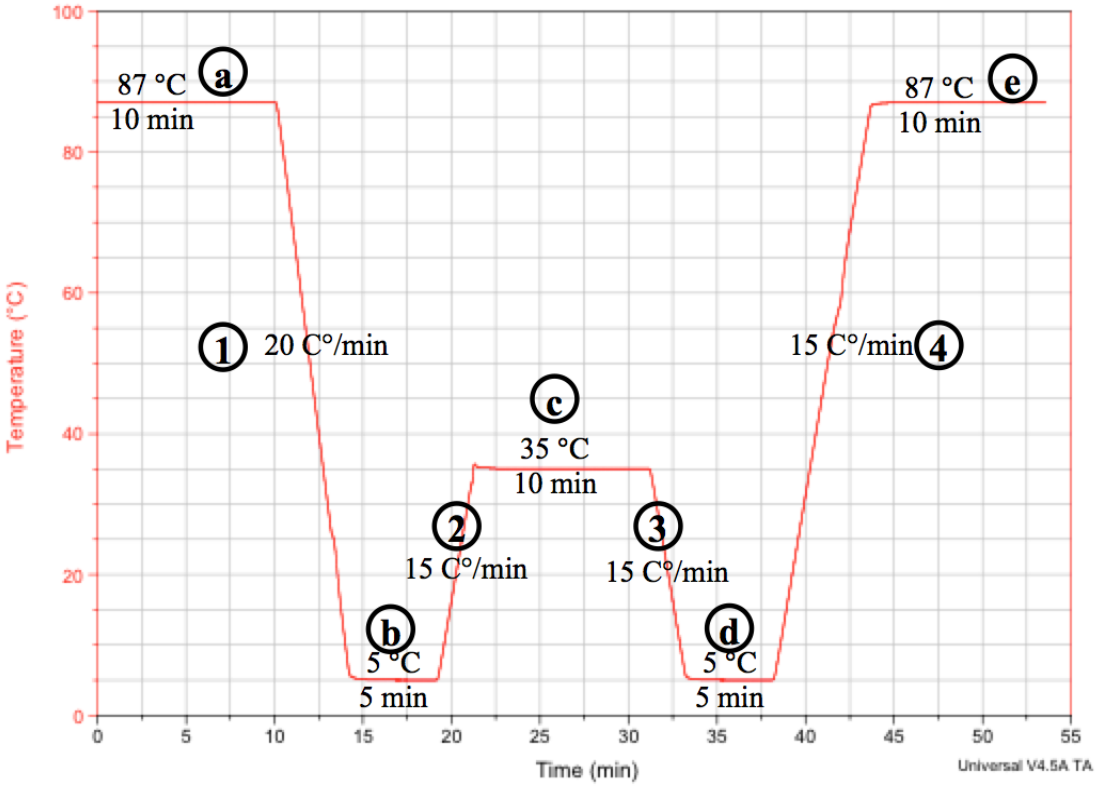

Figure 4-6. Tempering program of the MMM sample.

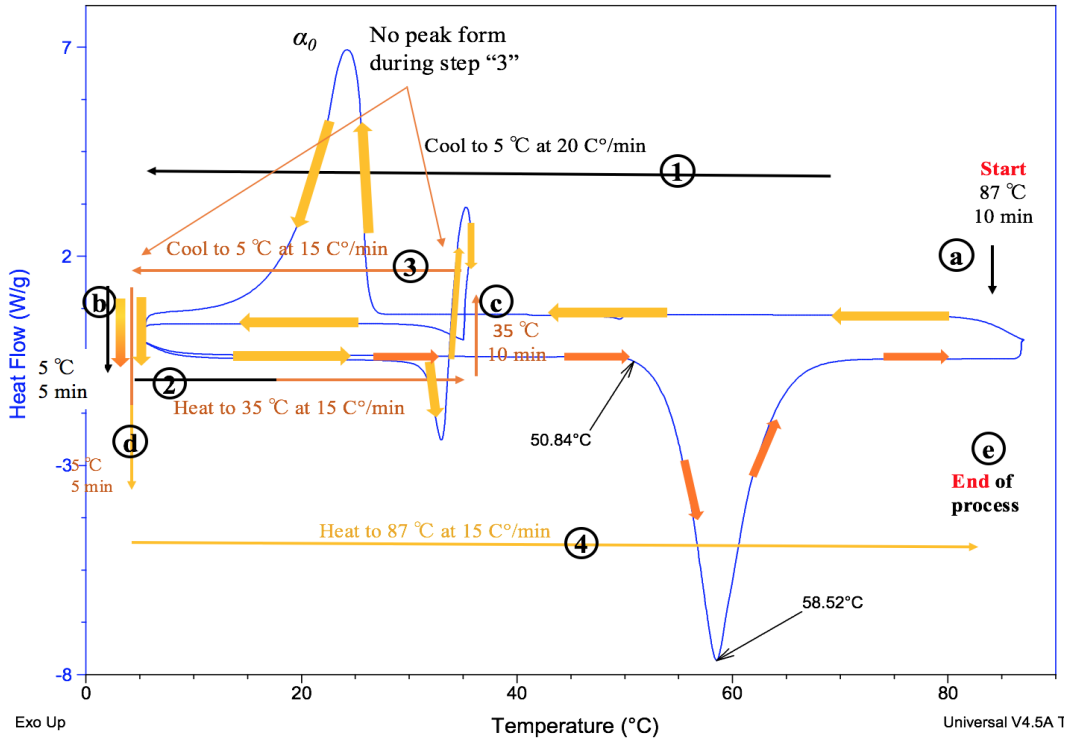

Figure 4-7. Thermogram of the tempering process of MMM. (For step numbers and letters see Figure 4-6). Arrows on the thermogram traces showing the temporal sequence of events, start from yellow arrows to orange arrows.

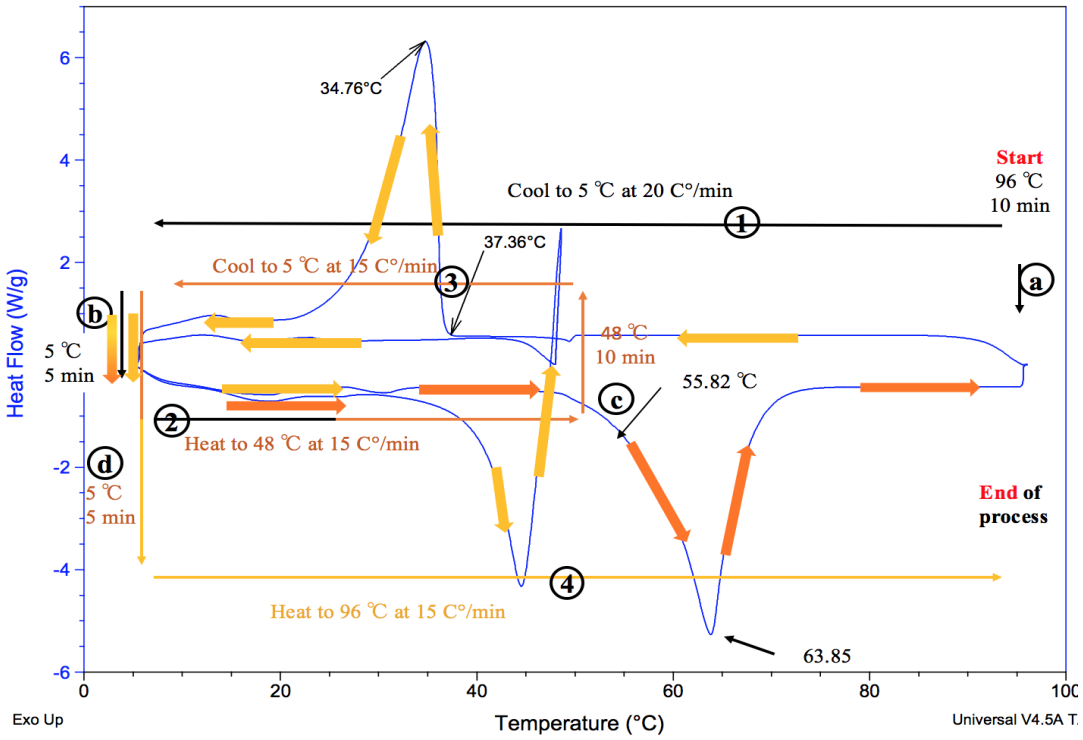

Figure 4-8. Thermogram of the tempering process of PPP. (For step numbers and letters see Figure 4-6).

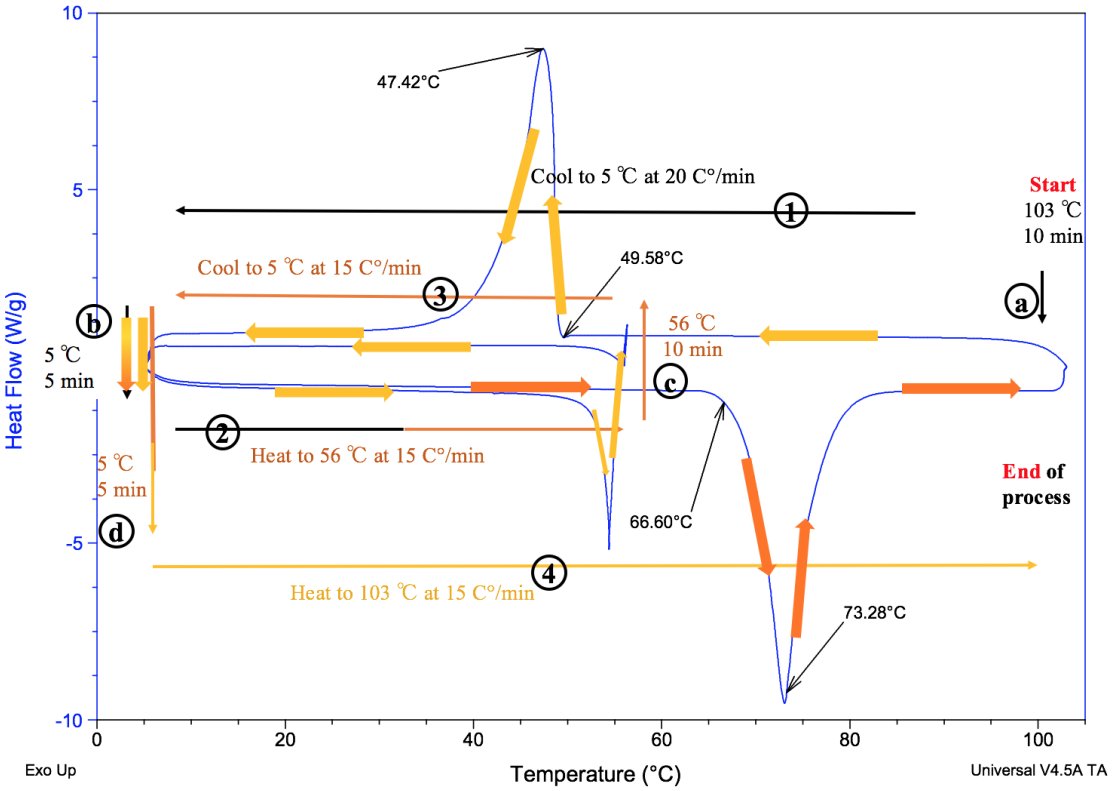

Figure 4-9. Thermogram of the tempering process of SSS. (For step numbers and letters see Figure 4-6).

The same type of tempering process was applied to PPP and SSS, as shown in Figure 4-8 and Figure 4-9. The onset melting temperature of PPP (step "4" in Figure 4-8) was around 55.82 °C, while the onset melting temperature of SSS (step "5" in Figure 4-9) was around 66.60 °C. Both of them were higher than the ***β'*** melting points of PPP and SSS, meaning that after the tempering process for PPP and SSS only the ***β*** polymorph was left.

4.2 Time-temperature boundaries of crystal memory in pure triacylglycerols

4.2.1 Trimyristin boundaries

The temperature profile shown in Figure 4-10 represents one of the experiments done to determine the time-temperature boundaries of the memory effect in MMM. A thermogram corresponding to this experiment is presented in Figure 4-11 and Figure 4-12. Each step is clearly labeled with a different color in order to facilitate the understanding of the different steps. The process was the same in all experiments until the end of step "d" (Figure 4-10). After step "d", steps "4", "e", and "5" were changed to locate the memory boundaries. Steps "f" and "6" were always the same, though their starting time sometimes happened earlier or later than 45 minutes during the overall experiment time, depending on the duration of the program for the segment "4e5".

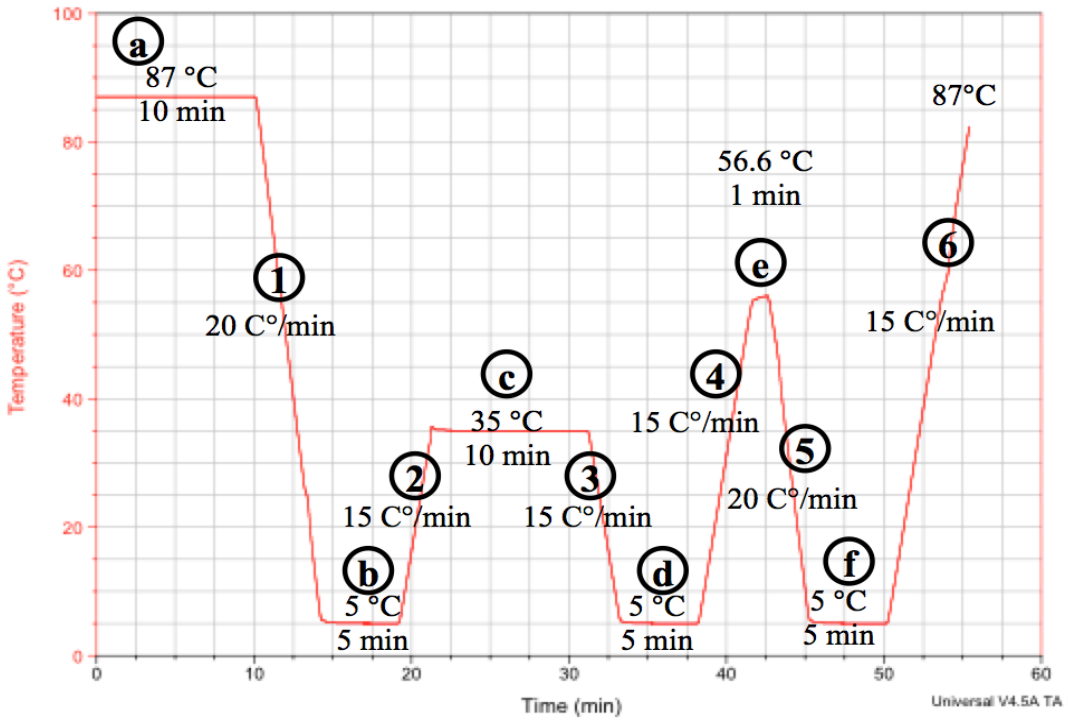

Figure 4-10. Temperature-time program used to characterize the memory effect for the MMM. This figure is the same as Figure 3.4, presented here for convenient access.

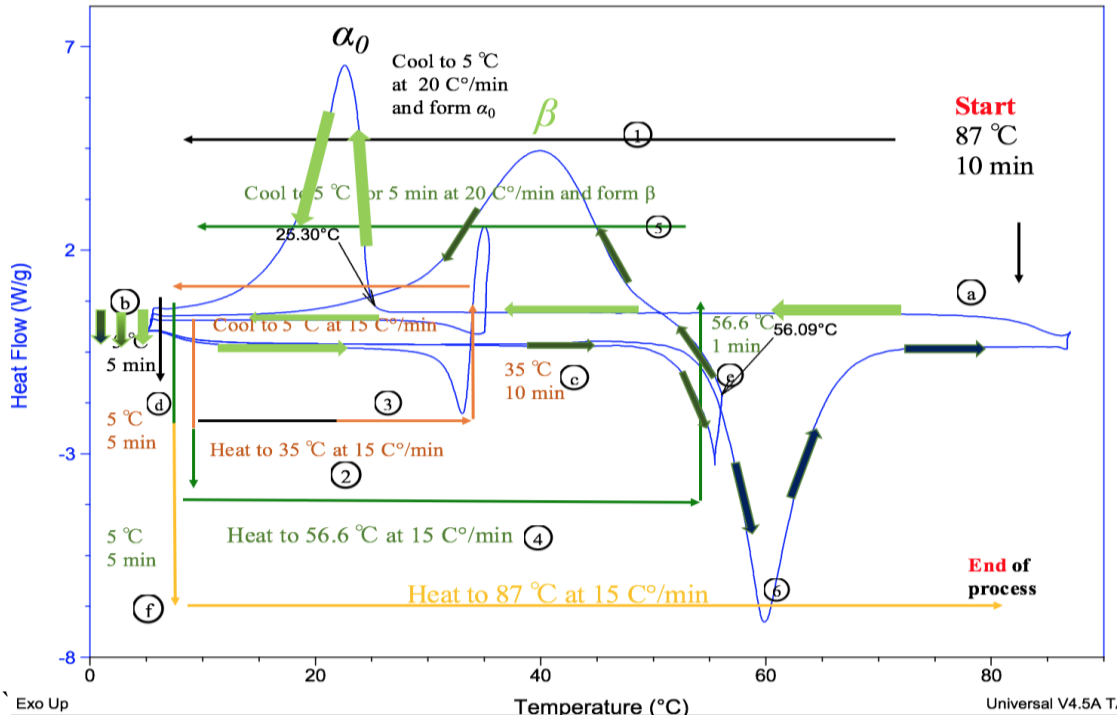

Figure 4-11. Thermogram from the program used to characterize the ***β*** memory effect for MMM, at 56.6 °C for 1 min (For step numbers and letters see Figure 4-10). Blue arrows indicate temporal sequence of events.

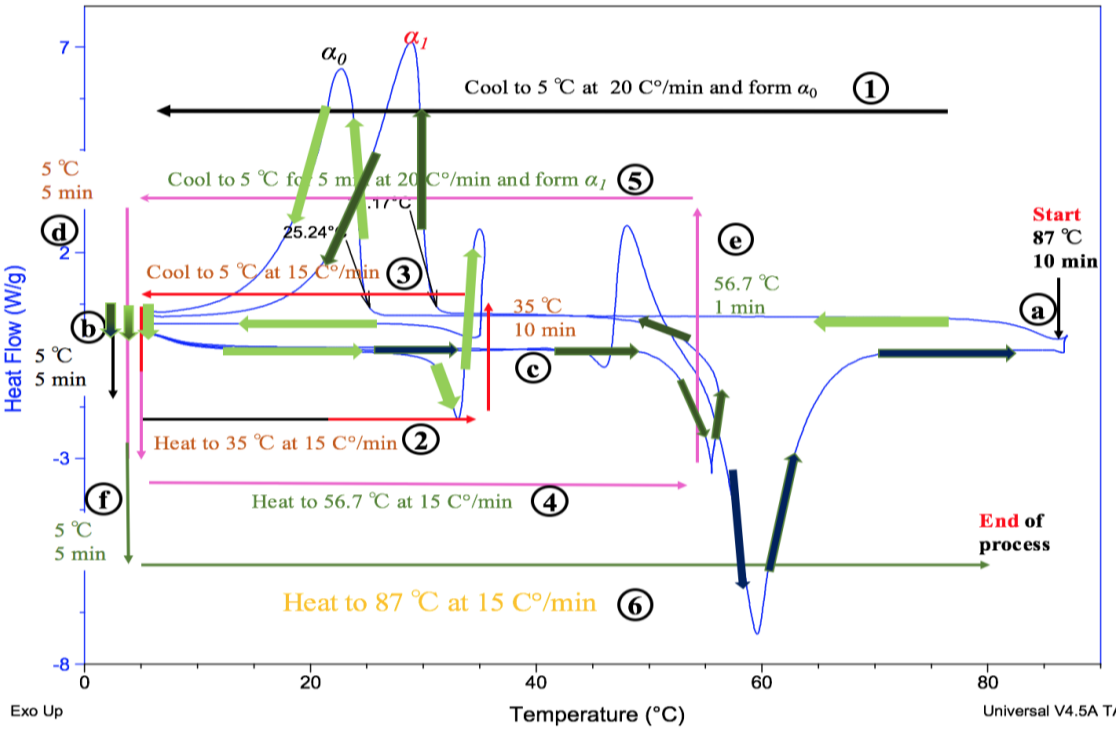

Figure 4-12. Thermogram from the program used to characterize the early ***α*** memory effect for MMM, at 56.7 °C for 1 min (For step numbers and letters see Figure 4-10).

The memory effect displayed by MMM in this experiment is similar to the 'memory effect' documented for cocoa butter and other fats, featuring the formation of a more stable polymorph directly from the melt due to some molecular structure or organization preserved in the liquid after the melting of the crystals. This type of memory will be referred to as "***β*** memory" throughout the rest of the thesis. The onset temperature of ***β*** crystallization (step "5" in Figure 4-11 and Figure 4-12) was around 55.98 °C, as indicated in Figure 4-13.

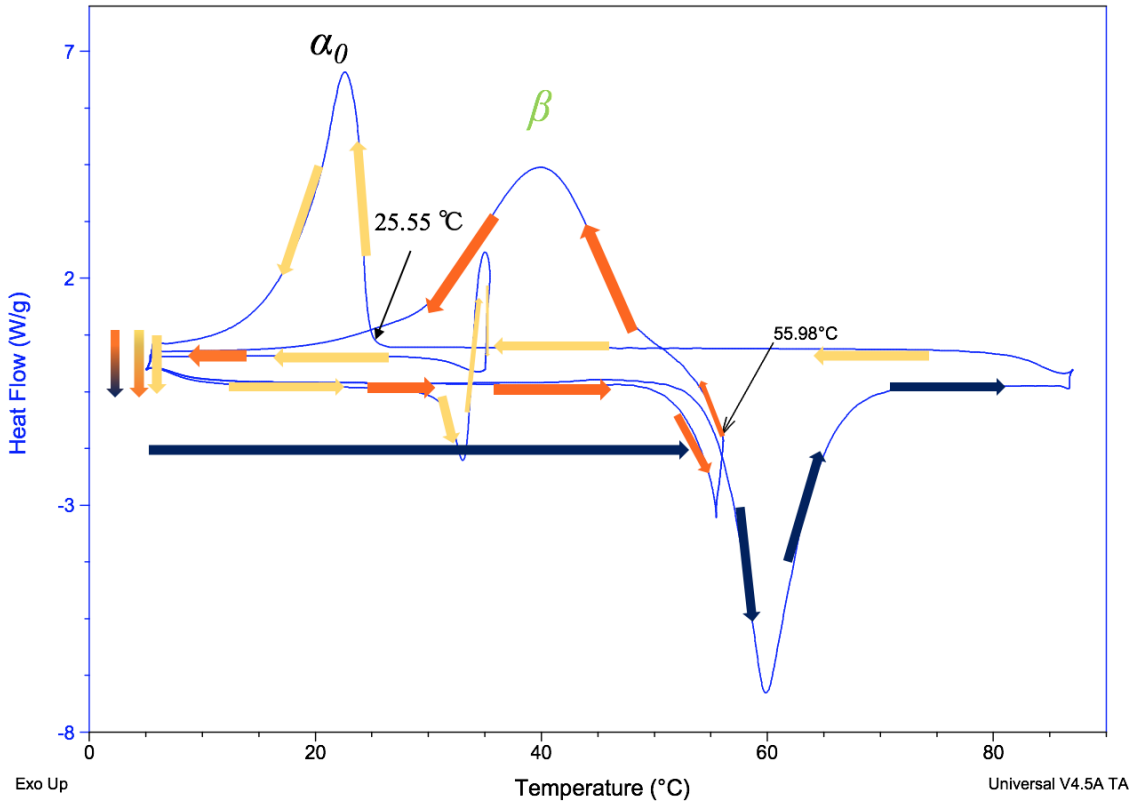

Figure 4-13. Example thermogram of "***β*** memory" effect of MMM, held at 56.6 °C for 1 min (For step numbers and letters see Figure 4-10).

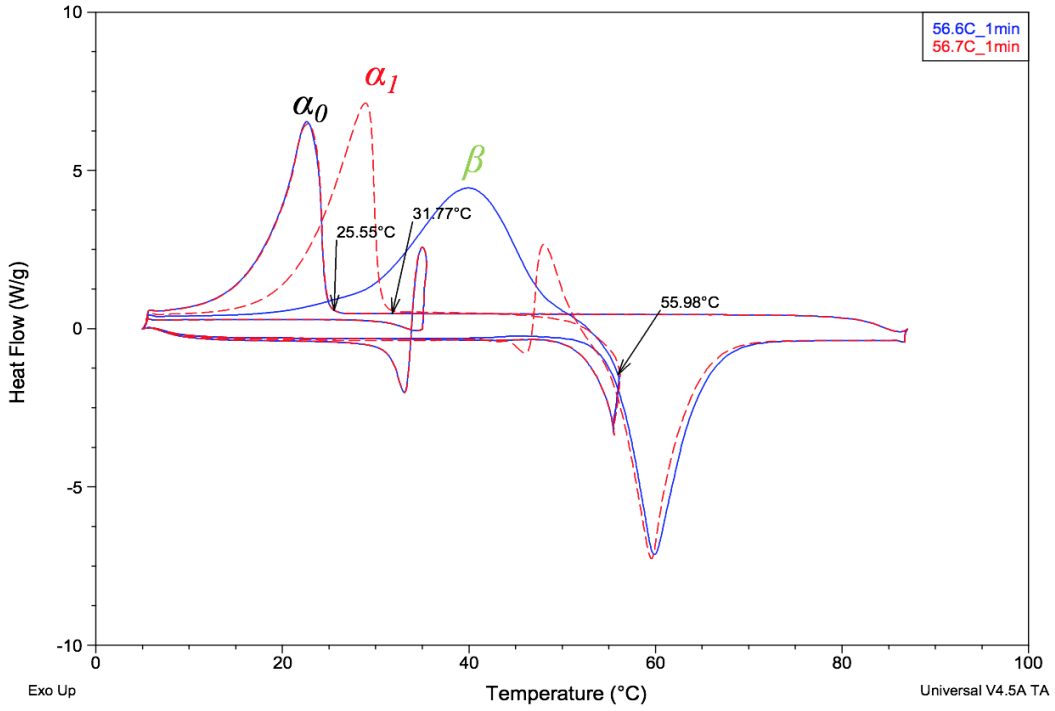

Figure 4-14. Thermograms of recrystallization of MMM, showing the two different types of memory effects detected from experiments. The blue line represents the formation of $\boldsymbol{\beta}$ memory, while the dashed red line represents the formation of early $\boldsymbol{\alpha}$ memory.

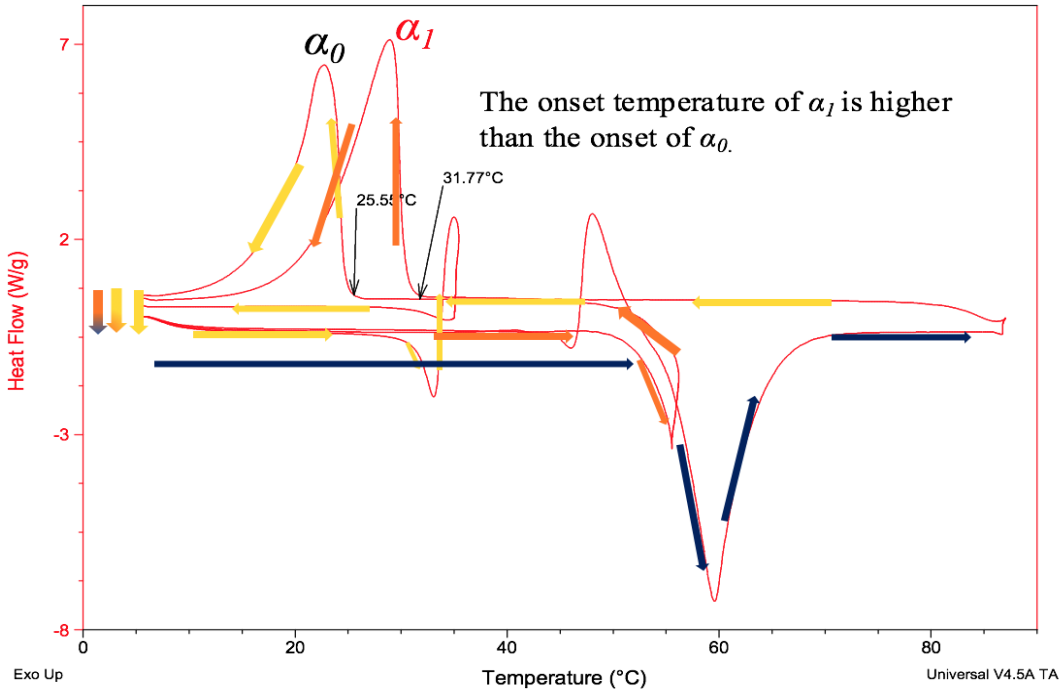

Figure 4-15. Example thermogram of "early $\boldsymbol{\alpha}$ memory" effect of MMM, after being held at 56.7 °C for 1 min (For step numbers and letters see Figure 4-10).

As previously observed in the experiments of Arnaud (2009), another type of memory was found for MMM. This memory involved the formation of an ***α*** crystal (α_1) that appeared to form at lower undercooling (i.e., higher temperature; step "5" in Figure 4-12) than the onset when cooling from the original melt (step "1" in Figure 4-12), defined as "early ***α*** memory" in this thesis.

These two different types of "memory effect" were called "early ***α*** memory" when referring to ***α*** crystals and "***β*** memory" when referring to ***β*** crystals. As shown in Figure 4-15, the liquid with "early ***α*** memory" started to crystallize at 31.77 °C (step "5" in Figure 4-12). The onset of the reference $\boldsymbol{\alpha}_0$ peak was 25.55 °C (step "1" in Figure 4-12). Thus, the onset temperature during the recrystallization was 6.25 C° higher. It was noted that, as the holding temperatures in step "e" were increased or the holding time at that temperature was made longer, this difference decreased. Hence, the memory effect was reduced until the point that it disappeared.

The overlaid thermograms for "early ***α*** memory" (Figure 4-16) and "***β*** memory" (Figure 4-17) show the endothermic peaks at the boundaries of the memory effect, with their time and temperature combinations labeled at the top right corner. A summary of the time-temperature boundaries of MMM is shown in Table 4-1.

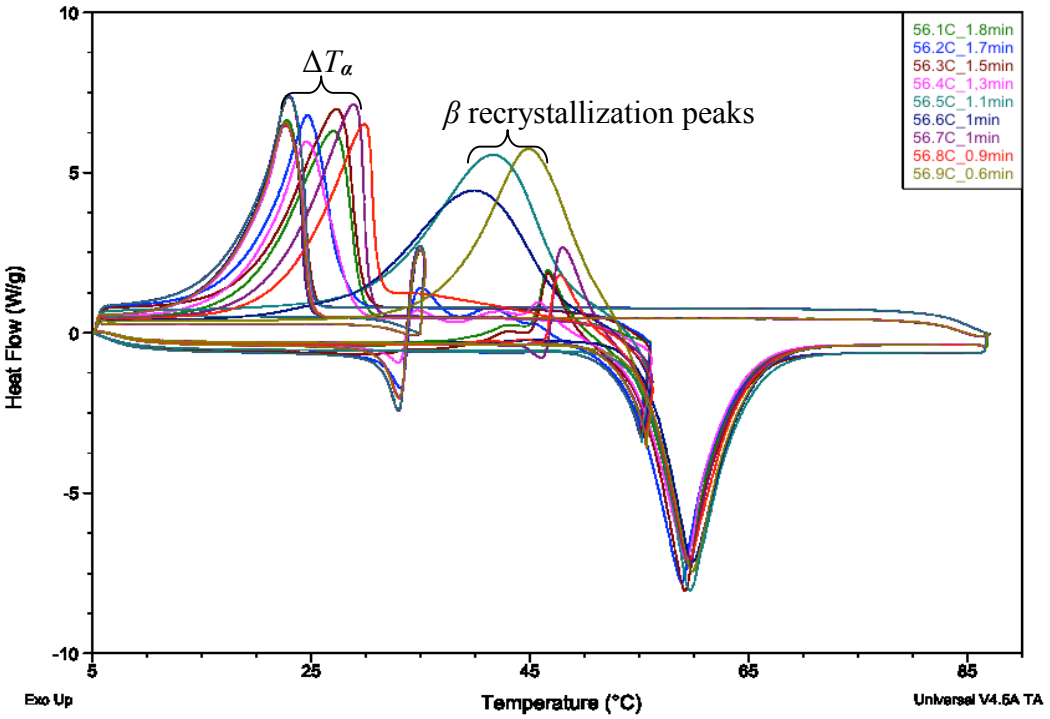

Figure 4-16. Overlaid thermograms of temperature-time boundaries for MMM. Different combinations of temperatures and times are labeled at the right top corner of the figure. The temperature at 56.5 °C, 56.6 °C and 56.9 °C were ended with β memory.

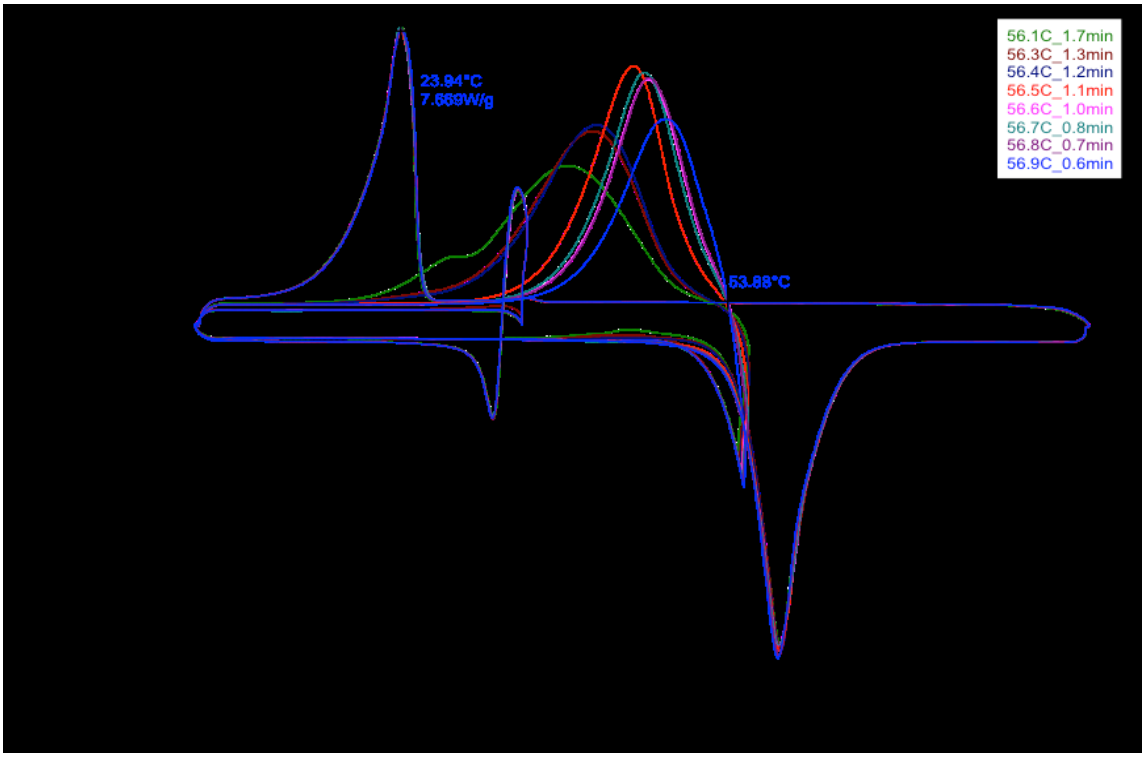

Figure 4-17. Overlaid thermograms of temperature-time boundaries of ***β*** memory for MMM. The onsets of ***β*** recrystallization are around 53.8 °C.

The time-temperature boundaries of the two types of crystal memory and their average are shown in Table 4-1 and Table 4-2. The temperature-time combinations follow the rule that higher holding temperatures will correspond to shorter holding times in order to persist memory effect.

Table 4-1. Time at each holding temperature that defined the boundary for "early ***α*** memory" of MMM. (At "*" the boundary became a "***β*** memory" boundary). Temperatures displayed in this table are the longest holding time that the early ***α*** memory persisted at different holding temperatures. The "*α* Time_1 (min)" is the holding time boundary at holding temperature for pan 1 and "*α* Time_2 (min)" is the holding time boundary at holding temperature for pan 2.

Holding Temperature (°C)	**56.0**	**56.1**	**56.2**	**56.3**	**56.4**	**56.5**	**56.6**	**56.7**	**56.8**	**56.9**
***α* Time_1 (min)**	>75	1.8	1.7	1.5	1.3	*	*	1.0	0.9	*
***α* Time_2 (min)**	>75	1.9	1.8	1.6	1.5	*	*	1.0	0.7	*
***α* Time average**	>75	1.85	1.75	1.55	1.4	*	*	1.0	0.8	*

Table 4-2. Time at each holding temperature that defined the boundary for "***β*** memory" of MMM. The "*β* Time_1 (min)" is the holding time boundary at holding temperature for pan 1 and "*β* Time_2 (min)" is the holding time boundary at holding temperature for pan 2.

Holding Temperature (°C)	**56.0**	**56.1**	**56.2**	**56.3**	**56.4**	**56.5**	**56.6**	**56.7**	**56.8**	**56.9**
***β* Time_1 (min)**	15	1.7	1.4	1.3	1.2	1.0	1.0	0.8	0.7	0.6
***β* Time_2 (min)**	20	1.6	1.5	1.4	1.3	1.2	1.1	0.8	0.7	0.5
***β* Time average**	17.5	1.65	1.45	1.35	1.25	1.1	1.05	0.8	0.7	0.65

In addition, the time to erase "early ***α*** memory" was always longer than the time to erase "***β*** memory". With increased time at a holding temperature, "***β*** memory" gradually transformed into "early ***α*** memory". For each temperature, all the memories were erased beyond a certain value of time. In fact, not all experiments end up with "early ***α*** memory": some of them, such as 56.5 °C, 56.6 °C and 56.9 °C, instead ended with "***β*** memory". In those cases, after reaching the time of the boundary, the memory was completely erased, without any transition into early ***α*** memory. These boundaries are shown in Figure 4-18.

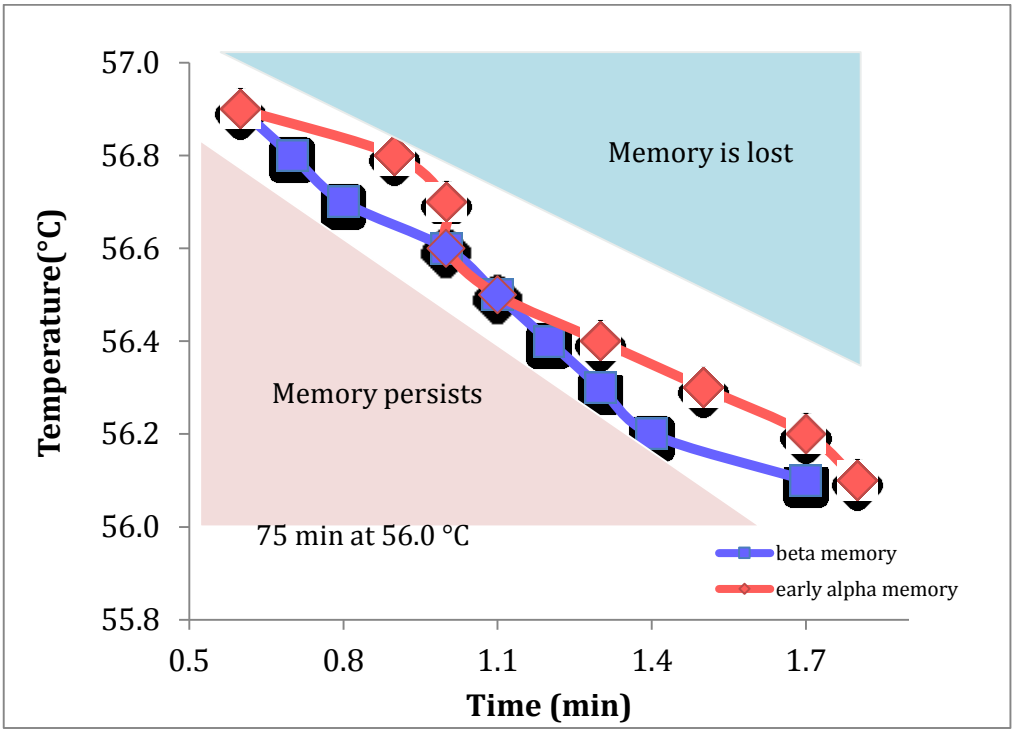

Figure 4-18. Time-temperature boundaries of two types of memory. The red points are for "early ***α*** memory", and the blue points represent the temperature and time combination of "***β*** memory".

During preliminary experiments, the ***β*** polymorph could only be melted at or above 56.0 °C. Thus, only temperatures ≥56.0 °C were used in the experiments. When the sample was held at 56.0 °C for 75 min (step "5" in Figure 4-10), it still showed "early ***α*** memory". Thus, the "early ***α*** memory" of MMM persisted for more than 75 min at that temperature. Yet, when the temperature was increased to 56.1 °C, the holding time boundary of "early ***α*** memory" suddenly dropped to 1.8 min. From there it kept decreasing with the increasing temperature up to 56.9 °C; after the temperature reached 57.0 °C, the memory effect was completely lost (Figure 4-18).

Two pans were made for each sample in order to make sure that the results of the experiments were reproducible. As shown in Figure 4-19 and Figure 4-20, the time differences between the two pans were small ($\Delta t \leq$ 0.2 s), with some of the points overlapping. A much more detailed discussion is presented below, as Figure 4-35 is discussed.

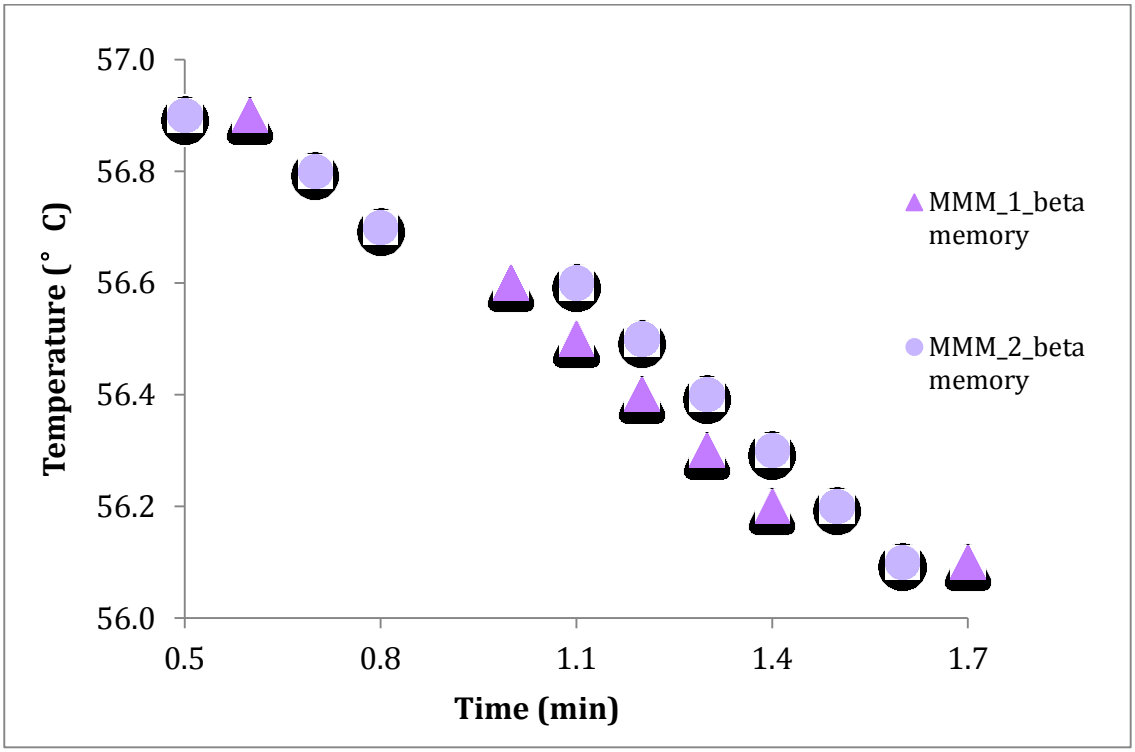

Figure 4-19. Temperature versus time plot of the "***β*** memory" of MMM_1 and MMM_2. The preliminary statistic analysis will be shown in 4.2.4.

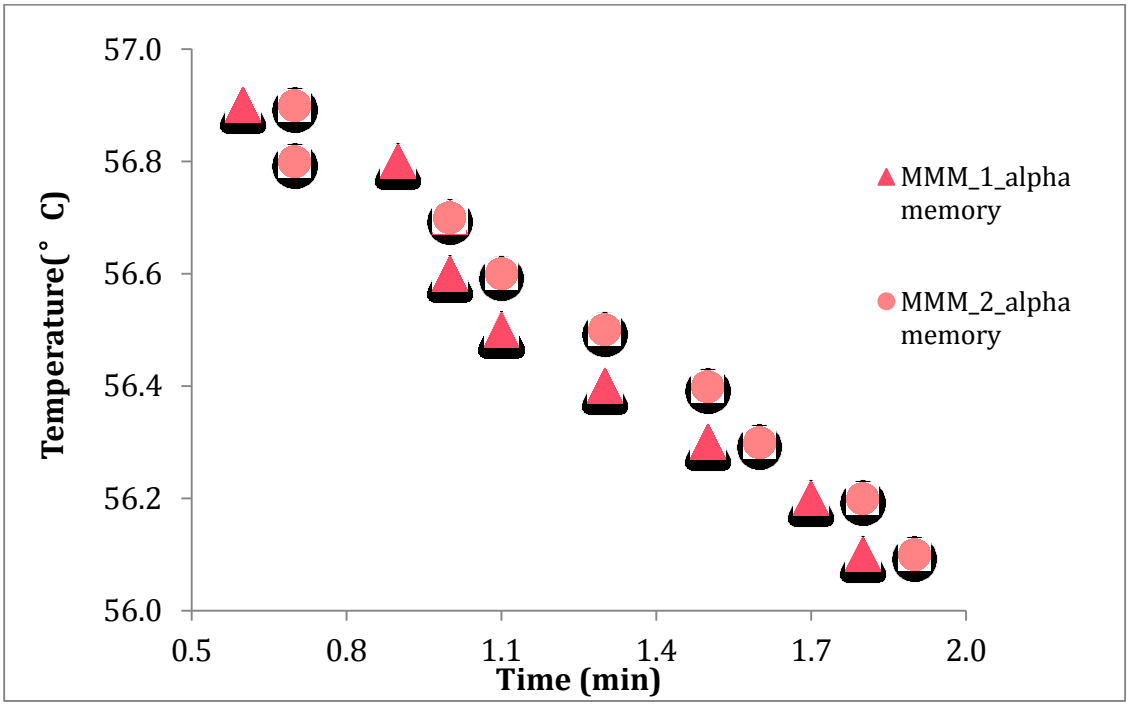

Figure 4-20. Temperature versus time plot of "early ***α*** memory" of MMM_1 and MMM_2. The preliminary statistic analysis will be shown in 4.2.4.

4.2.2 Tripalmitin boundaries

Figure 4-21 and Figure 4-22 show the DSC curves for the two types of "memory effect" in the PPP samples. In Figure 4-22, for longer times and low temperatures, both $\boldsymbol{\beta}$ and $\boldsymbol{\alpha}$ memories seem to coexist. Specifically, during cooling (step "5" in Figure 4-10), there was first a $\boldsymbol{\beta}$ recrystallization, then a small $\boldsymbol{\alpha}$ formation. Only at the longer times and higher temperatures did the "early $\boldsymbol{\alpha}$ memory" seem to be erased.

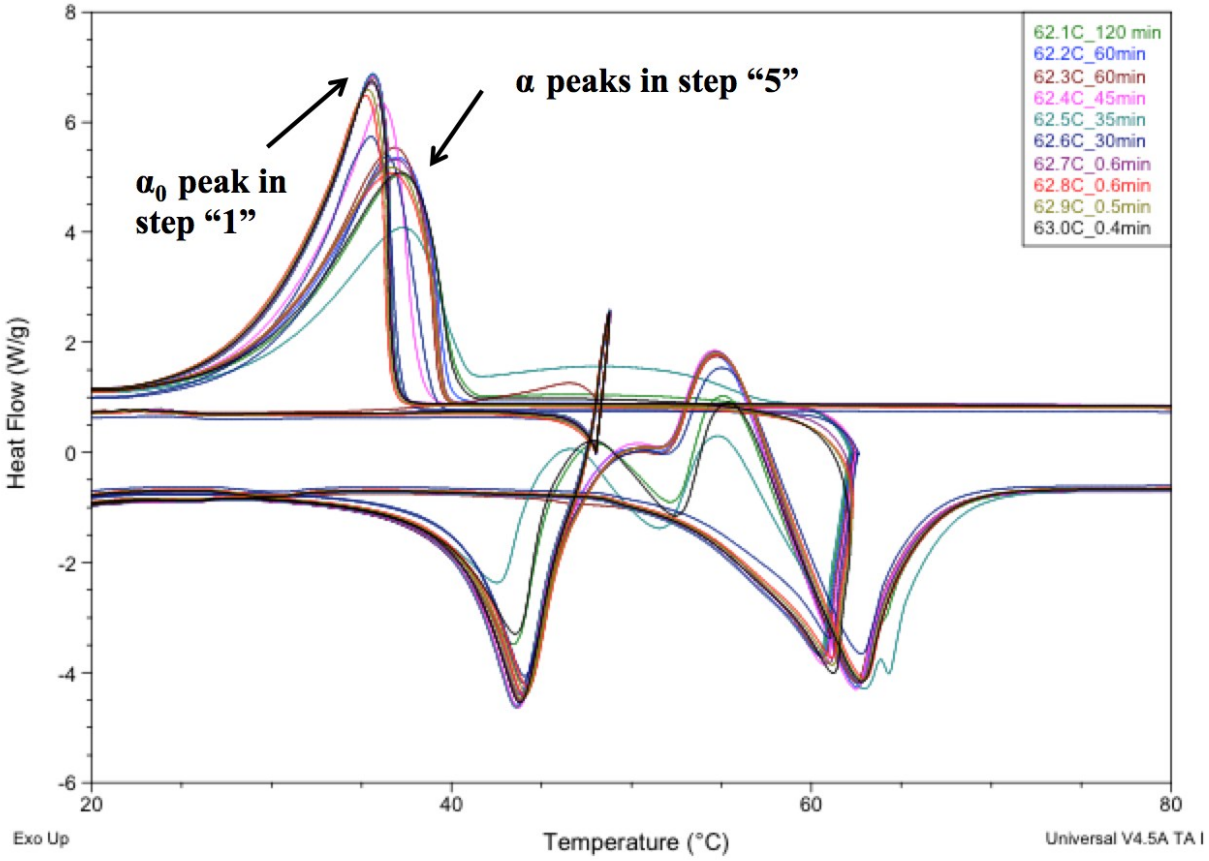

Figure 4-21. Overlay of temperature-time boundaries of "early $\boldsymbol{\alpha}$ memory" thermograms for PPP.

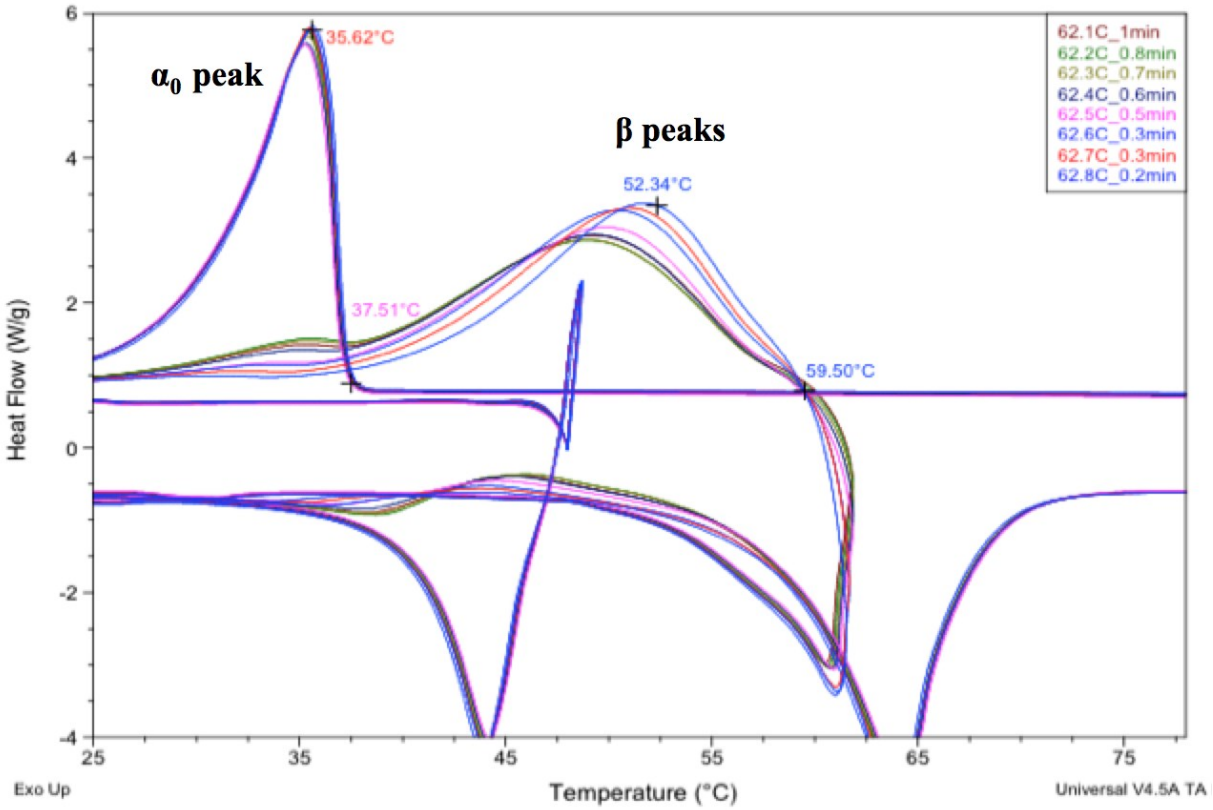

Figure 4-22. Overlaid thermograms of temperature-time boundaries of ***β*** memory for PPP.

The transformation from "***β*** memory" to "early ***α*** memory" is illustrated step-by-step in Figure 4-23 using different holding times at the same temperature of 62.7 °C in step "e". When the sample was held for 0.3 min in step "e", only the ***β*** peak appeared. As the time was extended to 0.5 min, a small ***α*** peak was seen along with the ***β*** peak. After a holding time of 0.6 min, the "***β*** memory" had been erased, and only an early ***α*** peak was observed. After holding for 0.1 min more, both memory effects were completely removed.

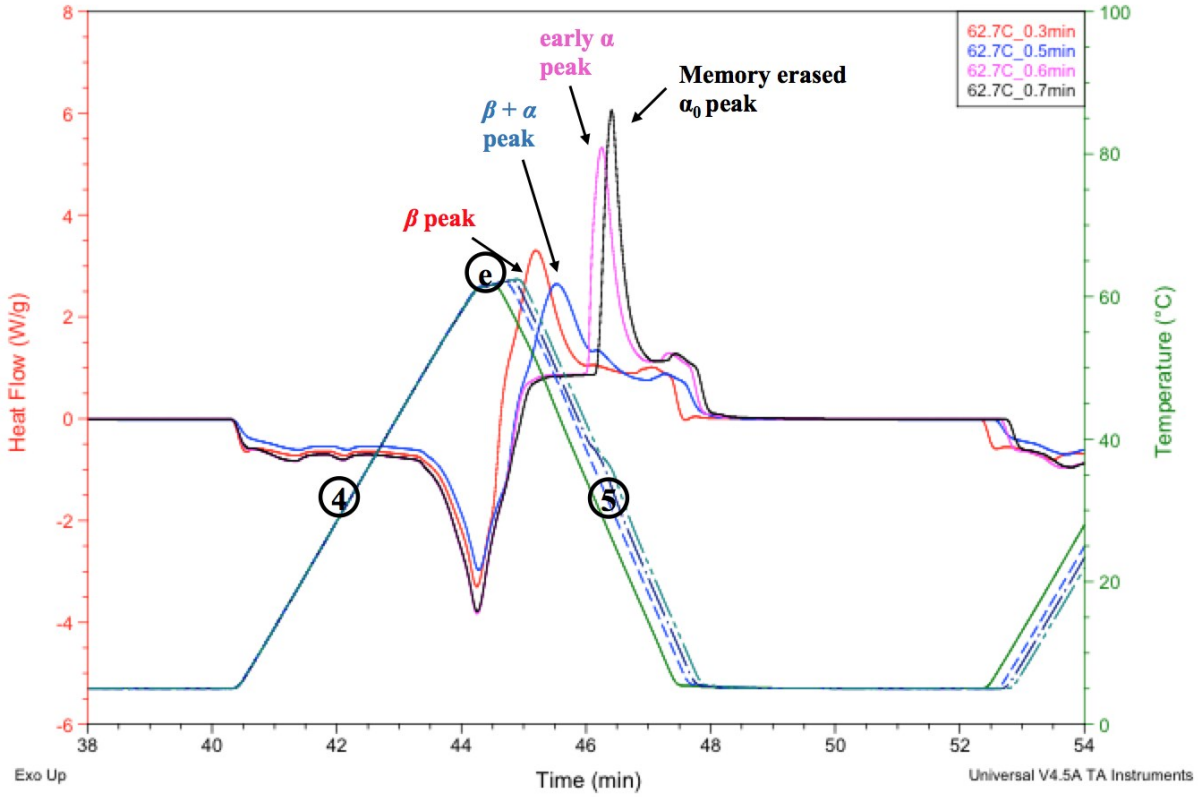

Figure 4-23. Transformation from "***β*** memory" to "early ***α*** memory" with different holding times for PPP at 62.7 °C (including steps "4", "e" and "5"). The X-axis is time, while the Y1 axis (left side) is the heat flow, and the Y2 axis (right side) is temperature.

The boundaries of two types of memory effect for PPP are shown in Table 4-3 and Table 4-4. As shown in Figure 4-24, a sharp difference appeared when the sample was heated (step "4" in Figure 4-10) above 62.7 °C. At that temperature or higher, the crystal memory was erased within just 0.6 min or less. However, at even 0.1 °C below 62.7 °C, the "memory effect" persisted for 30 min of holding time. There were clearly two different types of behavior, with a sharp transition between the two occurring between 62.6 and 62.7 °C. The times are plotted in Figure 4-24, one for the long times (a) and one for the short times (b).

Table 4-3. Time at each holding temperature (in step "e") that defined the boundary for "early ***α*** memory" of PPP. The "*α* Time_1 (min)" is the holding time boundary at holding temperature for pan 1 and "*α* Time_2 (min)" is the holding time boundary at holding temperature for pan 2.

Holding Temperature (°C)	**62.1**	**62.2**	**62.3**	**62.4**	**62.5**	**62.6**	**62.7**	**62.8**	**62.9**	**63.0**
***α* Time_1 (min)**	120	90	60	45	35	30	0.6	0.6	0.5	0.4
***α* Time_2 (min)**	120	90	60	45	37	32	0.7	0.6	0.5	0.4
***α* Time average**	120	90	60	45	36	31	0.65	0.6	0.5	0.4

Table 4-4. Time at each holding temperature (in step "e") that defined the boundary for "***β*** memory" of PPP. The "*β* Time_1 (min)" is the holding time boundary at holding temperature for pan 1 and "*β* Time_2 (min)" is the holding time boundary at holding temperature for pan 2.

Holding Temperature (°C)	**62.1**	**62.2**	**62.3**	**62.4**	**62.5**	**62.6**	**62.7**	**62.8**
***β* Time_1 (min)**	1.0	0.8	0.7	0.6	0.5	0.3	0.3	0.2
***β* Time_2 (min)**	1.2	1.0	0.9	0.7	0.6	0.4	0.3	0.2
***β* Time average**	1.1	0.9	0.8	0.65	0.55	0.35	0.3	0.2

From Figure 4-24 (a), it is clear that the "***β*** memory" can be erased with shorter time at lower holding temperatures than the "early ***α*** memory". For example, in Table 4-3, at 62.1 °C, the "early ***α*** memory" persisted even after 2h at the holding temperature, whereas the "***β*** memory" was lost after holding for only 1 min. The "***β*** memory" is thus a weaker memory that can be erased with shorter holding times and /or lower holding temperatures. Since it can be destroyed with less energy, it is safe to assume that its structure is much easier to disorder. Conversely, the "early ***α*** memory" can be assumed to be longer term, requiring longer holding times and /or higher holding temperatures to be erased. The "early ***α*** memory" of PPP was, comparatively, very hard to erase. Figure 4-25 and Figure 4-26 show the close agreement between the results obtained from both pans.

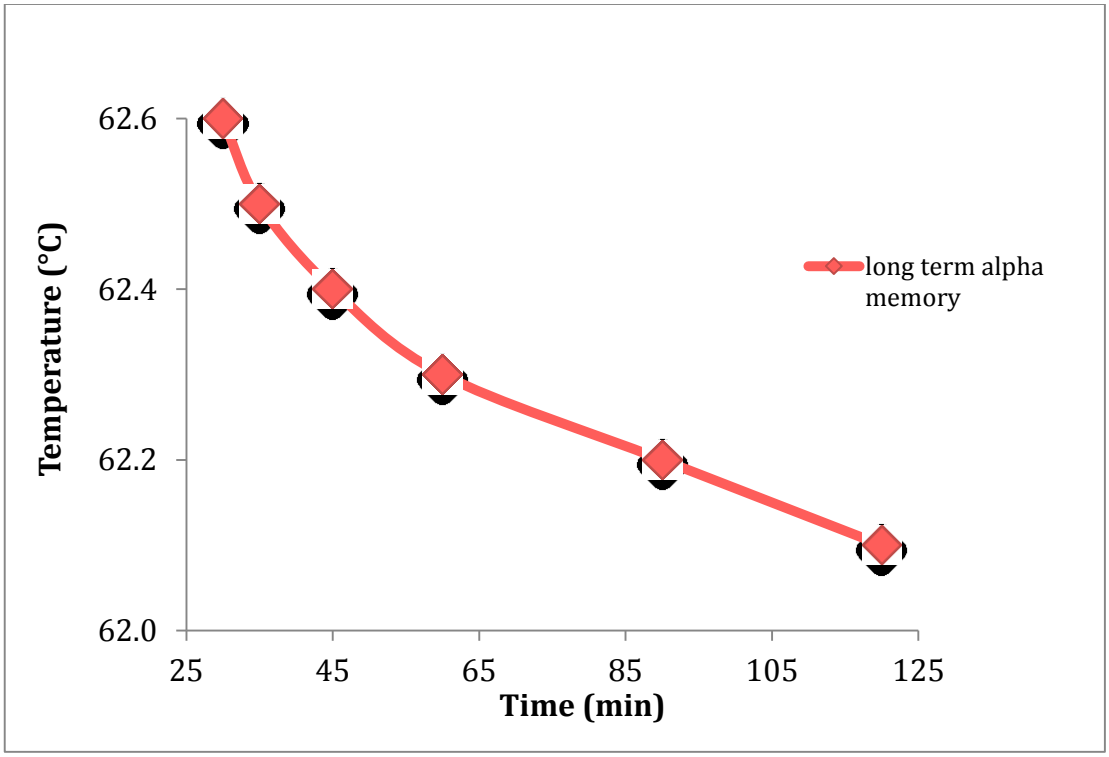

(a)

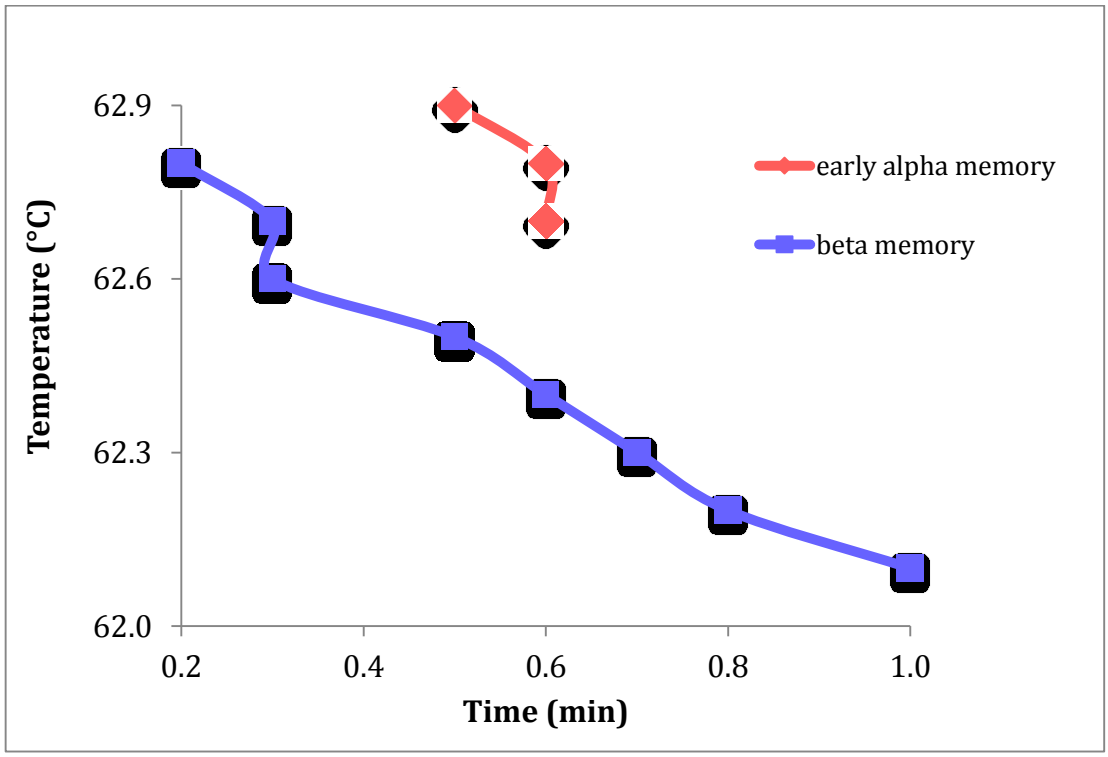

(b)

Figure 4-24. Time-temperature boundaries of PPP. (a) is the boundary of the long-term memory of "early α memory" and (b) is the boundary of short-term memory of "early α memory" (in red) and the boundary of "β memory" (in blue).

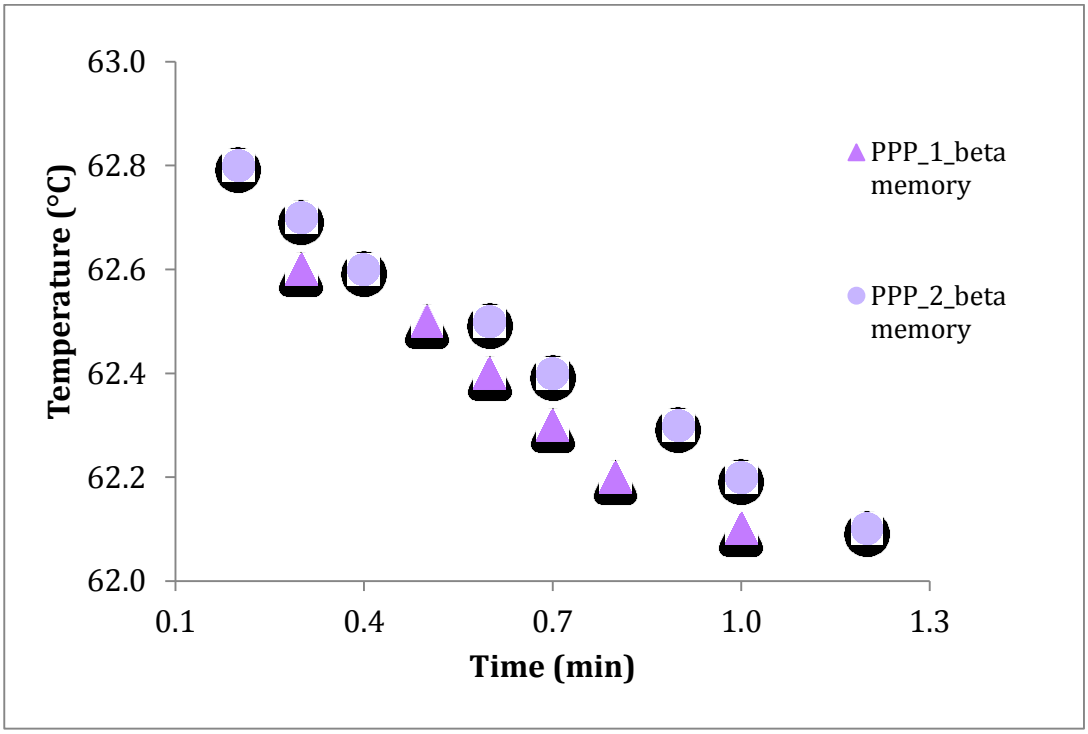

Figure 4-25. Temperature versus time plot of the "***β*** memory" for PPP_1 and PPP_2. The statistical analysis will be shown in 4.2.4.

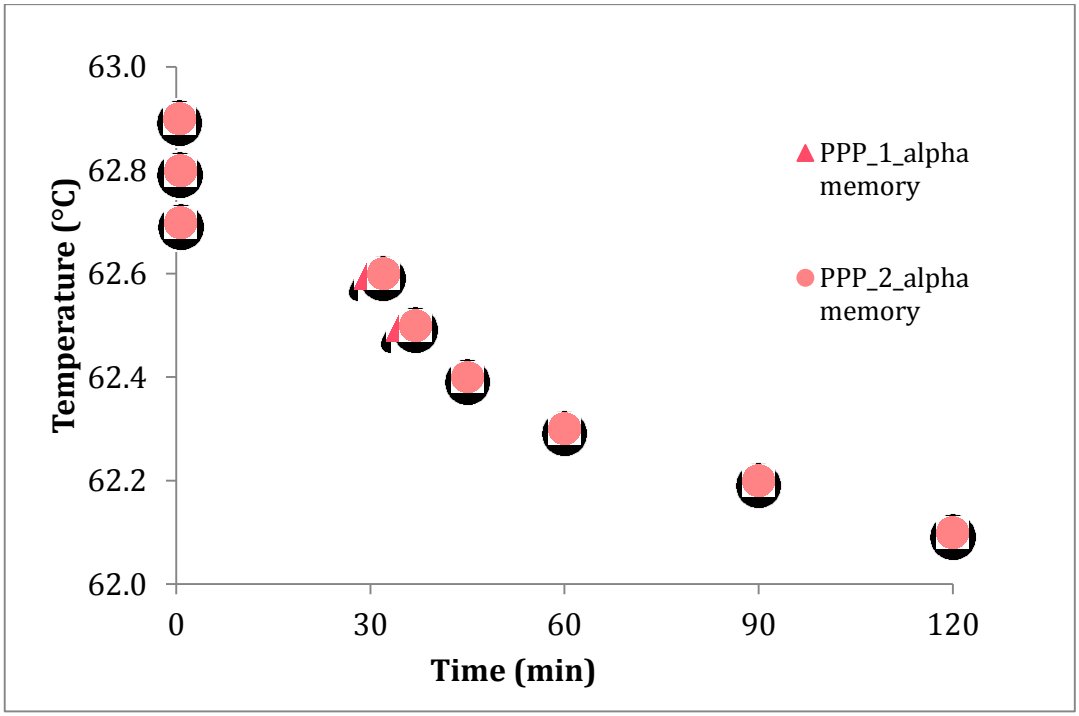

Figure 4-26. Temperature versus time plot of the "early ***α*** memory" for PPP_1 and PPP_2. The statistical analysis will be shown in 4.2.4.

4.2.3 Tristearin boundaries

As seen in Figure 4-27, the ***α*** crystallization memory peaks (in step "5") for SSS were very close to the α_0 reference peak (in step "1"), unlike those of the other two materials. It took a shorter time or lower relative holding temperatures for the transition from "***β*** memory" to "early ***α*** memory" to occur in SSS than in the other two pure TAGs. However, it took a longer time to erase the ***α*** memory. This indicates that SSS has some molecular characteristic that allows it to maintain its "early ***α*** memory" for a longer time compared to PPP and MMM. It was shown in the previous section that "early ***α*** memory" persisted in PPP much longer than in MMM.

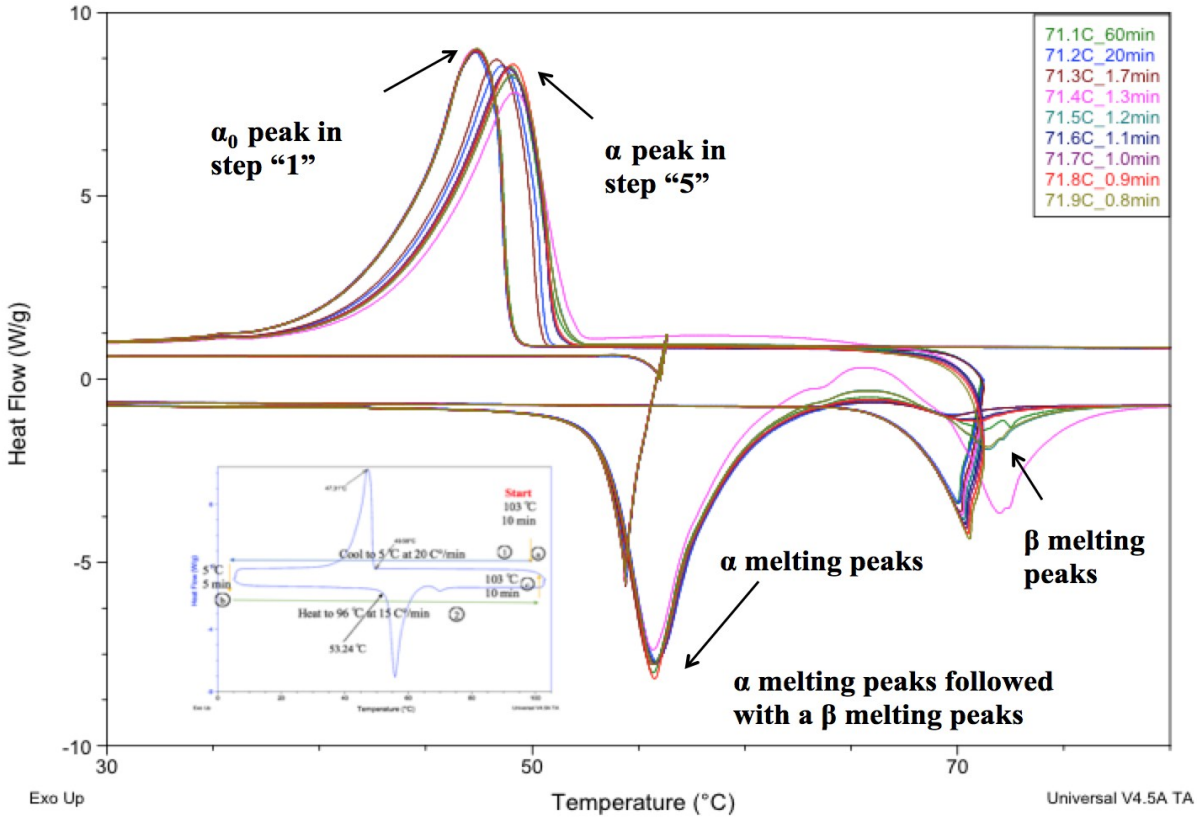

Figure 4-27. Thermograms overlay of temperature-time boundaries of "early ***α*** memory" for SSS (For step numbers and letters see Figure 4-10). Overlaid ***α*** memory peaks, close to the reference α_0 peak.

Thus, one possible hypothesis is that the structural origin of "early $\boldsymbol{\alpha}$ memory" is associated with alkyl chains, rather than with the polar glycerol core of the molecules. The "early $\boldsymbol{\alpha}$ memory" thus would require only a relative alignment of the alkyl chains, rather than a specific orientation, as required by "$\boldsymbol{\beta}$ memory". This is consistent with the ease of disruption of "$\boldsymbol{\beta}$ memory" and the persistence of "early $\boldsymbol{\alpha}$ memory" at temperatures below a critical threshold, associated with the energy between the alkyl chains.

The energy distribution in the liquid can provide an alternative explanation of why a certain level of coexistence of memory types is observed after some holding time-temperature combinations. If a liquid has structured regions, the distribution of energy between regions may be uneven, even if the average corresponds to the same temperature. Lower energy regions would keep the "$\boldsymbol{\beta}$ memory", whereas regions with higher energy, and therefore lower order, would only be able to keep "early $\boldsymbol{\alpha}$ memory".

Comparing Figure 4-27 with Figure 4-28, the differences between the two types of memory were present not only during the crystallization process (step "5" in Figure 4-10) but also during the melting process (step "6" in Figure 4-10). The formed materials were different, as evidenced by the difference in their melting peaks (step "6" in Figure 4-10). In the case of the "$\boldsymbol{\beta}$ memory", the peak was a clear simple $\boldsymbol{\beta}$ melting (Figure 4-28). However, the melting peaks (Figure 4-27) of the materials formed by recrystallization from "early $\boldsymbol{\alpha}$ memory" differed depending on the conditions of the holding time-temperature combinations. It can be surmised that the structure formed is slightly different when the holding temperatures are in the 71.3 °C to 71.7 °C range.

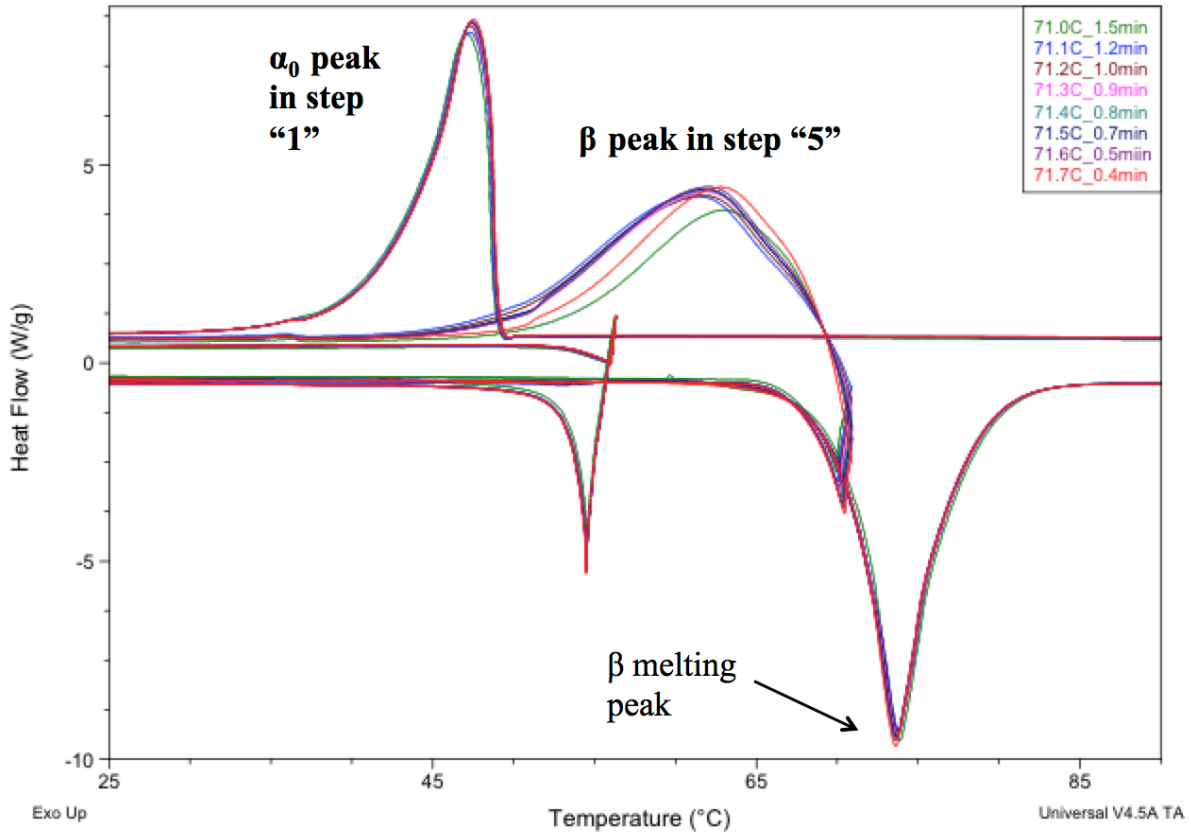

Figure 4-28. Thermograms overlay of temperature-time boundaries of ***β*** memory for SSS (For step numbers and letters see Figure 4-10). Represent the overlay of ***β*** memory peaks.

Table 4-5. Time at each holding temperature that defined the boundary for "early ***α*** memory" of SSS. The "*α* Time_1 (min)" is the holding time boundary at holding temperature for pan 1 and "*α* Time_2 (min)" is the holding time boundary at holding temperature for pan 2.

Holding Temperature (°C)	**71.0**	**71.1**	**71.2**	**71.3**	**71.4**	**71.5**	**71.6**	**71.7**	**71.8**	**71.9**
***α* Time_1 (min)**	120	60	45	1.8	1.5	1.2	1.1	1.0	0.9	0.8
***α* Time_2 (min)**	120	60	45	1.9	1.7	1.6	1.3	1.2	1.0	0.9
***α* Time average**	120	60	45	1.85	1.6	1.4	1.2	1.1	0.95	0.85

Table 4-6. Time at each holding temperature that defined the boundary for "***β*** memory" of SSS. The "*β* Time_1 (min)" is the holding time boundary at holding temperature for pan 1 and "*β* Time_2 (min)" is the holding time boundary at holding temperature for pan 2.

Holding Temperature (°C)	**71.0**	**71.1**	**71.2**	**71.3**	**71.4**	**71.5**	**71.6**	**71.7**	**71.8**	**71.9**
***β* Time_1 (min)**	1.5	1.2	1.0	0.9	0.8	0.7	0.5	0.4	-	-
***β* Time_2 (min)**	1.6	1.3	1.2	1.0	0.9	0.8	0.6	0.5	-	-
***β* Time average**	1.55	1.25	1.15	0.95	0.85	0.75	0.55	0.45	-	-

The difference of time in erasing "***β*** memory" and "early ***α*** memory" was most pronounced when the holding temperature was lower, especially near the lowest temperature at which the memory seems to be present. For example, when the system was heated up to 71.0 °C (step "4" in Figure 4-10), the time to erase "***β*** memory" was 1.5 min. At that temperature, the time to erase the "early ***α*** memory" was 120 min (step "5" in Figure 4-10).

As the temperature rises, the time difference between the two kinds of memory was reduced. Nonetheless, the time to erase ***β*** memory was always shorter than the time required for the removal of ***α*** memory, as shown in Figure 4-29.

The results from the two pans used to investigate "***β*** memory" and "early ***α*** memory" exhibit very small differences between them (Figure 4-30 and Figure 4-31). Their trends are discussed in detail in the next section.

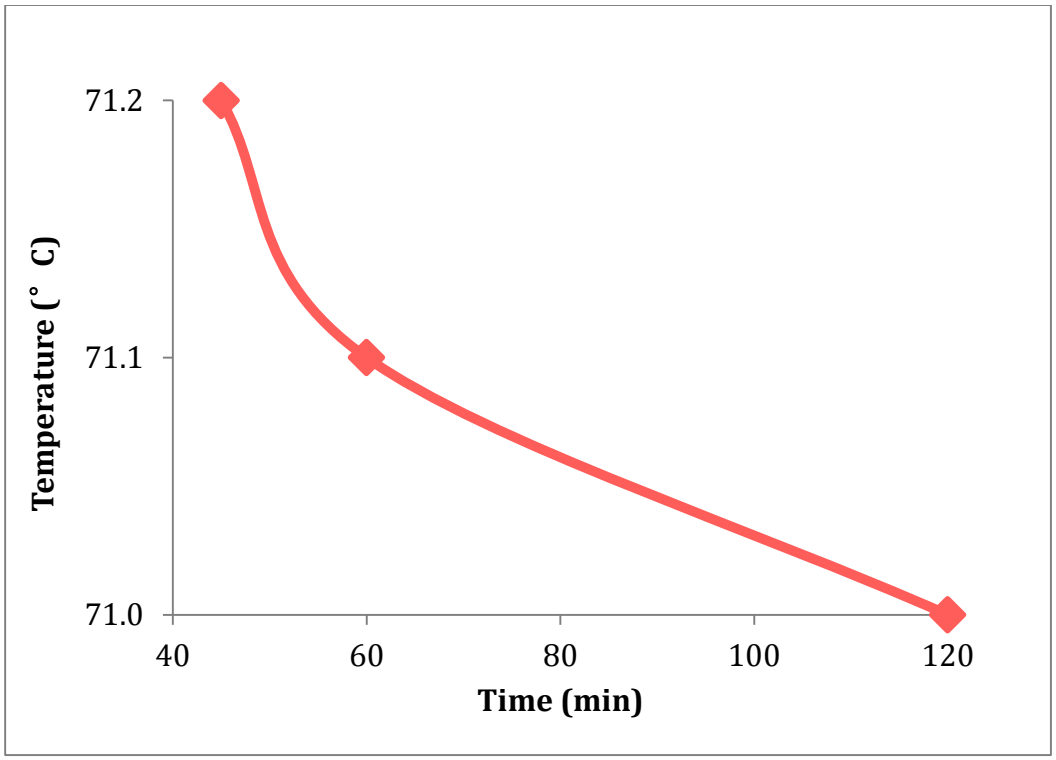

(a)

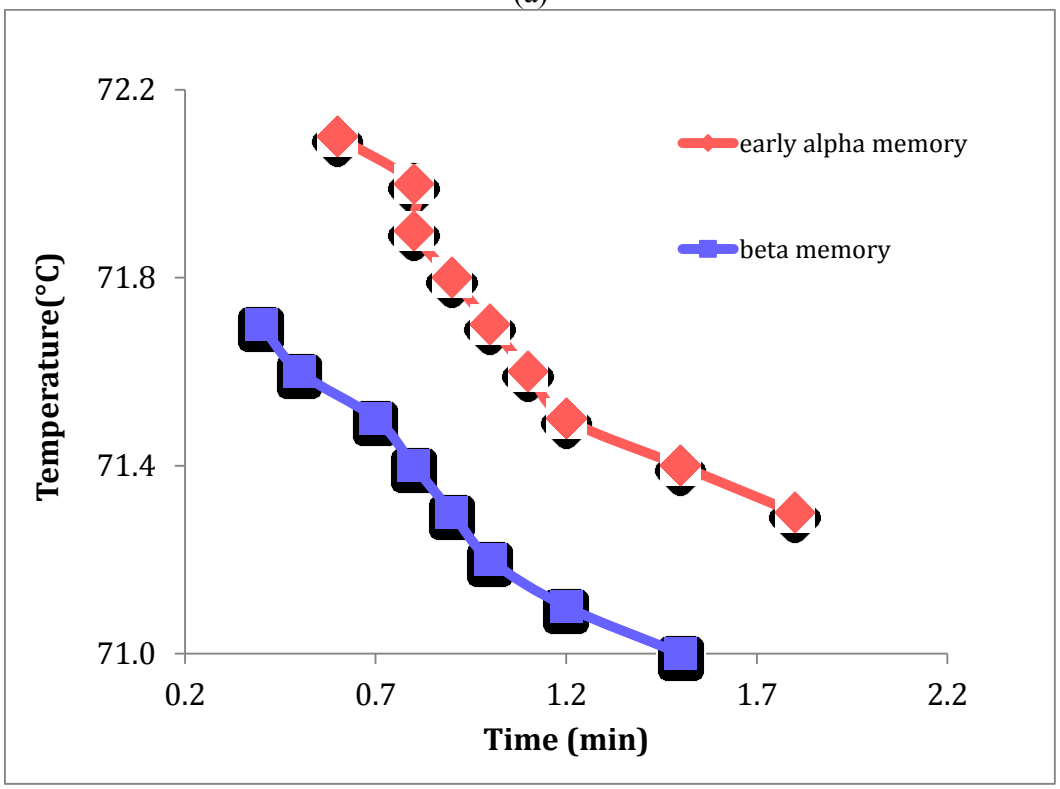

(b)

Figure 4-29. Time-temperature boundaries for memory effect of SSS. (a) is the boundary of the long-term memory of "early α memory" and (b) is the boundary of short-term memory of "early α memory" (in red) and the boundary of "β memory" (in blue).

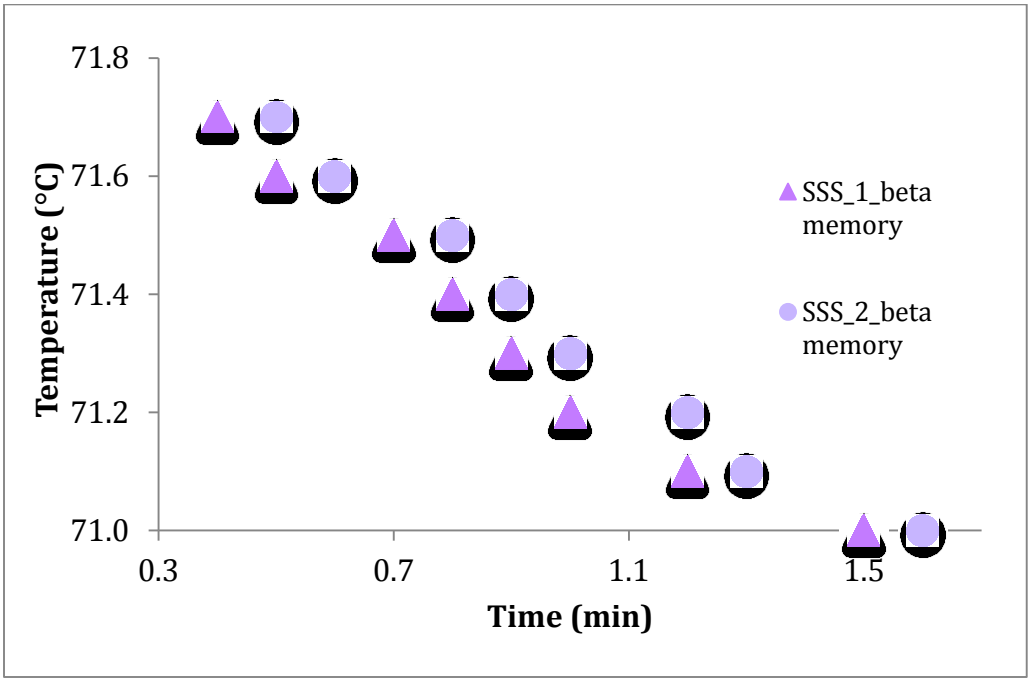

Figure 4-30. Temperature versus time plot of ***β*** memory for SSS_1 and SSS_2. The statistical analysis will be shown in 4.2.4.

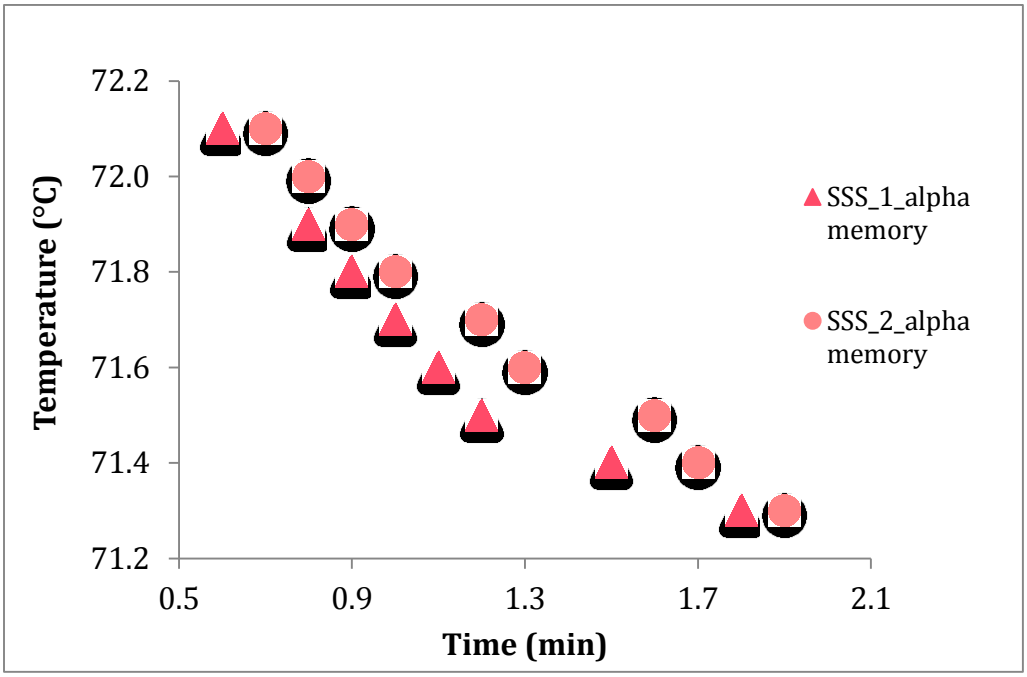

Figure 4-31. Temperature versus time plot of ***α*** memory for SSS_1 and SSS_2. The statistical analysis will be shown in 4.2.4.

4.2.4 Temperature – time boundaries of the crystal memory effect: comparative summary

Linear regression of the temperature-time data sets of the short time experiments provided reasonable estimates of the correlation between temperature and time, as seen in Figure 4-32 for MMM, in Figure 4-33 (b) and (c) for PPP, and in Figure 4-34 (b) and (c) for SSS. The linear relationship between holding temperature T_H (°C) and holding time t_H (min) was defined by a function with parameters T_{max} (intercept) and m_{st} (slope):

$$T_H = T_{\max} + m_{st} \cdot t_H$$

The values for these parameters are summarized in Table 4-7 and Table 4-8. The onset temperatures included in the plots are discussed later, in section 4.3.

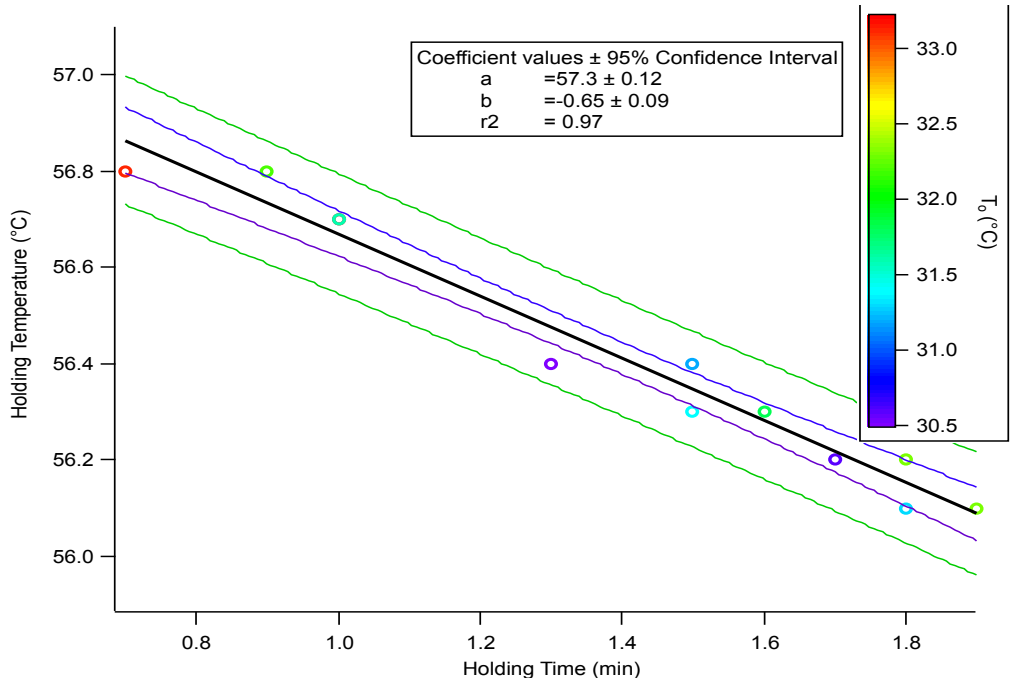

(a)

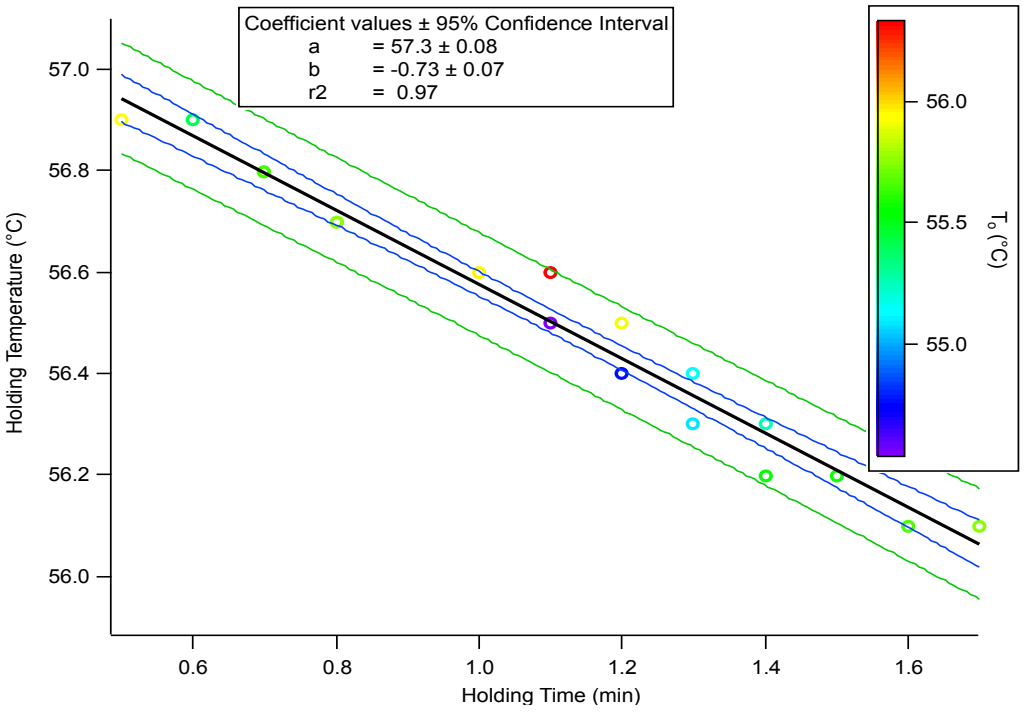

(b)

Figure 4-32. Memory boundaries for MMM. Plot of holding temperature T_H as a function of holding time t_H, showing the confidence intervals of the linear fit. The colors of the data represent the onset for (a) $\boldsymbol{T_{onset\_\alpha}}$ of "early $\boldsymbol{\alpha}$ memory" and (b) $\boldsymbol{T_{onset\_\beta}}$ of "$\boldsymbol{\beta}$ memory". The blue lines indicate the confidence intervals of the regression at 95%, whereas the green lines indicate the confidence intervals for the data at 95%. "a" in legend indicates the intercept, "b" is the slope of the line, and r2 is the coefficient of determination.

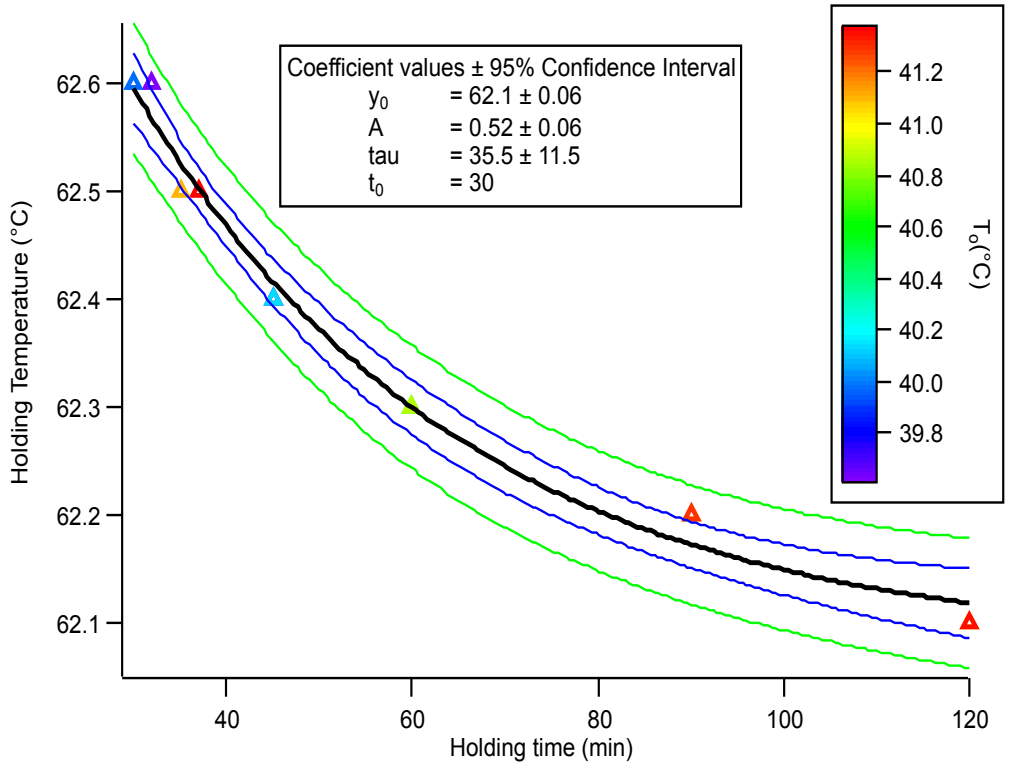
Coefficient values ± 95% Confidence Interval
y_0 = 62.1 ± 0.06
A = 0.52 ± 0.06
tau = 35.5 ± 11.5
t_0 = 30
Holding Temperature (°C)
62.6
62.5
62.4
62.3
62.2
62.1
40
60
80
100
120
Holding time (min)
41.2
41.0
40.8
40.6
40.4
40.2
40.0
39.8
T_o(°C)

(a)

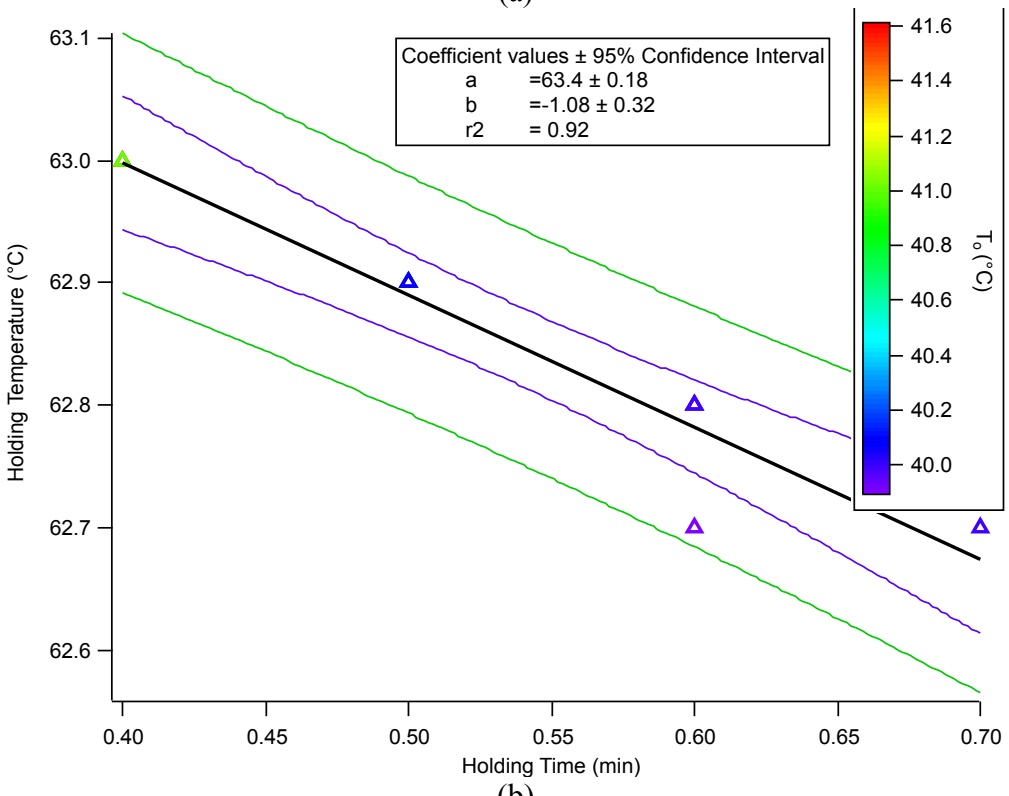
Coefficient values ± 95% Confidence Interval
a =63.4 ± 0.18
b =-1.08 ± 0.32
r2 = 0.92
Holding Temperature (°C)
63.1
63.0
62.9
62.8
62.7
62.6
0.40
0.45
0.50
0.55
0.60
0.65
0.70
Holding Time (min)
41.6
41.4
41.2
41.0
40.8
40.6
40.4
40.2
40.0
T_o (°C)

(b)

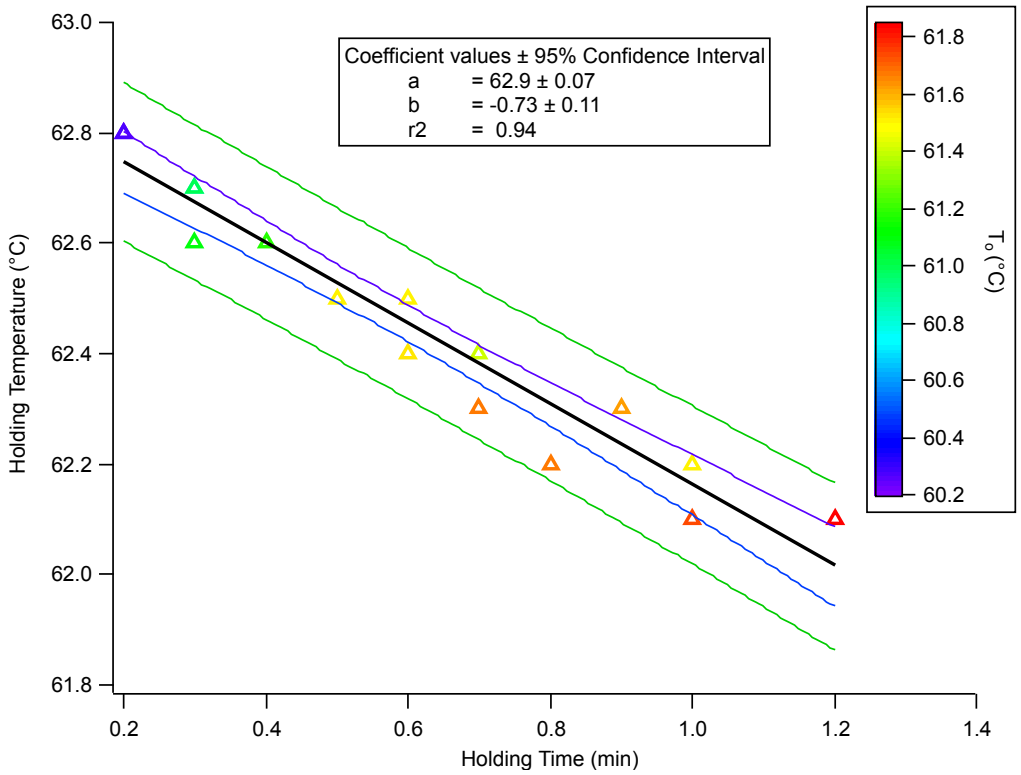

(c)

Figure 4-33. Memory boundaries for PPP. Plot of holding temperature T_H as a function of holding time t_H, showing the confidence intervals of the fit. The blue lines indicate the confidence intervals of the regression at 95%, whereas the green lines indicate the confidence intervals for the data at 95%. The colors of the data represent the onset for (a) $\boldsymbol{T_{onset\_\alpha}}$ of "early $\boldsymbol{\alpha}$ memory" with lower holding temperatures and long times, (b) $\boldsymbol{T_{onset\_\alpha}}$ of "early $\boldsymbol{\alpha}$ memory" with higher holding temperatures and short times and (c) $\boldsymbol{T_{onset\_\beta}}$ of "$\boldsymbol{\beta}$ memory. "a" in legend indicates the intercept, "b" is the slope of the line, and r2 is the coefficient of determination.

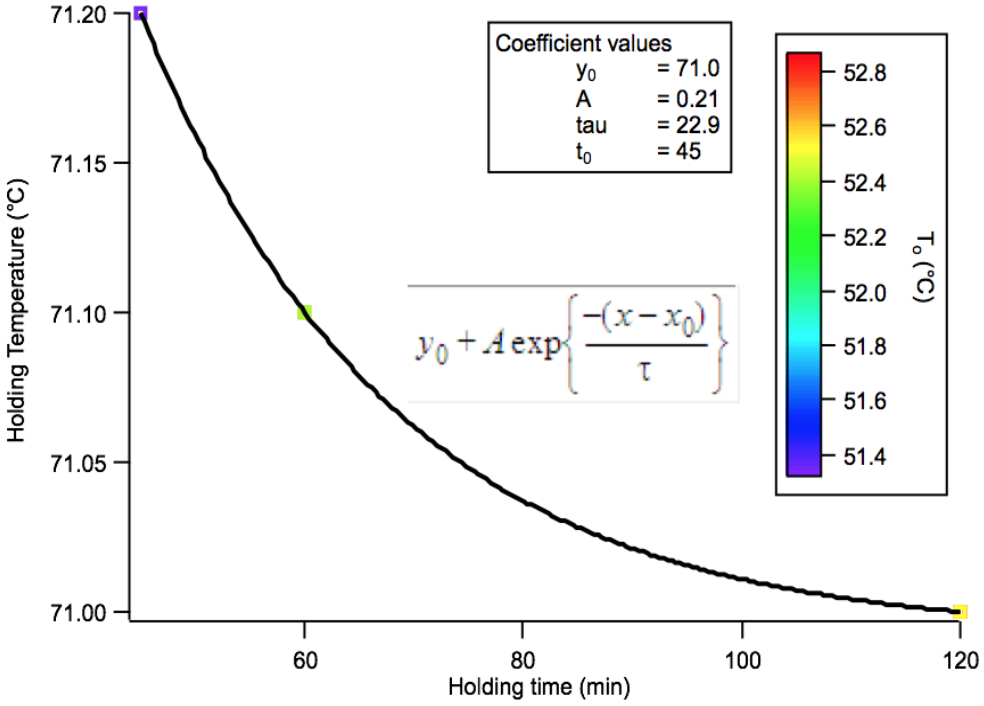
Coefficient values
y0 = 71.0
A = 0.21
tau = 22.9
t0 = 45
$y_0 + A\exp\left\{\frac{-(x-x_0)}{\tau}\right\}$
Holding Temperature (°C)
71.20
71.15
71.10
71.05
71.00
60
80
100
120
Holding time (min)
52.8
52.6
52.4
52.2
52.0
51.8
51.6
51.4
T₀ (°C)

(a)

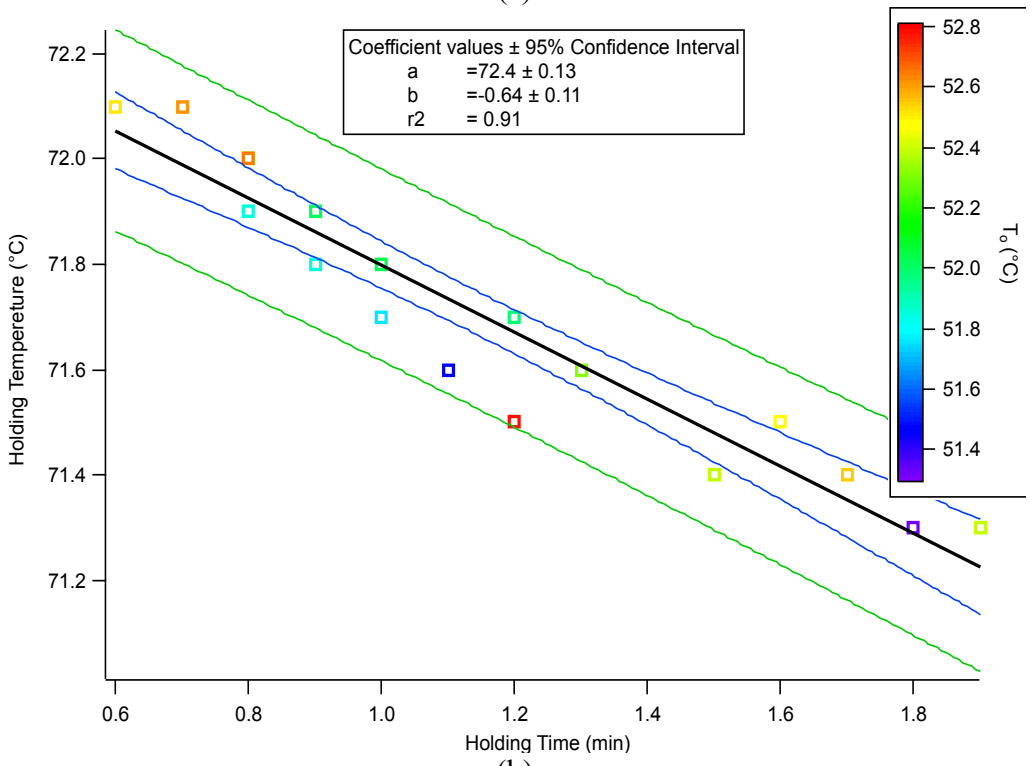
Coefficient values ± 95% Confidence Interval
a =72.4 ± 0.13
b =-0.64 ± 0.11
r2 = 0.91
Holding Tempereture (°C)
72.2
72.0
71.8
71.6
71.4
71.2
0.6
0.8
1.0
1.2
1.4
1.6
1.8
Holding Time (min)
52.8
52.6
52.4
52.2
52.0
51.8
51.6
51.4
T₀ (°C)

(b)

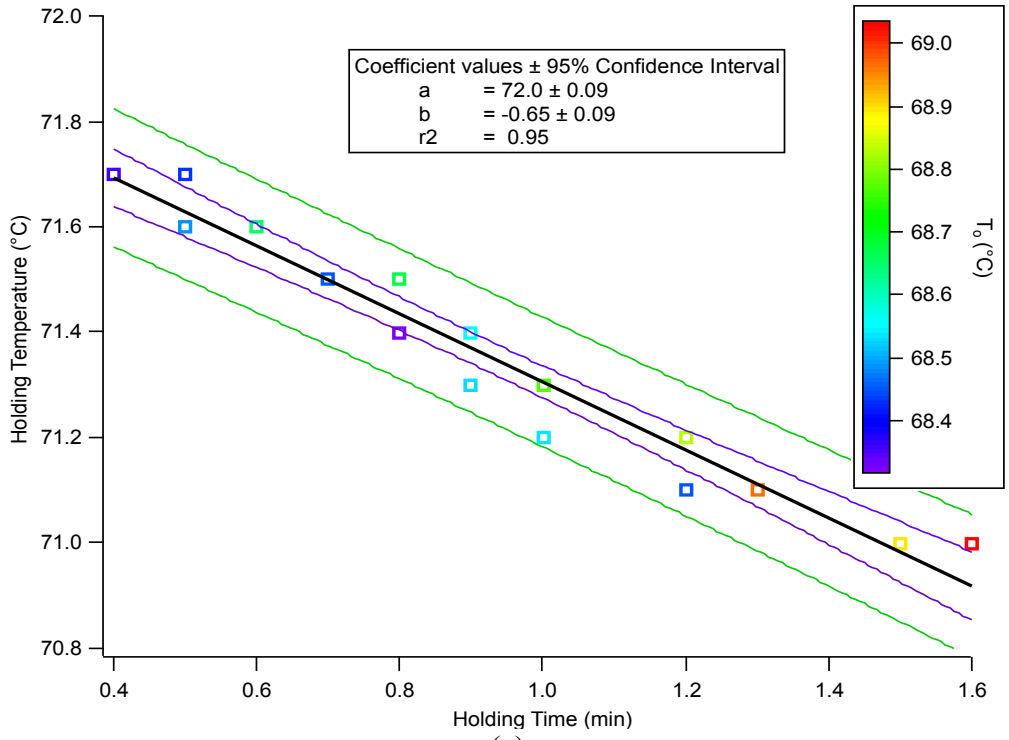

(c)

Figure 4-34. Memory boundaries for SSS. Plot of holding temperature T_H as a function of holding time t_H, showing the confidence intervals of the fit. The blue lines indicate the confidence intervals of the regression at 95%, whereas the green lines indicate the confidence intervals for the data at 95%. The colors of the data represent the onset for (a) $\boldsymbol{T_{onset\_\alpha}}$ of "early $\boldsymbol{\alpha}$ memory" with lower holding temperature, (b) $\boldsymbol{T_{onset\_\alpha}}$ of "early $\boldsymbol{\alpha}$ memory" with higher holding temperature and (c) $\boldsymbol{T_{onset\_\beta}}$ of "$\boldsymbol{\beta}$ memory". "a" in legend indicates the intercept, "b" is the slope of the line, and r2 is the coefficient of determination.

Table 4-7. Summary of linear parameters for the "$\boldsymbol{\beta}$ memory" boundaries.

Sample	**Intercept** (T_{max} °C)	±	**Slope** (m_{st} C°/min)	±
MMM	57.3	0.08	-0.73	0.07
PPP	62.9	0.07	-0.73	0.11
SSS	72.0	0.09	-0.65	0.09

Table 4-8. Summary of linear parameters for the "early $\boldsymbol{\alpha}$ memory" boundaries at high temperatures and short times.

Sample	**Intercept** (T_{max} °C)	±	**Slope** (m_{st} C°/min)	±
MMM	57.3	0.12	-0.65	0.09
PPP	63.4	0.18	-1.08	0.32
SSS	72.4	0.13	-0.64	0.11

Remarkably, the slopes of the linear fit to the short-time boundaries of the three materials were very similar for "$\boldsymbol{\beta}$ memory" and "early $\boldsymbol{\alpha}$ memory". The PPP $\boldsymbol{\alpha}$ value appears to be an outlier, as do the PPP holding temperatures.

The data for PPP (Figure 4-33 (a)) and for SSS (Figure 4-34 (a)) corresponded to experiments that required longer holding times. The data related to long-term memory were best described by the following exponential function:

$$T_H = T_{\min} + \Delta T_{sl} \cdot \exp\left(-\frac{(t_H - t_{\min})}{\tau}\right)$$

The parameters are summarized in Table 4-9. T_H is the holding temperature, T_{min} is the minimum holding temperature which holds the memory effect. ΔT_{sl} is the temperature interval between the long- term memory and the short- term memory, t_H is the holding time. The characteristic time constant τ is in minutes. The shortest time is t_{min}, at the highest temperature T_{sl} that exhibited this long time behavior.

Table 4-9. Summary of exponential parameters for the "early α memory" boundaries at low temperatures and long times.

Sample	ΔT_{sl} (C°)	T_{min} (°C)	$T_{sl} = T_{min} + \Delta T_{sl}$ (°C)	τ (min)	t_{min} (min)	t_{max} (min)
MMM β	*<0.1*	*56.0*	*56.0*	-	> 2	*75 (?)*
PPP	0.52	62.1	62.6	35.5	30	120
SSS	0.21	71.0	71.2	22.9	45	120

In experiments with MMM kept at 56.0 °C, β recrystallization occurred after keeping the material for 75 minutes. However, it is not entirely clear if the material was fully melted or not; further experiments may refine this boundary.

The temperature range, ΔT_{sl}, was very narrow in both PPP and SSS, but the times were quite long. This offers the opportunity to study this liquid state with NMR (Callaghan & Jolley, 1977; Komlosh & Callaghan, 2004) and with small angle neutron scattering, provided that a refined and precise temperature control system is in place.

4.3 Onset temperatures of recrystallization of the α and β polymorphs

The onset crystallization temperatures (T_{onset}) of α_0 were from step "1" and the other onset temperatures (T_{onset}) were from step "5" in Figure 4-35. For pure TAGs, the T_{onset} of α_0 was always lower than the T_{onset} of memory effect.

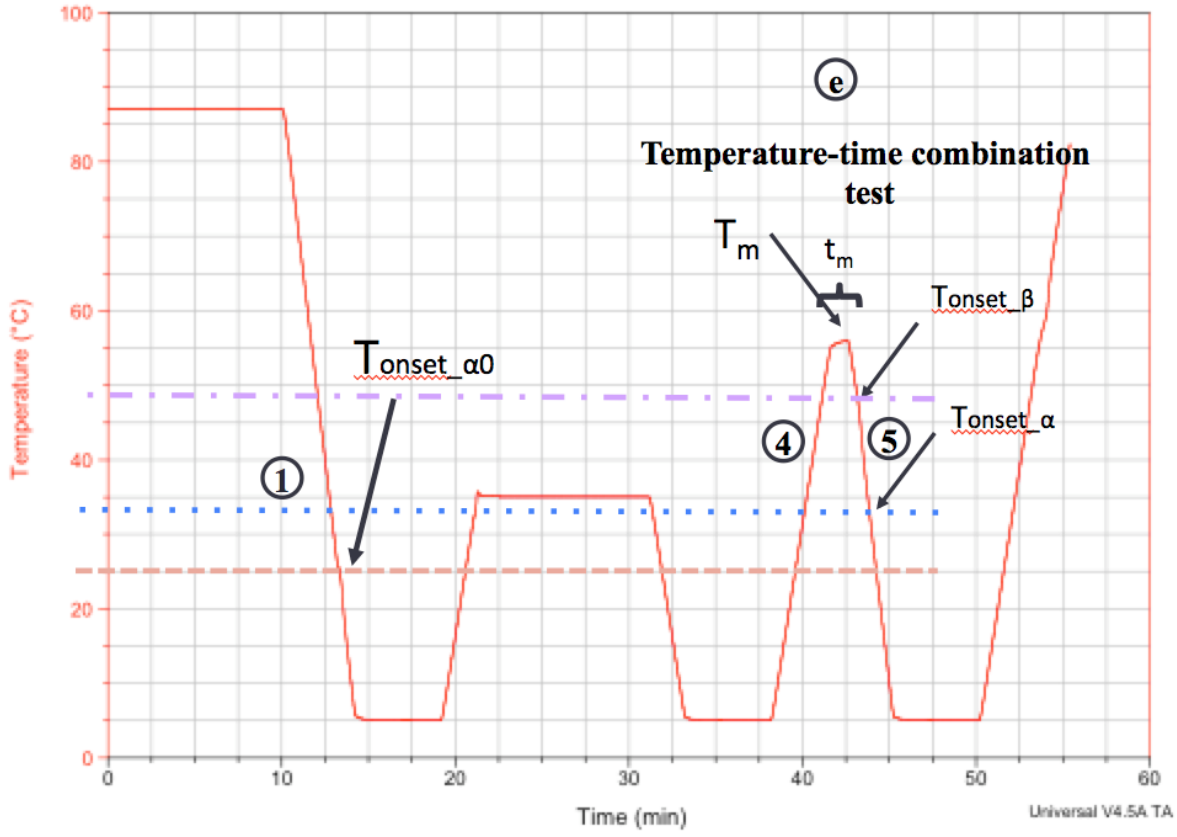

Figure 4-35. Experimental temperature - time profile showing the typical location of onset temperatures. ($\boldsymbol{T_{onset\_\alpha 0}}$ was lower than the other onset temperatures.)

4.3.1 Trimyristin onsets

Table 4-10 summarizes the reference onset temperatures (T_{onset}) in step "1" of $\boldsymbol{\alpha_0}$. Triplicate tests were done for each pan and two pans were made for each sample (As we mentioned in Chapter 3). The average T_{onset} values of $\boldsymbol{\alpha_0}$ were 26.3 ± 0.08 °C for pan 1 and 27.1 ± 0.07 °C for pan 2.

Table 4-10. Summary of the onset temperature ($T_{onset\_\alpha 0}$) during formation of $\boldsymbol{\alpha}$ polymorph of MMM from the amnesiac liquid.

Test	1	2	3	Average
$\mathbf{T_{onset\_\alpha 0}\_1}$ **(°C)**	26.41	26.22	26.32	**26.32**
$\mathbf{T_{onset\_\alpha 0}\_2}$ **(°C)**	27.04	27.22	27.14	**27.13**

As shown in Figure 4-35, $T_{onset\_\alpha 0}$ was the onset temperature of the first crystallization (step "1" in Figure 4-35). During step "e" in Figure 4-35, we programmed the holding temperature T_H and holding time t_H. When we recrystallized the sample after the temperature-time combination test (step "5"), we observed T_{onset_α} and T_{onset_β}.

Table 4-11 summarizes the onset temperatures of the crystallization (in step "5") of "early $\boldsymbol{\alpha}$ memory" (T_{onset_α}) in orange characters, and the onset temperatures of the crystallization (in step "5") of "$\boldsymbol{\beta}$ memory" (T_{onset_β}) in black characters. Each sample has two values, representing each of the two pans.

Table 4-11. Summary of the onset temperatures of recrystallization of "early $\boldsymbol{\alpha}$ memory" (T_{onset_α}) and the onset temperatures of recrystallization of "$\boldsymbol{\beta}$ memory" (T_{onset_β}) for MMM, as a function of the holding temperature. The onset temperatures of the crystallization (in step "5") of "early $\boldsymbol{\alpha}$ memory" (T_{onset_α}) are in orange characters, and the onset temperatures of the crystallization of "$\boldsymbol{\beta}$ memory" (T_{onset_β}) are in black characters.

Holding Temperature (°C)	56.1	56.2	56.3	56.4	56.5	56.6	56.7	56.8	56.9
$\mathbf{T_{onset\_\alpha}\_1}$ **(°C)**	31.26	30.63	31.44	30.54	-	-	31.56	32.21	-
$\mathbf{T_{onset\_\alpha}\_2}$ **(°C)**	32.33	32.26	31.82	31.23	-	-	33.21	33.13	-
$\mathbf{T_{onset\_\beta}\_1}$ **(°C)**	55.74	55.54	55.08	54.76	54.54	55.95	55.74	55.63	55.41
$\mathbf{T_{onset\_\beta}\_2}$ **(°C)**	55.65	55.56	55.24	55.11	55.91	56.32	55.81	55.74	55.94

T_{onset_α} and T_{onset_β} were plotted as a function of holding time in Figure 4-32. The color bar indicates range of the onset temperature during recrystallization, and the color of each circle represents the

onset temperature. A linear regression analysis of the temperature-time boundary is shown in Figure 4-32, Figure 4-33 (b and c) and Figure 4-34 (b and c). The blue lines indicate the confidence intervals of the regression at 95%, whereas the green lines indicate the confidence intervals for the data at 95%.

We calculated the difference between the average $T_{onset\_\alpha 0}$ and T_{onset_α}, and named it ΔT_{α}. The difference between the average $T_{onset\_\alpha 0}$ and T_{onset_β} was named $\Delta T_{\alpha\beta}$. Thus, the average $T_{onset\_\alpha 0}$ temperatures were used as a reference to compare the onsets of crystallization from the different experiments. These relative onset temperature differences were calculated for each pan.

Table 4-12 summarizes the average differences between $T_{onset\_\alpha 0}$ and T_{onset_α}, (ΔT_{α}), and the differences between $T_{onset\_\alpha 0}$ and T_{onset_β}, ($\Delta T_{\alpha\beta}$). The red characters show the differences between the onset temperatures of α and the onset temperatures of α_0, ΔT_{α}_1 and ΔT_{α}_2, respectively. In the other cells, the differences between the onset temperatures of β and the onset temperatures of α_0, $\Delta T_{\alpha\beta}\_1$ and $\Delta T_{\alpha\beta}\_2$, are displayed in blue characters.

Table 4-12. Summary of the differences between $T_{onset\_\alpha 0}$ and T_{onset_α} (ΔT_{α}) and the differences between $T_{onset\_\alpha 0}$ and T_{onset_β} ($\Delta T_{\alpha\beta}$) of MMM. The ΔT_{α} is present in red characters and $\Delta T_{\alpha\beta}$ is present in blue characters.

Holding Temperature (°C)	56.1	56.2	56.3	56.4	56.5	56.6	56.7	56.8	56.9
$\Delta T\alpha\_1$ (C°)	4.94	4.31	5.12	4.22	-	-	5.24	5.89	-
$\Delta T\alpha\_2$ (C°)	5.20	5.13	4.69	4.10	-	-	6.08	6.00	-
$\Delta T\alpha\beta\_1$ (C°)	29.42	29.22	28.76	28.44	28.22	29.63	29.42	29.31	29.09
$\Delta T\alpha\beta\_2$ (C°)	28.52	28.43	28.11	27.98	28.78	29.19	28.68	28.61	28.81

The ΔT data in Table 4-12 are plotted in Figure 4-36, (a) for ΔT_{α} and (b) for $\Delta T_{\alpha\beta}$, as a function of the holding temperature. In both cases, values were grouped into two clusters, below and above ~56.55 °C. In the case of ΔT_{α} below 56.5 °C the onset temperature difference decreased as the

holding temperature increases (holding time decreases). The points at 56.7 °C and 56.8 °C were higher, but a trend is not clear.

For $\Delta T_{\alpha\beta}$, the onset temperature decreased within each cluster with the increase of the holding temperature (and its corresponding time decrease). As with holding temperature above 56.5 °C, the onset temperature exhibited a sharp jump before decreasing again at higher holding temperatures. The sharp boundary at 56.55 °C suggests a change in the underlying process of molecular organization in the liquid. Further research should be done around this point using the NMR methods described by Callaghan (1977), as well as small angle neutron scattering experiments. The differences observed between the two pans point to the need of performing a larger number of replicates for future experiments.

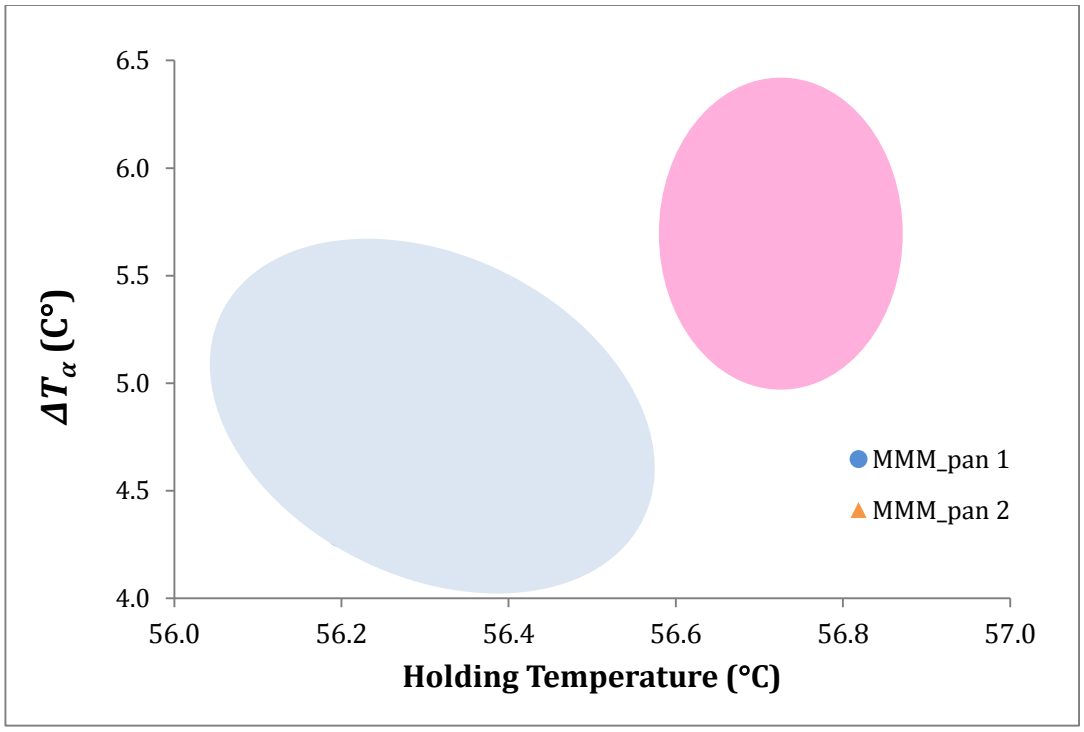

(a)

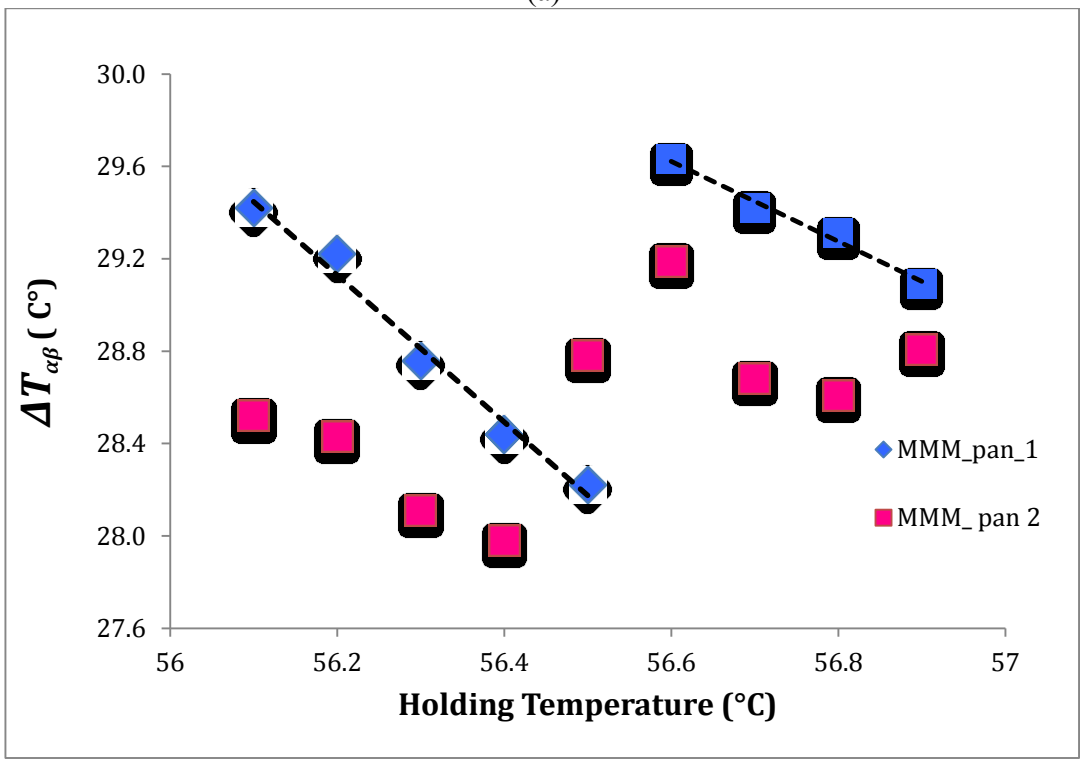

(b)

Figure 4-36. Onset temperature differences for MMM as a function of the holding temperature for the two pans studied. (a) α onsets (b) β onsets.

4.3.2 Tripalmitin onsets

Table 4-13 shows T_{onset} of α_0 for the three replicates for each pan of PPP. The average T_{onset} values were 37.4 ± 0.04 °C for pan_1 and 36.9 ± 0.17 °C for pan_2. These average values were used in the calculation of ΔT_{α} and $\Delta T_{\alpha\beta}$.

Table 4-13. Summary of the onset temperature ($T_{onset\_\alpha 0}$) during formation of α polymorph (step "1") of PPP.

Test	1	2	3	Average
$T_{onset_\alpha 0}$_1 (°C)	37.33	37.43	37.41	**37.39**
$T_{onset_\alpha 0}$_2 (°C)	36.68	37.11	36.89	**36.89**

The plots in Figure 4-33, based on the data from Table 4-1, Table 4-2 and Table 4-14. For low temperatures, the times needed to erase "early α memory" were long and appeared to increase exponentially with decreasing temperature (Figure 4-33 (a)). The fitted curve has a temperature of 62.62 °C and a time of 30 min at the origin. It decays asymptotically to a temperature of 62.1 °C as time becomes very large. This gives us an approximate range of time-temperature combinations needed to erase "early α memory" below 62.6 °C. Above this temperature, the relationship for "early α memory" between holding temperature and time for the other materials was linear.

Table 4-14. Onset temperatures of crystallization of "early α memory" (T_{onset_α}) and onset temperatures of the crystallization of "β memory" (T_{onset_β}) of PPP, at a variety of holding temperatures. The onset temperatures of the crystallization (in step "5") of "early α memory" (T_{onset_α}) are in orange characters, and the onset temperatures of the crystallization of "β memory" (T_{onset_β}) are in black characters.

Holding Temperature (°C)	**62.1**	**62.2**	**62.3**	**62.4**	**62.5**	**62.6**	**62.7**	**62.8**	**62.9**	**63.0**
T_{onset_α}_1 (°C)	41.33	41.28	40.87	40.14	41.09	39.98	39.94	39.99	40.05	40.96
T_{onset_α}_2 (°C)	41.03	41.14	40.49	39.84	41.36	39.62	39.95	39.95	39.95	41.58
T_{onset_β}_1 (°C)	61.73	61.67	61.66	61.62	61.50	61.09	60.99	60.28	-	-
T_{onset_β}_2 (°C)	61.84	61.51	61.62	61.4	61.51	61.18	60.75	60.20	-	-

Thus, even though Figure 4-33 (b) only contains four points of short holding times (t_H), we fitted a straight line to the data. The boundaries of the time-temperature combinations needed to erase the "β memory" are plotted in Figure 4-33 (c). The points follow a linear relationship. Higher holding temperatures required shorter holding times, as well as higher onset crystallization temperatures. Hence, the color distribution of the onset temperatures of PPP in Figure 4-33 (b) is regularly distributed.

Table 4-15. Summary of the differences between $T_{onset\_\alpha 0}$ and T_{onset_α} (ΔT_α) and the differences between $T_{onset\_\alpha 0}$ and T_{onset_β} ($\Delta T_{\alpha\beta}$) of PPP.

Holding Temperature (°C)	**62.1**	**62.2**	**62.3**	**62.4**	**62.5**	**62.6**	**62.7**	**62.8**	**62.9**	**63.0**
ΔT_{α}_1 (C°)	3.94	3.89	3.48	2.75	3.70	2.59	2.55	2.60	2.66	3.67
ΔT_{α}_2 (C°)	4.14	4.25	3.60	2.95	4.47	2.73	3.06	3.06	3.06	4.69
$\Delta T_{\alpha\beta}$_1 (C°)	24.34	24.28	24.27	24.13	24.11	23.70	23.60	22.89	-	-
$\Delta T_{\alpha\beta}$_2 (C°)	24.95	24.62	24.73	24.51	24.62	24.29	23.86	23.31	-	-

The onset temperatures followed two linear trends, transitioning from one to the other at 62.5 °C. The sharp jump observed in the onset temperatures of MMM was not seen in PPP. However, it seems that PPP also exhibited a "two regime" behavior, as seen in Figure 4-37.

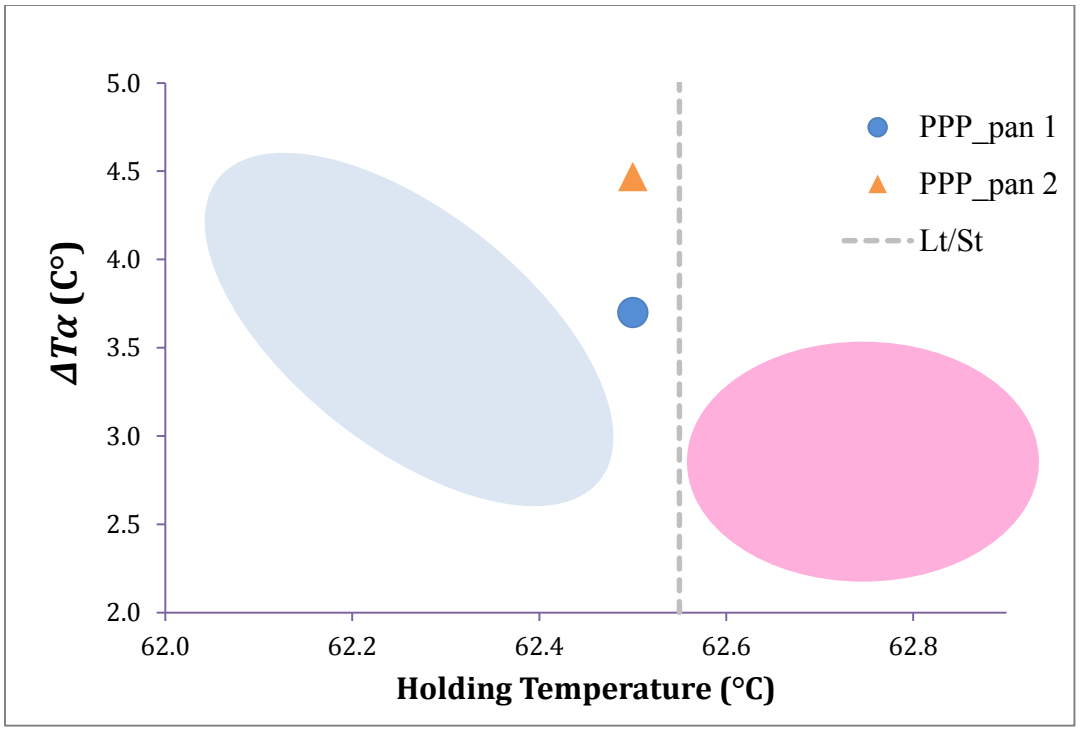

(a)

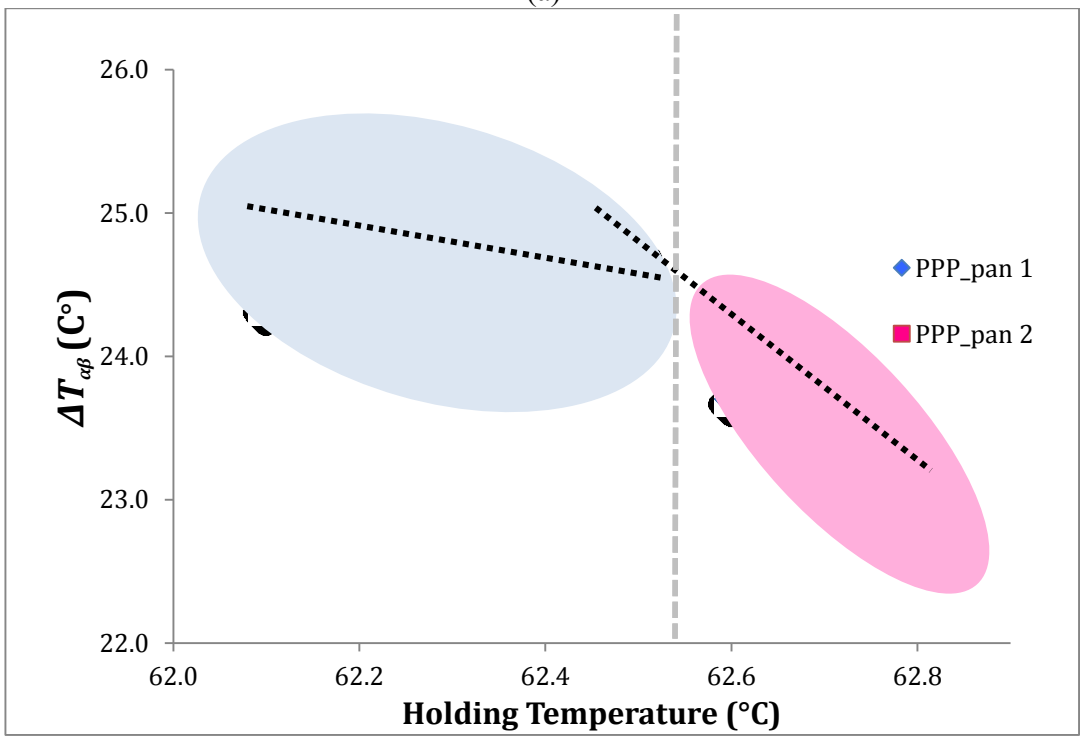

(b)

Figure 4-37. Onset temperature differences for PPP as a function of the holding temperature for the two pans studied. (a) α onsets (b) β onsets. Lines are for visual aid only.

4.3.3 Tristearin onsets

Table 4-16 shows the T_{onset} of α_0. As with the other materials, three replicates were done for each pan. The average T_{onset} values of α_0 were 49.2 ± 0.09 °C for pan 1 and 49.5 ± 0.12 °C for pan 2. These average values were used in the calculation of ΔT_{α} and $\Delta T_{\alpha\beta}$.

Table 4-16. Summary of the onset temperature ($T_{onset\_\alpha 0}$) during formation of α polymorph of SSS.

Test	1	2	3	Average
$T_{onset_\alpha 0}$_1 (°C)	49.11	49.34	49.22	**49.22**
$T_{onset_\alpha 0}$_2 (°C)	49.56	49.33	49.62	**49.50**

The data in Table 4-17 were plotted in Figure 4-34. As seen in panel (b), the colors of the symbols, representing temperature, did not follow a clear trend as a function of time. However, the relationship between onset temperature and the melting temperature in panel (c) did follow a trend: higher holding temperature resulted in higher onset recrystallization temperature.

Table 4-17. Summary of the onset temperatures of the crystallization of "early α memory" (T_{onset_α}) and the onset temperatures of the crystallization of "β memory" (T_{onset_β}) of SSS, as a function of the holding temperature. The onset temperatures of the crystallization (in step "5") of "early α memory" (T_{onset_α}) are in orange characters, and the onset temperatures of the crystallization of "β memory" (T_{onset_β}) are in black characters.

Holding Temperature (°C)	71.0	71.1	71.2	71.3	71.4	71.5	71.6	71.7	71.8	71.9
T_{onset_α}_1 (°C)	52.51	52.38	51.33	51.32	52.38	52.77	51.46	51.76	51.85	51.85
T_{onset_α}_2 (°C)	52.85	52.67	52.41	52.38	52.53	52.46	52.31	51.98	52.03	52.01
T_{onset_β}_1 (°C)	68.89	68.45	68.54	68.53	68.32	68.45	68.49	68.36	-	-
T_{onset_β}_2 (°C)	69.03	68.96	68.86	68.77	68.55	68.67	68.65	68.43	-	-

Table 4-18. Summary of the differences between $T_{onset\_\alpha 0}$ and T_{onset_α} (ΔT_α) and the differences between $T_{onset\_\alpha 0}$ and T_{onset_β} ($\Delta T_{\alpha\beta}$) of SSS. The ΔT_α is present in red characters and $\Delta T_{\alpha\beta}$ is present in blue characters.

Holding Temperature (°C)	**71.0**	**71.1**	**71.2**	**71.3**	**71.4**	**71.5**	**71.6**	**71.7**	**71.8**	**71.9**
ΔT_{α}_1 (C°)	3.29	3.16	2.11	2.10	3.16	3.55	2.24	2.54	2.63	2.63
ΔT_{α}_2 (C°)	3.35	3.17	2.91	2.88	3.03	2.96	2.81	2.48	2.53	2.51
$\Delta T_{\alpha\beta}\_1$ (C°)	19.67	19.23	19.32	19.31	19.10	19.23	19.27	19.14	-	-
$\Delta T_{\alpha\beta}\_2$ (C°)	19.53	19.46	19.33	19.27	19.05	19.17	19.15	18.93	-	-

The relative onset temperatures are plotted in Figure 4-38 for $\boldsymbol{\alpha}$ (panel a) and $\boldsymbol{\beta}$ (panel b). The ΔT_α onsets are divided into two groups: the low temperature group belongs to the long time memory experiments, while the high temperature group corresponds to the short time experiments. It will be necessary to perform more replicates before any trend can be identified with certainty. The values of $\Delta T_{\alpha\beta}$, plotted in panel b, on the other hand, followed two trends, transitioning from one to the other at 71.4 °C. A sharp jump was observed in the onset temperatures of MMM.

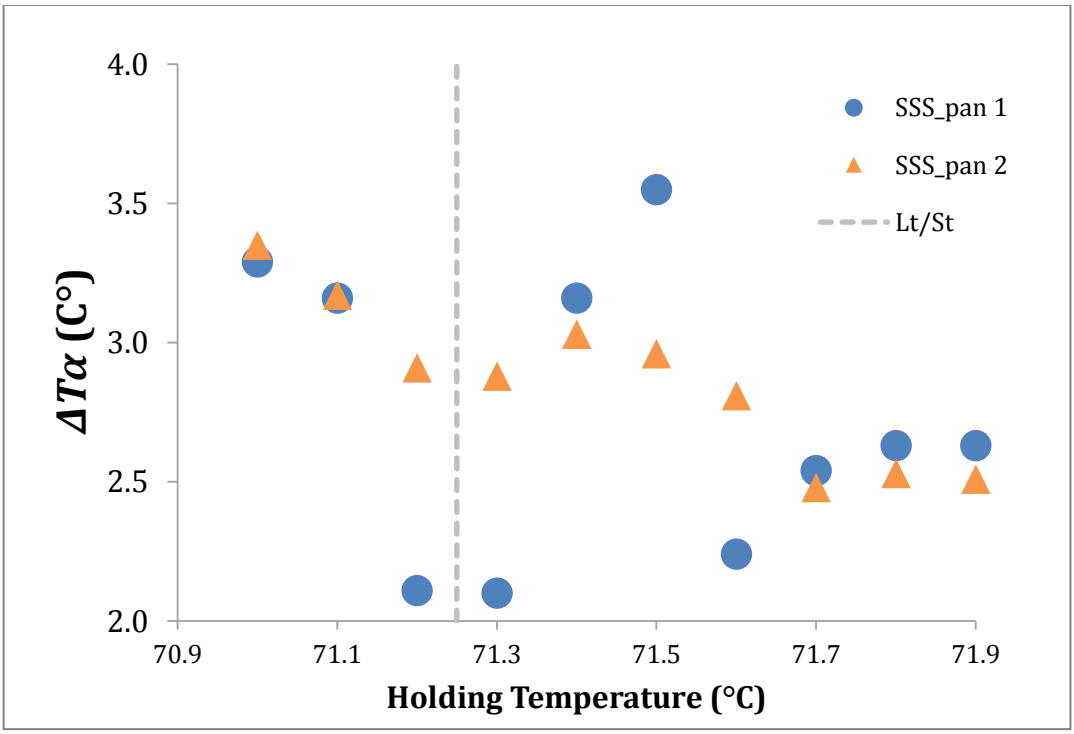

(a)

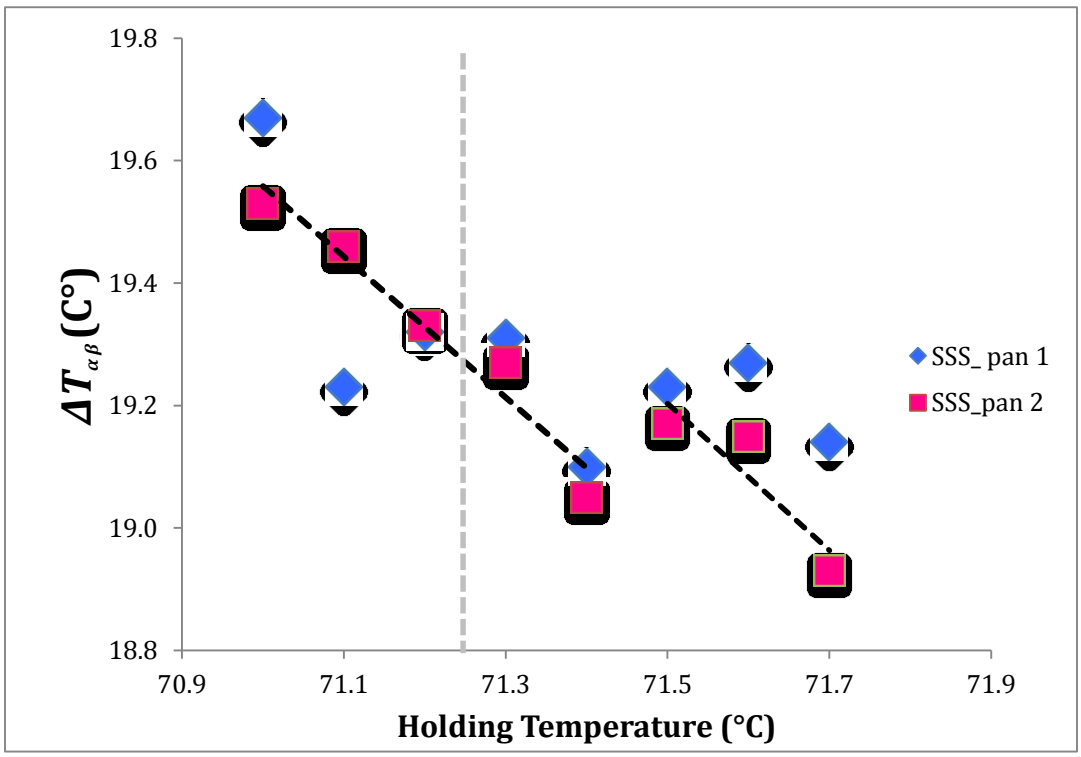

(b)

Figure 4-38. Onset temperature differences for SSS as a function of the holding temperature for the two pans studied. (a) α onsets (b) β onsets.

4.3.4 Onset temperatures of recrystallization from crystal memory: comparative summary

The crystal memory phenomenon occurs above a certain minimum temperature, T_{min}, and is equal to the lowest value at which the $\boldsymbol{\beta}$ polymorph began to melt. In our experiments, T_{min} was 71.0 °C for SSS; 62.1 °C for PPP, and 56.0 °C for MMM. T_{sl} is the temperature above which the memory effect can be erased with short time heating (as opposed to requiring a long heating time). As the holding temperature became higher, the holding time needed to erase the memory decreased rapidly. Above a maximum temperature, T_{max}, the memory effect will be erased completely. T_{max} was 72.5 °C for SSS, 63.5 °C for PPP, and 57.3 °C for MMM. The difference between T_{max} and T_{min} was about 1.5 °C for the three samples; specifically, PPP had a 1.4 °C and SSS had a 1.5 °C interval, while for MMM, the temperature interval was 1.3 °C, as shown in Figure 4-39 and Figure 4-19. Figure 4-19 shows T_{min}, T_{max}, T_{sl} and (T_{max}-T_{min}), the T_{sl} and T_{min} for PPP is significantly larger, suggesting that the memory of PPP can persist longer than for MMM or SSS.

Table 4-19. T_{min}, T_{max} and T_{sl} values for the three different materials

Sample	T_{min} (°C)	T_{sl} (°C)	T_{max} (°C)	T_{max} - T_{min} (C°)	T_{sl} - T_{min} (C°)
MMM	56.0	56.1	57.3	1.3	0.1
PPP	62.1	62.7	63.5	1.4	0.6
SSS	71.0	71.3	72.5	1.5	0.3

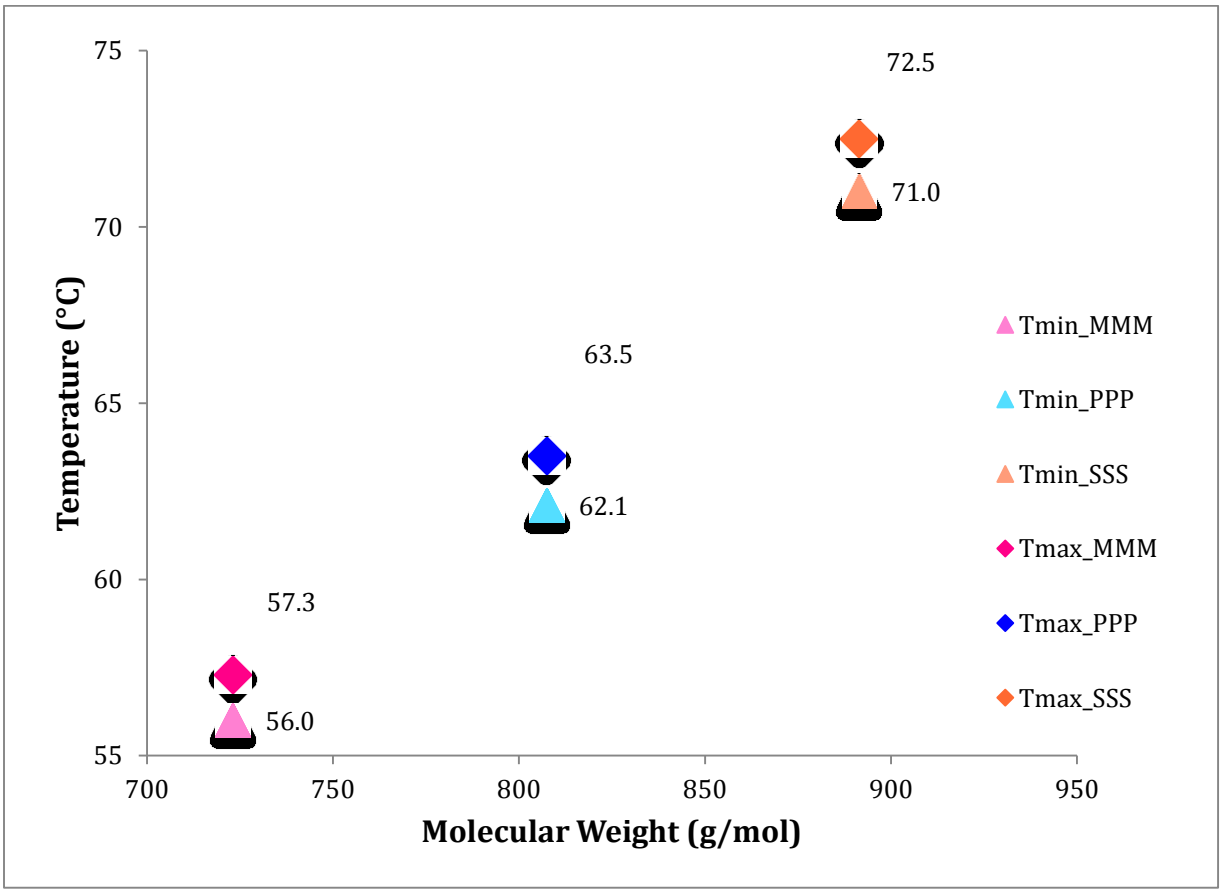

Figure 4-39. The relationship between T_{max} and T_{min} and molecular weight of the materials. The pink color represents MMM with a molecular weight 723.16 g/mol; purple represents PPP with a molecular weight 807.43 g/mol. Orange represents SSS with a molecular weight 891.48 g/mol. The "diamonds" stand for T_{max} while "triangles" stand for T_{min}.

Figure 4-41 summarizes ΔT_a values of all pure samples for all types of $\boldsymbol{\alpha}$ memory. The Y-axis is ΔT_a, the difference between T_{onset_α} and $T_{onset\_\alpha 0}$. The X-axis is ΔT_m, the difference between the holding temperature T_H and the minimal melting temperature T_{min}. Data sets with the same symbols include pan 1 and pan 2, showing that the general behavior of the two pans was very similar. The circles represent MMM ΔT_a was generally higher for MMM than for PPP and SSS.

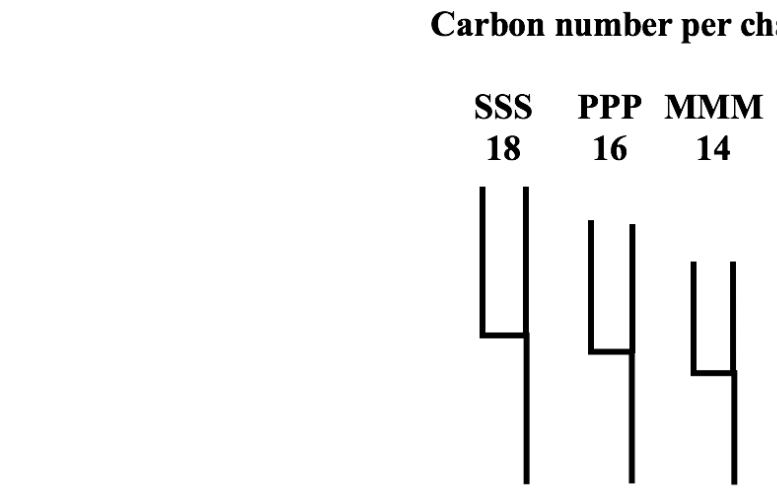

Figure 4-40. Qualitative representation of the effect of different carbon numbers per chain of MMM, PPP and SSS (Bailey et al.,).

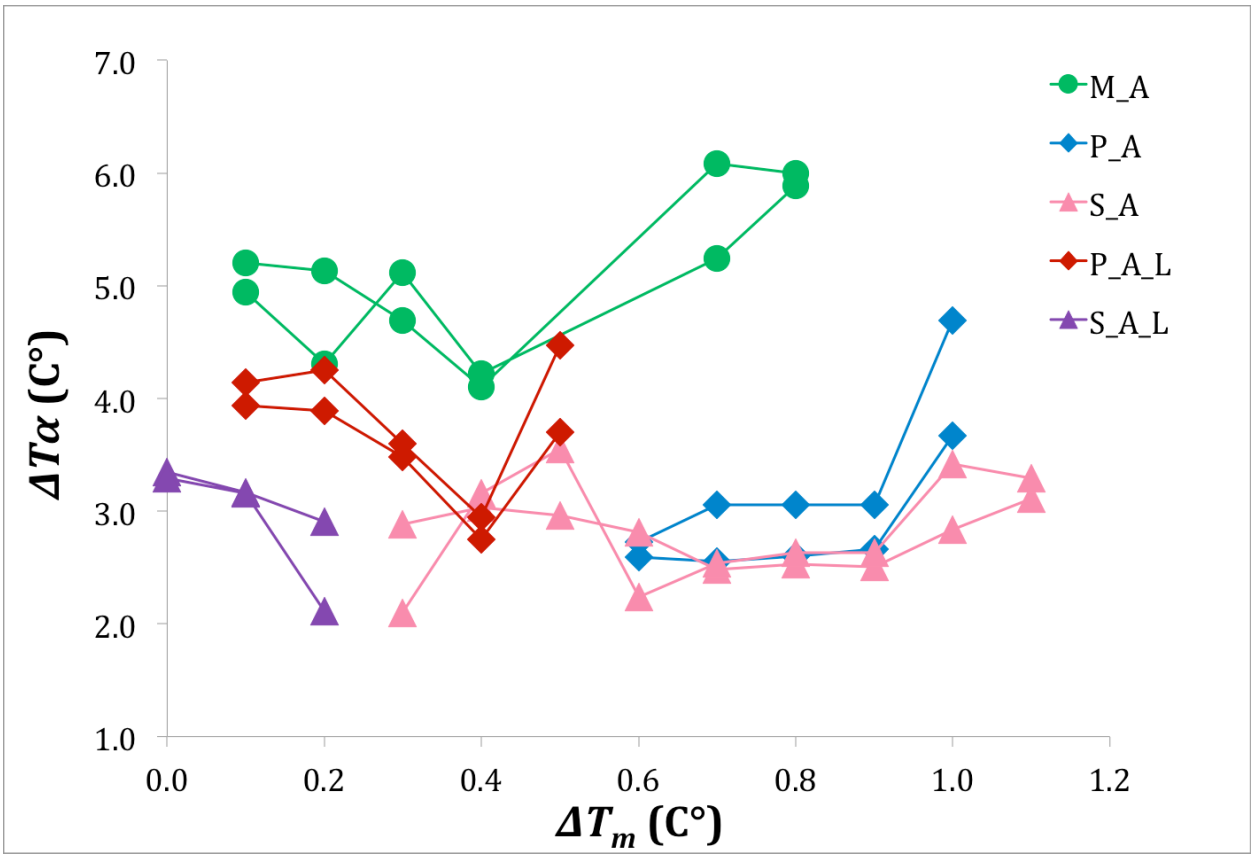

Figure 4-41. ΔT_a of the pure samples as a function of ΔT_m, the difference between the holding temperature and their experimental melting temperature (T_H - T_{min}). The circles represent MMM, PPP (diamonds) and SSS (triangles). P_A_L represent the long- term α memory of PPP and S_A_L is the long-term α memory of SSS, P_A is the short- term α memory of PPP and S_A is the short- term α memory of SSS.

For PPP and SSS, the time required to erase the memory at temperatures close to T_{min} was much longer than it was above T_{sl} (Figure 4-41). ΔT_m is the temperature between T_H and T_{min}. Thus, the plot in Figure 4-41 presents their results divided into two groups, labeled S_A and P_A for short times in SSS and PPP, and S_A_L and P_A_L for their corresponding long-times. The general distribution of the ΔT_a with respect to ΔT_m reveals that PPP and SSS followed a more or less similar trend, whereas MMM exhibited behavior similar to PPP or SSS at low temperatures, but shifted towards earlier recrystallization.

These results hint at the molecular mechanisms involved in the process, and offer an excellent starting point for further research into the "memory" liquid state.

The interactions between TAG molecules in a non-aqueous environment can be divided into two types: the attractive forces derived from the polar glycerol core, and the attractive forces present via van der Waals interactions among the alkyl chains. The glycerol core is common to the three species, while alkyl chain length varies: for MMM, PPP and SSS, the lengths are 14, 16 and 18 carbon atoms, respectively (Figure 4-40).

One possible explanation for the behavior observed here is that in the smaller molecules the prevailing re-crystallization interactions are dominated by the attraction of the glycerol cores. As the alkyl interactions become stronger, the long-time persistence of $\boldsymbol{\alpha}$ appears, and the material becomes more tolerant to higher overheating. Thus, the alkyl chains length contribute an increasing proportion of the attractive forces.

Quantification and exploration of this hypothesis is beyond the scope of this thesis, but this research has provided a precise set of conditions with which other researchers may pursue this possibility.

CHAPTER 5. RESULTS AND DISCUSSION – II TIME-TEMPERATURE BOUNDARIES OF CRYSTAL MEMORY IN BINARY MIXTURES OF TRIACYLGLYCEROLS

As described in Section 3.1.1 and 3.1.2, a limited number of experiments were carried out on triacylglycerol binary mixtures. When two TAGs are mixed, each TAG influences the melting properties of the others; the phase behavior of the resulting mixture is complicated, and not a simply a superposition of the two materials. The thermograms obtained in DSC experiments are further complicated by the presence of different polymorphic arrangements adopted by the crystals, as TAGs readily form solid solutions (i.e., crystals composed of different molecules at the lattice level, similar to substitution crystals). The affinity of the glycerol group and alkyl chains is strong enough to overcome the structural mismatch produced by chain length differences in the crystals. The present limited data agrees with the observed increase in the formation of solid solutions as the relative difference in chain length is reduced. Binary mixtures of saturated TAGs seldom form a single phase when cooled below their solid forming temperature. Instead, they tend to produce two or more types of crystals of different composition (solid solutions).

Each crystal type (i.e., each phase) is characterized both by its unique composition and polymorphic form. Thus, it is possible to have crystals that exhibit the same polymorphic form but different compositions, resulting in different melting properties. Similarly, there could be two phases, each with a composition and polymorphic form different from each another. The overall complexity of the material formed increases with the number of phases formed.

For the initial melting of the binary mixtures, the temperature used was higher than the melting temperature of the component with the highest melting point. At a temperature above the melting point of the higher melting component, all the lipids were expected to be in the liquid state. This liquid state is produced by the melting of phases of different compositions distributed locally in a

container. That means that to achieve a uniform concentration distribution, it is necessary to wait until the molecules can mix sufficiently to remove any concentration gradients via diffusion and convection. If convection is negligible, as with the DSC pans or x-ray capillaries, then the mixing relies solely on molecular diffusion.

The experiments conducted in this part of the research were devised to test the hypothesis that erasing the memory effect would take longer for mixtures of TAGs than for their pure constituents. The exploration of the binary mixtures, however, is not a simple extension of the study of the pure TAGs. Below, we will provide details regarding some of the complexities that are unique binary systems. This part of the thesis is more preliminary and is intended as a valuable starting point for a deeper research in the future.

During the experiments with binary mixtures, the blends did not form the β polymorph, as was observed for pure TAGs in their most stable phase. Instead, they formed β' polymorph crystals of different compositions. One explanation for this is that the solid solution of two different molecules makes it very difficult to reach the highly ordered state of the β polymorph within our experimental procedures. Thus, for the mixtures, the stable phase and memory explored correspond to the β' polymorph. The behavior of β' memory in the blended mixtures is analogous to that of β memory in the pure TAGs (Chapter 4).

The melting and crystallization temperatures of binary mixtures do not normally coincide with those of pure materials (e.g., for MMM (M) and PPP (P) for the α polymorph). In an isothermal mixture, the first equilibrium condition is that the chemical potential of a component must be the same in all the phases. The second condition is that all components must satisfy the first condition. For a binary system, this can be mathematically described by the solution of temperature and mole fractions of solid and liquid (T, x, y) to two simultaneous thermodynamic equations. They are often

written as follows (Batchu, 2014; Marangoni & Wesdorp, 2012), with T_m as the initial melting temperature of the solid being heated:

$$y_M = \breve{x}_M \cdot \gamma_M \cdot \exp\left[\frac{\Delta H_M}{R}\left(\frac{1}{T_m} - \frac{1}{T_M}\right)\right]$$

$$1 - y_M = \left(1 - \breve{x}_M\right) \cdot \gamma_P \cdot \exp\left[\frac{\Delta H_P}{R}\left(\frac{1}{T_m} - \frac{1}{T_P}\right)\right]$$

The same equations, written for the case of a liquid being cooled, with T_c as the initial crystallization temperature, are:

$$\breve{y}_M = x_M \cdot \gamma_M \cdot \exp\left[\frac{\Delta H_M}{R}\left(\frac{1}{T_c} - \frac{1}{T_M}\right)\right]$$

$$1 - \breve{y}_M = \left(1 - x_M\right) \cdot \gamma_P \cdot \exp\left[\frac{\Delta H_P}{R}\left(\frac{1}{T_c} - \frac{1}{T_P}\right)\right]$$

In equilibrium, the mole fraction of MMM in the liquid state, y_M, must be equal to the product of the mole fraction of MMM in the solid state, x_M, by an activity coefficient γ_M and an exponential temperature factor. Similarly, the mole fractions of PPP in the liquid and solid states, presented as (1- y_M) and (1- x_M), are related to its activity coefficient γ_P and its exponential temperature factor. The enthalpies ΔH_M and ΔH_P and the melting temperatures T_M and T_P, correspond to the $\boldsymbol{\alpha}$ polymorph of the pure components. An ideal equilibrium plot for the $\boldsymbol{\alpha}$ polymorph of the MMM-PPP blend, obtained by solving these equations, is presented in Figure 5-1. The red line is the theoretical liquidus line, the yellow line is the theoretical solidus line. The green dotted lines are 'tie lines', i.e. isothermal lines showing a solid and liquid composition that are in equilibrium at the corresponding temperature. These curves and lines were calculated in Excel using the

thermodynamic equations above, and the parameter values in Chapters 1 and 2. The conversion from mass fraction w_M to mole fraction x_M depends on the molecular weights M_M and M_P:

$$x_M = \frac{\frac{w_M}{M_M}}{\frac{w_M}{M_M} + \frac{w_P}{M_P}} = \frac{1}{1 + \frac{w_P}{w_M}\frac{M_M}{M_P}} = \frac{1}{1 + \frac{1 - w_M}{w_M}\frac{M_M}{M_P}}$$

The average mole fraction of MMM in 5M5P is $x_M = 0.528$. The vertical blue line is traced at this molar composition. The top dotted green line indicates the theoretical temperature of crystallization in a 'fully mixed' liquid, and the composition of the solid that would begin to form. If liquid with a composition $y_M = 0.528$ was being cooled, the ideal ($\gamma_M = \gamma_P = 1$) onset crystallization temperature would be $T_c = 40.52$ °C, and the solid formed would have a mole fraction $x_M = 0.234$. The bottom green line indicates the theoretical initial melting temperature of a 'fully mixed' solid, and the composition of the liquid that would begin to appear if this solid was being heated. The ideal onset melting temperature would be $T_m = 36.76$ °C, and the liquid formed would have a mole fraction $y_M = 0.813$. In these experiments, however, the mixed liquid material was cooled below this phase diagram before its crystallization actually started; as a result, it is not easy to make a theoretical assumption of which phases are supposed to form.

The experimental onset of crystallization for the first $\boldsymbol{\alpha}$ polymorph of 5M5P occurred around 33.7 °C, as indicated by the tip of the blue arrow in Figure 5-1. This is 6.8 C° below the ideal liquid curve and about 3 C° below the solid curve. Furthermore, most materials formed two phases upon crystallization, and sometimes three. Traditional phase diagrams of this kind are not adequate to describe this behavior; in fact, there are currently no fully satisfactory methods available to predict this type of behavior in TAG mixtures (Liu, 2014; Batchu, 2014). However, without better tools

at our disposal, the experimental results will be compared, when possible, to the ideal mixture scenarios.

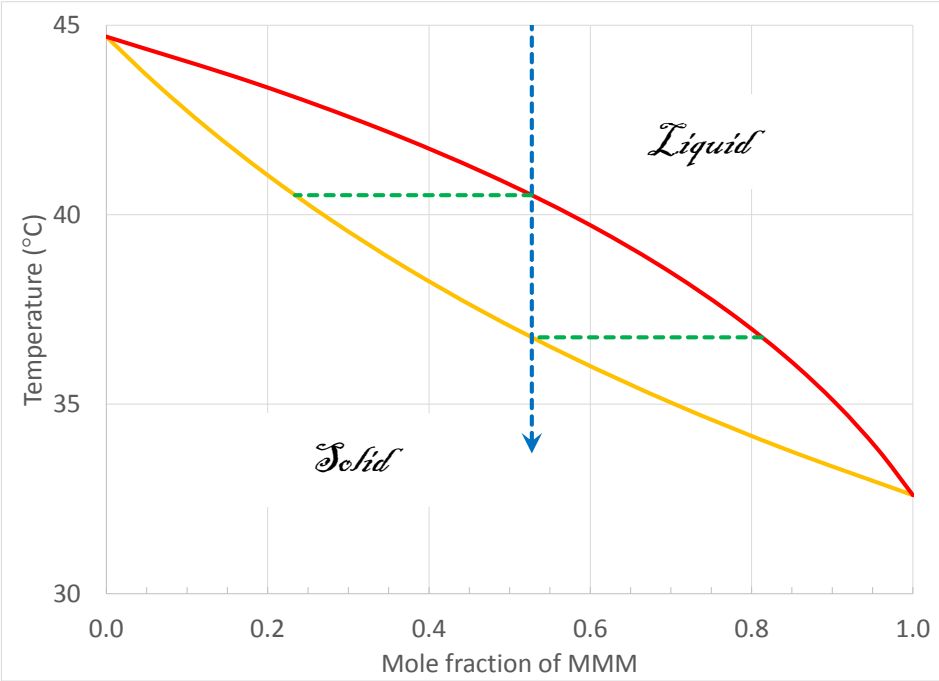

Figure 5-1. Ideal equilibrium plot for the MMM-PPP α polymorph. The red line is the theoretical liquidus line, the yellow line is the theoretical solidus line. The blue line is a cooling line traced at the molar composition of the mixture. The top dotted green tie line indicates the theoretical temperature of crystallization in a 'fully mixed' liquid. The bottom green tie line indicates the theoretical initial melting temperature of a 'fully mixed' solid. They were calculated in Excel using the thermodynamic equations and values from Chapters 1 and 2.

5.1 Time-temperature boundaries of crystal memory in the binary mixtures

5.1.1 Boundaries of 5M5P

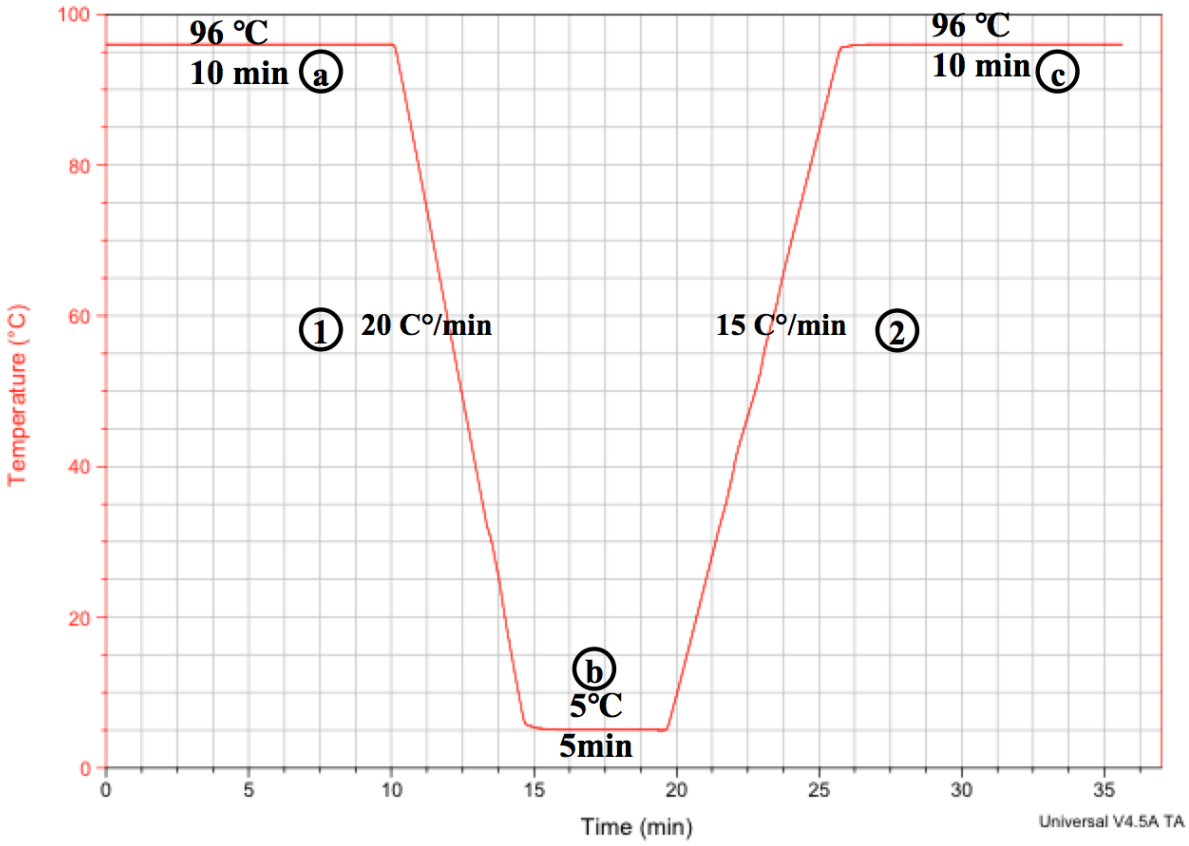

Figure 5-2. Temperature-time plot of 5M5P ***α*** polymorph formation and analysis.

Figure 5-2 shows the temperature-time process used to create and analyze the ***α*** polymorph for the 5M5P mixture. A similar process was used with 5P5S. We used 30 C° above the melting point of PPP, 96 °C, as the initial melting temperature (step "a" in Figure 5-2) for this mixture in order to ensure that the material was fully melted. The holding time at the melting temperature was 10 min, as in the experiments with pure TAGs. The holding time for the low temperature hold (step "b") was 5 min.

Figure 5-3 shows the ***α*** polymorph reference thermogram trace for 5M5P. During the initial cooling step at 20 C°/min (step "1" in Figure 5-2), two crystallization peaks were observed, at

31.42 °C and 26.91 °C (Figure 5-3), corresponding to the formation of two different mixed phases. Although MMM and PPP have different melting points, during crystallization they do not crystallize separately. Instead, it would appear that perhaps they first formed one solid solution phase rich in PPP, starting at 33.7 °C and peaking at 31.42 °C. Soon after, another phase rich in MMM appeared, peaking at 26.91 °C. In this case, it is likely that both phases belong to the α type polymorphic form. Though two different polymorphs can occur and coexist at the same time, that is unlikely under the present experimental conditions for this mixture. Given that the individual TAGs at this cooling rate produced the α polymorph, it is highly unlikely that they would form a more stable polymorph of a mixed composition, which is inherently more unstable. It is energetically more difficult to form a mixed β or β' crystal than it is to form a mixed α crystal. Therefore, it is perhaps reasonable to assume that both phases have an α polymorphic form, but with different compositions. We have called these phases α_P and α_M. Two additional phases were observed during the heating period, and were called β'_M and β'_P. These were also solid solution crystals rather than pure components.

During the heating period at 15 C°/min (step "2" in Figure 5-2), α_M started to melt first, at around 25 °C. The formation of its liquid may have fostered the melting-dissolution of the α_P phase. The different liquid phases being formed recrystallized as the β'_M and β'_P solid phases. As the heating continued, it would seem as if the β'_M phase started to melt, followed soon after by the β'_P phase. Past 70 °C, the mixture had melted and continued to heat up to 96 °C. After 10 minutes at 96 °C (step "a" in Figure 5-2), cooling at 20 C°/min (step "1" in Figure 5-2) produced the same onset as the control that had been held at 96 °C for 10 min. Therefore, it was concluded that 10 minutes at 96 °C (step "a" in Figure 5-2) was enough to bring the liquid back to its original state, without memory.

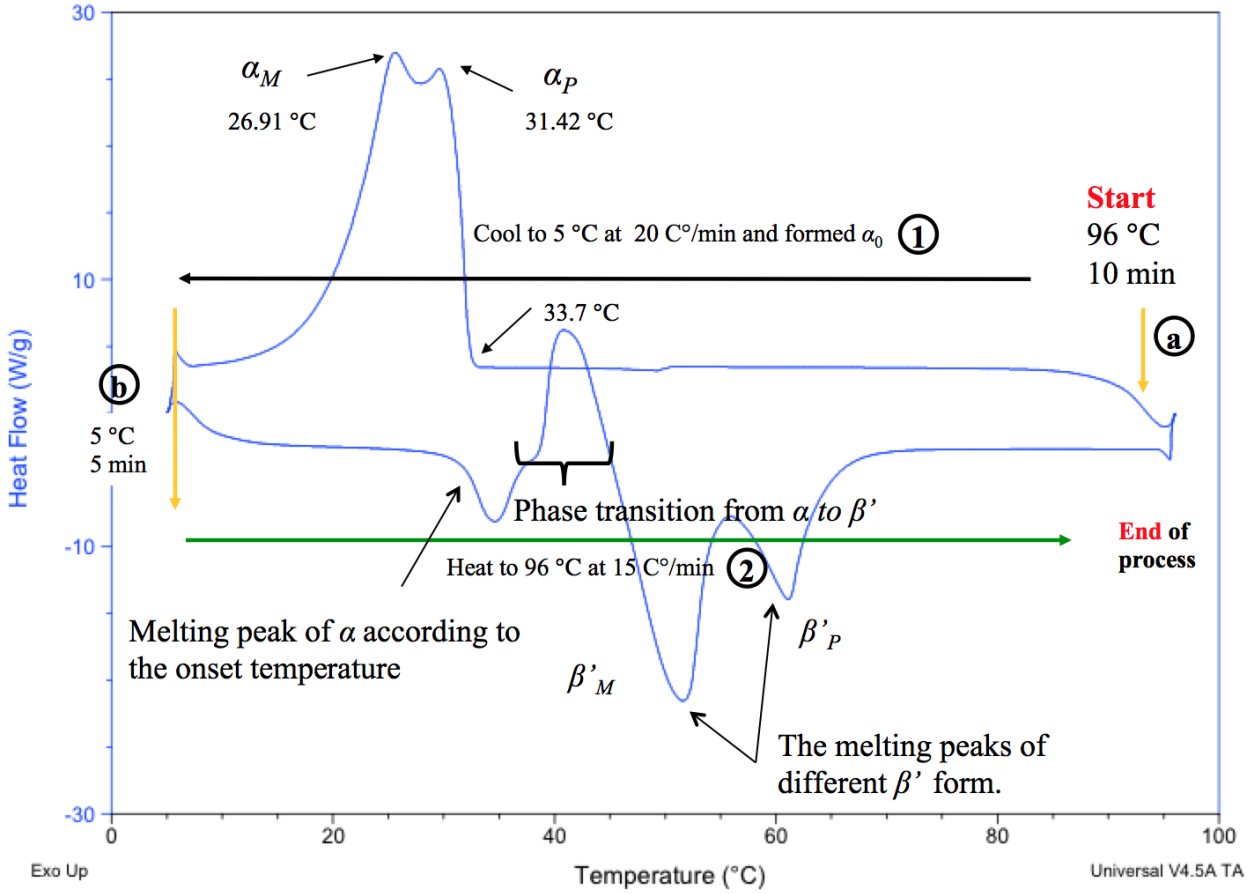

Figure 5-3. Thermogram of the process to form and analyze the $\boldsymbol{\alpha}$ polymorph in 5M5P, indicating the cooling and heating directions and conditions.

The formation of two phases requires the material to split while keeping its mass balance. In this case, the overall mole fraction, z_m, is 0.528. The two phases formed must have mole fraction such that $x_{M2} < z_m < x_{M1}$, with x_{M1} being the mole fraction of $\boldsymbol{\alpha}_M$ and x_{M2} being the mole fraction of $\boldsymbol{\alpha}_P$. The fraction of moles in the solid form, χ, that corresponds to $\boldsymbol{\alpha}_M$, the phase rich in MMM is then,

$$\chi = \frac{z_m - x_{M2}}{x_{M1} - x_{M2}}$$

From the thermogram alone it is not possible to exactly determine χ, but the areas were not very different, suggesting that its value was somewhere between 0.4 and 0.6. For example, values of

x_{M1} = 0.845 and x_{M2} = 0.14 produce a value of χ = 0.55. These values are used below to illustrate a qualitative interpretation of the formation of the solid.

The experimental onset temperatures of $\boldsymbol{\alpha}$ crystal formation during cooling were plotted on top of the ideal equilibrium diagram of MMM-PPP of Figure 5-1, resulting in Figure 5-4. Except for the liquid used for the initial cooling, the exact mole fractions are unknown, so they were estimated as a qualitative indicator in order to facilitate discussion.

The PPP-rich $\boldsymbol{\alpha}$ phase first started to form as the melt was cooled downwards from 33.7 °C. Because the crystalline fraction had a composition that had more PPP than the liquid, it depleted the liquid of PPP faster than that of MMM. This would cause the concentration of the liquid to shift towards MMM. Once the MMM-rich phase started to crystallize, this tendency was reduced.

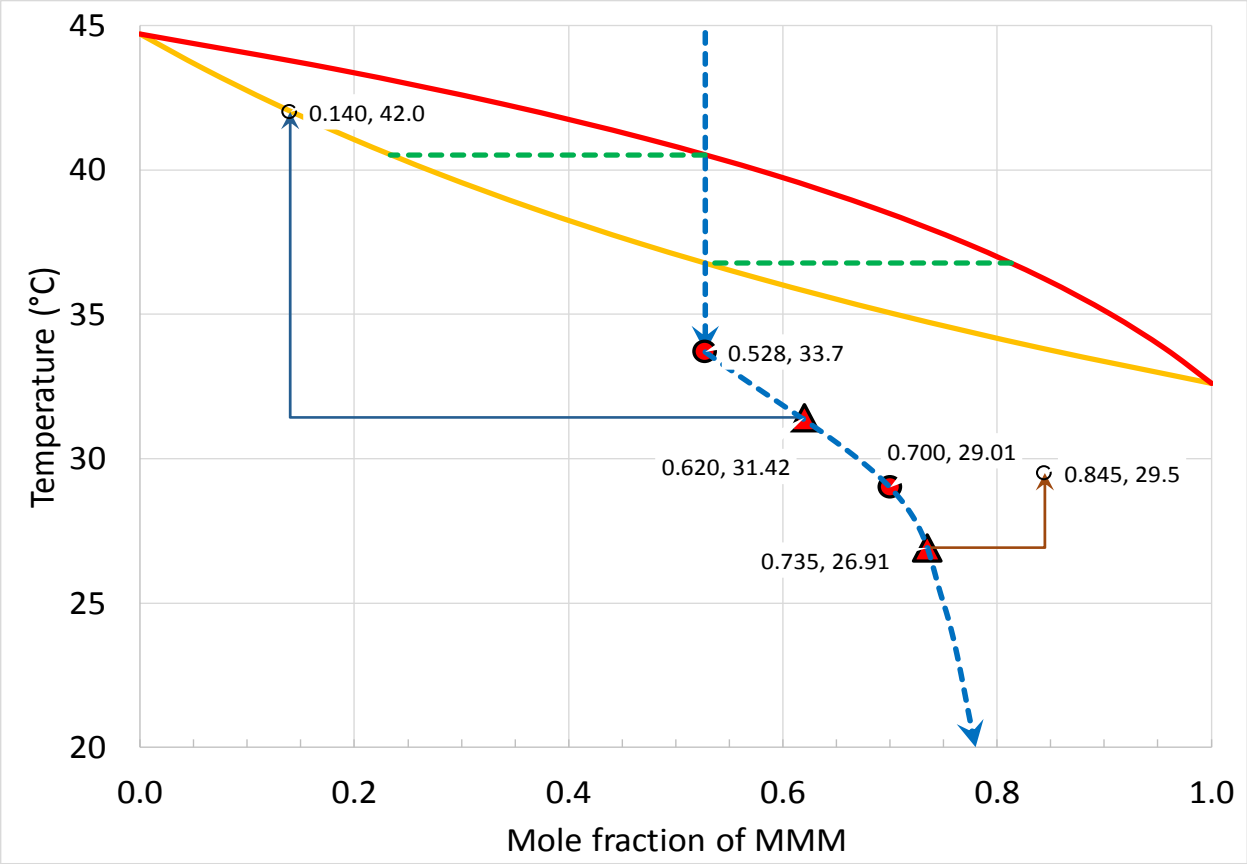

Figure 5-4. Experimental onset temperatures of α crystal formation during cooling plotted on top of the ideal equilibrium diagram of MMM-PPP of Figure 5-1, including the α_P onset temperature 33.7 °C (circle at $x_M = 0.528$), peak temperatures (triangles), and melting onsets (upwards arrows on solid lines). The hypothetical α_M onset temperature and other features of the plot are described in the text. The dashed blue line represents the mole fraction of the liquid, and its estimate after the onset of the first α phase. The circles represent the estimated onsets of the α phases. The triangles are placed at the temperatures corresponding to the maxima of the crystallization peaks in the thermograms. The arrows on the left and right indicate the melting temperature of the α phases.

The tempering regime for mixed TAGs was obtained by testing different conditions above the melting points of α MMM, and α PPP. Once the melting started (step "2" in Figure 5-3), at around 25 °C, the remainder of the solid was dissolved rapidly by the liquid. The recrystallized material seemed to behave similarly regardless of tempering conditions. Thus, the melting temperature was chosen to be 35 °C, just above the published melting point of α MMM. As in the pure TAGs experiments, a tempering time of 10 min was used (step "2", "c" and "3" in Figure 5-5).

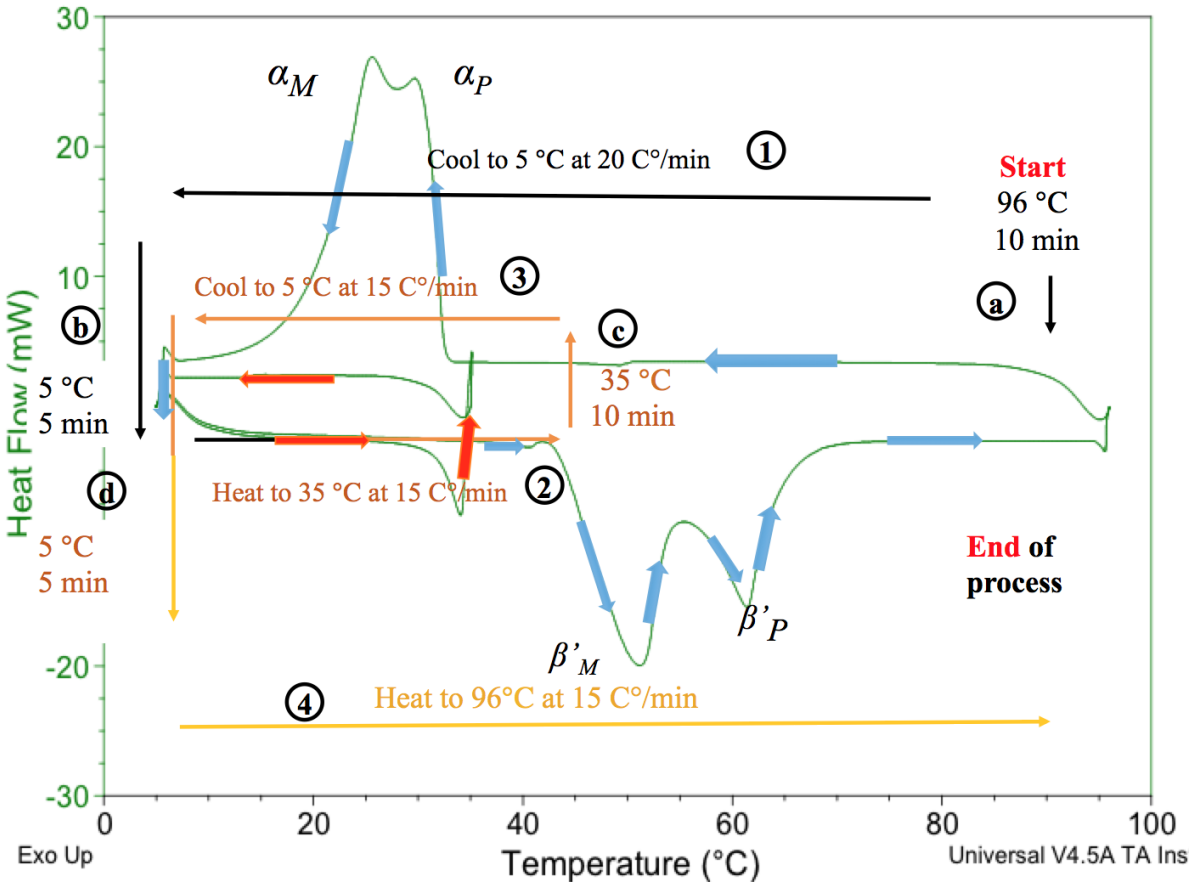

Figure 5-5. Thermogram of the tempering process of 5M5P, step "2", "c" and "3" (orange arrows) indicates the tempering process.

The plot in Figure 5-5 shows the heating trace of the material formed after tempering. When the temperature was below 40 °C, the faint melting indicated that the ***α*** material had virtually disappeared with minimal recrystallization (step "3" in Figure 5-5). The two big melting events during re-heating (step "4" in Figure 5-5) are similar to those observed during the heating period (step "2" in Figure 5-3) from the untempered ***α*** material, and corresponded to the melting of the β'_M and β'_P phases.

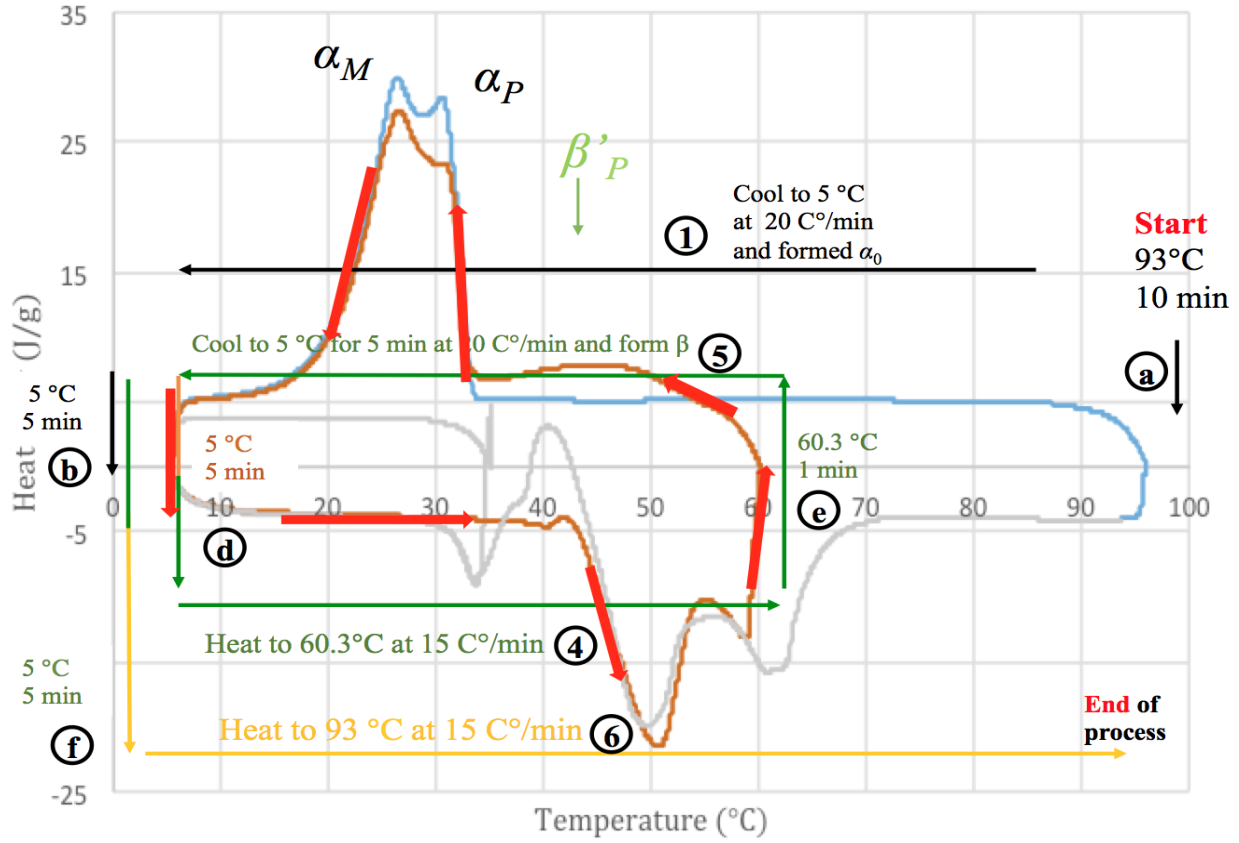

Figure 5-6. Thermogram from the program used to characterize the memory effect for 5M5P, with holding temperature and time of 60.3 °C and 1 min. Red indicates the process of temperature-time combination test (step "4", "e" and "5").

The thermogram in Figure 5-6 shows the process used to determine the presence of memory in 5M5P. From previous experiences and observations of other thermograms, the interpretation of this thermogram is that three phases were formed during recrystallization: phase α_M, might be fully recovered; phase α_P reappeared in a smaller proportion; and phase β'_P was newly formed. It appears that phase β'_P formed at the expense of using the liquid available for α_P, since α_P is present in a smaller proportion.

Similar experiments were conducted at different temperatures to determine how long the memory would persist (step "5"). The temperature-time boundaries are summarized in Table 5-1 and Table 5-2. The T_{min} of the 5M5P material was around 57.0 °C, while the T_{max} of 5M5P was higher than 60.6 °C.

Table 5-1. Time at each holding temperature that defined the boundary for "early ***α*** memory" of 5M5P. The "*α* Time_1 (min)" is the holding time boundary at holding temperature for pan 1 and "*α* Time_2 (min)" is the holding time boundary at holding temperature for pan 2.

Holding Temperature (°C)	**57.0**	**58.0**	**59.0**	**60.0**	**60.1**	**60.2**	**60.3**	**60.4**	**60.5**	**60.6**
***α* Time_1 (min)**	120	100	60	15	2.0	1.5	1.4	1.3	1.2	1.0
***α* Time_2 (min)**	120	100	60	18	2.3	2.0	1.6	1.4	1.3	1.1
***α* Time average**	120	100	60	16.5	2.15	1.75	1.5	1.35	1.25	1.05

Table 5-2. Time at each holding temperature that defined the boundary for "***β'*** memory" of 5M5P. The "*β'* Time_1 (min)" is the holding time boundary at holding temperature for pan 1 and "*β'* Time_2 (min)" is the holding time boundary at holding temperature for pan 2.

Holding Temperature (°C)	**57.0**	**58.0**	**59.0**	**60.0**	**60.1**	**60.2**	**60.3**	**60.4**
***β'* Time_1 (min)**	9	8	>1	>1	>1	>1	>1	0
***β'* Time_2 (min)**	12	10	>1	>1	>1	>1	>1	0
***β'* Time average**	10.5	9	>1	>1	>1	>1	>1	0

These data (Table 5-1 and Table 5-2) were used to construct Figure 5-7. The early ***α*** memory data did not follow the exponential trend that was observed in PPP and SSS. The time and temperature range for crystals to form are similar (~120 min); the ΔT_{sl} is 3.0 C°, the latter being much larger than the intervals of pure triacylglycerols, which were typically 0.5 C° or less (Section 4.3.4).

The time and temperature ranges of the short time boundary were similar to those of the pure materials, with a time interval of about 2 min and a temperature interval exceeding 0.6 C°. Linear regression revealed an estimate for T_{max} of 61.0 ± 0.1 °C for a time interval of 1 min, and a slope of -0.41 ± 0.08 C°/min, which is more gentle than those of pure materials (-0.64 to -0.73 C°/min), but represents a similar order of magnitude.

The boundaries of the "***β'*** memory" are shown in panel (c). Further experiments must be conducted in the future to refine the boundaries; however, its environs have been determined fairly well. The

value of $T_{max\_\beta'}$ was 60.4 °C, since no recrystallization into the ***β'*** form was observed at this temperature or above. T_{min} was around 57.0 °C, but requires further, more precise, determination. This range of ~3.4 C° in temperatures required to erase the "***β'*** memory" of 5M5P was somewhat broader than the ~1.5 C° needed for erasing the "***β*** memory" of pure materials. However, the time required to erase the "***β'*** memory" for the mixture, which is approximately 12 min, was much longer than for the pure samples, where the "***β*** memory" can be easily eliminated within 2 min of heating at the lowest holding temperature.

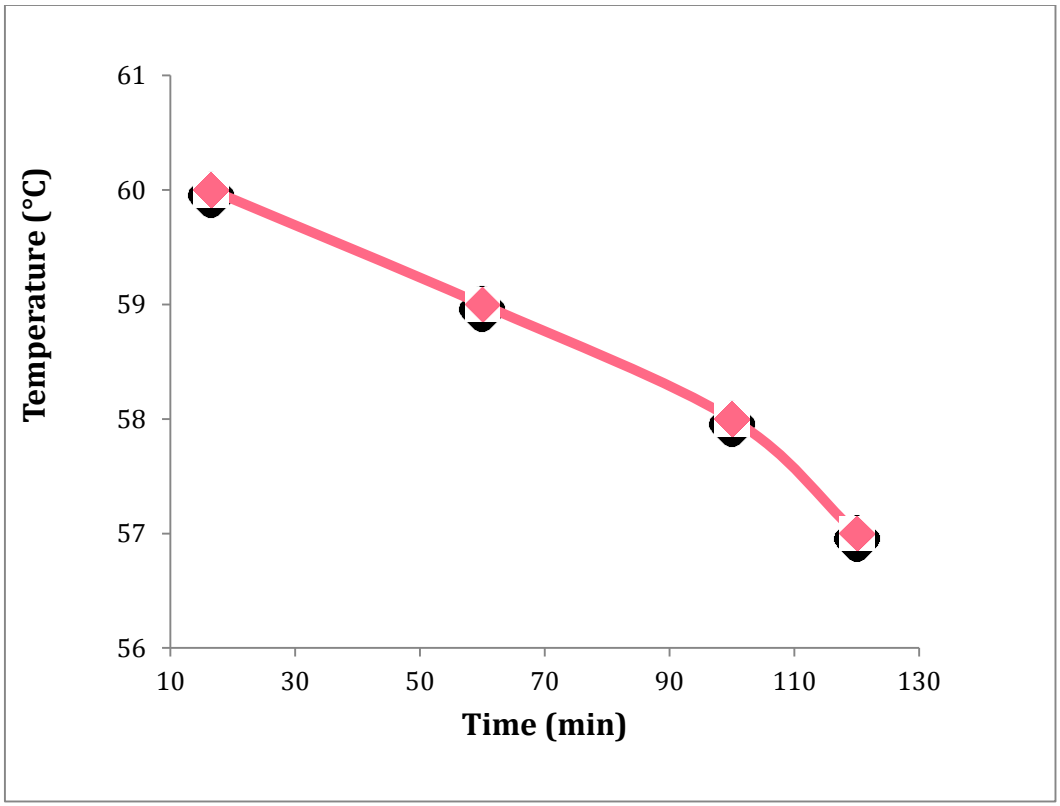
Temperature (°C)
61
60
59
58
57
56
10
30
50
70
90
110
130
Time (min)

(a)

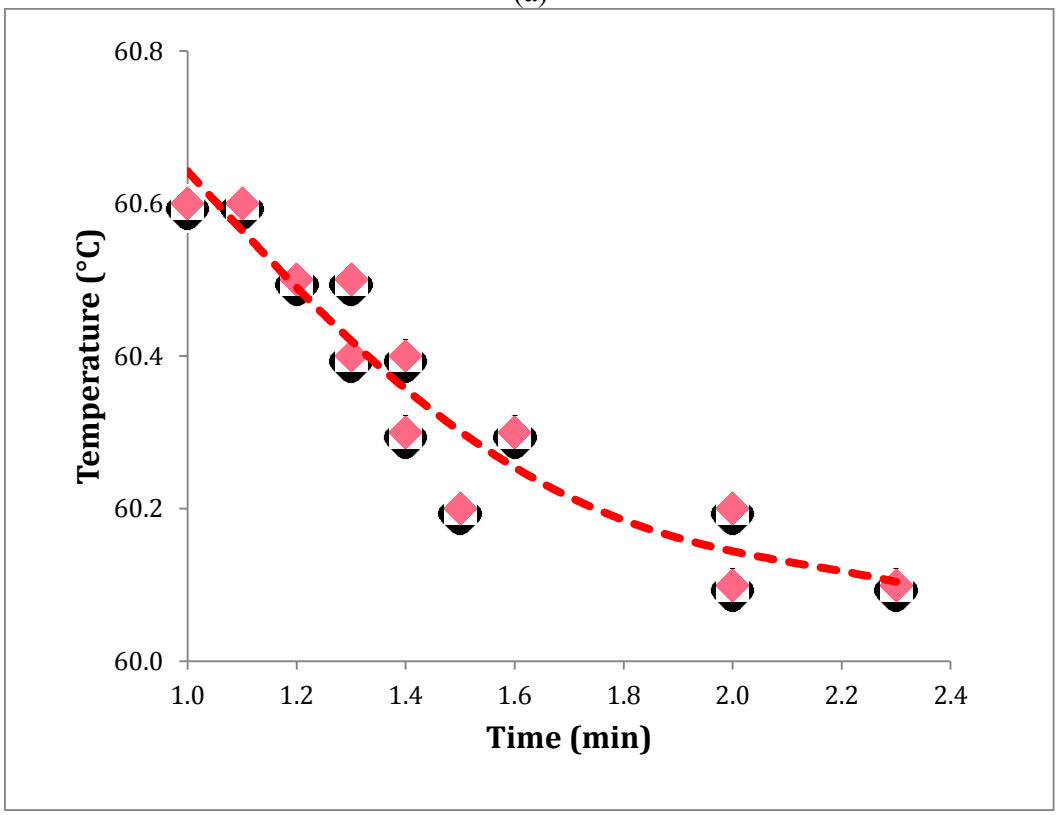
Temperature (°C)
60.8
60.6
60.4
60.2
60.0
1.0
1.2
1.4
1.6
1.8
2.0
2.2
2.4
Time (min)

(b)

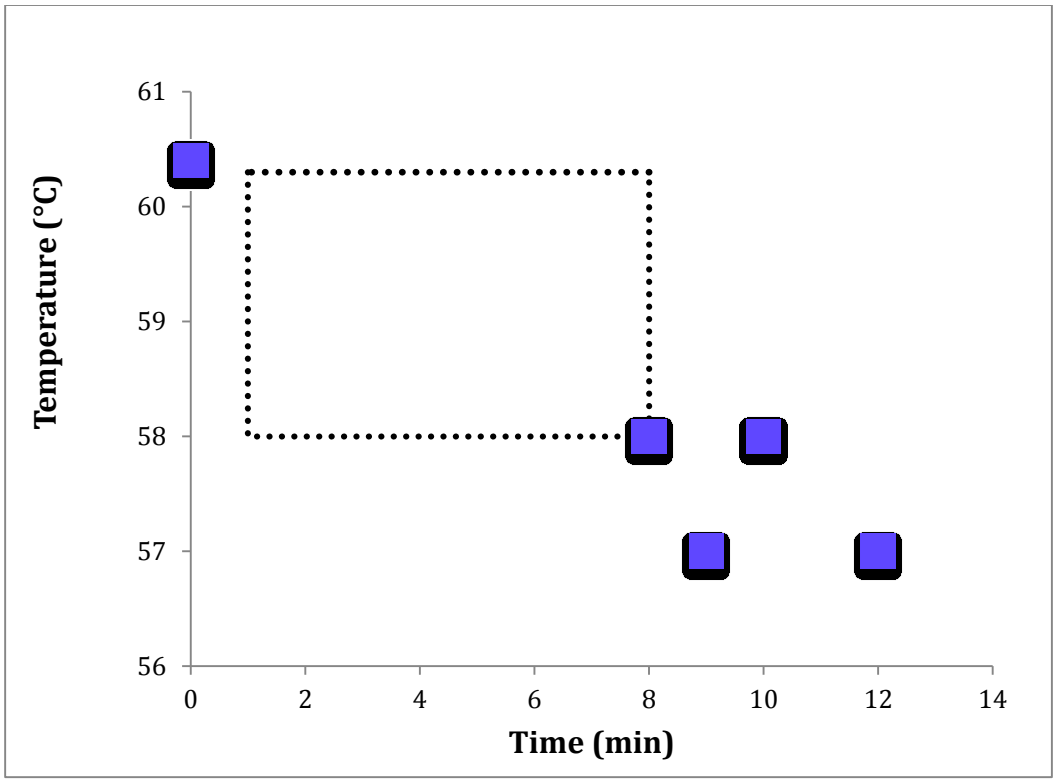

(c)

Figure 5-7. Time-temperature boundaries for memory effect of 5M5P. The red line represent the boundaries of "early α memory" and the blue line represent the boundaries of "β' memory". Panel (a) shows the long time temperature-time boundaries of "early α memory" linked by a red solid line, panel (b) shows the short time temperature-time boundaries of "early α memory" data, and an empirical fit as a red dashed line, and panel (c) shows the boundaries of "β' memory" for 5M5P in blue dots, the black dotted square indicates the region that needs further data.

Three steps were tentatively identified for the process of erasing the β' memory effect of 5M5P. A selected set of thermograms representing holding times and temperatures, overlaid in Figure 5-8, highlights this interesting behavior. The holding times were 1 min, except for 59.0 °C, for which the time was 0.6 min. At the lowest holding temperature, 58.0 °C (see legend), the thermogram shows two β' recrystallization peaks: the β'_P phase presumed at a higher temperature (~ 47 °C), and the β'_M presumed at a lower temperature (~38 °C). As the holding temperature increased to 59.0 °C, the β'_P area became larger, even with the shorter holding time, while the β'_M peak became smaller. After holding for 1 min, the peak of phase α_M appeared.

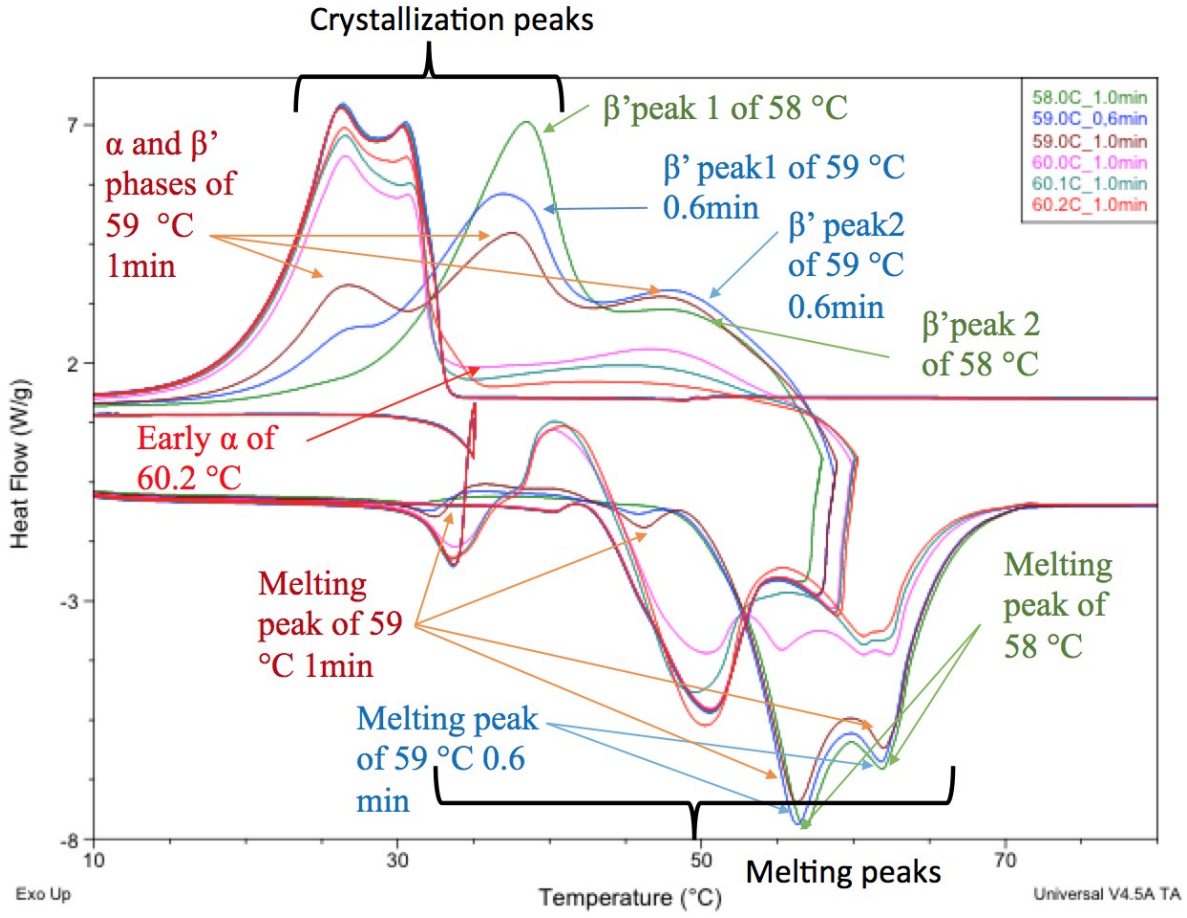

Figure 5-8. Overlaid thermograms of temperature-time boundaries for 5M5P. There are two ***β'*** peaks at 58.0 °C for 1 min and 59.0 °C for 0.6 min. When the holding time was increased to 1 min at 59.0 °C, three different phases (two *β'* phases and one *α* phase) were formed during recrystallization.

Table 5-3. Melting points of the ***α*** and ***β'*** polymorphs of MMM and PPP (Takeuchi *et al.*, 2002).

TAG m.p. (°C)	***α***	***β'***
MMM	32.6	45.9
PPP	44.7	55.7

The melting points of the different polymorphs of MMM and PPP, collated in Table 5-3, were compared to the onset temperatures observed for 5M5P. The higher temperature recrystallization peaks (step "5") appeared to belong to the mixtures of $\boldsymbol{\beta'_P}$ and $\boldsymbol{\beta'_M}$. Further verification via X-ray

diffraction is, however, necessary. Four different phases were observed during the final melting (step "6" in Figure 5-8) of the material recrystallized after holding at 59.0 °C for 1 min (labeled with orange arrows).

The difference in melting points between mixtures and pure materials, shown as endothermic peaks (valleys in Figure 5-8), were not solely due to an averaging of the properties of the constituents. In particular, there are peculiarities of the structures of the solid-solution crystals that do not exist in the pure materials. This difference arises from the lamellar nature of the TAG crystals. When PPP is majoritarian in the lamellae, MMM can be interspersed by substitution, leaving some voids if necessary. This will not have a very disruptive effect on the attractive forces between the methyl-methyl planes that keep the lamellae together. However, if the phase forming the lamellae is predominantly MMM, inserting a PPP molecule disrupts the topography of the methyl plane and makes formation of the crystals more difficult. In keeping with that, liquid rich in MMM tends to return to its $\boldsymbol{\alpha_M}$ polymorphic form upon recrystallization. Liquid richer in PPP, on the other hand, more easily recrystallizes in the $\boldsymbol{\beta'}_P$ phase. The proportion of the phases at the end of the recrystallization reflects this tendency.

The traces in Figure 5-9 were chosen to show the separation of the 5M5P recrystallization peaks (in step "5") formed after holding for 1 min at different holding temperatures (step "e"). The thermogram shows that the $\boldsymbol{\alpha}_P$ peak (peak 2) formed earlier than the $\boldsymbol{\alpha}_M$ peak (peak 1). The $\boldsymbol{\alpha}_M$ peak corresponds to the phase that has a higher proportion of MMM, with a lower melting point and a lower carbon number in the alkyl chains. The other peak corresponds to the phase rich in PPP, which has a higher melting point.

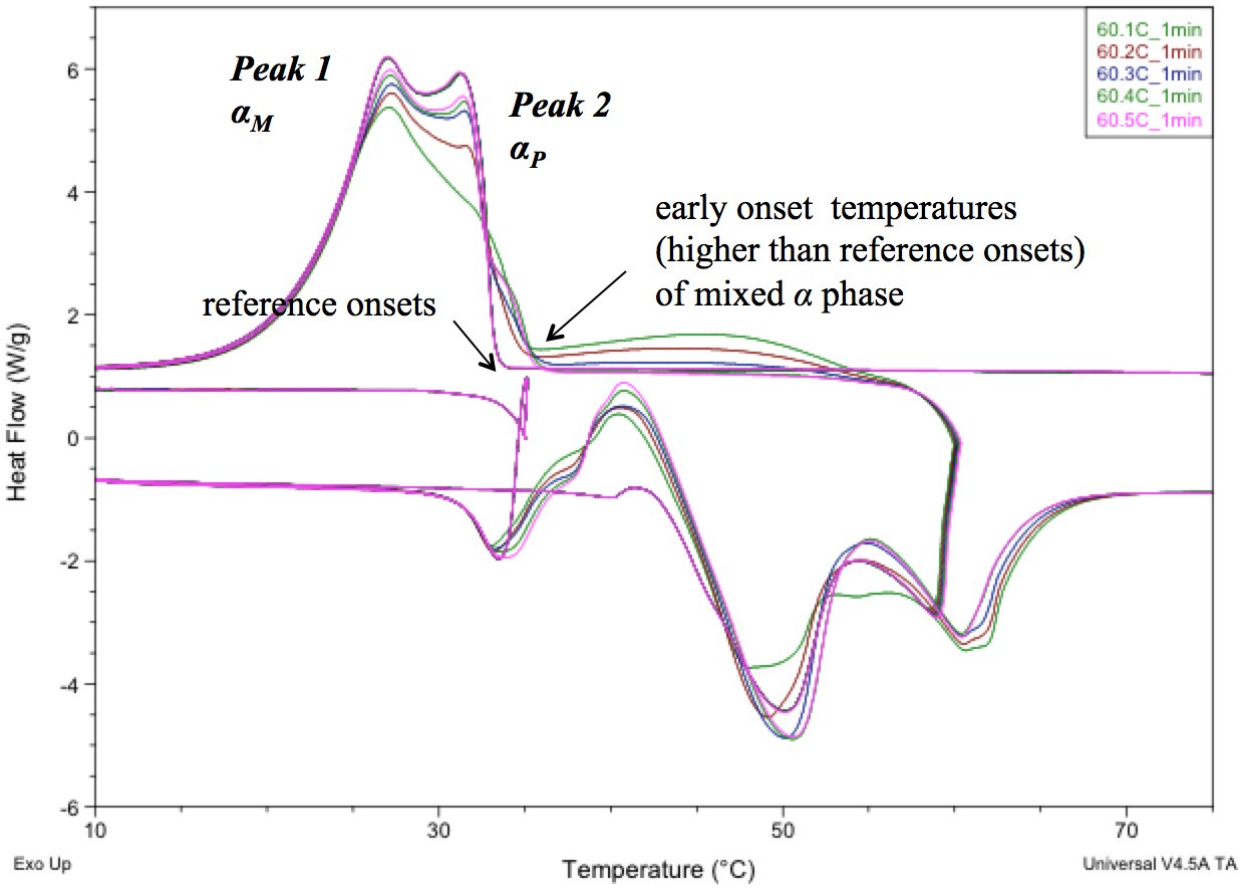

Figure 5-9. Peak separation as a result of the combined ***α*** and of ***β'*** memory effects of 5M5P. The early combined ***α*** (α_M) and onset can be clearly seen, both in the presence and absence ($T_H \geq 60.4$ °C) of ***β'*** recrystallization.

Figure 5-9 also shows how the early ***α*** onset happened in the mixture, both in the presence ($T_H < 60.4$ °C) and absence ($T_H \geq 60.4$ °C) of ***β'*** recrystallization. For T_H between 60.1 °C and 60.3 °C, the early onset occurred after a recrystallization of ***β'*** that reduced the magnitude of the α_P peak. It was thus concluded, as indicated before, that the liquid that recrystallized contributed to formation of the β'_P phase, and was not available to contribute to the formation of the α_P phase. For $T_H \geq 60.4$ °C, the early event may have been a more concentrated (in PPP) α_P phase, since the other two ***α*** peaks appear to have decreased. An additional recrystallization was also seen around 40 °C, during melting of the material held at 60.5 °C.

5.1.2 Boundaries of 5P5S

Figure 5-10 shows the temperature-time plot for 5P5S, reflecting the same process that was followed for SSS. We used a melting temperature of 103 °C (30 C° above the melting point of ***β*** SSS (step "a") in order to make sure that the sample was fully melted and homogeneous.

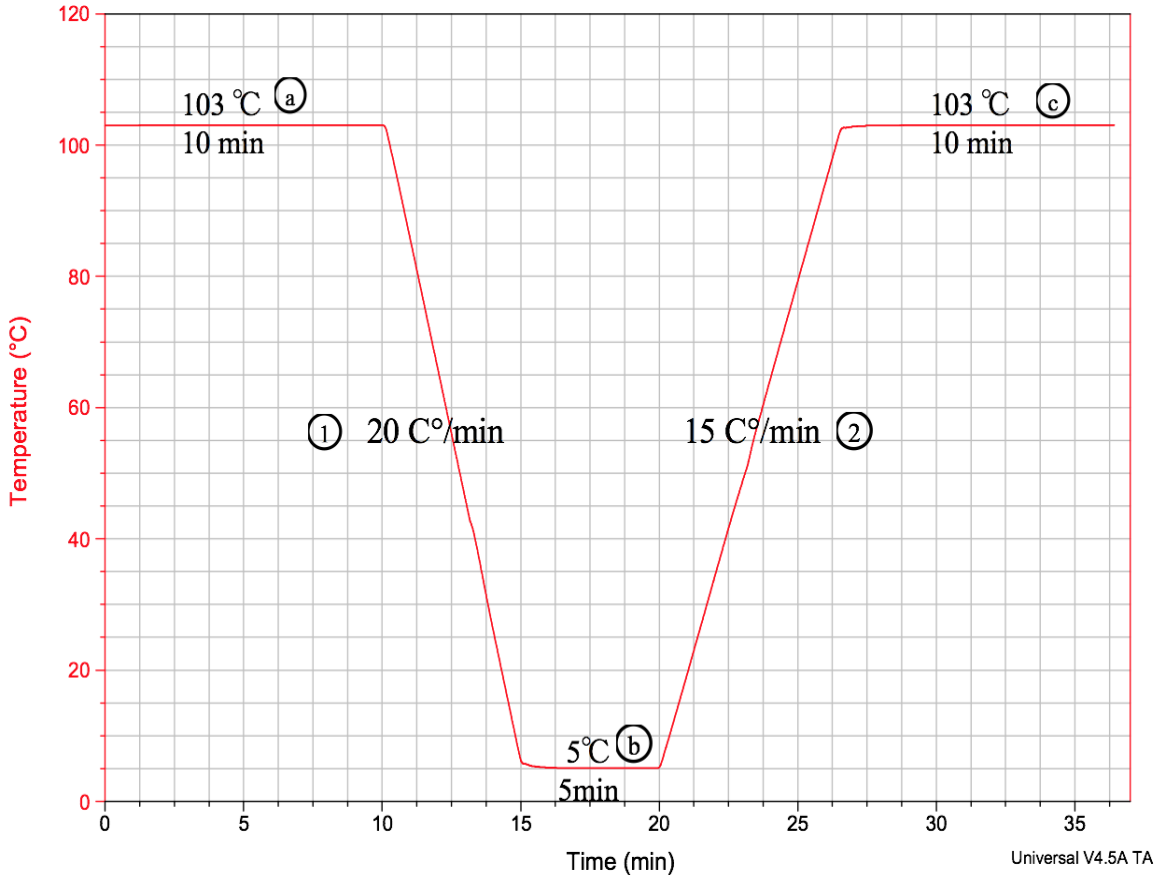

Figure 5-10. Temperature-time plot of 5P5S ***α*** polymorph formation and analysis.

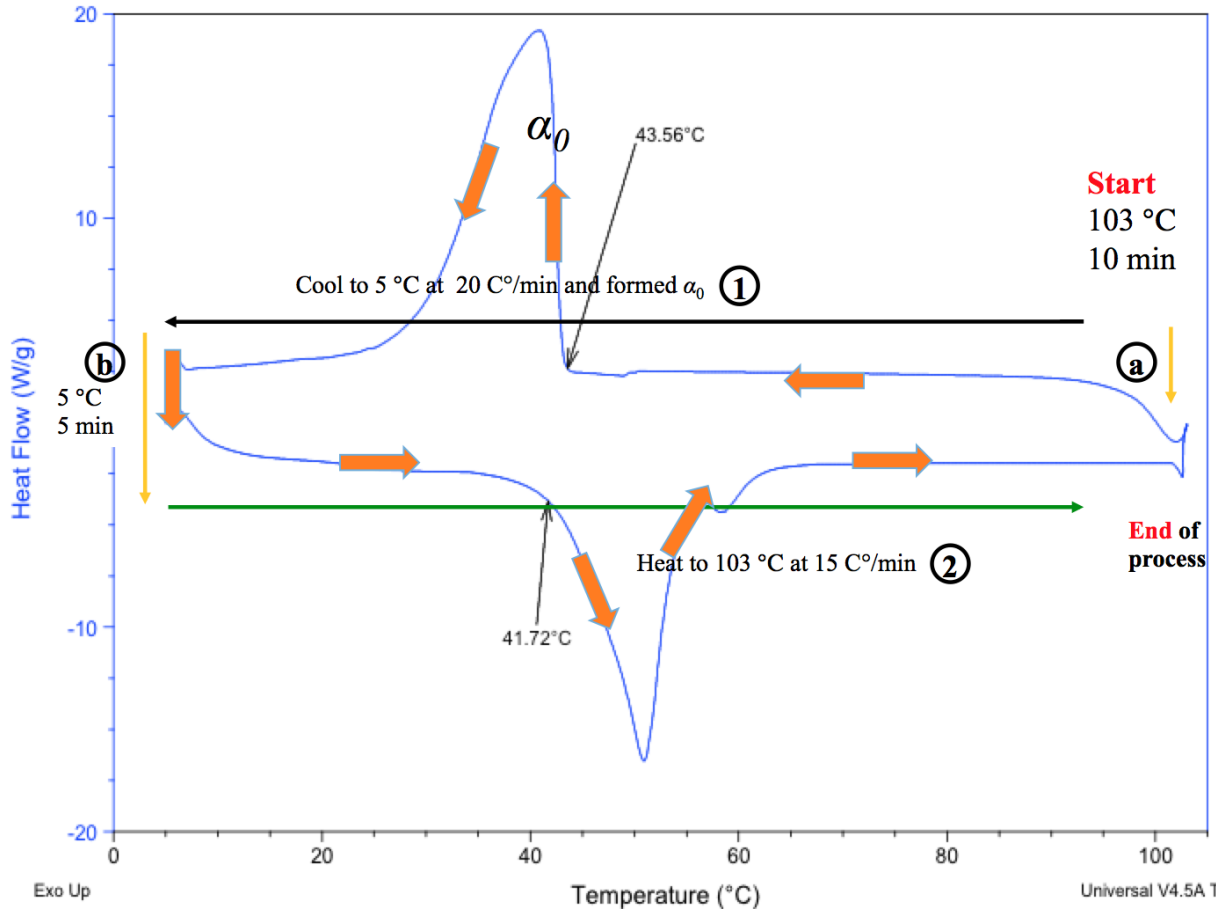

Figure 5-11. Thermogram of the process to form and analyze the ***α*** polymorph in 5P5S, indicating the cooling and heating directions and conditions.

During initial crystallization (step "1" in Figure 5-11), instead of forming two separate peaks, 5P5S exhibited only one broad peak, as shown in Figure 5-11. When the pure materials were mixed in a 50%:50% weight proportion, the ratio of the difference in alkyl chain lengths could be calculated as the difference in carbon number (according to Figure 5-12) divided by the average of the carbon number. For MMM and PPP, this ratio was 2/ ((14+16)/2) = 1/7.5. For PPP and SSS, it was 2/ ((16+18)/2) = 1/8.5, which is a larger ratio (smaller quotient). These values characterized how different the molecules "feel" in terms of the attractive alkyl forces, and the disruption of the crystalline structures. Thus, MMM and PPP feel "more different" towards each other than do PPP and SSS. Moreover, the total attractive forces between MMM and PPP are weaker than between

PPP and SSS due to the van der Waal's attractive forces, which are roughly proportional to the carbon number of the constituents in the TAG crystal. Therefore, the affinity between PPP and SSS is much greater than that between MMM and PPP, as the relative length is less dissimilar and there is more attraction between the two molecules. We were not surprised, therefore, to see one broad trailing peak in the thermogram. It is possible that there are two overlapping peaks, α_S and α_P, but, if so, they are not clearly resolved due to their proximity to each other during the crystallization process.

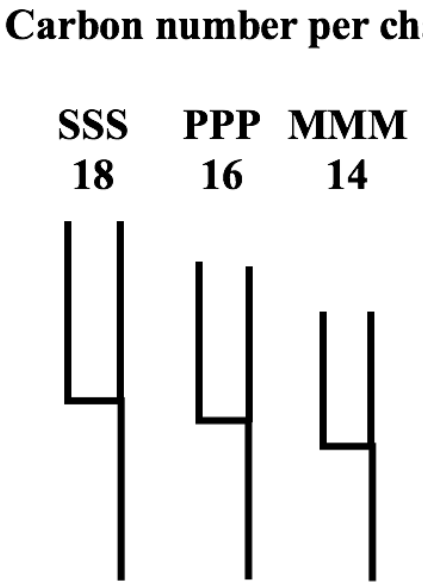

Figure 5-12. Qualitative representation of the effect of different carbon numbers per chain of MMM, PPP and SSS (Bailey *et al*.,).

Figure 5-13 shows an ideal phase diagram of α crystallization of 5P5S was calculated in a similar manner as the one built for 5M5P (see Figure 5-1 and Figure 5-4). As in those Figures, the red line is the theoretical liquidus line, the yellow line is the theoretical solidus line. The green dotted lines are 'tie lines', i.e. isothermal lines of solid and liquid compositions in equilibrium.

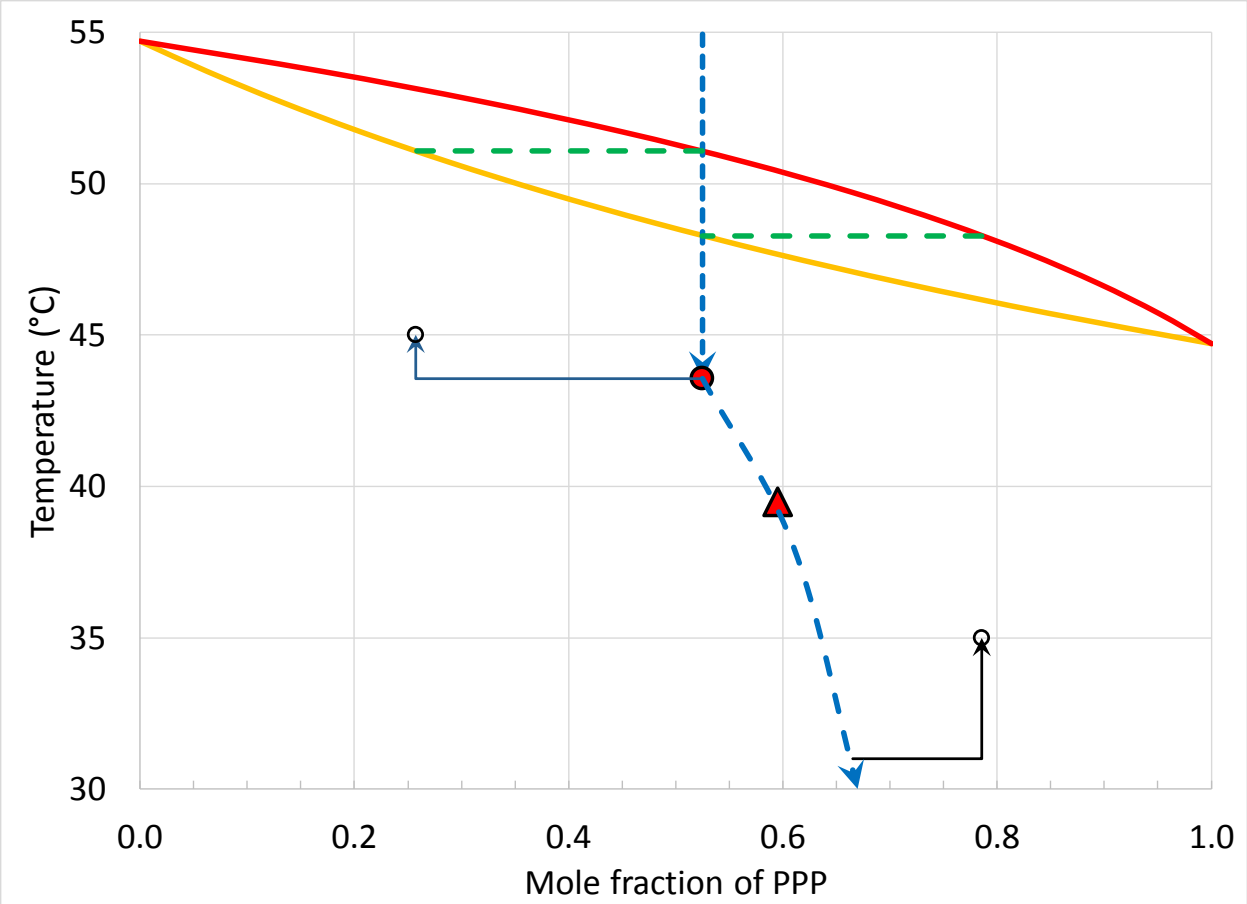

Figure 5-13. Ideal phase diagram for ***α*** crystallization of 5P5S. The equilibrium phase diagram was built in Excel using a similar method as that for Figure 5-4. For an explanation of the trjectory of the liquid (blue dotted line) and the other symbols, please see the text.

The curves and lines were calculated in Excel using the same thermodynamic equations above, and the parameter values in Chapters 1 and 2 for PPP and SSS. On top of them were plotted the onset of crystallization (circle) and the summit of the crystallization peak (triangle) temperatures, as a function of the composition of the liquid phase. The mole fraction of PPP in 5P5S was x_M = 0.525. The blue dashed line represents the cooling of liquid that stays at this concentration until it reaches the onset of crystallization (circle). Crystallization would produce a phase richer in SSS, leaving behind a liquid enriched in PPP, as qualitatively illustrated by the blue dashed line below

the onset. The two thin arrows point at the temperatures estimated for the melting of the α phases from the thermograms, α_S (~ 45.0 °C) and α_P (~ 35.0 °C).

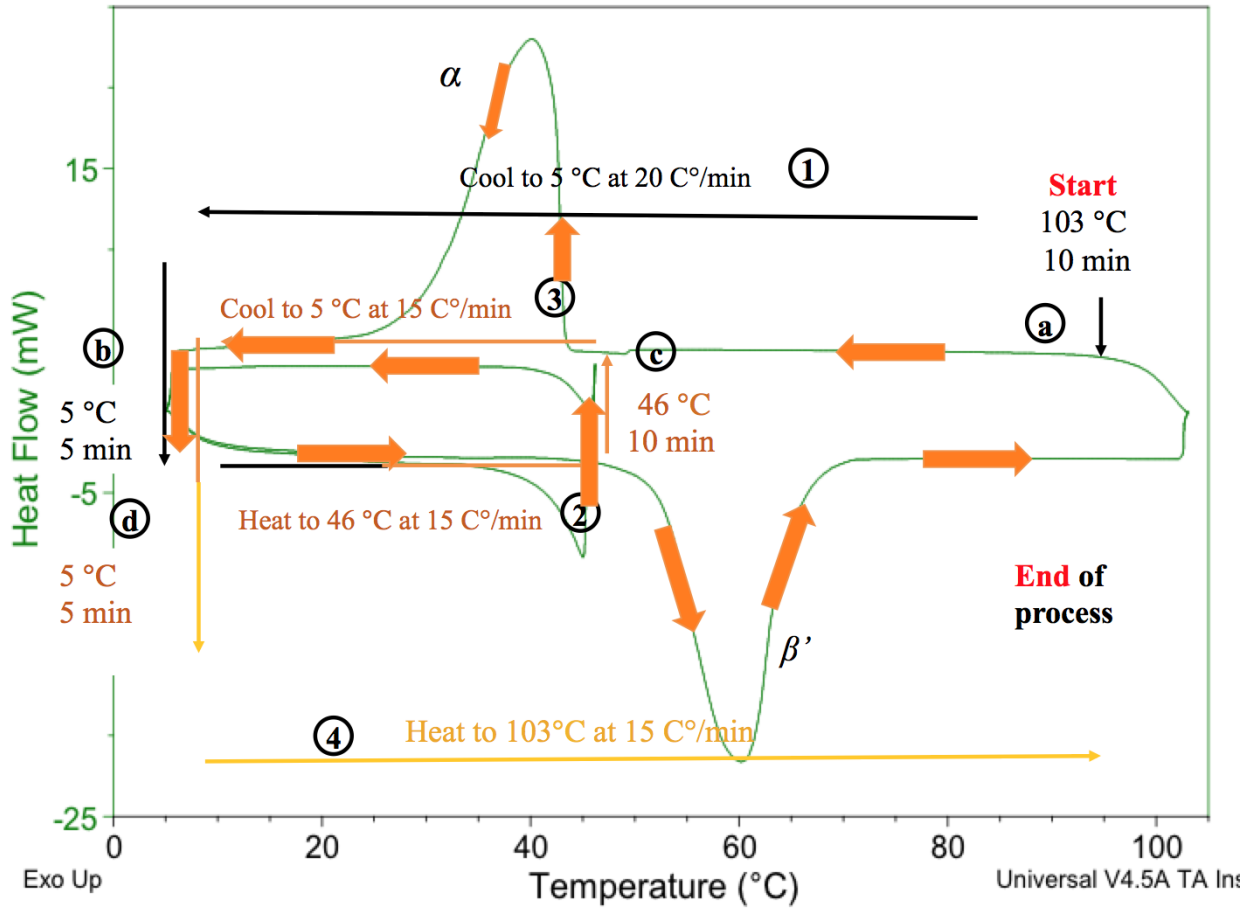

Figure 5-14. Thermogram of the process to form and analyze the ***β'*** polymorph in 5P5S, indicating the cooling and heating directions and conditions.

The tempering process was done by heating at 15 C°/min to 46.0 °C and holding the sample there for 10 minutes (steps "2" and "c" in Figure 5-14) followed by cooling back to 5.0 °C at 15 C°/min (step "3" in Figure 5-14).

During heating (step "4" in Figure 5-14), 5P5S was fully melted when the temperature reached approximately 67 °C, which is quite similar to the temperature at which 5M5P fully liquefied when heated at 15 C°/min (step "1" in Figure 5-14). This illustrates the difficulty of predicting the effect that the mixing has on the melting point of these blends. One might expect that a PPP-SSS blend

would have a higher final melting point than a MMM-PPP blend with similar polymorphic forms. However, we do not have any quantitative information of the energies of interaction between different molecules. Those energies no doubt play an important role in these solid solution crystals. The procedure of finding memory boundaries after the tempering process is summarized in Figure 5-15.

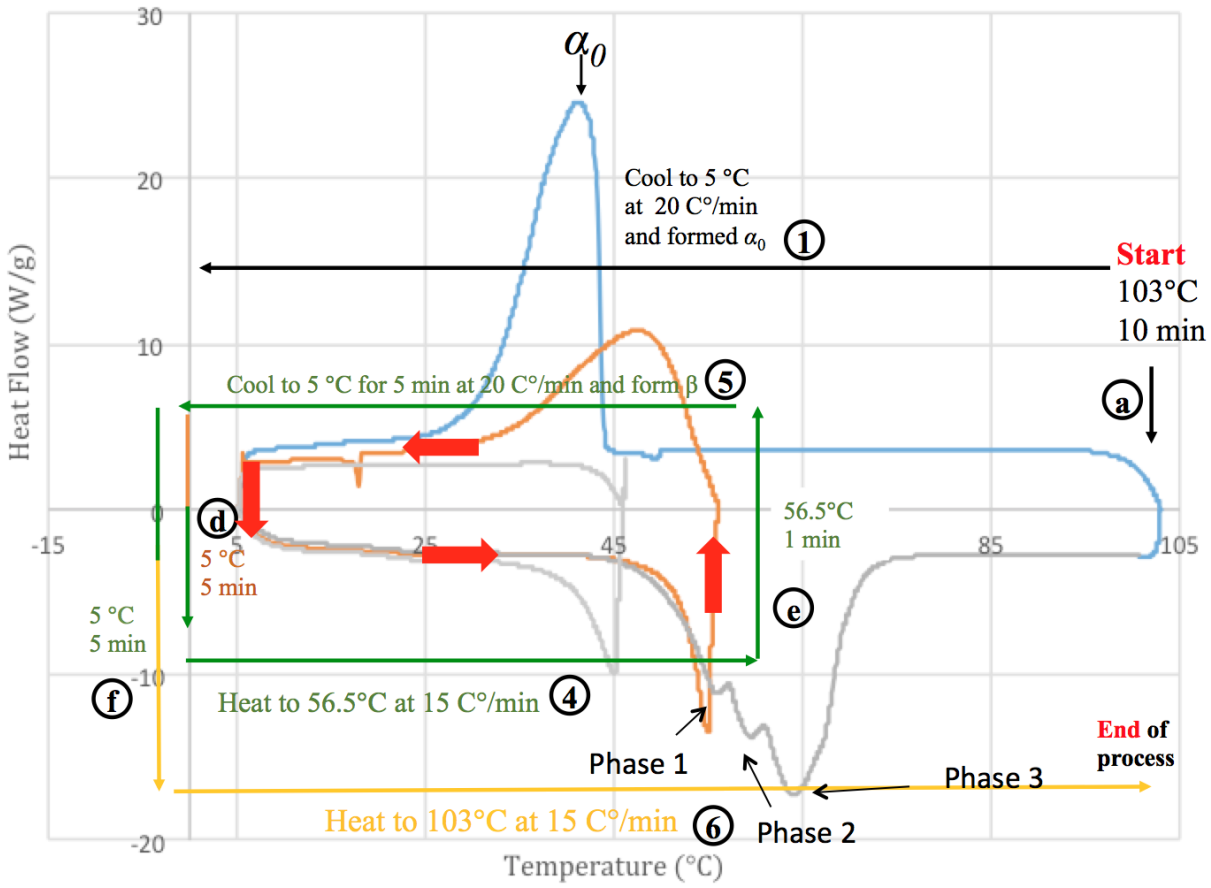

Figure 5-15. Thermogram from the program used to characterize the ***β'*** memory effect for 5P5S, at 56.5 °C for 1 min. Red indicates the process of temperature- time combination test (step "4", "e" and "5").

The peak of recrystallization (step "5") significantly shifted to a higher temperature with respect to the peak α_0. It is hard to tell whether the recrystallization peak belongs to the ***β'*** or ***β*** polymorphs

without results from X-ray diffraction, which were not available for this study. The current results only revealed that the sample starts to crystallize at a higher temperature compared to the α_0 crystallization peak. With the above caveat, we will call it "***β'*** ". A complex melting pattern appeared in the final melting stage, suggesting the presence of three different phases.

The approximate temperature-time boundaries for 5P5S are collected in Table 5−4 and Table 5−5. The averaged data have been plotted in Figure 5−16.

Table 5-4. Time at each holding temperature that defined the boundary for "early ***α*** memory" of 5P5S. The "α Time_1 (min)" is the holding time boundary at holding temperature for pan 1 and "α Time_2 (min)" is the holding time boundary at holding temperature for pan 2.

Holding Temperature (°C)	**55.0**	**56.5**	**57.0**	**57.5**	**58.0**	**59.0**	**60.0**
***α* Time_1 (min)**	30	20	18	15	12	6	2
***α* Time_2 (min)**	25	18	15	13	10	5	1
***α* Time average**	27.5	19	16.5	14	11	5.5	1.51

Table 5-5. Time at each holding temperature that defined the boundary for " β' memory" of 5P5S. The "β' Time_1 (min)" is the holding time boundary at holding temperature for pan 1 and "β' Time_2 (min)" is the holding time boundary at holding temperature for pan 2.

Holding Temperature (°C)	**55.0**	**56.5**	**57.0**	**57.5**	**58.0**	**59.0**	**60.0**
***β'* Time_1 (min)**	15	12	10	7	4	1	0.3
***β'* Time_2 (min)**	17	13	11	9	5	2	0.5
***β'* Time average**	16	12.5	10.5	8	4.5	1.5	0.4

The lowest temperature at which the memory effect happened for 5P5S was T_{min} = 55.0 °C, which is the same as the lowest temperature observed in 5M5P (T_{min} = 55.0 °C, Table 5-1). The two blends contain pure PPP, whereas the other component is quite different in terms of the melting points, enthalpies, and molecular masses of MMM and SSS. Yet, it turns out that the T_{min} and T_{max}

of both mixtures were similar, both near the melting point of ***β'*** PPP, 55.7 °C (Table 5-6). It is possible that PPP somehow played a dominant role in both mixtures.

Table 5-6. Melting points of the ***α*** and polymorphs ***β'*** of PPP and SSS.

TAG m.p. (°C)	***α***	***β'***
PPP	44.7	55.7
SSS	54.7	64.3

The boundary conditions for ***α*** and beta type (***β'***) memory are plotted in Figure 5-16. According to the data in Table 5-4 and Table 5-5, plotted in Figure 5-16, the temperature boundary of the ***α*** form crystal memory was just above the melting point of ***α*** SSS, which was around the melting point of ***β'*** PPP.

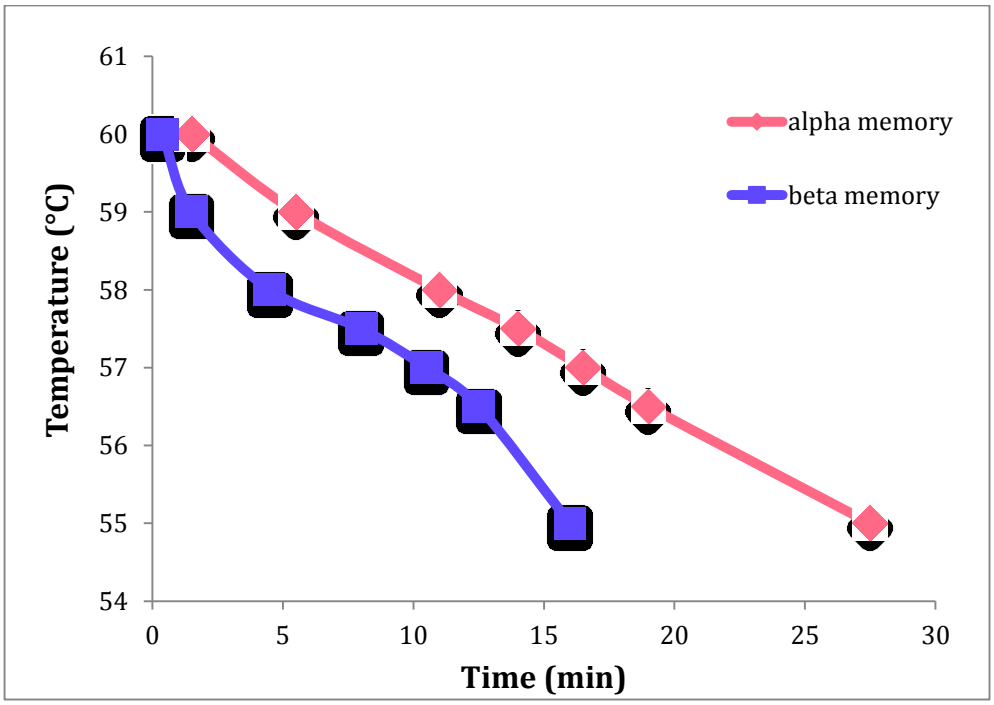

Figure 5-16. Boundaries of temperature-time combination of two different memories of 5P5S. Red line indicates the boundary of alpha type (***α***) memory while blue line represents the boundary of beta type (***β'***) memory.

Linear regression of the holding temperatures as a function of holding times for the ***α*** form yielded $T_H = (60.1 \pm 0.1) - (0.18 \pm 0.01) \times t_H$, with t_H in minutes. The shape of the ***β'*** boundary was not linear, and no attempt was made to describe it mathematically.

Even though the melting temperature of ***α*** PPP and ***β'*** MMM were both around 55 °C, the temperature range (5.5 C°) and time span (~ 15 min β' and 30 min α) of the 5P5S boundary were broader than those of the pure TAGs. Thus, the hypothesis that the mixtures require longer times than the pure materials to erase the memory effect is supported by the data presented in the current study.

The exception may be the long holding times of early ***α*** memory in pure PPP and SSS at their lowest temperatures. They exhibit very narrow temperature ranges (less than 0.6 C°). In the mixtures, the times were of the same order of magnitude, but the temperature range was much broader.

The overlaid thermograms for 5P5S in Figure 5-17 illustrates several temperature-time combinations at the boundary of the α memory effect (from step "e").

The holding time needed for 5P5S at 55.0 °C was much longer than at higher temperatures, and recrystallization produced a ***β***'-type peak with an early onset temperature, with a small ***α*** peak was formed in the end. As the holding temperature increased to 58.0 °C (step "e") and the time decreased, larger amounts of $\boldsymbol{\alpha_P}$ were formed, along with smaller amounts of ***β'***. Three different phases were produced during the recrystallization process at a holding temperature of 59.0 °C: $\boldsymbol{\alpha}_P$, $\boldsymbol{\alpha}_S$, and ***β'***. After holding at 60.0 °C for 1 min, only $\boldsymbol{\alpha}_P$ and $\boldsymbol{\alpha}_S$ recrystallized, albeit at considerably higher onset temperatures.

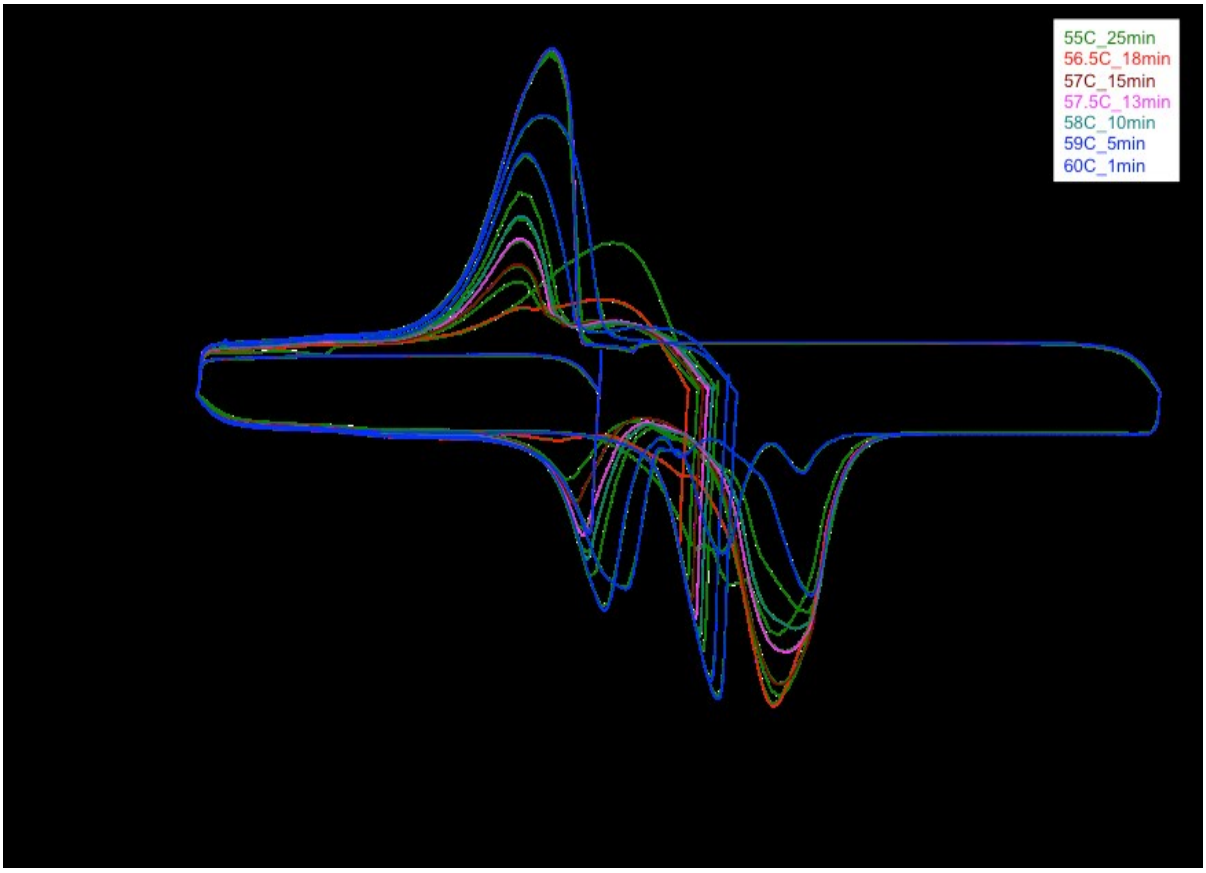

Figure 5-17. Overlaid thermograms of temperature-time boundaries of ***α*** memory for 5P5S.

Figure 5-18 contains the overlay of the thermograms used to determine the boundaries of the ***β***' memory of 5P5S, which are plotted in Figure 5-16. The temperature-time boundaries of "***β***' memory" were broader than those seen with other materials. The results suggest that, under these holding temperature and time combinations, the recrystallization at higher temperatures produced at least two phases, one rich in SSS, perhaps ***β***'$_S$, and another rich in PPP, most likely ***β***'$_P$. The complexity of the melting profiles, along with the lack of supporting X-ray diffraction data, made a clear interpretation very difficult.

With these experiments, we have created a preliminary map of the memory boundaries of these two important homologous blends of saturated triacylglycerols; these boundary temperatures are summarized in Figure 5-18 and Table 5-7.

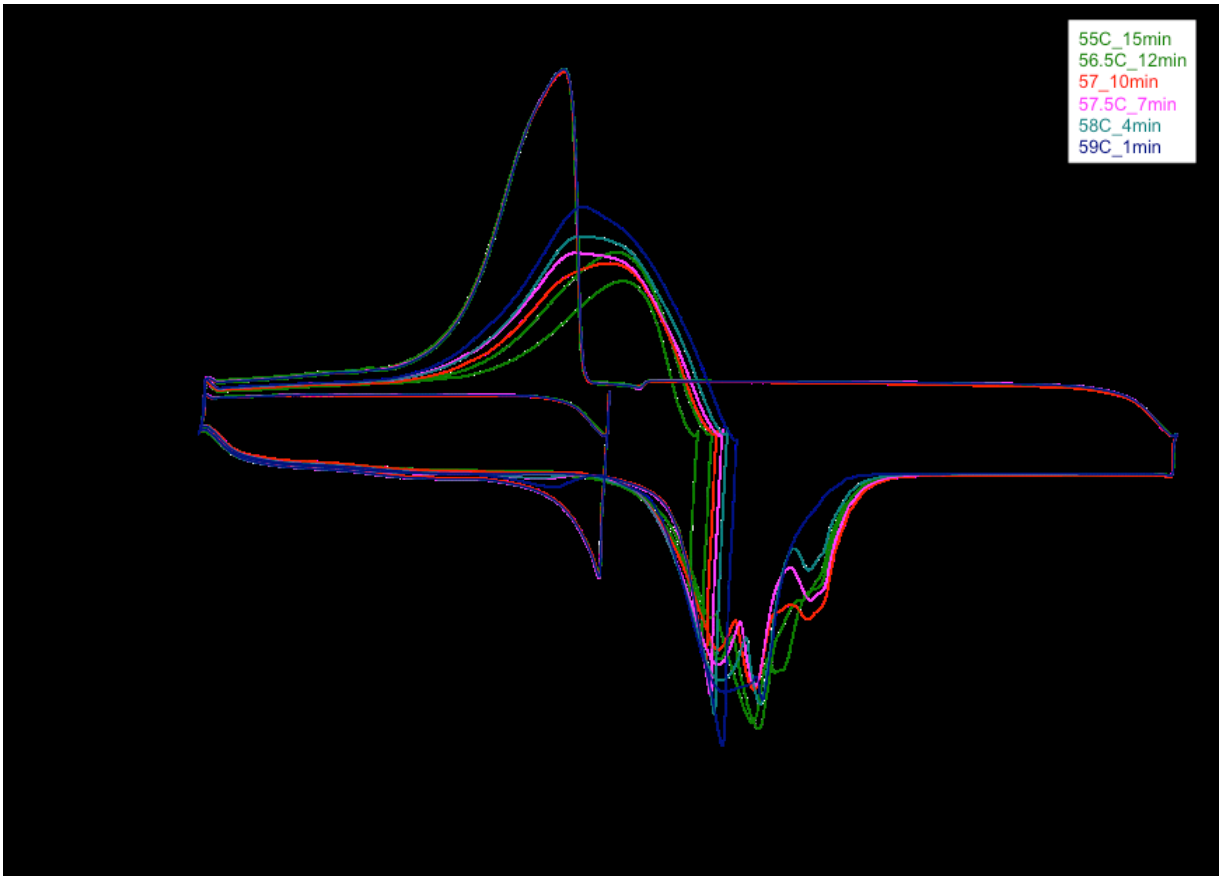

Figure 5-18. Thermograms for the boundaries of the ***β***' memory of 5P5S.

Table 5-7. Limit temperatures of the memory effect in the 5M5P and 5P5S blends.

°C	5M5P	5P5S
T_{min}	57.0	55.0
T_{max}	60.6	60.0

One explanation for the extended holding times needed to erase memories in mixed TAGs relates to the fact that crystals formed from TAG mixtures are solid solutions. Two phases are formed, and they have different compositions, and they are spatially distributed. Upon melting, the mixed molecules in one micro region are in a different composition environment than those in an adjacent microregion. Thus, the molecules start a diffusion process, leading back into a homogeneous

molecular distribution, as had been present in the original hot liquid. Because crystallization produces many small areas of different molecular distributions, the melting simply makes these areas liquid, without instantaneously removing the concentration gradients between them. Therefore, the molecules have to diffuse to reduce these differences until the melt is homogeneous. This is not necessary in the pure substance, since all the molecules are the same. Thus, the memory effect seems to consist of two phenomena: thermal separation of the molecules, which was discussed in the context of pure triacylglycerols, and the diffusion of different molecules in the liquid state, which requires longer times, and was observed in the mixtures.

5.2 Onset temperatures of recrystallization of the α and β' polymorphs

5.2.1 Onset temperatures of 5M5P

Table 5-8 shows the onset temperature of the first crystallization (step "1" in Figure 5-14) from the completely melted and homogeneous liquid, T_{onset} for the α_0 phase. Three repeating experiments were performed for each DSC pan and two pans were made for each sample. The average T_{onset} values of α_0 were 33.7 ± 0.05 °C for pan 1and 33.6 ± 0.04 °C for pan 2. These average values were used in the calculation of ΔT_α and $\Delta T_{\alpha\beta'}$.

Table 5-8. T_{onset} of the reference phase α_0 from the experiments with 5M5P.

Test	1	2	3	Average
$T_{onset_\alpha 0}$_1 (°C)	33.79	33.67	33.72	**33.73**
$T_{onset_\alpha 0}$_2 (°C)	33.57	33.64	33.66	**33.62**

Table 5-9. Summary of the onset temperatures of the crystallization of "early ***α*** memory" (T_{onset_α}) and the onset temperatures of the crystallization of "***β***'memory" ($T_{onset\_\beta'}$) of 5M5P, as a function of the holding temperature. The onset temperatures of the crystallization (in step "5") of "early ***α*** memory" (T_{onset_α}) are in orange characters, and the onset temperatures of the crystallization of "***β*** memory" (T_{onset_β}) are in black characters.

Holding Temperature (°C)	**57.0**	**58.0**	**59.0**	**60.0**	**60.1**	**60.2**	**60.3**	**60.4**	**60.5**	**60.6**
T_{onset_α}_1 (°C)	35.22	34.69	35.27	34.73	34.66	35.44	35.21	35.28	35.32	35.53
T_{onset_α}_2 (°C)	35.10	35.08	35.13	34.96	34.77	35.10	35.01	35.03	35.13	35.22
$T_{onset_\beta'}$_1 (°C)	54.76	55.83	56.91	57.06	-	-	-	-	-	-
$T_{onset_\beta'}$_2 (°C)	53.76	54.98	57.78	57.93	-	-	-	-	-	-

Table 5-10. Summary of the differences between $T_{onset\_\alpha 0}$ and T_{onset_α} (ΔT_α) and the differences between $T_{onset\_\alpha 0}$ and $T_{onset\_\beta'}$ ($\Delta T_{\alpha\beta'}$) of 5M5P. The ΔT_α is present in red characters and $\Delta T_{\alpha\beta}$ is present in blue characters.

Holding Temperature (°C)	**57.0**	**58.0**	**59.0**	**60.0**	**60.1**	**60.2**	**60.3**	**60.4**	**60.5**	**60.6**
ΔT_{α}_1 (C°)	1.50	0.97	1.55	1.01	0.94	1.72	1.49	1.56	1.60	1.81
ΔT_{α}_2 (C°)	1.48	1.46	1.51	1.34	1.15	1.48	1.39	1.41	1.51	1.60
$\Delta T_{\alpha\beta'}$_1 (C°)	21.04	22.11	23.19	23.34	-	-	-	-	-	-
$\Delta T_{\alpha\beta'}$_2 (C°)	20.19	21.41	24.21	24.36	-	-	-	-	-	-

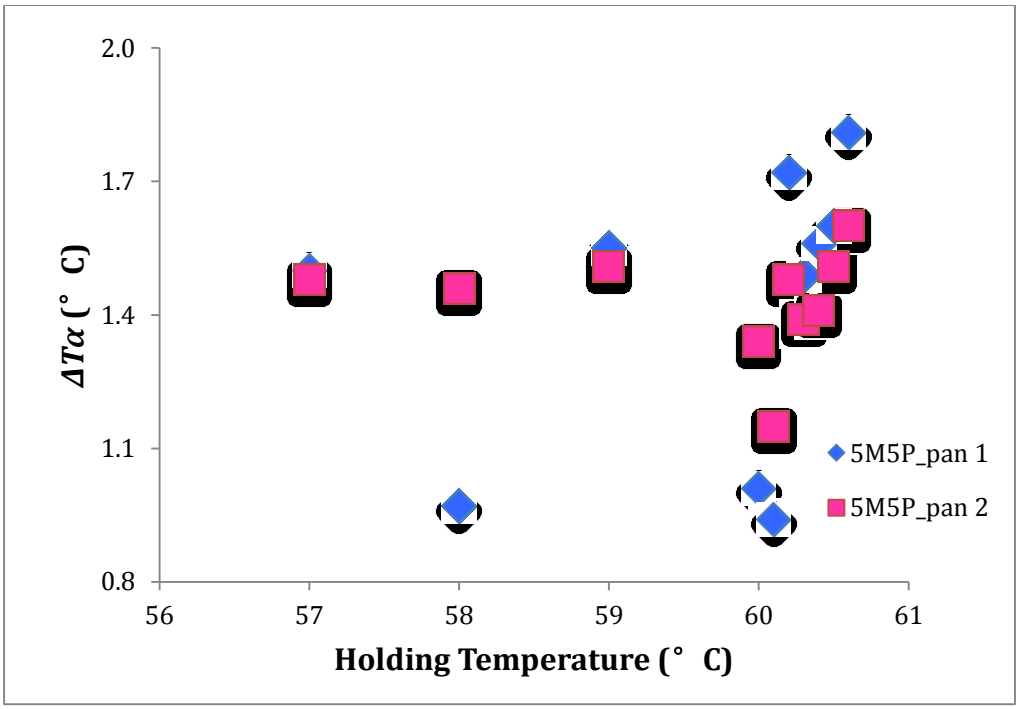

Figure 5-19. Onset temperature differences ΔT_α for the α recrystallization as a function of the holding temperature for the two 5M5P samples (Table 5-10). Blue diamonds represent data from pan 1, whereas pink squares represent data from pan 2.

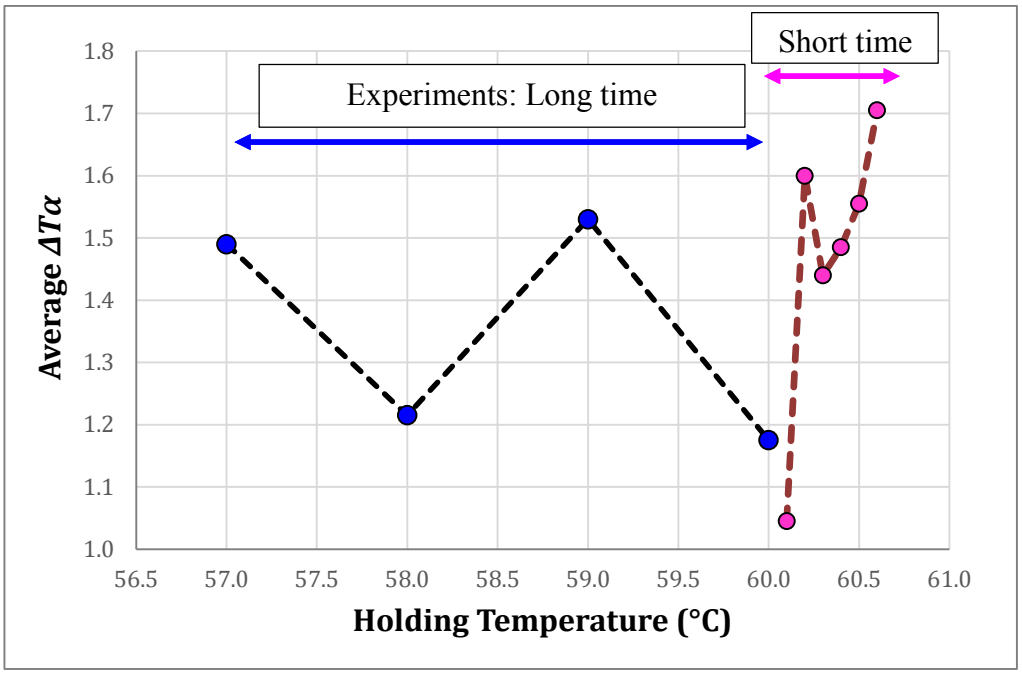

Figure 5-20. Summary of the averaged values from the experimental pairs of ΔT_α as a function of holding temperature, plotted as lines instead of points. The black line and blue points correspond to long time data up to 60 °C, the brown line and pink to points to short time data above 60 °C.

The ΔT_α data from Table 5-10 were plotted in Figure 5-19, showing in blue the values from one pan and in pink those from the other pan. The values ranged from 0.94 to 1.8 C°, indicating the presence of a memory effect. However, no distinct trend was clear with respect to the change in onset temperature ΔT_α due to the holding temperature. Perhaps there is an increasing trend in ΔT_α above 60 °C. This can be better seen if the ΔT_α data from Table 5-10 are averaged before plotting them, and identified according to holding time/temperature, as shown in Figure 5-20. The black line and blue points correspond to long time data up to 60 °C, the brown line and pink to points to short time data above 60 °C. A larger number of replicates and points will be needed to confirm this in a future study of these mixtures. The two temperature sets corresponded to two distinct time regions, short or long, though this is not self-evident from the plot. The data below a holding temperature of 60.0 °C corresponded to long times, whereas the data above corresponded to short times. Thus, the ascending trend in ΔT_α the average holding temperature above 60.0 °C corresponded to decreasing times and increasing temperatures in the short time region. The short times somewhat reduced the precision of onset temperature determination in these experiments, in comparison with the longer-time experiments. The absence of trend in the longer-time experiments may correspond to a pseudo-equilibrium state of the liquid state, with a range in ΔT_α between 1.2 and 1.5 C°.

5.2.2 Onset temperatures of 5P5S

Table 5-11. T_{onset} of the reference phase α_0 from the experiments with 5P5S.

Test	1	2	3	Average
$T_{onset_\alpha 0}$_1 (°C)	44.42	44.39	44.37	44.39
$T_{onset_\alpha 0}$_2 (°C)	44.16	44.25	44.22	44.21

Table 5-11 shows the T_{onset} of α_0 for 5P5S. Three replicates were done for each pan and two pans were made for each sample, as with the other materials studied. The average T_{onset} values of α_0 for were 44.4 ± 0.02 °C for pan 1 and 44.2 ± 0.04 °C for pan 2. These average values were used in the calculation of ΔT_{α} and $\Delta T_{\alpha\beta'}$, shown in Table 5-12 and Table 5-13.

Table 5-12. Summary of the onset temperatures of the crystallization of "early α memory" (T_{onset_α}) and the onset temperatures of the crystallization of "β' memory" ($T_{onset\_\beta'}$) of 5P5S, as a function of the holding temperature. The onset temperatures of the crystallization (in step "5") of "early α memory" (T_{onset_α}) are in orange characters, and the onset temperatures of the crystallization of "β memory" (T_{onset_β}) are in black characters.

Holding Temperature (°C)	55.0	56.5	57.0	57.5	58.0	59.0	60.0
T_{onset_α}_1 (°C)	43.21	42.89	44.32	47.67	43.09	43.04	45.21
T_{onset_α}_2 (°C)	41.06	41.23	43.39	47.7	42.78	42.27	43.47
$T_{onset_\beta'}$_1 (°C)	55.98	56.21	57.13	59.45	58.92	61.04	59.34
$T_{onset_\beta'}$_2 (°C)	55.03	55.98	57.01	58.89	58.04	59.77	59.08

Table 5-13. Summary of the differences between $T_{onset\_\alpha 0}$ and T_{onset_α} (ΔT_{α}) and the differences between $T_{onset\_\alpha 0}$ and $T_{onset\_\beta'}$ ($\Delta T_{\alpha\beta'}$) of 5P5S. The ΔT_{α} is present in red characters and $\Delta T_{\alpha\beta}$ is present in blue characters.

Holding Temperature (°C)	55.0	56.5	57.0	57.5	58.0	59.0	60.0
ΔT_{α}_1 (C°)	-1.00	-1.32	0.11	3.46	-1.12	-1.17	1.00
ΔT_{α}_2 (C°)	-3.33	-3.16	-1.00	3.31	-1.61	-2.12	-0.92
$\Delta T_{\alpha\beta'}$_1 (C°)	11.77	12.00	12.92	15.24	14.71	16.83	15.13
$\Delta T_{\alpha\beta'}$_2 (C°)	10.64	11.59	12.62	14.50	13.65	15.38	14.69

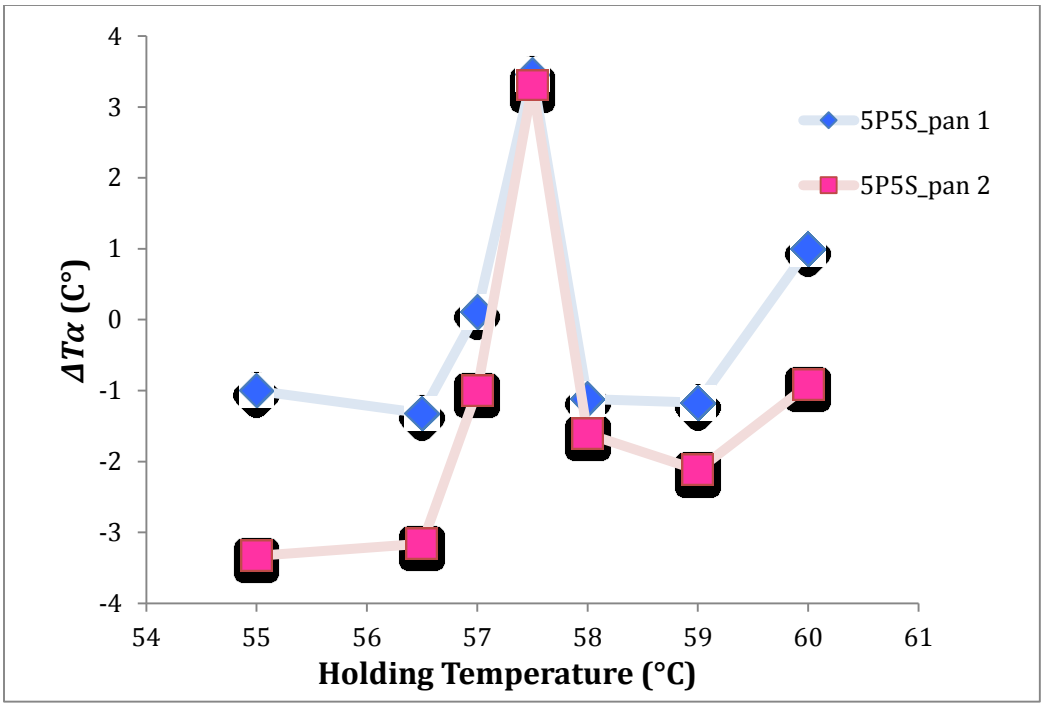

Figure 5-21. Onset temperature differences for the ***α*** recrystallization as a function of the holding temperature for the two 5P5S samples.

It is difficult to determine the effect of the holding temperature on the onset temperatures for 5M5P and 5P5S, which are shown in Figure 5-19, Figure 5-20 and Figure 5-21. As with the pure materials, there seemed to be different regions with trends of behavior separated by sharp boundaries. In general, the patterns followed by the ΔT_α were the same in the two pans, suggesting that the behaviors are not random. Studies with smaller temperature intervals with more exploratory times are required before any conclusions can be drawn regarding the behavior of these mixed materials. These preliminary experiments hopefully will serve as a guide for further research. Negative ΔT_α values indicate that the liquid structures formed were less prone to crystallize.

5.2.3 Onset temperatures of the *β'* polymorphs of 5M5P and 5P5S

The trends in the onset temperature differences, $\Delta T_{\alpha\beta'}$, for recrystallization of the ***β'*** polymorphs of 5M5P and 5P5S, as a function of the holding temperatures, can be seen in Figure 5-22. The

tendencies were relatively smooth compared to the ΔT_{α} data obtained for the ***α*** polymorph. In general, as the holding temperature increased, the onset of recrystallization occurred at a higher temperature, even though the holding times were shorter. In both cases, the range of the onset was around 5 C°, though for 5M5P the memory was only studied above 57.0 °C. The error bar shown near each material data shows ± one standard deviation, as calculated from the data with respect to their own local means.

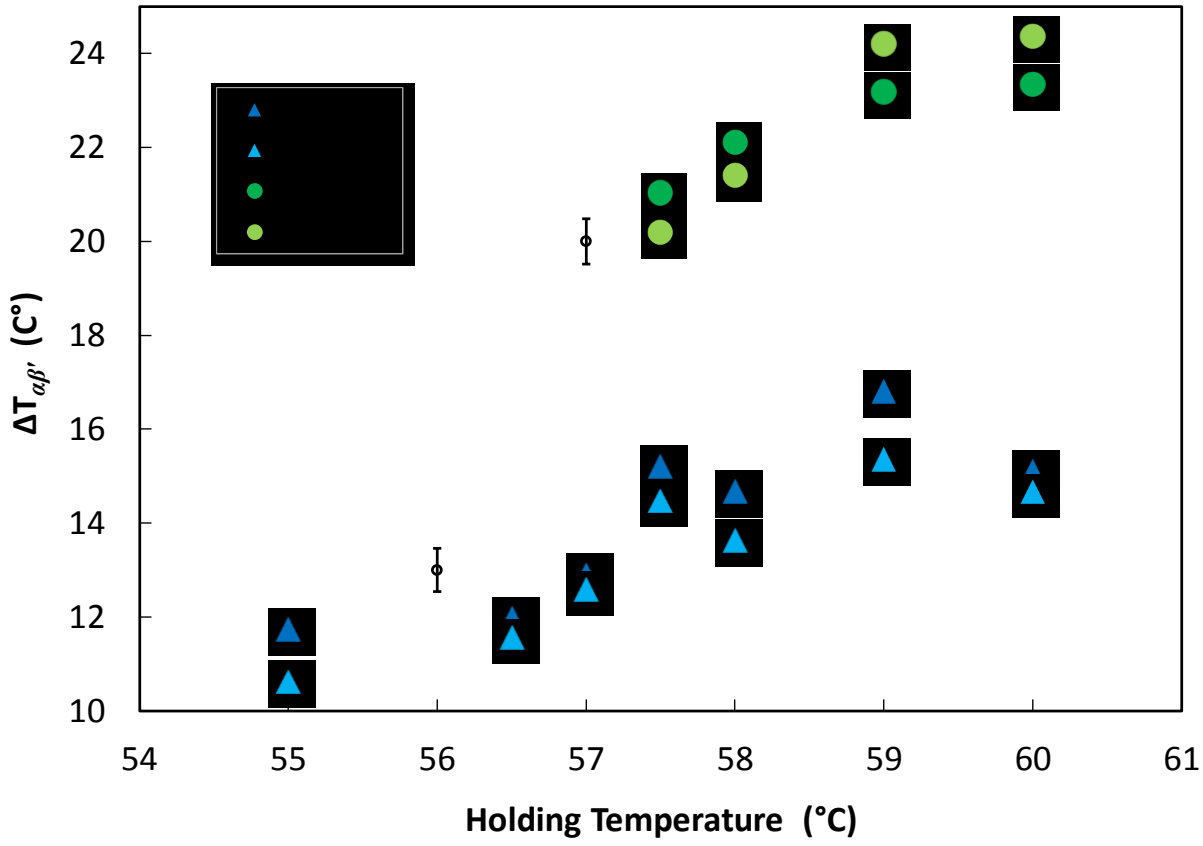

Figure 5-22. Onset temperature differences $\Delta T_{\alpha\beta'}$ for recrystallization of the ***β'*** polymorphs of 5M5P and 5P5S, as a function of the holding temperature, including the two pans of each material. The error bar shown near each material data shows ± one standard deviation, as calculated from the data.

5.3 Illustrative example: simulation of diffusion from binary regions of different composition in mixtures

As was explained in the introduction to this section and at the end of section 5.1.2, after a crystallization process from a binary liquid composed of saturated TAG, it is common to find two or three crystalline phases coexisting. Each phase is a collection of solid solution nanocrystals solutions. The nanocrystals of each phase have approximately the same composition, which differs from the composition of the nanocrystals of other phases. The total or average composition of the bulk, composed by the various phases, adds up to the same as the original fully melted liquid. The nanocrystals that have approximately the same composition and polymorphic form inside a particular spatial region will have their melting range and enthalpy and sometimes this will be clear in the DSC. In any case, after a relatively fast melting in the absence of mixing, the liquid will retain almost intact the original distribution of diverse compositional zones.

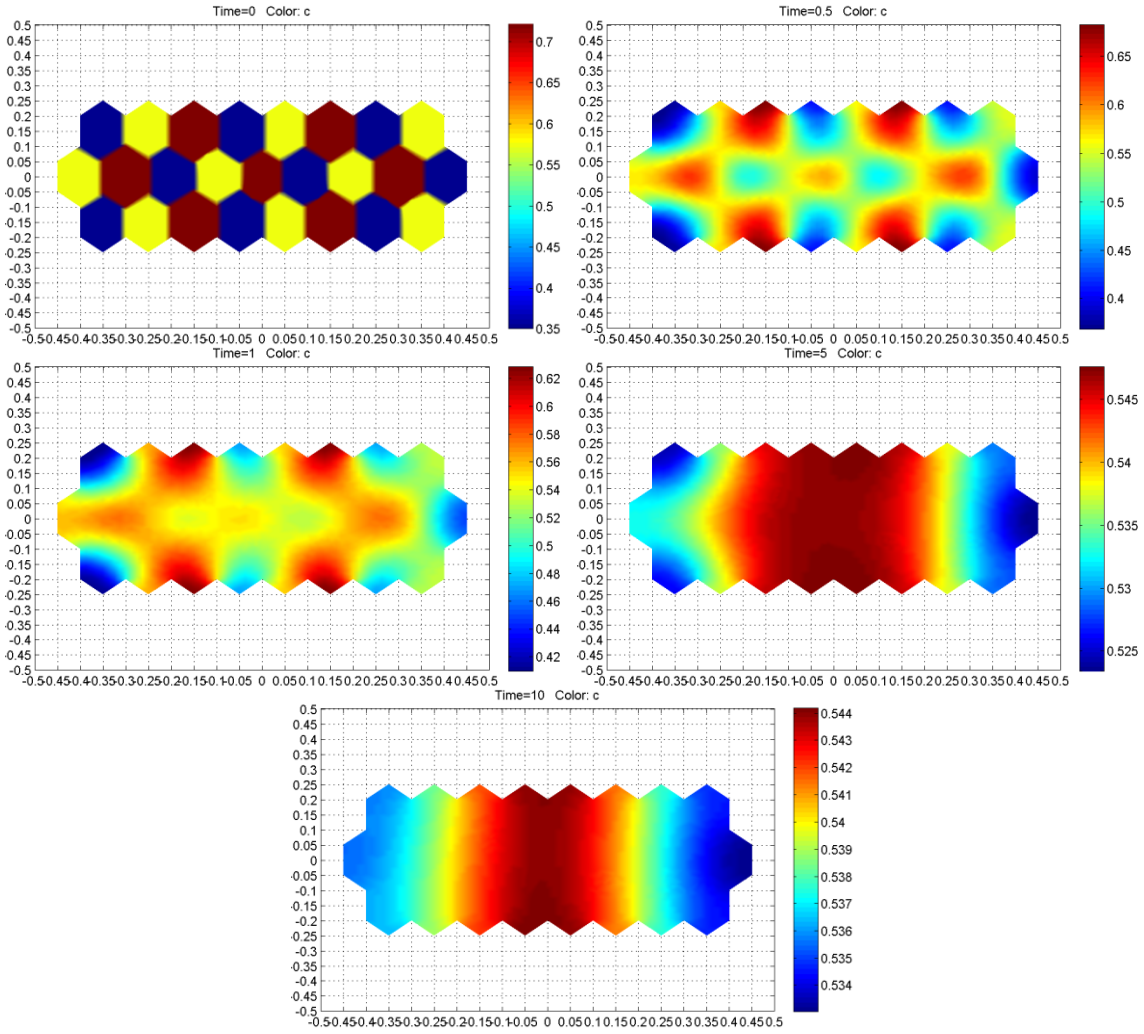

Figure 5-23. Concentration distribution of MMM simulated for binary TAG diffusion from small domains of about 100 microns. Time sequence shown after 0, 0.5, 1, and 10 minutes. The color bar is relative, bracketed between the minimal and maximal concentrations.

Molecular diffusion will then take place until the molecular distribution is again that of the original hot liquid. If it is assumed that the molecular distribution of the original liquid is random, one can perform a relatively simple simulation to estimate the time needed for the domains to become even.

Figure 5-23 shows a graphical representation of a simulation done by Dr. Mazzanti of a portion of a binary mixture, featuring close to 50% of each component. It was assumed that the sample had crystallized in three different phases, in domains that were about 120 microns in diameter. In this example, the bulk binary sample is 5M5P, the solid phase represented by the brown color is

composed of 71% MMM and 29% PPP. The solid blue phase has 35% MMM, and the solid yellow phase has 56% MMM. It was assumed that they melted very rapidly, transitioning into the liquid state while preserving their compositions and spatial distribution. After diffusing for 0.5 min at the holding temperature, the materials blurred the boundaries between the domains. The total range of the color bar becomes smaller since the maximum and minimum concentrations are less far apart. This trend continued as the simulation time continued. To monitor the progress of the diffusion, two criteria were used; these are plotted in Figure 5-24.

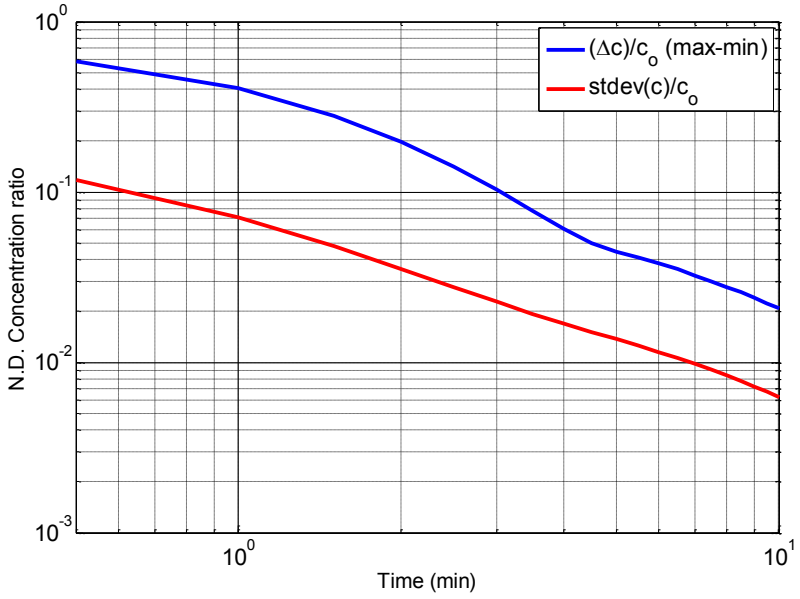

Figure 5-24. Log-log plot of the ratio of the concentration and the standard deviation in the simulation of 5M5P diffusion. The blue line represents the difference between the maximum and minimal concentrations divided by the average initial concentration, c_0. The red line is the standard deviation divided by the average initial concentration, c_0.

The overall average was approximately 0.5. The log plot shows that the time to reach a given homogeneity target (e.g., 0.001 in stdev (c)/c_o) could not be predicted simply by a log-log linear plot.

It is not easy to define what level of homogeneity corresponds to an amnesiac liquid (i.e., a liquid

that will crystallize at 20 C°/min and produce the same α_0 crystallization as a liquid held for a very long time at high temperature). Nonetheless it can be argued that the characteristic size of the inhomogeneity has to be on the order of nucleus size, somewhere below 100 nm. The tolerable difference in concentration between these regions could be estimated using basic molecular statistics mechanics, but that falls beyond the scope of this work and is left as a suggested focus for future research.

If the size of the phase domains had been about 50 μm (instead of 100 as μm, as in the example above), the approximate reduction of time to reach the same standard deviation would be a factor of (100/50) ^ 2 = 4. At the same temperature, a process that would take 8 minutes from the 100 μm phase regions would take only 2 min from 50 μm regions. The regions are not easy to identify using microscopy, but it would be a very useful project to complement this study.

From the experiments, it was clear that 10 min at 93.0 °C for 5M5P or at 103.0 °C for 5P5S was more than enough to return the liquid to its original amnesiac state. This was confirmed by the crystallization from the melt at 20 C°/min, which produced the exact same α_0 crystallization, regardless of the previous history of crystallization or recrystallization. Both temperatures were considerably higher than the T_{max} for 5M5P and 5P5S, which were both approximately 61.0 °C. Thus, it is not possible to estimate the domain size or other diffusional characteristics from them. Nonetheless, the model built here can be used in future works with the combinations of time temperatures of the boundaries to provide an estimate of domain sizes and compositions.

CHAPTER 6. CONCLUSIONS AND SUGGESTIONS FOR FUTURE WORK

The primary goal of this research was to use DSC to conduct the first systematic investigation on the time-temperature boundaries of the "crystal memory effect" in selected pure TAGs.

This research was limited to saturated monoacid TAGs, with experiments using one melting rate, 15 C°/min, followed by a recrystallization rate of 20 C°/min. Despite such limits, we have a sound methodology that can be used by other researchers in the study of the memory effect and its boundaries. Here, we used this methodology primarily to define the type of memory and better understand the associated onset temperatures. Combined with exploration of other systems, such information should provide the experimental basis for a better quantitative theoretical explanation of the connection between melting, liquid structure and nucleation theory with respect to TAGs.

In summary, three pure saturated TAGs and two TAG mixtures were crystallized and tempered in DSC sample pans under controlled temperature and time profiles that were developed for each material. The thermograms corresponding to these temperature-time profiles were obtained using a heat flux DSC. The combinations of holding time and temperature needed to erase the memory effect that affected the recrystallization were determined, as were the onset temperatures of recrystallization.

Two types of memory were identified. The first one, the "early α memory", reflects the fact that, upon recrystallization, the onset temperature for the formation of the α crystals had a higher onset temperature than the original α_0 onset temperature. This early α phase memory was similar to that identified by Arnaud and by the cocoa butter researchers. The second one is called "β' memory" or "β memory", and refers to the recrystallization of the more stable phase directly from the melt.

This "***β*** memory" survived when the liquid was held at lower temperatures with shorter holding times, but was eliminated at higher temperatures or longer times. In most cases, the "early ***α*** memory" persisted at higher holding temperatures and longer holding times combinations than "***β*** or ***β'*** memory".

The overall temperature range (T_{max} - T_{min}) of memory elimination in SSS, PPP and MMM was 1.5 C°, 1.4 C° and 1.3 C°, respectively. Thus, the crystal memory of pure saturated TAGs can be erased by heating the coldest point in the sample to a few degrees above the melting point of the ***β*** polymorph, for about one minute at 15 C°/min or less. Therefore, compared with the usual procedure of heating at least 20 C° above the melting point for 10 minutes, much time could be saved during future pure TAGs phase transition experiments.

For the pure TAGs, the holding time needed for erasing the memory decreased as the temperature increased, with a very similar slope in most cases (~ -0.7 C°/min). The holding time needed to erase "***β*** memory" was much shorter than the time needed to erase "early ***α*** memory". For MMM, the holding time needed to delete "early ***α*** memory" was usually around 2 min, and the range of temperatures for memory elimination was 1.3 C°. There was no clear evidence of "long term memory" in MMM. However, for PPP and SSS, the boundaries were divided into separate sections reflecting "long term" and "short term".

"Long term" memory required much longer holding times (e.g., 60 min) than "short term" memory (typically < 2 min). The temperature interval, ΔT_{sl}, for "long term" PPP was 0.52 C°, whereas for SSS it was 0.21 C°. This narrow temperature band represents a particularly interesting liquid state, worthy of future NMR, SAXS and SANS exploration.

The onset temperatures of crystallization, ΔT_a, followed a general trend with respect to ΔT_m for PPP and SSS. MMM exhibited behavior similar to PPP or SSS at low temperatures, though shifted

towards earlier recrystallization at higher holding temperature or longer holding time. This phenomenon suggests that there is a balance between the forces of attraction associated with glycerol and alkyl chains. The liquid retains some additional structures inherited from its originating solid state when compared to an amnesiac liquid, and the way these additional structures are retained depends on the balance of those forces.

For the binary triacylglycerol mixtures, 5M5P and 5P5S, the time and temperature ranges of memory elimination were much broader than for pure TAGs. Each blended material was composed of two kinds of molecules with different sizes, melting points, and enthalpies. It was expected that the temperature limits of 5P5S would be higher than for 5M5P; however, the results did not show this. Thus, even for the simplest binary mixtures the prediction of properties and behavior in TAGs remains a challenging task.

It was clear, however, that the times required to erase "***β'*** memory" and the short term "early ***α*** memory" in the blends were longer (~15 min) than the corresponding times in the pure TAGs (<2 min). The temperature range was broader: 3.5 – 6 C° for the blends vs. 1.3 C° for pure TAGs. These observations confirm the hypothesis that, in mixtures, a very important part of the memory mechanism is the diffusion of the molecules from an initially heterogeneous liquid into a homogeneous liquid. Further exploration of these binary mixtures will continue to provide insights regarding their memory effects.

Together, the results clearly demonstrate that the destruction of the memory consists of at least two mechanisms that are distinct but nonetheless related:

1) Thermal separation of the molecules is responsible for destroying the initial liquid structure and appears to occur in both pure and blended TAGs; occurring it occurs quickly and just a few degrees

above melting the materials. This mechanism depends on the balance of forces between the alkyl and glycerol core sections of the molecules.

2) Occurring in blended but not pure TAGs, diffusion or convection drives the mixing of the molecules towards restoration of the homogeneous distribution of concentrations in the liquid. This extra process requires a much longer time and higher temperatures. It depends on the sizes of the domains and on the differences in the initial concentrations between the domains.

It is important to note that these experiments did not address all factors that could affect the behaviors of TAGs. For example, cooling and heating rates, kept constant in these experiments, play an important role in the persistence of the structures after melting TAGs. Shear forces and promotion of mixing may also bring important changes to these boundaries. Further, complex or multicomponent mixtures of TAGs are likely to have their own unique memory profiles. A comprehensive understanding of TAG behavior, and application of such for manufacturing or other purposes, requires the use of combined methods such as DSC, synchrotron XRD, NMR, microscopy, and others. This thesis provides a vital foundation for building that knowledge.

BIBLIOGRAPHY

Acevedo, N. C., & Marangoni, A. G. (2010). Characterization of the Nanoscale in Triacylglycerol Crystal Networks. *Crystal Growth and Design,* 10(8), 3334–3339. http://doi.org/10.021/cg100469x

Al-Qatami, O. A. M. (2011). Thermal study of a triglyceride mixture, MSc Thesis, Dalhousie University.

Callaghan, P. T. (1977). The use of 13C spin relaxation to investigate molecular motion in liquid tristearin. *Chemistry and Physics of Lipids*, *19*(1), 56–73. http://doi.org/10.1016/0009-3084(77)90081-0

Callaghan, P. T., & Jolley, K. W. (1977). An irreversible liquid–liquid phase transition in tristearin. *The Journal of Chemical Physics*, *67*(10), 4773. http://doi.org/10.1063/1.434607

Callaghan, P.T., & Jolley, K. W. (1980). Translational motion in the liquid phases of tristearin, triolein and trilinolein. *Chemistry and Physics of Lipids, 27*(1), 49–56. http://doi.org/10.1016/0009-3084(80)90047-X

Campos, R., Narine, S. S., & Marangoni, A. G. (2002). Effect of cooling rate on the structure and mechanical properties of milk fat and lard. *Food Research International*, *35*(10), 971–981. http://doi.org/10.1016/S0963-9969(02)00159-X

Cebula, D., McClements, D., Povey, M., & Smith, P. (1992). Neutron Diffraction Studies of Liquid and Crystalline Trilaurin. *Journal of the American Oil Chemists' Society*, *69*(2), 130–136. http://doi.org/10.1038/nature09648

Chumpitaz, L. D. A., Coutinho, L. F., & Meirelles, A. J. A. (1999). Surface tension of fatty acids and triglycerides. *Journal of the American Oil Chemists' Society*, *76*(3), 379–382. http://doi.org/10.1007/s11746-999-0245-6

Danley, R. L. and Caulfield, P. A. (2001). "DSC Baseline Improvements Obtained by a New Heat Flow measurment Technique", *Proc. 29th Conf. N. Amer. Therm. Anal.Soc.*

Foubert, I., Vanrolleghem, P. A., & Dewettinck, K. (2003). A differential scanning calorimetry method to determine the isothermal crystallization kinetics of cocoa butter. *Thermochemica Acta*, *400*(2), 131–142. http://doi.org/10.1016/S0040-6031(02)00484-7

Foubert, I., Vanrolleghem, P. A., Vanhoutte, B., & Dewettinck, K. (2002). Dynamic mathematical model of the crystallization kinetics of fats. *Food Research International*, *35*(10), 945–956. http://doi.org/10.1016/S0963-9969(02)00157-6

Greiner, M., Reilly, A. M., & Briesen, H. (2012). Temperature- and pressure-dependent densities, self-diffusion coefficients, and phase behavior of monoacid saturated triacylglycerides: Toward molecular-level insights into processing. *Journal of Agricultural and Food Chemistry*, *60*(20), 5243–5249. http://doi.org/10.1021/jf3004898

Gunstone, F. D., & Padley, F. B. (1997). Lipid technologies and applications. *Food Chemistry*. http://doi.org/10.1016/S0308-8146(97)00213-6

Hagemann, J. W., & Rothfus, J. A. (1993). Evidence for resonance-assisted hydrogen bonding from crystal-structure correlations on the enol form of the β-diketone fragment. *Journal of the American Oil Chemists' Society*, *70*(3), 211–217. http://doi.org/10.1021/ja00185a035

Hampson, J. W., & Rothbart, H. L. (1983). Triglyceride Specific Heat Determined by Differential Scanning Calorimetry. *Journal of the American Oil Chemists' Society*, 60(6), 1102–1104. http://doi.org/10.1007/BF02671334

Harwood, J. (1989). Gas chromatography and lipids: A practical guide: *Phytochemistry*. *28*(1), 3251–3252. http://doi.org/10.1016/0031-9422(89)80324-3

Hernqvist, L. (1984), On the Structure of Triglycerides in the Liquid State and Fat Crystallization. *Fette, Seifen, Anstrichmittel*, *86*: 297–300. http://doi.org/10.1002/lipi.19840860802

Herrera, M. L., & Hartel, R. W. (2000). Effect of processing conditions on crystallization kinetics of a milk fat model system. *Journal of the American Oil Chemists' Society*, *77*(11), 1177–1188. http://doi.org/10.1007/s11746-000-0184-4

Himawan, C., Starov, V. M., & Stapley, A. G. F. (2006). Thermodynamic and kinetic aspects of fat crystallization. *Advances in Colloid and Interface Science*, *122*(13), 3–33. http://doi.org/10.1016/j.cis.2006.06.016

Holz, M., Heil, S. R., & Sacco, A. (2000). Temperature-dependent self-diffusion coefficients of water and six selected molecular liquids for calibration in accurate 1H NMR PFG measurements. *Physical Chemistry Chemical Physics*, *2*(20), 4740–4742. http://doi.org/10.1039/b005319h

Kawamura, K. (1979). The structure of multivariate Poisson distribution. *Kodai Mathematical Journal*. *2*(3), 337–345. http://doi.org/10.2996/kmj/1138036064

Kloek, W., Walstra, P., & van Vliet, T. (2000). Nucleation kinetics of emulsified triglyceride mixtures. *Journal of the American Oil Chemists' Society*, *77*(6), 643–652. http://doi.org/10.1007/s11746-000-0104-7

Kraack, H., Deutsch, M., & Sirota, E. (2000). Measurements of homogeneous nucleation in normal-alkanes. *Journal of Chemical Physics,* 112, 6873-6885. http://dx.doi.org/10.1063/1.481263

Krishna, R., & Van Baten, J. M. (2005). The Darken relation for multicomponent diffusion in liquid mixtures of linear alkanes: An investigation using Molecular Dynamics (MD) simulations. *Industrial and Engineering Chemistry Research*, *44*(17), 6939–6947. http://doi.org/10.1021/ie050146c

Larsson, K. (1966). Classification of glyceride crystal forms. *Acta Chemica Scandinavica*. *20*(5), 2255-2260. http://doi.org/10.3891/acta.chem.scand.20-2255

Larsson, K. (1972), Molecular Arrangement in Glycerides. *Fette, Seifen, Anstrichmittel*, 74: 136–142. http://doi.org/10.1002/lipi.19720740302

Loisel, C., Keller, G., Lecq, G., Bourgaux, C., & Ollivon, M. (1998). Phase transitions and polymorphism of cocoa butter. *Journal of the American Oil Chemists' Society*. *75*(14), 425-439. http://doi.org/10.1007/s11746-998-0245-y

Matovic, M., van Miltenburg, J. C., Los, J., Gandolfo, F. G., & Flöter, E. (2005). Thermal Properties of Tristearin by Adiabatic and Differential Scanning Calorimetry. *Journal of Chemical & Engineering Data*, *50*(5), 1624–1630. http://doi.org/10.1002/ejlt.200800181

Marty, S., Schroeder, M., Baker, K. W., Mazzanti, G., & Marangoni, A. G. (2009). Small-molecule diffusion through polycrystalline triglyceride networks quantified using fluorescence recovery after photobleaching. *Langmuir : The ACS Journal of Surfaces and Colloids*, *25*(15), 8780–8795. http://doi.org/10.1021/la900255u

Mazzanti, G., Guthrie, S. E., Sirota, E. B., Marangoni, A. G., & Idziak, S. H. J. (2003). Orientation and phase transitions of fat crystals under shear. *Crystal Growth and Design*, *3*(5), 721–725. http://doi.org/10.1021/cg034048a

Metin, S., & Hartel, R. W. (2005). Crystallization of Fats and Oils. *Bailey's Industrial Oil and Fat Products.* 1:2. http://doi.org/10.1002/047167849X.bio021

Morad, N. A., Idrees, M., & Hasan, A. A. (1995). Specific heat capacities of pure triglycerides by heat-flux differential scanning calorimetry. *Journal of Thermal Analysis*, *45*(6), 1449–1461. http://doi.org/10.1007/BF02547438

Narine, S. S., & Marangoni, A. G. (1999). Relating structure of fat crystal networks to mechanical properties: A review. Food Research International, 32(4), 227–248. http://doi.org/10.1016/S0963-9969(99)00078-2

Phipps. L.W. (1962). Dependence on Temperature of the Viscosity and Density of Supercooled Triglycerides. *Nature*, *193*, 541-542. http://doi.org/10.1038/193541a0

Pink, D. A., Hanna, C. B., Sandt, C., MacDonald, A. J., MacEachern, R., Corkery, R., & Rousseau, D. (2010). Modeling the solid-liquid phase transition in saturated triglycerides. *Journal of Chemical Physics*, *132*(5). http://doi.org/10.1063/1.3276108

Rabelo, J., Batista, E., Cavaleri, F. V. W., & Meirelles, A. J. A. (2000). Viscosity prediction for fatty systems. *Journal of the American Oil Chemists' Society*, *77*(12), 1255–1262. http://doi.org/10.1007/s11746-000-0197-z

Ribeiro, A. P. B., Masuchi, M. H., Miyasaki, E. K., Domingues, M. A. F., Stroppa, V. L. Z., de Oliveira, G. M., & Kieckbusch, T. G. (2015). Crystallization modifiers in lipid systems. *Journal of Food Science and Technology*, *52*(7), 3925–3946. http://doi.org/10.1007/s13197-014-1587-0

Rodríguez-Valverde, M. A, Cabrerizo-Vílchez, M. A., & Hidalgo- Álvarez, R. (2003). The Young Laplace equation links capillarity with geometrical optics. *European Journal of Physics*, *24*(2), 159–168. http://doi.org/10.1088/0143-0807/24/2/356

Rousset, P. (2002). Modeling Crystallization Kinetics of Triacylglycerols. In Marangoni, A. G & Narine, S. S, *Physical Properties of Lipids*. ISBN:0-8247-0005-8

Sato, K. (2001). Crystallization behaviour of fats and lipids — a review. *Chemical Engineering Science*, *56*(7), 2255–2265. http://doi.org/10.1016/S0009-2509(00)00458-9

Sato, K., & Garti, N. (2001). Crystallization processes in fats and lipid systems. *Chemical Engineering Science*, 56(7), 2255–2265. http://doi.org/10.1039/C3CE26657E

Sato, K., & Ueno, S. (2011). Crystallization, transformation and microstructures of polymorphic fats in colloidal dispersion states. *Current Opinion in Colloid and Interface Science*, *16*(5), 384–390. http://doi.org/10.1016/j.cocis.2011.06.004

Sato, K., Ueno, S., & Yano, J. (1999). Molecular interactions and kinetic properties of fats. *Progress in Lipid Research*, *38*(1), 91–116. http://doi.org/10.1016/S0163-7827(98)00019-8

Takeuchi, M., Ueno, S., & Sato, K. (2002). Crystallization kinetics of polymorphic forms of a molecular compound constructed by SOS (1,3-distearoyl-2-oleoyl-sn-glycerol) and SSO (1,2-distearoyl-3-oleoyl-rac-glycerol). *Food Research International*, *35*(10), 919–926. http://doi.org/10.1016/S0963-9969(02)00154-0

Thomas, L. C. (2005). Modulated DSC® Paper #1 Why Modulated DSC®; An Overview and Summary of Advantages and Disadvantages Relative to Traditional DSC. TA Instruments, New Castle, USA.

Timms, R. E. (1984). Phase behaviour of fats and their mixtures. *Progress in Lipid Research*, *23*(1), 1–38. http://doi.org/10.1016/0163-7827(84)90004-3

Turnbull, D., & Fisher, J. C. (1949). Rate of Nucleation in Condensed Systems. *The Journal of Chemical Physics*, *17*(1), 71. http://doi.org/10.1063/1.1747055

van Langevelde, A., van Malssen, K., Hollander, F., Peschar, R., & Schenk, H. (1999). Structure of mono-acid even-numbered β-triacylglycerols. *Acta Crystallographica Section B Structural Science*. http://doi.org/10.1107/S0108768198009392

van Malssen, K., Peschar, R., & Schenk, H. (1996). Real-Time X-Ray Powder Diffraction Investigations on Cocoa Butter . I . Temperature-Dependent. *Journal of the American Oil Chemists' Society*, *7*(10), 1209–1215. http://doi.org/10.1007/BF02525449

Vand, V., & Bell, I. P. (1951). A direct determination of the crystal structure of the β form of trilaurin. *Acta Crystallographica*, *4*(5), 465–469. http://doi.org/10.1107/S0365110X5100146X

Widlak, N., Hartel, R. W., & Narine, S. S. (2001*). Crystallization and Solidification Properties of Lipids*. Champaign, Illinois: AOCS Press. ISBN:1-893997-21-9.

Appendix A

A.1 Additional data from the studies of Arnaud on SSS

A.1.1 Cyclic data

The cyclic methodology used by Arnaud to explore the effect of melting, heating and cooling upon recrystallization is quite different from the methodology used in this thesis. However, since the material is the same, some degree of confirmation or refutation of the hypotheses may come from the results of these experiments. Figure A-1 and Figure A-2 show the temperature time cycles used for the SSS experiments. There is an "accumulation and amplification" effect of any previous memory events. The time scales are somewhat more complicated, because the heating time is (T_{hot} – 40)/10 in minutes, and the cooling time is (T_{hot} – 40) in minutes. They change each cycle, since T_{hot} was increased by 1 C° for each cycle. There was not waiting time either at T_{hot} or at 40 °C.

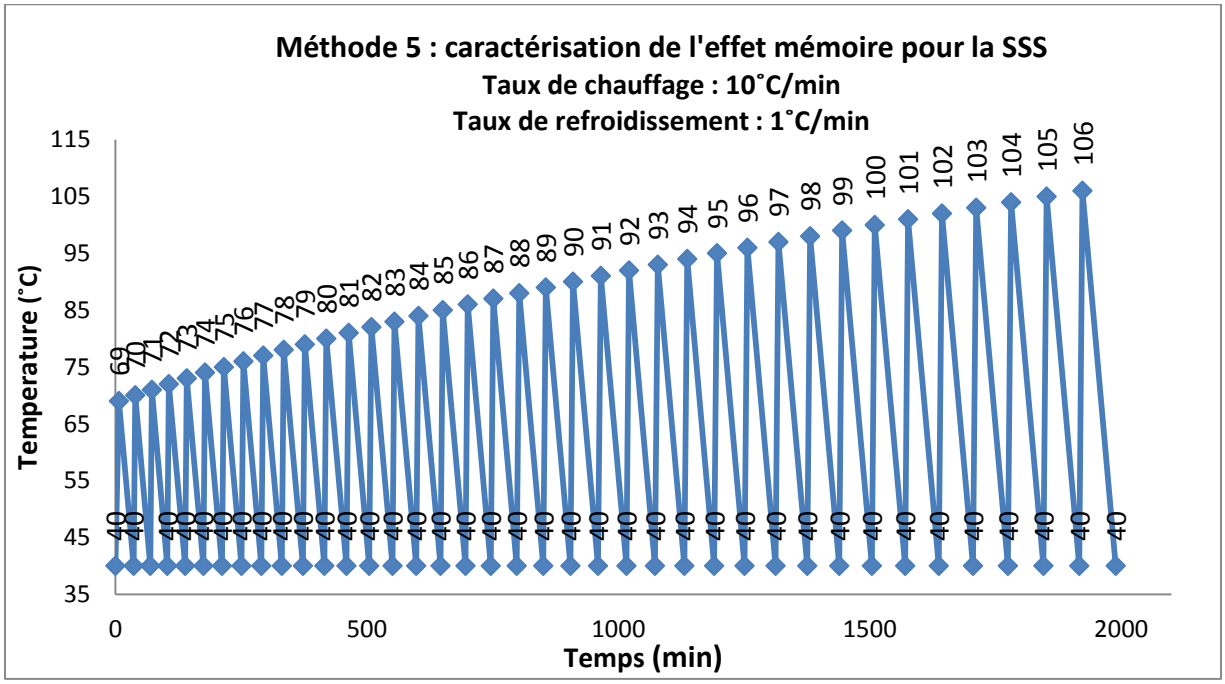

Figure A-1. Program used to characterize the memory effect for the SSS with 10˚C/min heating rates.

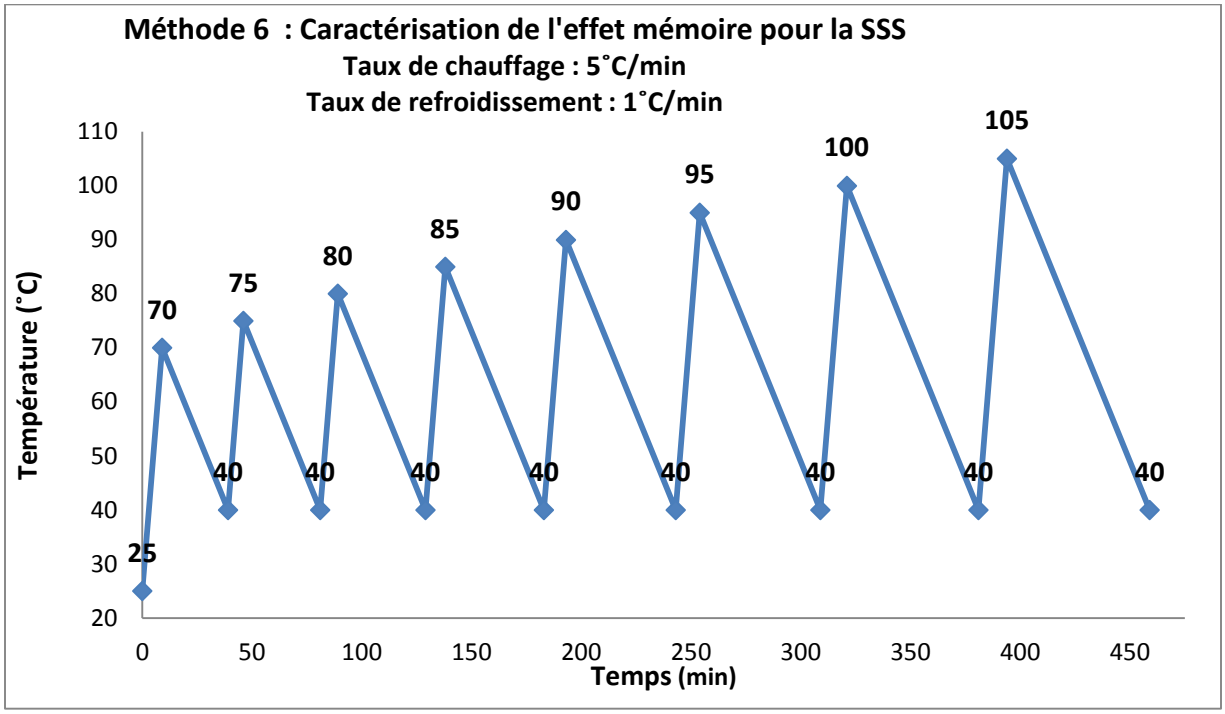

Figure A-2. Program used to characterize the memory effect for SSS and know his behavior over a range of temperatures with broader temperature intervals.

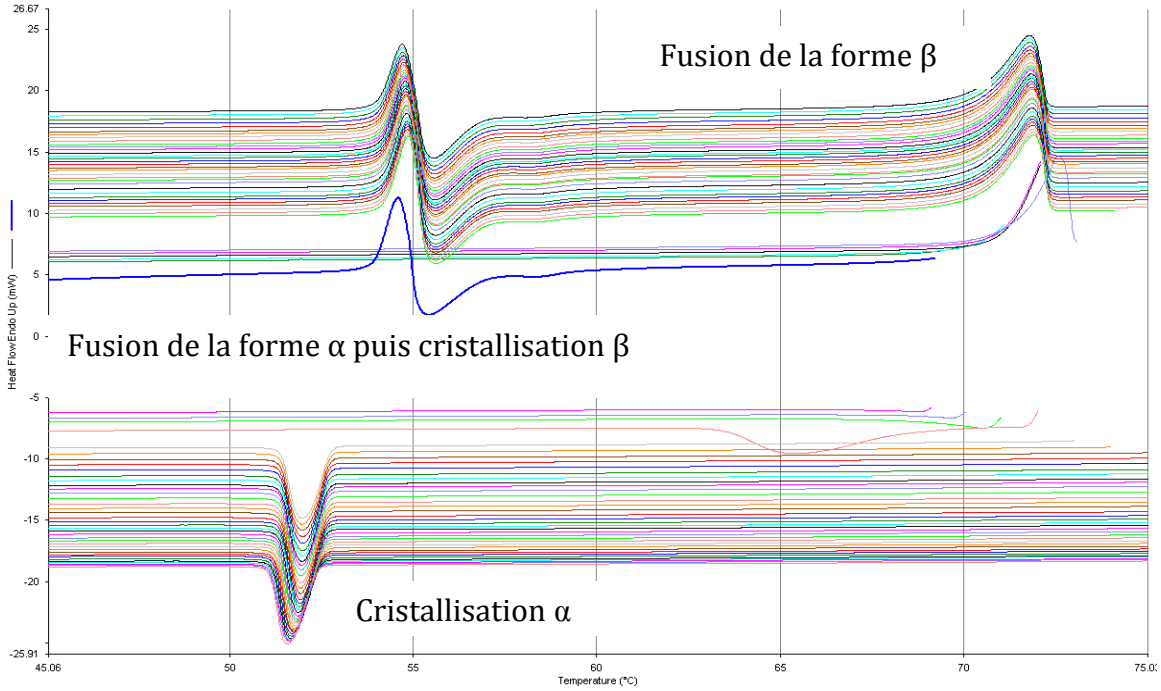

Figure A-3. Example of the crystallization and melting curves generated for the SSS, test 2 with method 4 (A12).

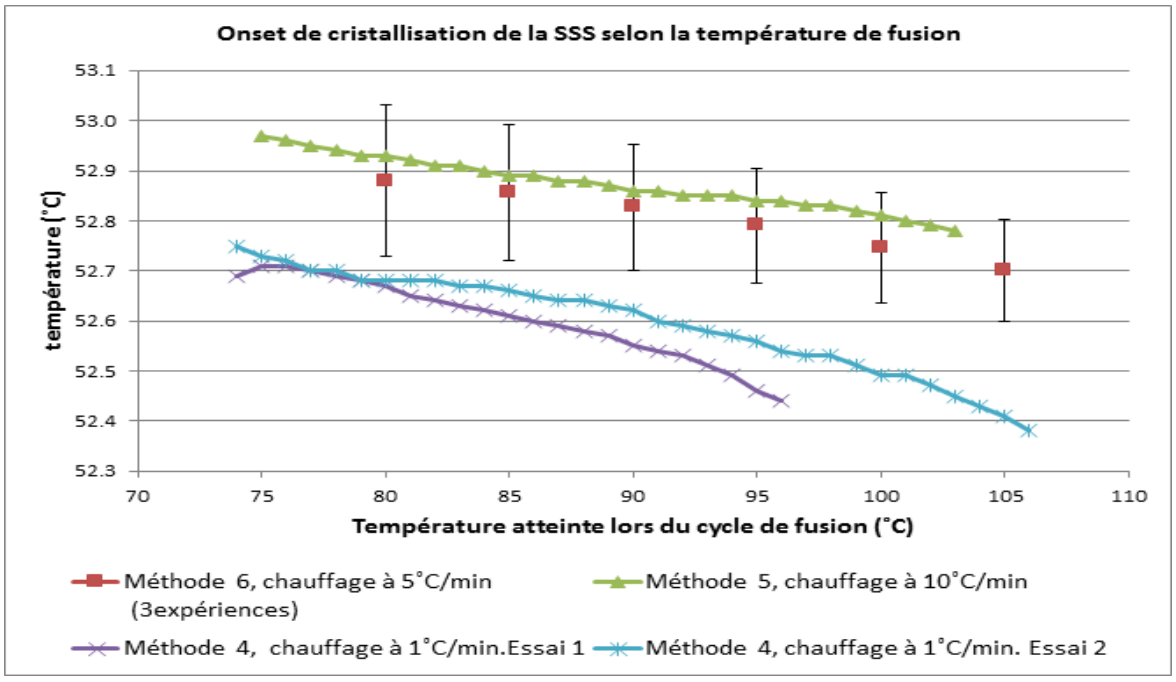

Figure A-4. Variation in the onset of crystallization of *α* SSS depending on the method used and the applied melting temperature.

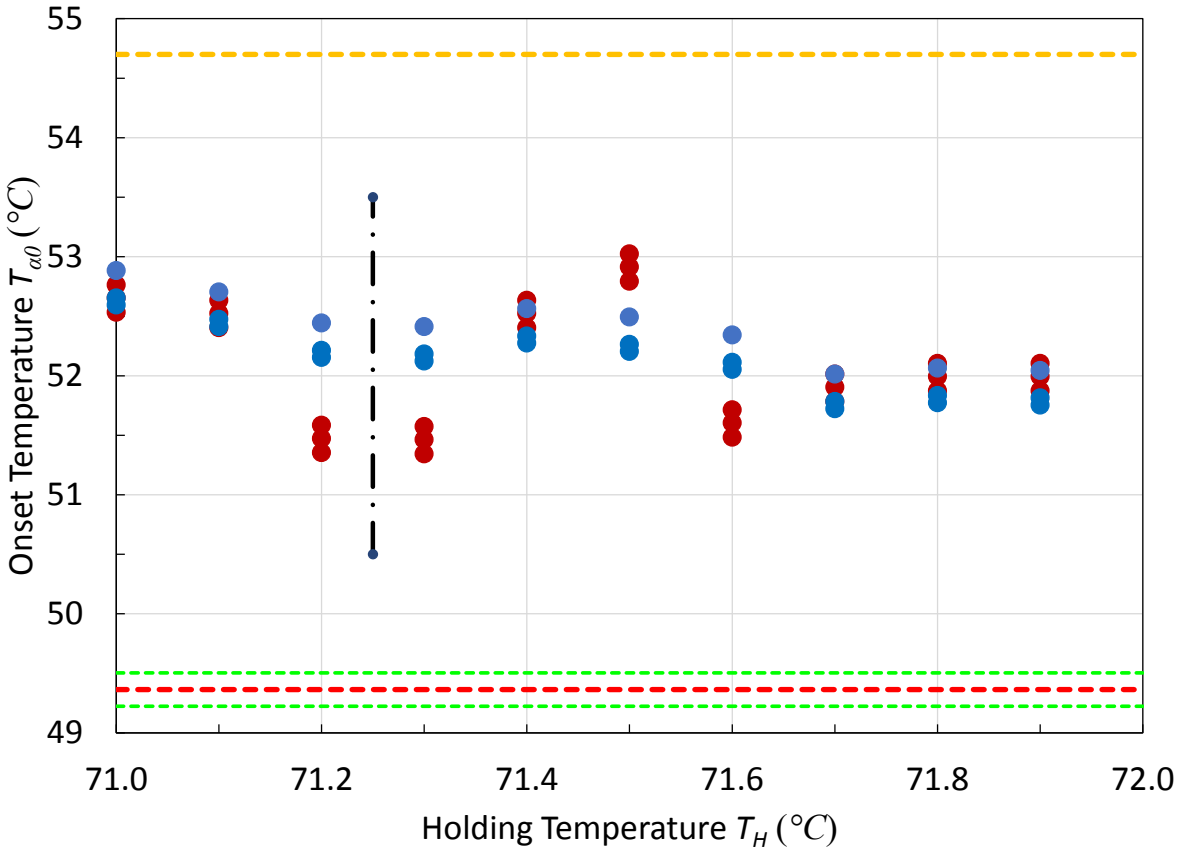

Figure A-5. Onset temperatures for α SSS for two pans as function of the holding temperature. (details are explained in the text)

In Figure A-5 the blue dots are for pan_1 and the red dots for pan_2. The orange dashed line marks 54.7 °C, the literature value for the melting point of α SSS. The range of the onset temperatures accounts for the variability of the onset of the $T_{\alpha 0}$ values, that had an overall average of 49.4 °C, when cooling at 20 C°/min (red dashed line). The green dashed lines mark the range of the $T_{\alpha 0}$ values. The vertical black line indicates the boundary between experiments that took long time, at lower temperatures, and short times, at higher temperatures.

The range of onset variation in the data from Arnaud is very similar to the range observed in our study. Unfortunately, the time study conducted for the other TAGs by Arnaud was not done for SSS. A reference liquid was also not provided, i.e. an experiment where the liquid was left a long

time at a high temperature, and cooled down at the cooling rate being explored, which for their SSS experiments was 1 C°/min. From our experiments, even the early α memory was erased above 72 °C. It is possible that the cycling procedure somehow enhances the organization of the liquid molecules. However, when the cycle is, for instance, heating at 10 C°/min to 102 °C, and then cooling back to 53 °C, the total time spent in the liquid state, i.e. above 72 °C while heating, and above 53 °C while cooling, is 3 minutes in heating and 49 minutes on cooling. It is quite contrasting from our experimental point of view that some memory was retained. We performed experiments with SSS in our DSC, after erasing memory, cooling at 1 C°/min, and observed an onset αtemperature of 52.7 °C. Though small calibration differences exist between calorimeters, this value is very close to the experiments done by Arnaud at the heating and cooing rates of 1 C°/min, and perhaps cast some doubt about the drift in their results.

In any case, it is possible that the cyclic process produced larger, more perfect crystals by annealing them. Therefore, upon melting, larger organized liquid regions (domains) were formed, which were then able to withstand harsher thermal treatments.

A.1.1 Onset temperatures in Trilaurin from Arnaud's study

The objective of their work was to show qualitatively that the memory effect indeed existed, and that was worth exploring. Due to the difference in methodology, it is not possible to do a very meaningful quantitative comparison between the results for this shorter TAG with the longer TAGs studied in the thesis.

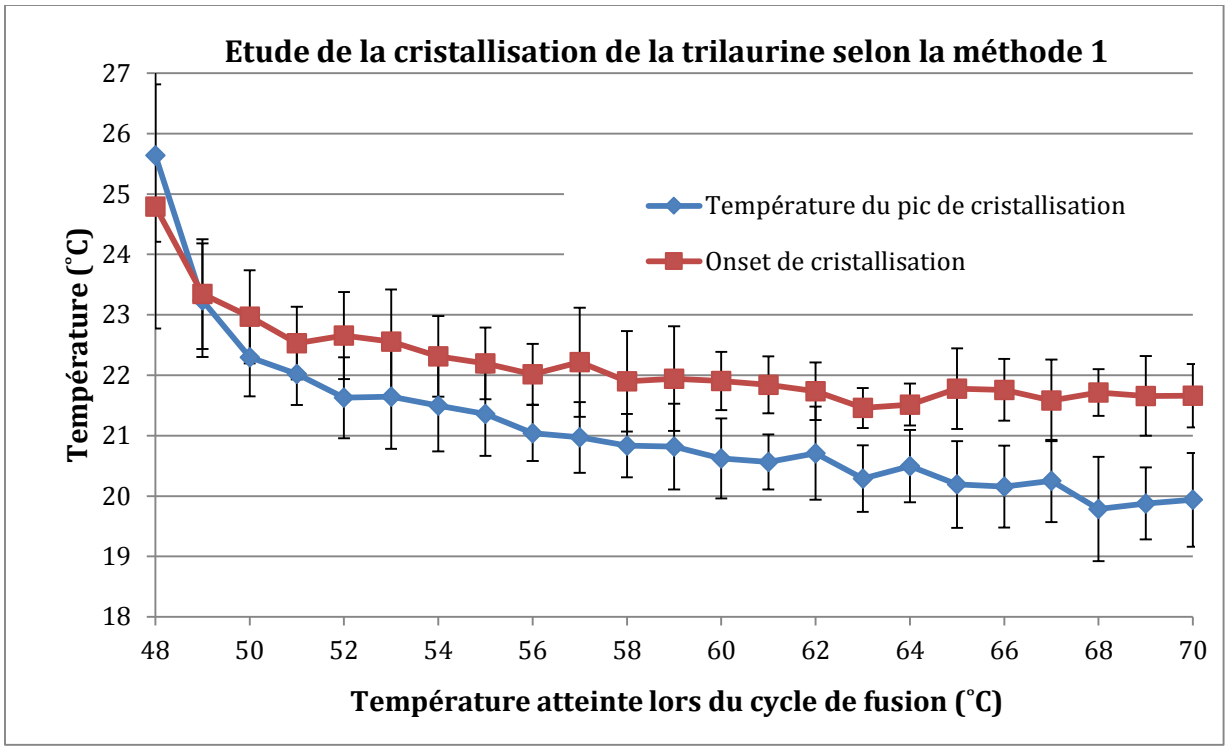

Figure A-6. Average for 6 experiments A1 to A6, the onset and the peak of crystallization for each temperature of fusion.

However, it is useful to include here that trilaurin did have a $T_{\alpha 0}$, for Arnaud's experimental conditions, of 21.8 °C. The value of T_{max} was ca. 68 °C, for the cyclic process.

Figure A-6 clearly shows that as temperatures increased, the onset temperature decreased, until it reached a plateau around 21.8 °C, when the memory effect disappeared. The hot temperature was above 68 °C. The β polymorph of LLL melts at 46.5 °C (Takeuchi *et al.*, 2002), so the material was heated about 21 C° above its last solid state before losing its memory. It is well established that under a cooling rate of 1 C°/min LLL crystallizes in the β' polymorph, whose melting point is 35 °C (Takeuchi *et al.*, 2002). Thus the undercooling without the memory effect, at that cooling rate was 13.2 C°. On the other hand, after the first cycle it recrystallized at 24.8 °C, i.e. the undercooling was 10.2 C°. Thus the initial ΔT_{α} was around 3 C°, which is of the same order as we have observed for the other pure TAGs studied.

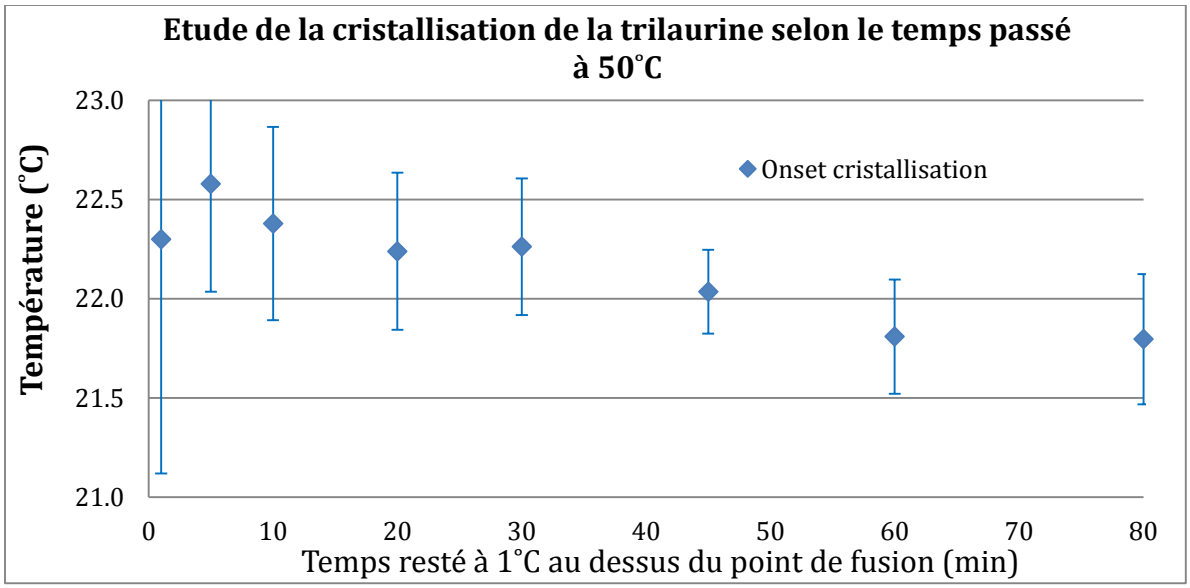

Figure A-7. Onset of crystallization of the LLL according to the time spent to 50˚C. Experiments in triplicate (Annexes A7, A8, A9).

After 60 minutes at 50 °C, the memory is also erased, and the crystallization onset is again at 22.8 °C, as it is after 80 minutes at that temperature. The trend of the intermediate data, from 1 to 45 minutes, is affected by the previous experiments, since no effort was made to erase their influence. It does not have any obvious shape that would suggest a function to be fitted to them. A straight line, anchored at the point t_H = 60 min and T_α = 24.8 °C, would yield the equation $T_\alpha = -0.0114 \cdot t_H + 22.494$, valid only for $t_H \leq 60$ min. The holding temperature reported is 50 °C, which is called "1 C° above the melting point of LLL". However, the reported melting point of β LLL is 46.5 °C. Hence, the heating would have been 3.5 C° above the melting point of LLL. It is interesting that at such relatively high range above the melting point this memory effect was observed. It is likely, again, the result of the annealing procedure, that yielded very large crystals, and therefore, upon melting, very large liquid domains. The very weak signals in the thermograms of the study on tricaprylin done by Ms. Arnaud led us to leave that part of her document out of our discussion.

A.2 Simulations of diffusion in a DSC pan

It was shown in Chapter 4 that the time required to erase the memories above T_{sl} is usually less than one minute, and the temperature required is just about 1.5 C° above the melting point of the crystals. In Chapter 5, the blends showed that the times required were often much longer, in the range of 15 minutes. In those cases, the temperatures were less than 6 C° above the melting point of the binary blends, which is much less than the additional temperature employed in most studies to make sure that crystal memory is erased.

In any case, it seems clear that, for the mixtures, diffusion plays an important role in maintaining the memory effect. Once two phases of different compositions have been crystallized in many different regions, each one of these microscopic spaces has a composition that is different from the microscopic spaces of the other phase. When the material melts, the liquid does not instantaneously recovers a uniform distribution of the molecules. Initially, in the best case, scenario, the liquid is a heterogeneous space of micro-domains of two different compositions. As time goes by, the molecules diffuse from regions where they have higher concentrations to regions where their concentrations are lower, until a dynamic equilibrium is established. Therefore, from a compositional point of view, the liquid becomes homogeneous.

This section intends to provide additional insight into the diffusion processes that take place inside a DSC pan when the liquid is heated to the holding temperature. The liquid is produced by the melting of two or more phases of different composition, which occupy many thousands of small, interspersed regions in the crystallized material, some in one composition, some in another.

A.2.1 Axisymmetric equations for diffusion

To model the diffusion in the pans, it is convenient to use the binary mass transfer equations in an axisymmetric geometry, invariant in the angular direction. These are parabolic partial differential equations, function of the radius and the height, i.e. in cylindrical coordinates:

$$\frac{\partial c}{\partial t} = \frac{\partial}{\partial r}\left(D\frac{\partial c}{\partial r}\right) + \frac{\partial}{\partial z}\left(D\frac{\partial c}{\partial z}\right) + D\frac{1}{r}\frac{\partial c}{\partial r}$$
$$\frac{\partial c}{\partial t} = \nabla\cdot\left(D\nabla c\right) + D\frac{1}{r}\frac{\partial c}{\partial r}$$

The concentration is expressed in units of mass per unit volume. These equations are derived for equi-volumetric local fluxes, i.e. it is assumed that the volume fluxes of the two species are equal. This is the same as neglecting the difference in density between the two materials. The bulk density of MMM, PPP and SSS are well known. For instance, at 70 °C, their densities are 0.879, 0.874 and 0.869 mg/mm^3 (Bennett *et al.*, 1995 ; M.Matovic & Miltenburg, 2005). The diffusivity values, on the other hand, are rough estimates. Furthermore, the exact physical distribution of the initial solids is unknown, and in fact, it is quite variable. For the approximate estimations intended in this thesis, the model was formulated neglecting the differences in density.

A.2.2 Surface tension and axisymmetric equations for surface shape

Because the pan has a small radius, for about 2 mm, surface tension becomes an important factor in defining the shape of the liquid in the pan, and therefore the trajectories of the diffusion. To estimate the shape of the liquid in the pan it is necessary to estimate the magnitude of the surface tension of the liquid, as well as the shape of the meniscus formed on the top. The sketch in Figure

A-8 shows how the surface of the liquid in the pan will not remain flat, as depicted in (a), but will form a notably concave meniscus, as illustrated in (b).

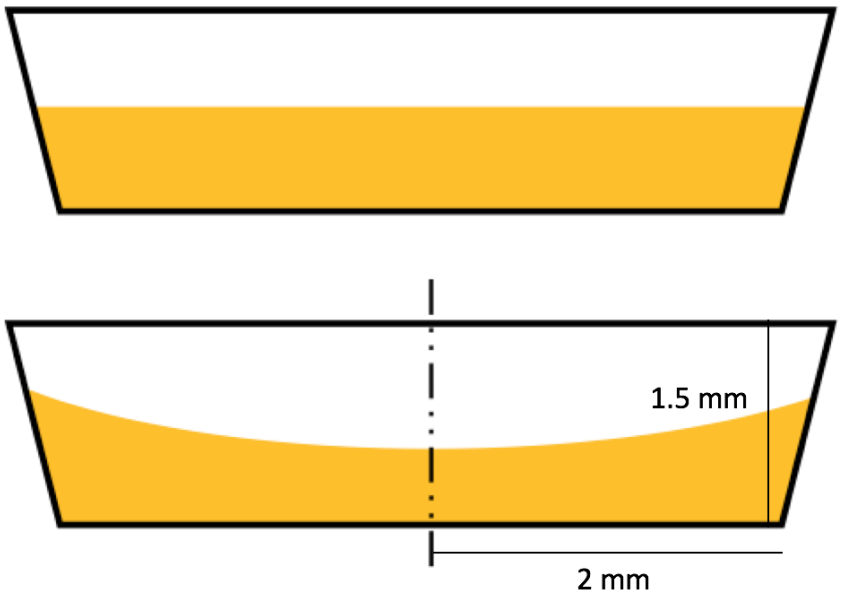

Figure A-8. Sketch showing the considerable change in shape due to surface tension in a liquid sample placed in a DSC pan. (a) No surface tension effect. (b) With surface tension.

For PPP the surface tension has been reported as 28.3 mNm at 80 °C, and values at other temperatures are available, as seen in Figure A-9 (Chumpitaz *et al*., 1999). The surface tension of the triglyceride of C8 is in the same plot, ~ 26 mNm. Therefore, the surface tension increases with the number of carbons. The similar slopes at around -0.06 mNm/C°, suggest an almost parallel dependence on temperature for the TAGs. No exact data were found for MMM or SSS. With two data points, only a linear estimation is possible. This gives a value for C14 of 27.7 mNm, and of 28.9 mNm for C18. For comparison, the surface tension for dodecane is around 20 mNm at 80 °C. The differences between the surface tensions of P-M and S-P are ~ 0.6 mNm, or 2% of their values. Thus, an average for the mixtures value can be used without concerns.

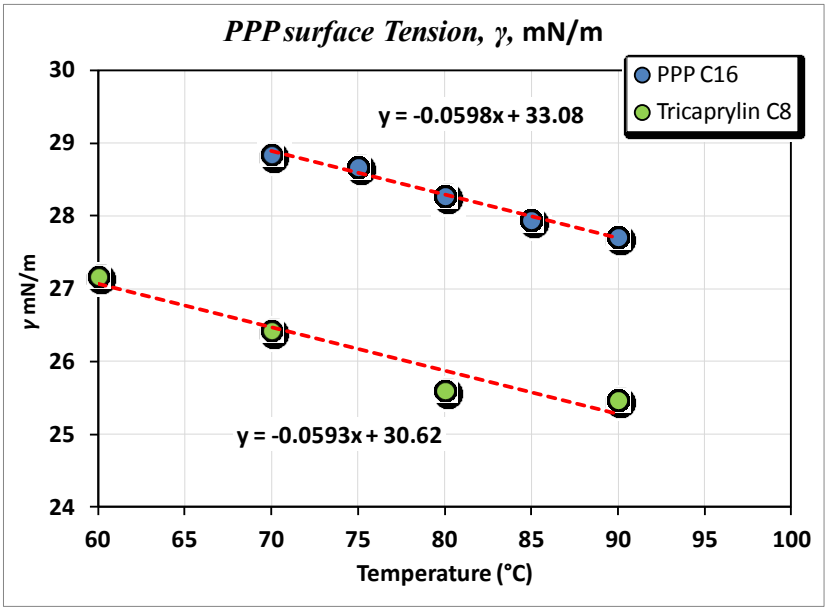

Figure A-9. Surface tension of PPP. (Chumpitaz *et al.*, 1999)

With the value of the surface tension, it is possible to calculate the shape of the meniscus. Under hydrostatic equilibrium, the Young-Laplace equation (Rodr gez-Valverde, Cabrerizo-V lchez, & Hidalgo- lvarez, 2003) can be expressed as

$$\gamma\left[\frac{1}{R_1}+\frac{1}{R_2}\right]=\frac{2\gamma}{R_0}+\Delta\rho g z \Rightarrow \frac{1}{\hat{R}_1}+\frac{1}{\hat{R}_2}=2+\frac{\Delta\rho g R_0^2}{\gamma}\hat{z} \qquad \hat{z}=z/R_0 \quad r=R/R_0$$

$$\frac{1}{\hat{R}_1}=\left(\frac{1}{R_1}\right)/R_0$$

$$\frac{1}{\hat{R}_1}+\frac{1}{\hat{R}_2}=2+\beta\hat{z} \qquad \beta=\frac{\Delta\rho g R_0^2}{\gamma} \qquad \frac{1}{\hat{R}_2}=\left(\frac{1}{R_2}\right)/R_0$$

$$\frac{1}{\hat{R}_1}=\frac{-\hat{z}'}{r\left(1+(\hat{z}')^2\right)^{1/2}} \qquad \frac{1}{\hat{R}_2}=\frac{-\hat{z}''}{\left(1+(\hat{z}')^2\right)^{3/2}}$$

The surface tension γ, determines the shape of the surface under the influence of gravity. The parameter R_0 is the radius of the ideal sphere at the center. However, the actual solution is likely not exactly spherical. However, a good spherical approximation solution is often found using the radius of the largest sphere, R_e. The second order differential equation is expressed as composed

of two terms, R_1 and R_2. The terms have been made non-dimensional (represented by a hat) by dividing them over R_0. The Bond number $\boldsymbol{\beta}$ is the ratio of gravitational to surface tension forces. Gravity is "g", 9.81 m^2/s, and $\Delta\rho$ is the difference in density between the liquid and the air. The vertical distance is z, and the non-dimensional radial distance is r.

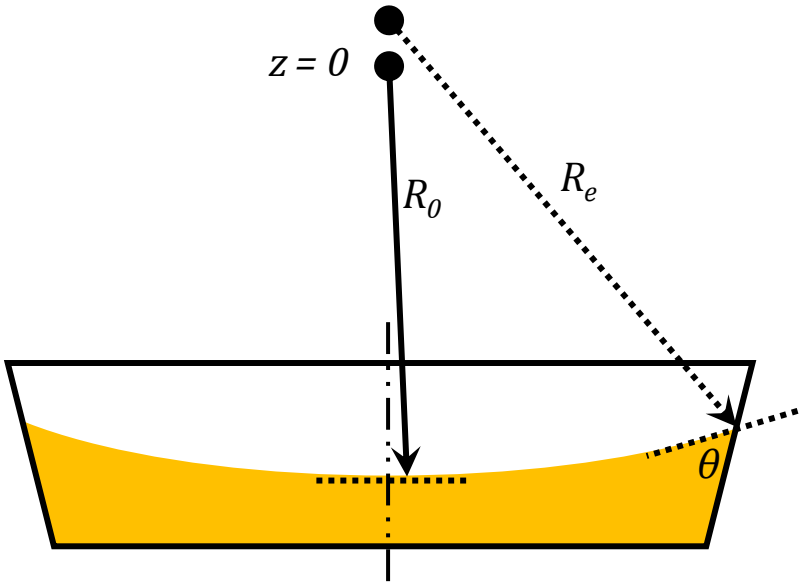

Figure A-10. Tangent plot on the surface of sample.

The second order differential equation

$$\hat{z}'' = -\left[\left(2+\beta\cdot\hat{z}\right)+\frac{\hat{z}'}{r\left(1+\left(\hat{z}'\right)^2\right)^{1/2}}\right]\left(1+\left(\hat{z}'\right)^2\right)^{3/2}$$

can be solved numerically with boundary conditions:

$$\hat{z}\big|_{r=0} = -1.0 \qquad \hat{z}'\big|_{r=0} = 0.0 \qquad \hat{z}'\big|_{r=r_{\max}} = \tan\left(\frac{\pi}{2}-\theta\right)$$

Where θ is the contact angle inside the liquid. Though the exact angle of contact is not known, observation of the pans when loaded provided an approximate estimate of around 60 degrees.

The density of liquid tristearin was estimated at 0.863 mg/mm^3 at 80 °C. The value found for R_0 in the case of that liquid tristearin was 3.5 mm. The difference between the bottom of the meniscus and its edge was thus 0.44 mm. With this value, and the radius of the pan, which is 2 mm, it was possible to calculate the equivalent radius for a sphere that has the same edge and bottom point.

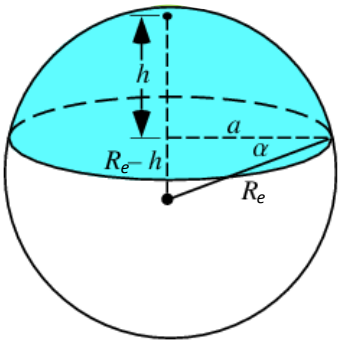

$$R_e = \frac{a^2 + h^2}{2h} \qquad V_{cap} = \frac{\pi}{6} h\left(3a^2 + h^2\right)$$

The equivalent radius R_e was 4.8 mm. The spherical approximation represents the surface quite well, as shown in Figure A-11 for SSS. The distance above the bottom of the meniscus, Δz, is plotted as a function of the radius.

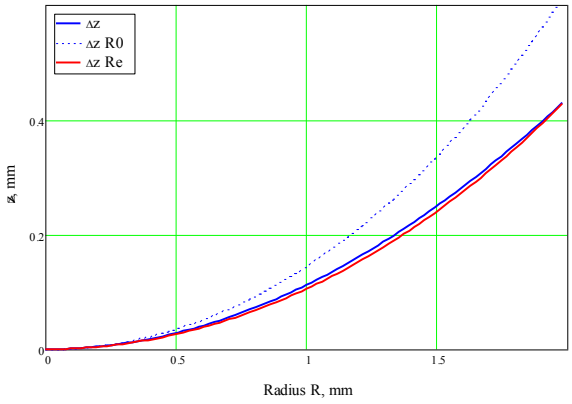

Figure A-11. Distance above the bottom of the meniscus versus the radius for liquid tristearin at 80 °C.

The solution was computed in Mathcad, a mathematical software. The solid blue line is the exact solution to the differential equation. The dotted line follows the minimal sphere, of radius R_0. The

red line follows the sphere of radius *Re*, which provides a very good approximation for the shape of the surface.

This approximation makes it much easier to draw the axisymmetric geometry in the finite element application of Matlab. The partial differential equations tool (PDEtool) was used to solve the 2D axisymmetric problem. The masses of the TAG mixtures were calculated for a typical 10 μL sample, and the corresponding heights were found. The slope of the wall of the pan, almost vertical, was neglected.

A.2.3 Diffusivity of saturated TAGs

The self-diffusivities at 80 °C were estimated from (Callaghan, 1977; Callaghan, & Jolley, 1980) and (Yucel & Uysal, 2003) and (Greiner, Reilly, & Briesen, 2012; Holz, Heil, & Sacco, 2000): $\boldsymbol{D_{ss}} \approx 0.000047$. This value is much smaller, for eample, than that for dodecane, that corresponds to one of the chains of trilaurin, $\boldsymbol{D_{dd}} \approx 0.0019$ mm^2/s.

The Fickian diffusivity D_{12}, here called D_{ds}, for a binary mixture can be estimated from the self-diffusivity of each component, as measured or estimated between two limits: in a liquid made of its own molecules, and in a liquid made of molecules of the other liquid, i.e. at infinite dilution. Following the treatment of Krishna and Baten (2005, Ind. Eng. Chem. Res., 44, 6939-6947)

$$D_{ds} = x_d \cdot D_d + x_s \cdot D_s = (1 - x_s) \cdot D_d + x_s \cdot D_s$$

$$D_d = (1 - w_s) \cdot D_{dd} + w_s \cdot D_{d\infty} \qquad D_s = (1 - w_s) \cdot D_{s\infty} + w_s \cdot D_{ss}$$

$$w_s = \frac{u}{u + (1-u)\rho_r} \quad x_s = \frac{u}{u + (1-u)M_\rho} \quad \rho_r = \frac{\rho_d}{\rho_s} \quad M_r = \frac{M_s}{M_d} \quad M_\rho = M_r \cdot \rho_r \quad u = \frac{c_s}{\rho_s}$$

Here, x_d is the mole fraction of the longer TAG, x_s is the mole fraction of the shorter one, w_s is the weight fraction of the shorter TAG, ρ_s is the liquid density of the shorter TAG, ρ_d is the density of liquid longer TAG, M_s is the molecular weight of the shorter TAG, M_d is the molecular weight of the longer TAG. The non-dimensional ratios ρ_s, M_r and M_ρ are defined in the equations. The non-dimensional concentration of the smaller TAG, $\boldsymbol{u}$, is calculated as the ratio of the mass concentration of the smaller TAG at a given location in the solution, c_s in kg/m3, divided by the density of the pure liquid smaller TAG, ρ_s.

D_{dd} is the self-diffusivity of the larger TAG molecules in pure liquid TAG, whereas $D_{d\infty}$ is the self-diffusivity of a liquid smaller TAG molecule infinitely diluted in the larger TAG. Similarly, D_{ss} is the self-diffusivity of the smaller TAG in itself, and $D_{s\infty}$ is the self-diffusivity of a molecule of the larger TAG infinitely diluted in the smaller TAG. D_d and D_s are the self-diffusivities of the larger TAG and smaller TAG in the mixed solution. They are combined to produce the binary, or Fickian, diffusivity, D_{ds}.

The self-diffusivities D_{ss} and D_{dd} of the smaller and the larger TAG were estimated using the equation proposed by (Callaghan, & Jolley,1980):

$$D = D_o e^{\left(\frac{-\Delta E}{R_g T}\right)}$$

$$D_o = a_D + b_D \cdot \eta_0$$

$$\Delta E = 8.04 \cdot \ln(n_c) - 6.11$$

Where the parameters ΔE and D_o for the two materials are given in by (Gunstone, 1994; Phipps, 1962; Cavaleri & Meirelles, 2000; Callaghan & Jolley, 1980)

The reference self-diffusivity D_o is related to the viscosity of the liquid TAG, as discussed by (Callaghan, & Jolley,1980). We used the data available for two TAGs to estimate the correlation between D_o and viscosity, as indicated in Table A-3 and in Table A-2.

Table A-1. Parameters to estimate the reference self-diffusivity as a function of viscosity at 70 °C.

TAG	D_o **x** 10^{-7}	η_0
SSS	4.79	18.63
OOO	9.37	13.81
	Parameter	
	a_D	22.5
	b_D	-0.95

$$D_o = a_D + b_D \cdot \eta_o$$

To estimate the viscosities of the TAGs at different temperatures, the correlations developed by Phipps (Phipps, 1962) were used:

$$\log_{10}(\log_{10}(\eta_0)) = a_\eta + b_\eta \cdot T$$

Table A-2. Parameters to estimate the viscosity of liquid TAGs, and the viscosity estimated at 70 °C.

C_n	a_η	b_η x 10^{-3}	η_0
12	0.3414	5.05	9.387
14	0.3649	4.68	12.294
16	0.3894	4.47	15.582
18	0.3972	4.19	18.633

The values of D_o reported in Table A-3 were estimated using the linear equation and the parameters in Table A-1.

Table A-3. Parameters to estimate the self-diffusivities D_{ss} and $D_{dd.}$

	n_c	ΔE kJ/mol	D_o m^2/s	Ref.
Trilaurin	42	23.9	1.36E-06	Method (Callaghan & Jolley, 1980)
Trimyristin	48	25.0	1.08E-06	Density and viscosities (Phipps, 1962)
Tripalmitin	54	26.0	7.69E-07	Actual data (Callaghan & Jolley, 1980)
Tristearin*	60	27.1	4.79E-07	
Dodecane	12	13.7	2.04E-07	Calculated from (Holz, Heil, & Sacco, 2000)
Rg			8.314E-03	kJ/(mol·K) Universal gas constant

Values of parameters used for these calculations are listed in Table A-4.

Table A-4.Example of parameters for self- diffusion calculations.

M_ρ	4.276	Mr·ρr
M_r	5.234	Ms/Md
ρ_r	0.817	ρd/ρs
ρ_s	863	kg/m^3
ρ_d	705	kg/m^3
M_s	891.48	kg/kmol
M_d	170.33	kg/kmol

	m^2/s (80 °C)	Ref.
D_{ss}	4.70E-11	(Callaghan & Jolley, 1980)
$D_{s\infty}$	2.01E-10	(Krishna & Baten, 2005)
D_{dd}	1.92E-09	(Holz, Heil, & Sacco, 2000)
$D_{d\infty}$	1.61E-10	(Krishna & Baten, 2005)

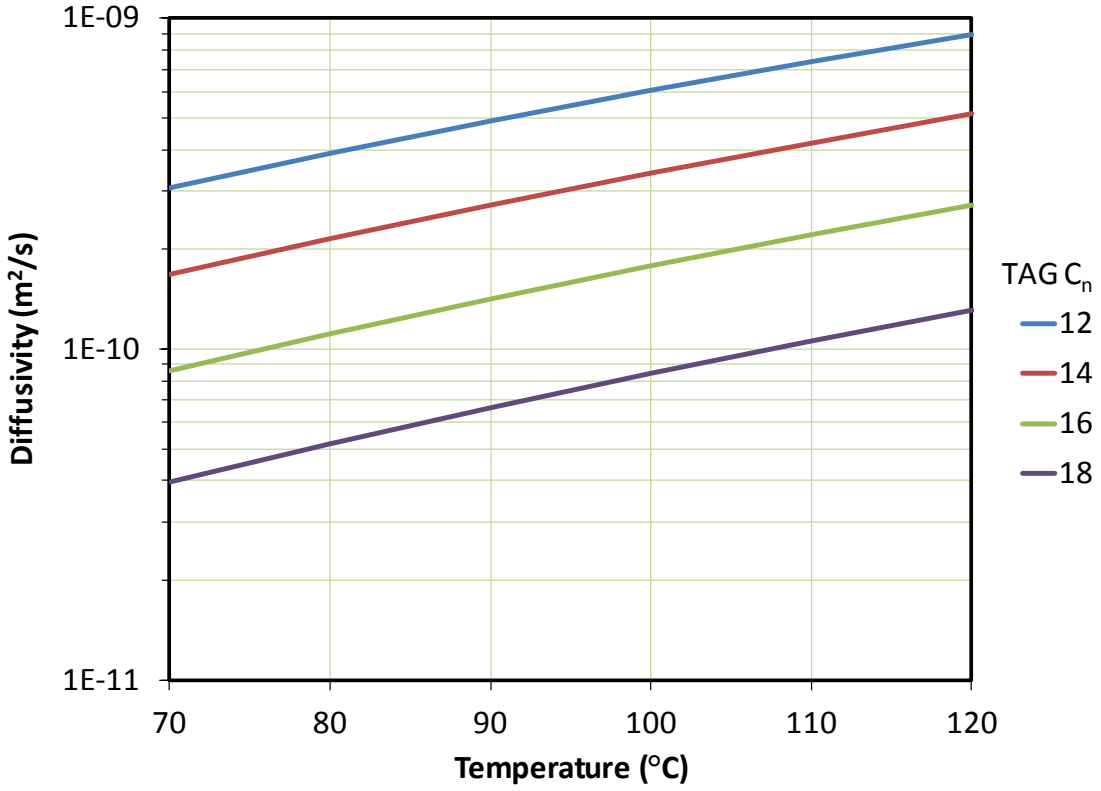

Figure A-12. Diffusivity of saturated TAGs, estimated following the concepts of (Callaghan & Jolley, 1980).

Table A-5. Parameters for the linear estimation of the density of liquid TAGs as a function of temperature, $\rho = a_\rho + b_\rho \cdot T$, T in °C. (Phipps 1962) The reference density ρ_0 is also tabulated.

C_n	a_ρ	b_ρ x 10^{-4}	ρ_0 (mg/mm^3) at 70.0 °C
12	0.9830	7.24	0.9323
14	0.9279	7.02	0.8788
16	0.9222	6.84	0.8743
18	0.9149	6.62	0.8686